ISBN 0-315-54952-1

CREEP ANALYSIS OF PLATE-LOAD AND PRESSUREMETER TESTS IN FROZEN SAND

by

PAUL RICHARD LACH

A THESIS
PRESENTED TO THE UNIVERSITY OF MANITOBA
IN PARTIAL FULFILLMENT OF THE
REQUIREMENTS FOR THE DEGREE OF
MASTER OF SCIENCE
IN
CIVIL ENGINEERING

WINNIPEG, MANITOBA

THE UNIVERSITY OF MANITOBA

LIBRARY

AUTHOR LACH, Paul Richard

TITLE CREEP ANALYSIS OF PLATE-LOAD AND PRESSUREMETER TESTS IN FROZEN SAND

THESIS M.Sc., 1989

I, the undersigned, agree to refrain from producing, or reproducing, the above-named work, or any part thereof, in any material form, without the written consent of the author:

CREEP ANALYSIS OF PLATE-LOAD AND PRESSUREMETER TESTS IN FROZEN SAND

BY

PAUL RICHARD LACH

A thesis submitted to the Faculty of Graduate Studies of the University of Manitoba in partial fulfillment of the requirements of the degree of

MASTER OF SCIENCE

ABSTRACT

The purpose of this study was to assess the validity of a constitutive model proposed by Rahman (1988), through the creep analyses of a plate-load and pressuremeter tests conducted in frozen sand. Both types of test subject the soil to multi-axial stress conditions representative of actual field problems.

A multi-stage plate-load creep test was performed using a 50 mm thick, 300 mm diameter, steel circular plate, which rested on the surface of a frozen sand. The test consisted of incrementally loading the plate and allowing creep deformation to occur under each increment. Four loads, which produced average bearing pressures of 0.88, 1.80, 2.68, and 3.44 MPa, were applied. The test was carried out over a period of about one year.

Two multi-stage pressuremeter creep tests were performed using Oyo Elastmeter 100 pressuremeter equipment. The tests were conducted in separate boreholes, at different locations in the same frozen sand investigated in the plate-load test program. Test No. 1 comprised four stages in which mean cavity pressures of 0.86, 1.77, 2.83, and 3.47 MPa were applied. The total test duration was 120 days. Test No. 2 comprised three stages in which mean cavity pressures of 0.85, 1.79, and 2.78 MPa were applied. The total test duration was 80 days.

Creep deformation analyses of both the plate-load and pressuremeter test problems were subsequently performed. The constitutive relationships developed by Rahman (1988) provided a basis for the analyses. The agreement between observed plate displacements and those predicted by analysis was poor. Several factors may have contributed to the poor agreement, but these could not be defined in a quantitative manner. On the other hand, for the pressuremeter problem, the agreement between observed and predicted creep strains was generally satisfactory. Therefore, no definite conclusion was drawn regarding the validity of the Rahman (1988) constitutive model.

ACKNOWLEDGEMENTS

The writer wishes to express his sincere gratitude to his advisor, Dr. L. Domaschuk, for his guidance and assistance during the preparation of this thesis.

The writer also wishes to extend special thanks to Dr. N. Rajapakse, Dr. D. Shields and Dr. E. Lajtai, who provided helpful suggestions and constructive criticism. Appreciation is expressed to Dr. J. Graham, and Dr. A. Shah for their advice and instruction. Thanks are also extended to Dr. L. Fransson, Mr. B. Turnbull, and Mr. E. Lemke for their contributions to the experimental phase of this study.

The writer also wishes to gratefully acknowledge the support and encouragement provided by Dr. F. Azizi, Dr. N. Chandler, Mr. S. Duncan, Mr. R. Kenyon, Mr. K. Leung, Mr. B. Lingnau, Mr. K. Osiowy, Mr. J. Oswell, Mr. N. Piamsalee, Mr. U. Puswewala, Mrs. V. Ring, Dr. F. Saadat, Mr. R. Serrette, Mrs. I. Trestrail, Mr. A. Wan, and Mr. J. Yin.

The writer also wishes to acknowledge the financial assistance provided by the Natural Sciences and Engineering Research Council of Canada.

The writer is greatly indebted to his parents for their understanding and sacrifices during his education.

TABLE OF CONTENTS

LIST OF FIGURES

LIST OF TABLES

CHAPTER 1

INTRODUCTION

1.1 GENERAL

Permafrost underlies almost 20% of the land area of the world. Its extensive occurrence in northern regions, including nearly one-half of the U.S.S.R. and Canada, and much of Alaska, is of particular concern to geotechnical engineers. Development and utilization of natural resources and the need for highways, pipelines, and other constructed facilities in Arctic regions have brought about increased interest in cold regions science and technology. In North America and the Soviet Union, the development of permafrost regions is advancing rapidly and engineering design and construction principles have to be formulated to ensure safe, functional and economical solutions. The field of frozen soil mechanics has also received further attention due to the growing use of artificial ground freezing for soil stabilization, particularly in soft ground tunnelling. A knowledge of the deformation and strength characteristics of frozen soils is essential for the design of structures or foundations comprising frozen soils, and the analysis of their behavior.

From the point of view of the science of materials, frozen soil is a natural particulate composite, consisting of four different constituents: solid grains (mineral or organic), ice, unfrozen water, and gases. Its most significant dissimilarity, when compared with other particulate materials, including unfrozen soils, is the continual restructuring of its matrix under applied stresses and varying temperature. Frozen soil exhibits substantial deformation under sustained loading. Engineering design, therefore, generally requires that stresses should not only be small enough to avert failure, but that deformations that develop during the lifetime of concern should also be maintained within tolerable limits. Hence,

the study of creep is of great importance. A primary thrust of cold regions engineering research involves the modelling of the stress-strain-time behavior of frozen soil.

Two general approaches have been adopted in the development of most of the existing theories of creep. These were termed micromechanistic and macroanalytical by Ladanyi (1972). The former approach provides a physical theory capable of describing creep behavior in terms of previously established concepts of physics. The latter approach provides an engineering theory based on certain macroscopic experimental findings. Due to the presence and interaction of various substances in different phases, the phenomena that control the mechanical behavior of frozen soil are complex and as yet have not been adequately investigated. Some of the studies which have attempted to provide fundamental explanations (physical theories) of observed behavior include those of Vyalov (1957, 1973), Goughnour and Andersland (1968), Chamberlain et al. (1972), Sayles (1973), Pusch (1980), Ting (1981, 1983), Ladanyi (1981, 1985), and Orth (1985). In particular, Ting (1981) provided a comprehensive study of various physical mechanisms controlling the strength and deformation behavior of frozen soil-ice systems. At the same time, it is recognized that the obligation to perform engineering design work, and to undertake construction in areas underlain by permafrost, requires basic relations that are broad in scope and adequately represent the behavior of frozen soil in practice. Recent literature reviews of various constitutive relations for frozen soils and ice were provided by Ting (1981), Rahman (1988), and Puswewala (1988).

In the most general case, the constitutive model for a material must express a relationship among the state of stress, state of strain, time, temperature, moisture and ice content, and other variables considered pertinent to the problem. The relative influence of each of these factors has been the subject of several studies. However, the actual deformation behavior and strength of frozen soil

mobilized in-situ, under the loading and thermal boundary conditions, which might arise in practice, is not readily estimated with accuracy. The gap between theory and practice in frozen soil engineering may be partially attributed to the lack of opportunity to investigate prototype behavior. This is now changing with growing interest in resource development in the North. More occasions are arising in which the in-situ behavior of frozen soil is studied and in which permafrost samples are made available to laboratories for testing.

A constitutive formulation, representative of a range of frozen soils, may be established based on laboratory test results. Nevertheless, there still remains the practical problem of determining the stresses and deformations in a frozen soil when several soils and complicated displacement and stress boundary conditions exist.

1.2 STATEMENT OF THE PROBLEM

Most of the existing constitutive theories for frozen soil and ice come from the study of metals, and fail to consider the fundamental differences in the behavior of metals and frictional frozen soils. The theories generally do not account for superimposed hydrostatic stress and do not consider volumetric strains in their formulation. In most cases, uniaxial creep test results are extended to the general state of stress by using equivalent stress and strain relationships from classical plasticity theory. Moreover, short term, high stress tests are usually conducted and the results are extrapolated to predict long term behavior.

Rahman (1988) proposed a constitutive model for frozen soil which accounts for the influence of the hydrostatic stress on creep behavior. As well, volume changes were measured and their effect on creep behavior was assessed.

Singh and Mitchell (1968) indicated that to be of practical use in providing a general description of the creep characteristics of soils, a proposed model must satisfy the following criteria: (1) it must be applicable for a reasonable

range of stresses; (2) it must describe the behavior of a range of soil types; and (3) it must contain parameters that are easily determined. In addition to Singh and Mitchell's criteria, the fundamental criterion of being applicable in the analysis of field problems was suggested by Emery (1971).

1.3 OBJECTIVES AND SCOPE OF THE INVESTIGATION

The present study is a continuation of the work of Rahman (1988). The general purpose of the study was to assess the practicality and validity of the constitutive model for frozen sand, proposed by Rahman. The specific objectives of the study were as follows:

1. To carry out a relatively long-term plate-load creep test using a rigid circular plate resting on the surface of the same frozen sand.
2. To carry out two relatively long-term pressuremeter creep tests in the same frozen sand.
3. To analyze the plate-load and pressuremeter problems, based on the Rahman constitutive model and to appraise the results. Specifically, this included the following three steps:
   (a) the modification of an existing finite element computer program to incorporate the creep constitutive relationsips;
   (b) the application of the program in the analysis of each of the above-mentioned experimental problems; and
   (c) the comparison of the observed creep response and that predicted by analysis.

Each test and the results are described separately in Chapters 2 and 3 of the thesis. The analyses and subsequent predictions of creep are considered in Chapter 4. Finally, Chapter 5 presents a discussion of results of the analyses along with conclusions regarding the overall study.

CHAPTER 2

PLATE-LOADING CREEP TEST: EXPERIMENTAL PROGRAM

2.1 - INTRODUCTION - REVIEW OF PUBLISHED EXPERIMENTAL DATA

Experimental information pertaining to the creep-deformation of frozen soil under a loaded area is at present relatively scarce. Studies carried out in the Soviet Union constitute the bulk of the currently available data on the deformation of frozen soil and ice beneath model and full-scale footings. In the following, a general review is provided of the results of published data concerning loading tests performed on frozen soil and ice. Discussion is limited primarily to test results and observations, due to a lack of similarity of objectives and methods in the experimental programs considered.

Vyalov (1959) reported the results of experimental investigations conducted at the Igarka Permafrost Research Station, Academy of Sciences of the U.S.S.R. In these studies, circular flat-faced punches of diameters 50, 71 and 101 mm, respectively, were pressed into large blocks of undisturbed frozen soils (loam, sandy loam, sand). The average soil temperature was -0.4°C. Tests were carried out at varying depths within the blocks under constant loads and also under loadings which were increased in a stepwise manner. Additional tests were performed in-situ using circular plates 505 mm in diameter. In this case, a stiff, varved clay containing a large number of ice lenses up to 50 mm thick, was investigated. The temperature of the soil was -0.5°C.

Unfortunately, complete information regarding the rheological properties of the soil tested was not provided in the report. However, observations concerning the character of deformation of the soil provided a general understanding of the physical phenomena occurring during such loading tests. According to Vyalov, the mode of failure of frozen soil under a rigid plate is distinct from that of

unfrozen soil. Heaving of the soil surface, generally observed in stiff unfrozen soils, was absent in a variety of frozen soil types subjected to both long and short-term loading. A more apparent characteristic was the appearance of cracks on the surface of the soil, directed radially from the axis of the plate. In addition, as in unfrozen soils, a dense region or 'kernel' was formed immediately beneath the base of the plate. The formation of Prandtl-type slip surfaces was not observed in these experiments.

To study long-term settlement, Vyalov (1978, 1979) also tested sandy loam soils in the field over a period of 19 years, using 3 settlement plates having a diameter 705 mm. The temperature of the soil at the level of the base of the plates was between -0.1 and -0.5°C. Loads were applied to the plates in increments. The settlement of field plate No. 1 under an initial pressure of 150 kPa stabilized after 6 months. The total settlement was only 7 mm. Field plate No. 2, under pressures of 125 and 250 kPa, experienced settlements of 5.5 and 21 mm that stabilized after 46 and 167 days, respectively. Plate No. 3 was initially loaded for equal time increments of short duration (Δt = 48 hr.). Under the final pressure increment, selected to approximate the long-term strength of the soil, settlements of all three plates continued steadily. The settlement stopped after 17 years, when the soil temperature was lowered as a result of the removal of insulation. The shape of the settlement curves observed throughout almost the entire testing period was nonlinear, emphasizing the uncertainty of predicting long-term settlement of foundations in warm frozen soils, from the results of short-term creep tests.

The creep data was represented in a form analogous to Schleicher's equation (Tsytovich, 1976) for a circular foundation loaded at the surface of an elastic half-space. In this case, the elastic modulus was regarded as a variable influenced by stress and time. Vyalov adopted a power relation to describe the dependence of plate creep settlement on both time and pressure as:

$$s/d = Bp^{1/m} t^{\beta}, \qquad (2.1)$$

in which s is the plate settlement, d is the plate diameter, p is the applied pressure, t is the elapsed time, and m, β and B are parameters obtained from experiments.

The values of parameters m, β and B in equation 2.1 for this investigation, which represents the longest continuous test record of this kind published to date, are specified in Table 2.1. According to Vyalov, substitution of the average values of these parameters into equation 2.1 then facilitates estimation of the magnitude of settlement which can be expected for real foundations on frozen soils of the investigated type.

TABLE 2.1 - PARAMETERS OF EQUATION (2.1)
(AFTER VYALOV, 1978, 1979)

Test Plate Number	m	β	$B(Pa^{-1/m} \cdot yr^{-\beta})$
1	0.57	n.a.	n.a.
2	0.57	0.167	$3.98 \cdot 10^{-3}$
3	0.57	0.137	$5.58 \cdot 10^{-3}$

Zaretskii (1972) proposed a linear-fractional representation (i.e. a hyperbolic type of dependence) of settlement on both stress and time to describe the attenuating creep settlements of foundations in plastic frozen soils, for stresses less than the long-term strength. However, experimental results reported concern only the time-dependence of the plate settlement expressed as:

$$s = s_{\infty} \frac{t}{T + t} \qquad (2.2)$$

in which t is the time, and s_{∞} and T are material constants, for the case of constant applied pressure. Table 2.2 presents values of T and attenuated settlement, s_{∞}, for the experiments of Maksimov (1967) and Vyalov (1959).

According to Zaretskii, the parameter T, which characterizes the intensity of attenuation of settlement, may be expressed as:

$$T = T_o \frac{p_o - p_\infty}{p_\infty - p} \qquad (2.3)$$

where p_∞ is the limiting long-term pressure, p_o is the instantaneous limiting pressure, and T_o is a creep parameter of the soil, independent of applied pressure. With increase of load, the period of stabilization increases, and for $p = p_\infty$ non-attenuated deformation is characterisitic. On the basis of the relation 2.3, for any values of T corresponding to different degrees of loading, such as those presented in Table 2.2, the critical pressure, p_∞ , may be approximated.

TABLE 2.2 - PARAMETERS OF EQUATION (2.2) FOR THE EXPERIMENTS OF MAKSIMOV (1967) AND VYALOV (1959) * AS REPORTED BY ZARETSKII (1972)

Soil	Area of Plate (cm^2)	Duration of Experiment (hr)	Load (kg/cm^2)	Parameter, T(hr)	S_∞ (mm) Calc.	S_∞ (mm) Actual
Fine frozen sand	4900	1680	4 - 8	151	17.8	15.5
at T = -0.5°C	4900	2400	8 - 12	482	34.4	30.0
Gravelly soil	4900	2400	20 - 30	163	4.4	4.3
at T = -0.5°C	4900	4320	30 - 40	254	12.7	12.3
Banded Clay at T = - 0.5°C*	90	2100	0 - 13	37.5	12.5	12.5

Vyalov et al. (1973) provided a qualitative assessment of the results of plate bearing tests in ice. The experiments were carried out in order to examine the influence of applied loads, the size and depth of the plate, and the structure and temperature of the ice investigated on the resulting settlement. Tests involving rigid circular plates of diameter 32, 160 and 320 mm were conducted

at various depths within the ice. Several tests performed in ice at -2.3°C showed similar deformation behavior and differed only values of the steady-state settlement rate. The rate of settlement was found to decrease with depth of the plate and to increase in approximate proportionality with the diameter of the test plate. Representation of the deformation behavior observed in these studies, as presented by the authors, incorporated a power law dependence on stress and accounted for temperature effects through an approach suggested by Voytkovskiy (1960). The influence of ice-structure on settlement rate was assessed through tests conducted on both multiple-veined ground ice and artificial ice, frozen in layers. The study indicated that within the stressed zone there was a breakdown and refinement of crystals, accompanied by a decrease in size of air bubbles and their concentration beyond the zone. The ice underwent a redistribution of density resulting in the formation of a dense region or 'kernel' beneath the plate.

Johnston and Ladanyi (1974a) described a test program conducted by the Division of Building Research of the N.R.C.C. at Thompson and Gillam, Manitoba, to evaluate the creep behavior and load capacity of 203, 254 and 381 mm diameter plate anchors installed at various depths within permafrost. The soils investigated were ice-rich stratified silts and clays. The average soil temperature was -0.3°C. It can be expected that within certain limitations of deformation and depth of embedment, the upward movement of a deep plate anchor would result in displacement behavior similar to that which would occur if the same anchor was pushed into the soil. All anchors were stage-loaded in increments of either 0.9 or 2.3 tonnes; each load increment being maintained until a constant rate of displacement was obtained. The duration of application of a single load increment ranged from 1 to 18 hours. Most tests were completed in less than 40 hours. The anchor test results lead to general conclusions on the frozen soil behavior similar to those expressed by Vyalov (1959) with regard to plate bearing

tests. In-situ examination revealed no failure surfaces but only a cone of frozen soil solidly attached to the plate. The resulting displacement-time curves were represented by a linear expression in which the intercept and slope representing the pseudo-instantaneous displacement and the steady-state displacement rate, respectively, were fitted as hyperbolic functions of the applied net uplift pressure. However, values of the corresponding parameters reported were influenced by various factors, including anchor depth (silt content increased with depth at the test site), anchor diameter, depth-to-diameter ratio, soil temperature and degree of disturbance during installation.

Ladanyi and Johnston (1974b) made use of the elastic analogue (Hoff, 1954) in the development of a solution which provides the rate of cavity expansion, within a medium, under a constant internal pressure. A relationship between the displacement of a deep circular footing and the expansion of a cylindrical cavity was then obtained by equating the volume displacements of soil produced in each case. The authors successfully employed the cavity expansion theory in the analysis of the test results presented by Ladanyi and Johnston (1974a).

Ladanyi and Paquin (1978) performed a series of laboratory deep plate loading tests with 35.7 mm diameter punches embedded in a saturated frozen sand. The temperature of the sand was -6°C. Three tests were carried out at depths of 152, 305 and 457 mm in a steel tank 600 mm in diameter and 900 mm high. All of the tests were stage-loaded, but the duration of the increments and the loading sequence was different in each case. The main purpose of the study was to investigate the effect of time, load and loading history on the settlement rate. The time necessary to attain a steady-state rate in these tests varied between 1 and 5 days, depending on the applied load. The instantaneous settlement was negligible. The relationship between settlement rate at the end of any stage and the applied pressure was expressed as a power law. In addition, from results when the load in these tests was cycled in several stages, it was

concluded that the settlement rate is influenced by both load and loading history, but becomes practically independent of the latter after the penetration resistance of the soil has been fully mobilized. The authors further demonstrated that a satisfactory prediction of settlement rates can be obtained by using a theory based on the spherical cavity expansion creep model (Ladanyi and Johnston, 1974b). Triaxial tests carried out on frozen soil samples taken directly from the testing tank provided the necessary soil properties to allow comparison between observed behavior and theoretical predictions.

Sego and Morgenstern (1985) carried out a series of punch indentation laboratory experiments in ice. The tests were performed using a constant displacement rate press and a 19.05 mm diameter circular punch, on samples of polycrystalline ice 100 mm in diameter. Ice temperatures in separate tests ranged from about -0.8 to -1.0°C. The duration of each test was approximately 10 days. A typical plot of punch resistance versus time at a constant displacement rate showed a definite peak resistance and asymptotic (post peak) resistance. According to the authors, the decrease in punch resistance with increasing punch penetration may be associated with a change in the size and orientation of the ice crystals beneath the penetrating punch. In the low-stress zone of the sample, little or no disturbance of the ice crystals occurred. A small-strain finite element computer code was developed to study plane strain and axisymmetric loading in a material whose creep behavior is governed by a flow law of the form of Glen's law as generalized to multiaxial stress states by Ladanyi (1972). Close agreement was found in comparison of the experimental peak resistance data, the results of an analysis using the cavity expansion model (Ladanyi and Johnson, 1974b), and the results of the finite element analysis for a penetrating punch with depth-to-diameter ratio of 0 and 5. A flow law derived from the results of uniaxial compression creep experiments was used in both the cavity expansion and finite element analyses. Both the results of finite element analysis and

experimental evidence suggested a lack of influence of depth of burial on punch resistance, in conflict with the data presented by Vyalov et al. (1973). The authors indicated that the discrepancy may have been due to the difference in magnitude of the strain to which the ice was subjected in each investigation.

Sayles (1985) presented the results of creep settlement tests performed on a concrete strip footing measuring 910 by 250 mm, founded on the surface of ice-rich aeolian silt permafrost. The tests were carried out at an ambient temperature of -2.0°C in the controlled environment of the U.S.A. C.R.R.E.L. Permafrost Tunnel Facility near Fox, Alaska. The tests involved the application of four pressures, 0.193, 0.385, 0.579 and 0.770 MPa, for test periods of 500, 250 and 145 days, respectively. Between loadings, the footing was allowed to rebound for at least 48 hours. The test results were reported as plots of footing settlement versus time for each of the applied pressures, with the exception of the 0.579 MPa test in which equipment failure produced inconsistent settlement values. Reasonable agreement was found between measured settlement values and those computed by different analytical methods that utilize results from unconfined compression creep tests. These methods included a cavity expansion model proposed by Ladanyi (1975), a thermodynamic creep model proposed by Fish (1983), and a procedure suggested by Nixon (1978) which utilizes influence factors determined from non-linear finite element analyses.

Lunne and Eidsmoen (1988) recently published preliminary results of an investigation involving long-term plate load tests on frozen Svea clay on Svalbard, Norway. The Svea clay is a marine clay with a salt content of about 35 g/ℓ and with ice lenses up to 10 mm thick, oriented both horizontally and almost vertically. Six steel plate footings, 1 m in diameter and 22 mm thick, were installed to depths varying between 1.2 and 2.2 m. Maximum settlement rates coincided with maximum temperatures recorded just below the plates, and settlements ceased for all of the plates as the soil temperature decreased near the end of the first

year. Prior to testing, maximum settlement rates were predicted based on parameters derived from laboratory creep tests and a simple power law. The shallowest plates (1.2 m depth) were subjected to applied vertical pressures of 52 kPa. The warmest soil temperature below these plates was -2.5 to -3°C and the corresponding maximum creep rates were 2 to 2.5 mm/month, which was significantly less than the rate predicted based on laboratory tests. The deepest plates (2.2 m depth) were subjected to applied vertical pressures of 100 to 134 kPa. The warmest soil temperature below these plates was -4.5°C and the corresponding maximum creep rates were 1 to 4 mm/month, which was reasonably close to predicted values.

To the writer's knowledge, the aforementioned studies constitute the only investigations reported in the literature where the creep behavior of frozen soil has been examined through experiments performed on model or full-scale test plates, or footings under both laboratory and field conditions.

2.2 EQUIPMENT AND MATERIALS

2.2.1 Test Facility

The tests were conducted in a 2.5 m square pit, 2 m deep, made of reinforced concrete, 200 mm thick. The walls and floor of the pit were insulated with 200 mm and 100 mm thick blocks of rigid insulation placed respectively, on the exterior and interior sides. Platecoil panels made of 14 gauge carbon steel and measuring 737 mm by 2108 mm were installed separately along the sides and base of the pit to provide two independent flow networks. A 3 hp air-cooled compressor unit was used to circulate refrigerant through the panels. Thermostatically controlled solenoid expansion valves permitted separate temperature control of the side and bottom panels. However, the system did

not allow for simultaneous temperature control of both networks. The test pit was housed in a 5 m square, 3 m high, walk-in type cold room refrigerated by a 5 hp air-cooled compressor unit.

2.2.2 Soil Description - Placement and Freezing Procedures

The soil used in this investigation was a uniform quartz-carbonate, medium-grain sand identical to that tested in the study conducted by Rahman (1988). A representative particle size distribution curve is shown in Figure 2.1. The coefficient of uniformity of the sand is 2.0.

The soil was deposited in a loose saturated state to a thickness of 1.8 m within the test pit. A polyethylene liner, 0.5 mm thick, was used to separate the sand from the platecoil panels in order to prevent adfreeze forces from acting on the panels. A 100 mm layer of wet sand was initially placed at the bottom of the pit. Four vertical strings of thermocouples mounted on long wood stakes were embedded in the soil at locations starting from the pit center and extending to a wall panel. Thermocouples (type TNBS) were spaced at 200 mm intervals along each string. A drawing indicating the relative locations of all thermocouples within the test pit is presented in Figure 2.2. After installation of the thermocouple strings, the sand layer at the bottom of the pit was frozen. The procedure used to place the remainder of the sand is described as follows.

A rectangular tank 2.8 m by 0.7 m and 0.6 m high was constructed out of sheet metal to be used for wetting the sand prior to its placement. The tank was built with a metal divider at a distance of 0.4 m from one end in order to create a reservoir. The bottom half of the divider was perforated so that water could flow freely into and out of the reservoir. Uniformly graded stone having a maximum size of 38 mm was placed in the bottom of the remainder of the tank. A sand container 2.4 m long and 0.7 m wide was constructed and set inside the upper half of the tank so that it rested upon the surface of the stone layer.

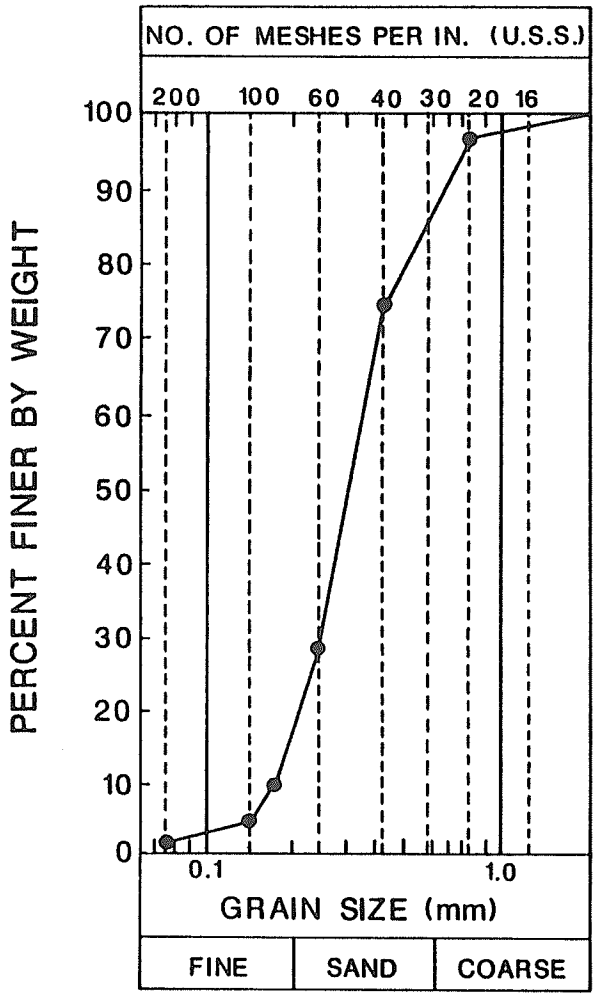

FIGURE 2.1 GRAIN-SIZE DISTRIBUTION OF THE SAND

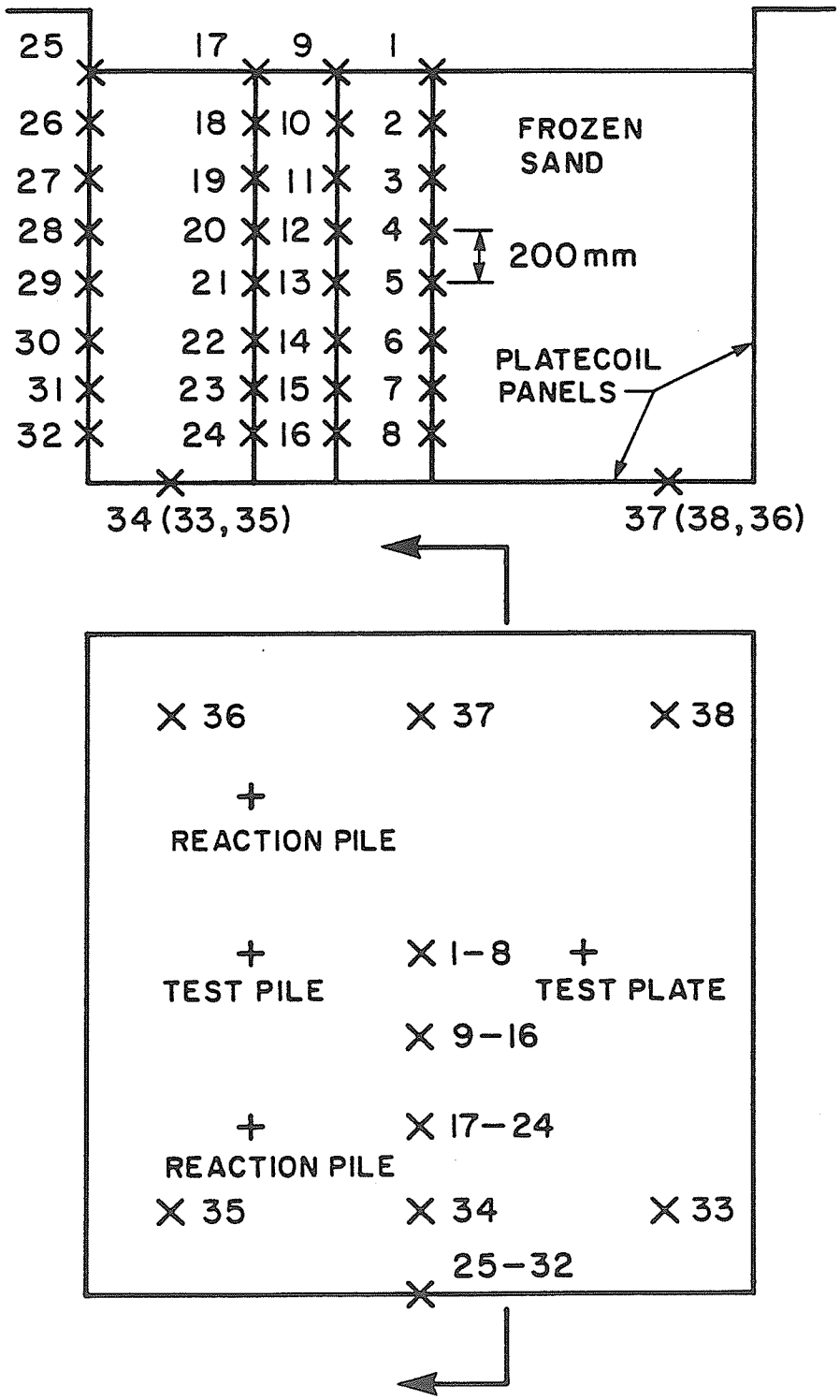

FIGURE 2.2 LOCATION OF ALL THERMOCOUPLES IN THE TEST PIT

The base of the container was made of expanded steel having approximately 6 mm openings. A layer of air dry sand, about 150 mm thick, was placed in the container. Water was subsequently pumped into the reservoir from which it flowed through the stone layer and up into the sand. The sand was left in a partially saturated state following drainage of the water to a level below the bottom of the container. The container with the sand was then removed from the tank and lowered into the pit, just below the surface of a 300 mm layer of cold (0°C) water retained above the sand in place. The sand flowed out of the container and was thus deposited by sedimentation. Openings were provided in the bottom of the container through which the thermocouple strings passed as the container was lowered and raised. Sand was placed to a depth of 1.8 m in this manner, as was previously noted. The top surface of the sand was levelled off manually, resulting in some disturbance within a thin upper layer of the soil.

The soil mass was then frozen unidirectionally upward by setting a temperature of -30°C at the base panels, closing off the side panels, and maintaining the ambient air temperature at 0°C. Since the sand had been cooled to near freezing during its placement, it only took about 2 days to bring it to temperature equal to or less than 0°C. Following a period of 16 days, the temperature of the soil varied linearly from 0°C at the top to -30°C at the base of the pit. To attain the proposed test temperature of -3°C, the base panels were closed off while the side panel and air temperatures were set at -3°C. As previously indicated, it was not possible to simultaneously circulate refrigerant through both the side panel and bottom panel circuits at the same temperature with the particular arrangement of a single compressor and thermostatically controlled expansion valves. A steady state temperature distribution with a slight vertical gradient was achieved after a period of several weeks. Temperature profiles are shown in Figure 2.3 for the following cases: immediately after sand placement; 2 days after initiation of the freezing process (all temperatures at

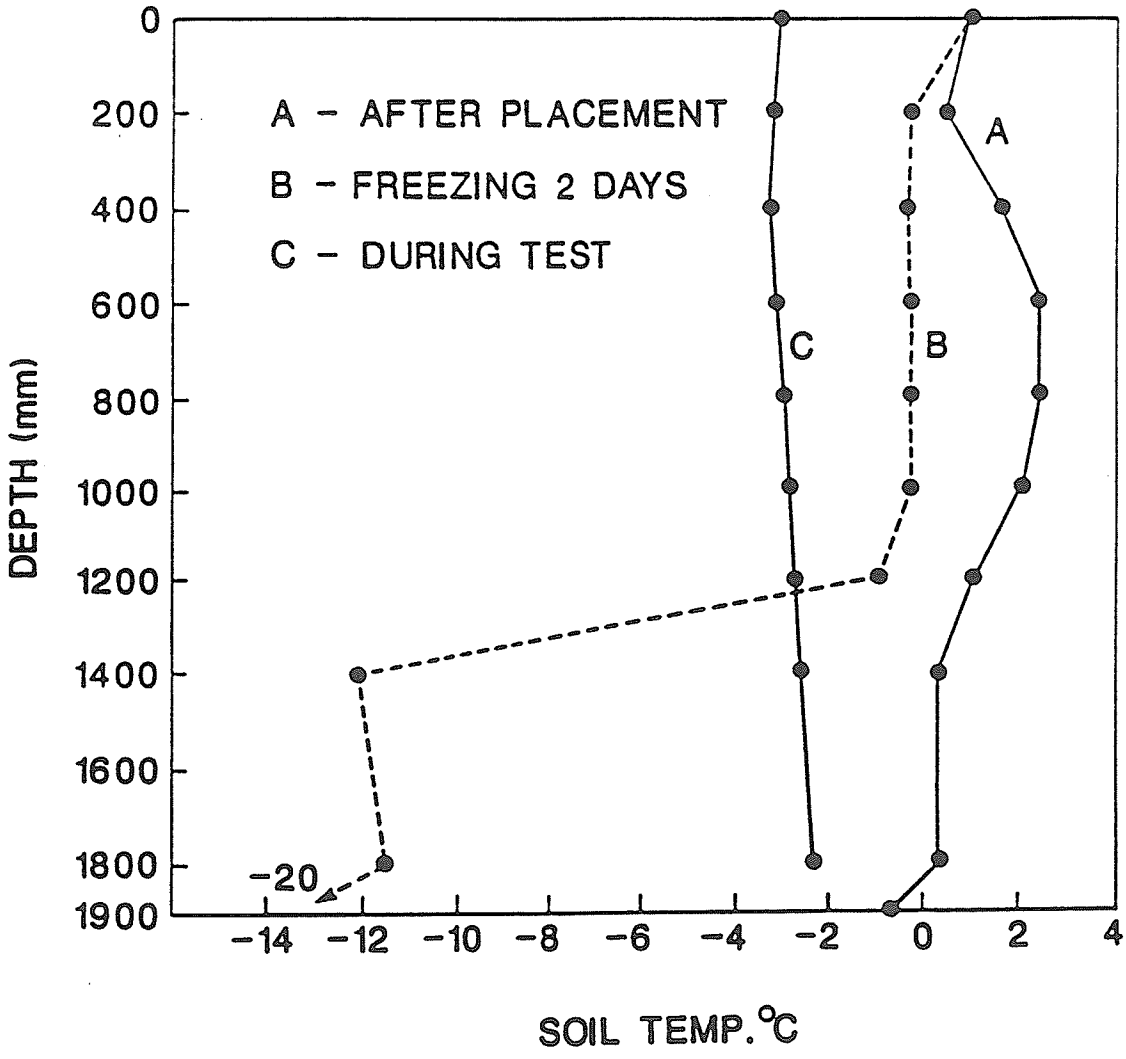

FIGURE 2.3 SOIL TEMPERATURE PROFILES FOR THE TEST PIT

or below 0°C); and during the initial stages of the test.

Unit weight and ice content profiles of the frozen soil were determined by coring at the beginning of the test and subsequent to its completion. These results are presented in Figure 2.4. The range of dry unit weights was 15.2 to 16.2 kN/m^3. The range of total moisture contents was 20.5 to 23.8%. The variation in water (ice) content near to the surface may be attributed to sublimation and occasional watering of the surface, which was done to minimize sublimation. No visible ice segregation was evidenced within the soil mass during coring.

2.2.3 Plate - Load Test Instrumentation

A schematic representation of the test pit and plate-load test apparatus is presented in Figure 2.4. The test set-up and instrumentation are also shown in Figure 2.5.

The plate-load test was performed using a 50 mm thick, 300 mm diameter, steel circular plate resting on the surface of the frozen soil. A second steel plate, 50 mm thick was stacked on the test plate to ensure rigidity. Constant loads (axial and concentric) were applied to the plate arrangement through a hydraulic ram activated by means of a dead-weight loading system. Plate displacement was monitored by means of a displacement transducer and corroborated by an independently attached dial gauge at a second location. The displacement transducer installed was a linear variable differential transformer (Hewlett Packard Model 7DCDT-500) with a displacement range of ±12.7 mm and a maximum nonlinearity of ±0.5% of full scale. The dial gauge allowed displacement measurements to be read to within ±0.005 mm. Both the displacement transducer and dial gauge were mounted on separate stable, non-magnetic bars fixed to the walls of the test pit.

Reaction for the applied loads was provided by a rigid structural steel frame positioned over the test pit. The frame consisted of two beams (W460

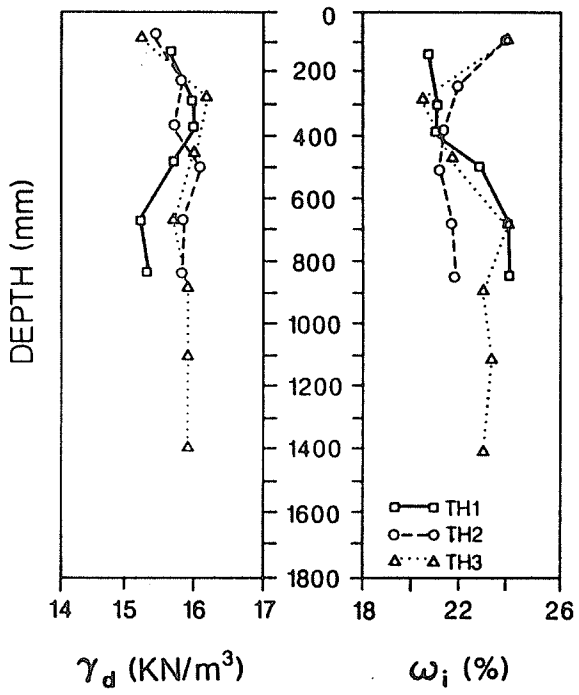

(a) Unit Weight and Soil Moisture Profiles

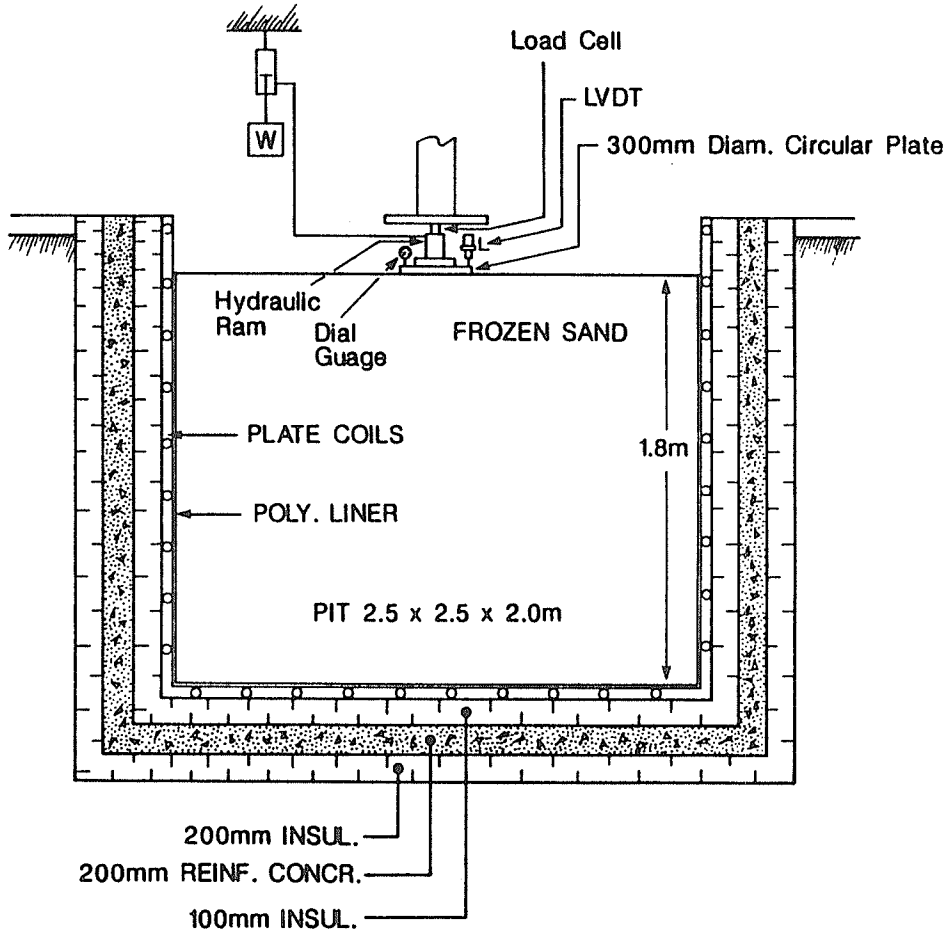

(b) Cross Section of Pit

FIGURE 2.4 (a) UNIT WEIGHT AND ICE CONTENT PROFILES (TH1 - BEGINNING OF TEST; TH2 AND TH3 - END OF TEST);
(b) SECTION THROUGH PIT AND PLATE-LOAD TEST APPARATUS

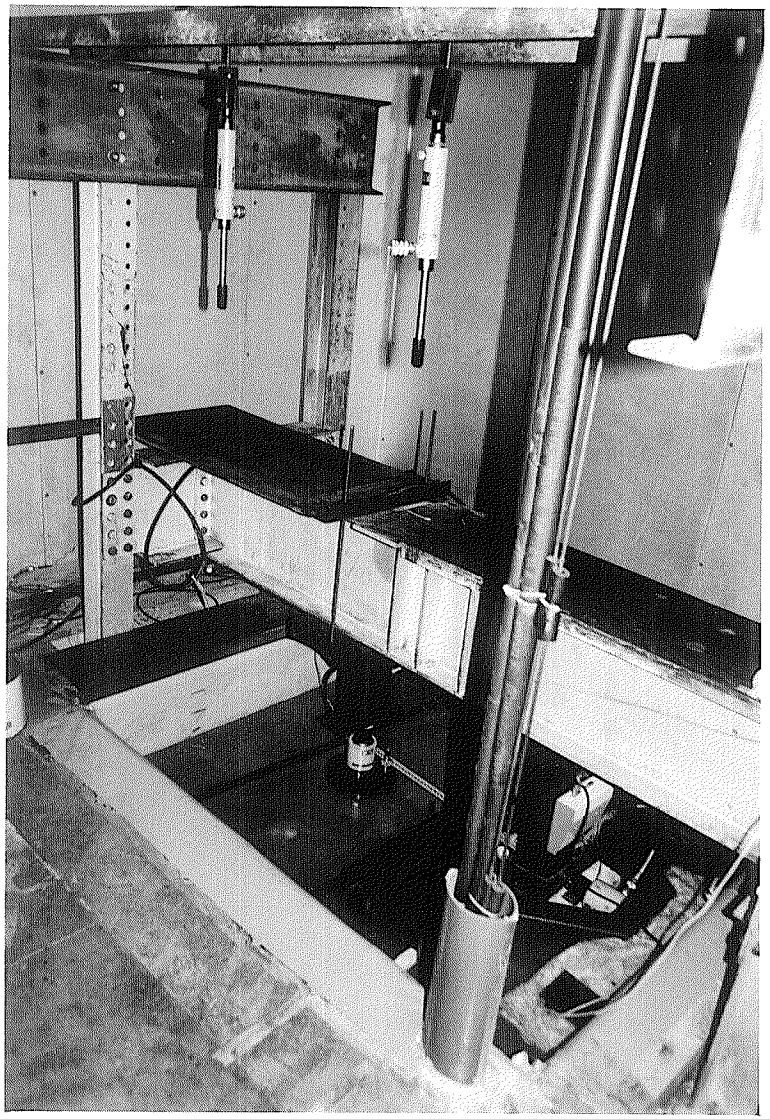

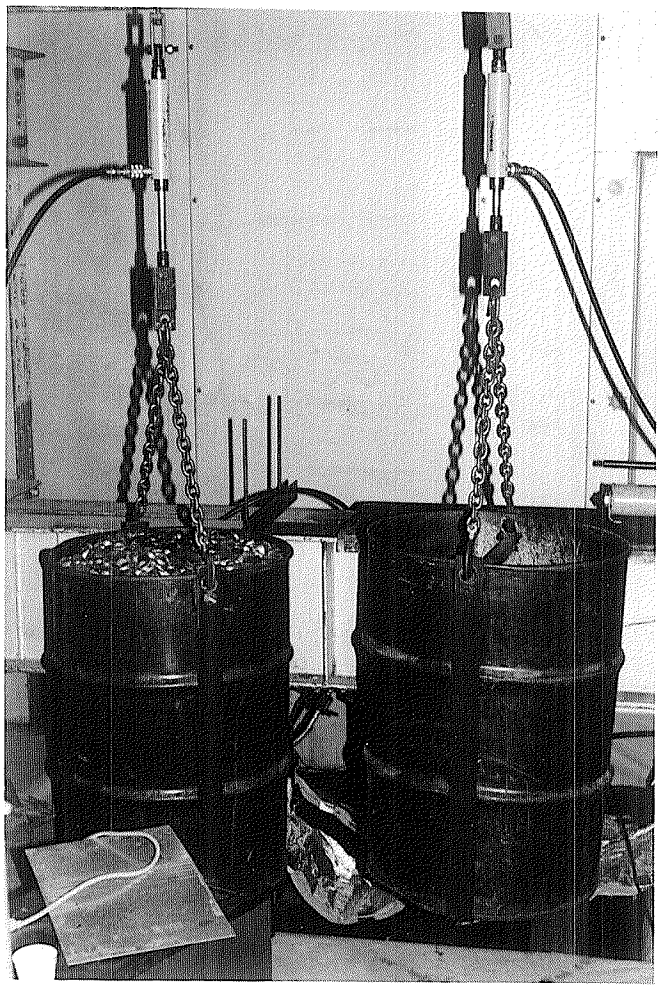

FIGURE 2.5 PLATE-LOAD TEST SET UP AND INSTRUMENTATION

x 82), approximately 2.6 m in length, which spanned the pit and were bolted to smaller beams (W460 x 74), about 1.0 m in length at their ends. These members were in turn fixed to four columns (W150 x 30) of 2.4 m height, anchored to the floor near the corners of the pit. Two channels (C380 x 50) of 2.5 m length were fixed close to the top of the columns. An identical section, 3.1 m in length, from which the loading apparatus was suspended, rested on these members and spanned across the pit along one side. In the following, the specific loading arrangement employed in this investigation is described.

A 35 kN double-acting hydraulic cylinder (RD-46) * was connected to a channel spanning the pit. A large oil drum was suspended from the cylinder plunger and steel punchings were placed within the barrel to provide dead-weight as required. High pressure hose was attached to the pull-action cylinder port.

In this loading arrangement, dead-weight was used to pull the plunger downward and thereby to create hydraulic pressure within the system. The high pressure hose was connected to a 450 kN capacity single-acting cylinder (RCL-502) mounted on the plate assemblage in the pit. Hydraulic pressure produced by the dead-weight loading pushed this second cylinder plunger upward against the reaction frame. Loads were transferred to the frame through a 200 kN capacity column-type compression load cell, and an arrangement of structural steel members comprising a 20 mm thick plate welded to a 150 mm square hollow structural section, 0.4 m in length, in turn welded to a channel section (C310 x 45) connected to the frame with a bracket.

The loading system hydraulic circuit also included manual shut-off valves (V-8) and needle valves (FFG 2003 T). This allowed for isolation of each system component to permit oil to be bled from the circuit and to provide for jacking-up

---

* ENERPAC product designation

of the hydraulic cylinder when it reached the end of its travel. This also permitted relatively rapid application of a loading increment and allowed for sustained loading in the case of a breakdown of a system component.

A microcomputer-based data aquisition system was used for continual monitoring and periodic recording of load, deflection and temperature measurements. The system comprised the following basic components: Fluke Helios I Computer Front End with option assemblies - Thermocouple/DC Volt Scanners (3), Isothermal Input Connectors (3), and a High Performance A/D Converter; RS-232-C direct connection with host computer; IBM-PC (compatible) system with hard drive and printer for data storage and hard-copy data output. The Front End executed commands received from the host computer, ran the measurement control hardware and sent appropriate responses back to the host. In this investigation, commands were issued through a computer program FLUKEH. BAS written in BASIC with optional programs for graphical output written in TURBO PASCAL. All connections between the Front End and the process to be monitored were made through option assemblies. The Thermocouple/DC Volt Scanner was a one micro volt, 20-channel thermocouple and multi-voltage range relay scanner. The Isothermal Input Connector routed a maximum of 20 thermocouple or voltage input channels to the scanner. The High Performance A/D Converter provided high accuracy analog to digital conversion of scanner input voltages (17 bit resolution).

Displacement transducer (LVDT) and load cell calibrations were performed at the beginning and checked at the end of the test program. Re-calibration of thermocouples following the completion of testing was not possible. All calibration procedures were carried out within the cold room at the test temperature.

2.3 TEST PROCEDURES

A multi-stage plate-loading test was performed. This test consisted of the application of a constant load to the plate arrangement and measurement of the displacement of the plate with time. The applied load was increased to a new level when the rate of plate displacement approached zero. Four step loadings were applied in this fashion, producing mean constant pressures at the base of the test plate of 0.880, 1.804, 2.675 and 3.438 MPa, which was the capacity of the loading system.

Some difficulty was encountered in maintaining the load constant due to friction in the hydraulic cylinder from which the dead-weight loading was suspended. Several techniques were tried to rectify this situation, including such means as wrapping the cylinder with heating coils and attaching mechanical vibrators to the cylinder. It was found that the most effective means of maintaining the load essentially constant was to periodically bleed off a small quantity of oil from the system so as to cause some displacement of the cylinder plunger and thereby reduce the static friction. This procedure was carried out on a daily basis throughout the duration of the test program, but met with only limited success. Complete alleviation of the problem in future investigations may require custom modification to specific system components, or a reassessment of methods used to develop hydraulic pressure within the system.

2.4 TEST RESULTS

2.4.1 Test Data - Summary

The plate pressures, plate displacement, and the temperature of the soil at the base of the plate are shown as a function of time in Figure 2.6, for the entire investigation. For clarity, individual plots of applied pressure, soil temperature, and plate displacement are displayed in Figures 2.7, 2.8, and 2.9, respectively. Plate displacement rates are also presented as a function of time

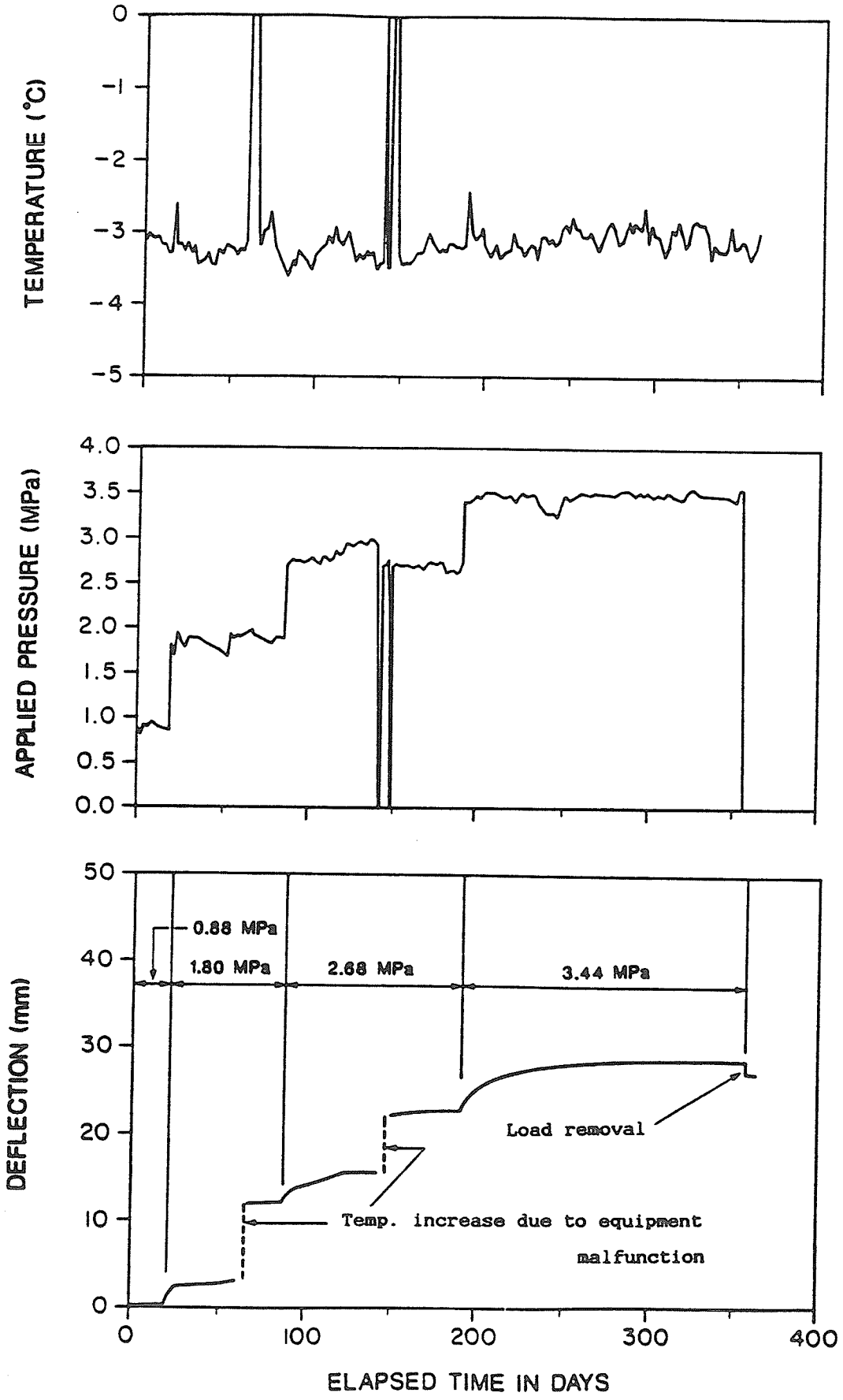

FIGURE 2.6 SOIL TEMPERATURE AT THE PLATE BASE, APPLIED BEARING PRESSURE, AND PLATE DISPLACEMENT VERSUS TIME

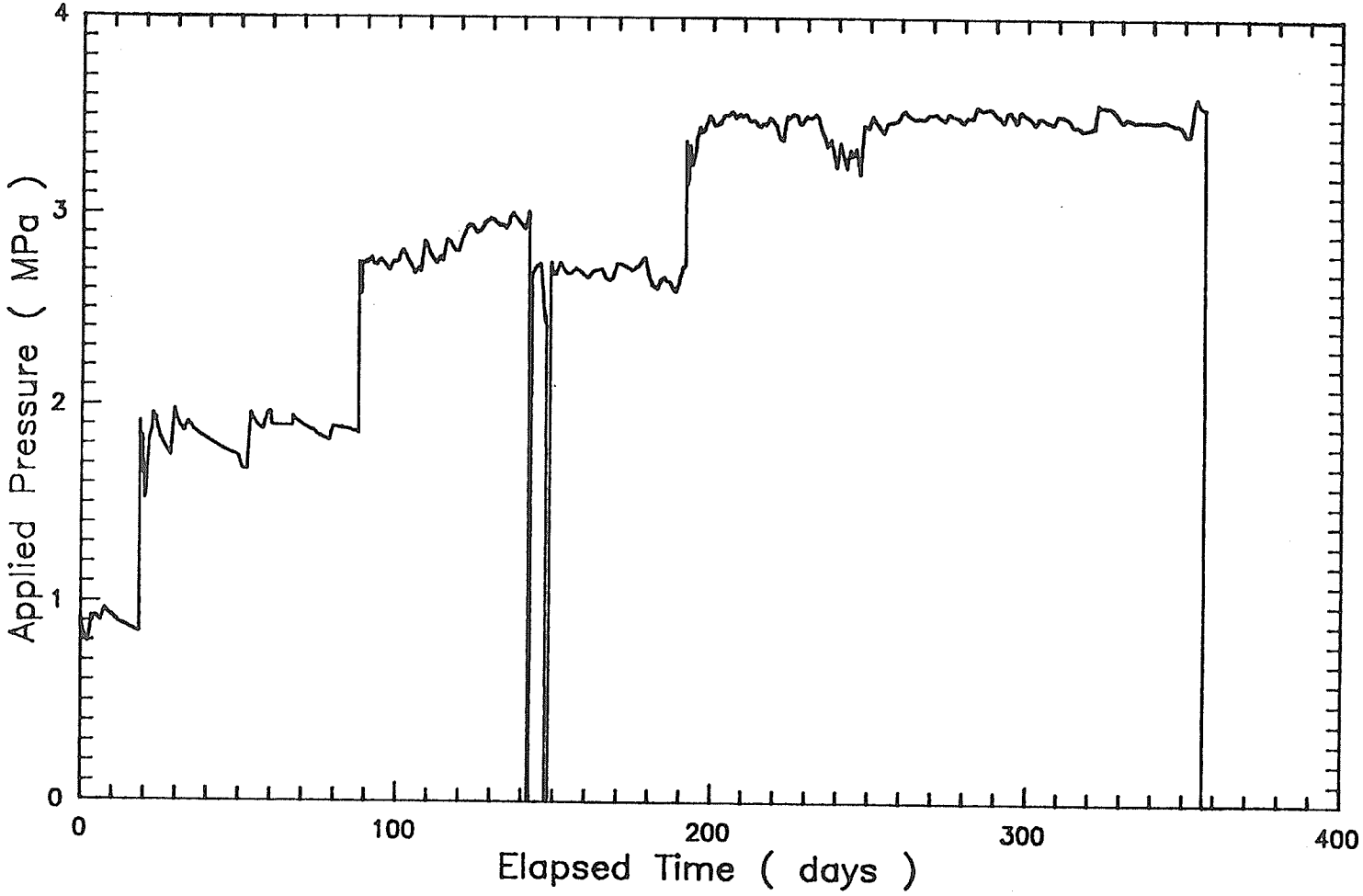

FIGURE 2.7 APPLIED BEARING PRESSURE VERSUS TIME

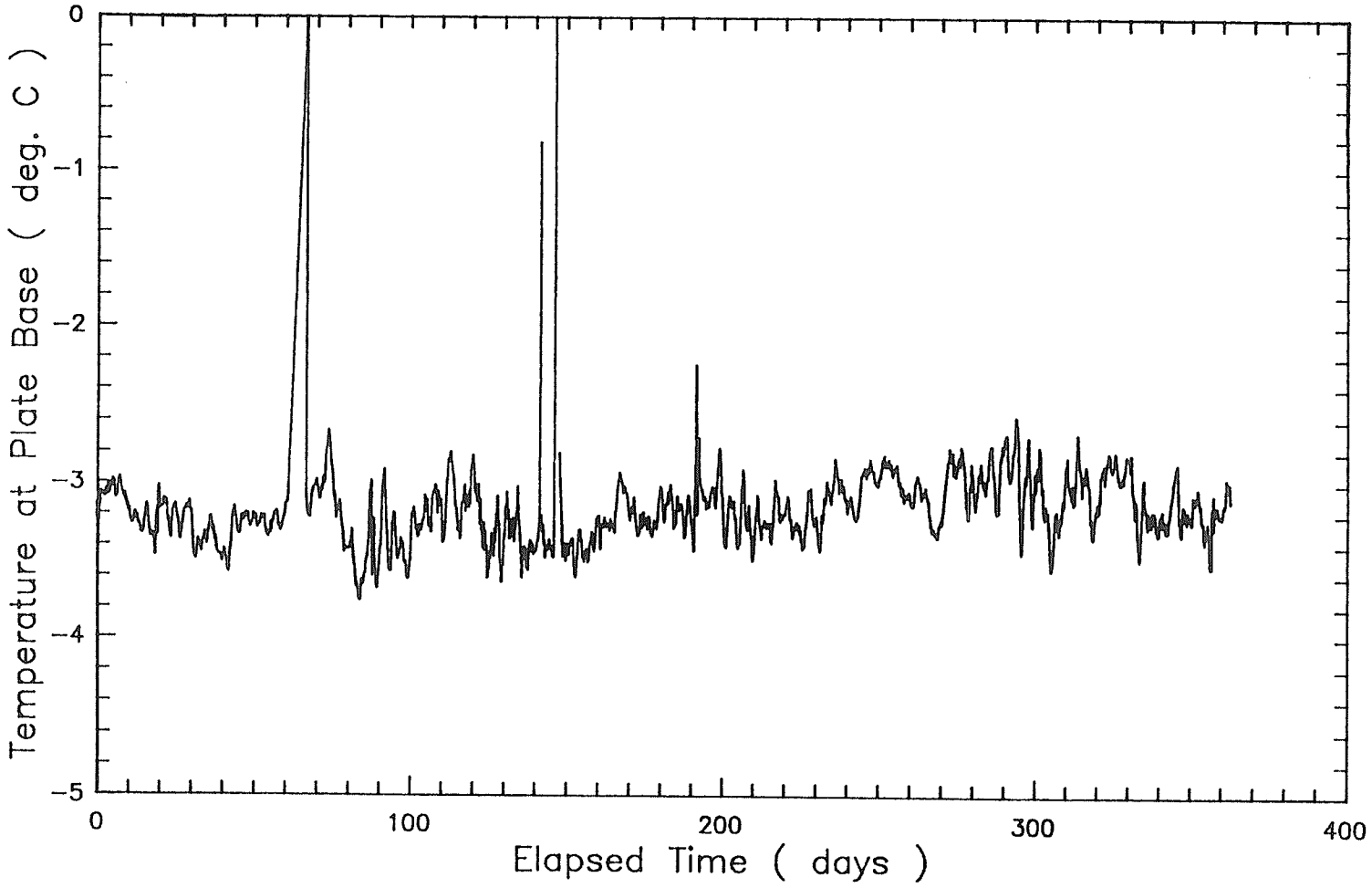

FIGURE 2.8 SOIL TEMPERATURE AT THE BASE OF THE PLATE VERSUS TIME

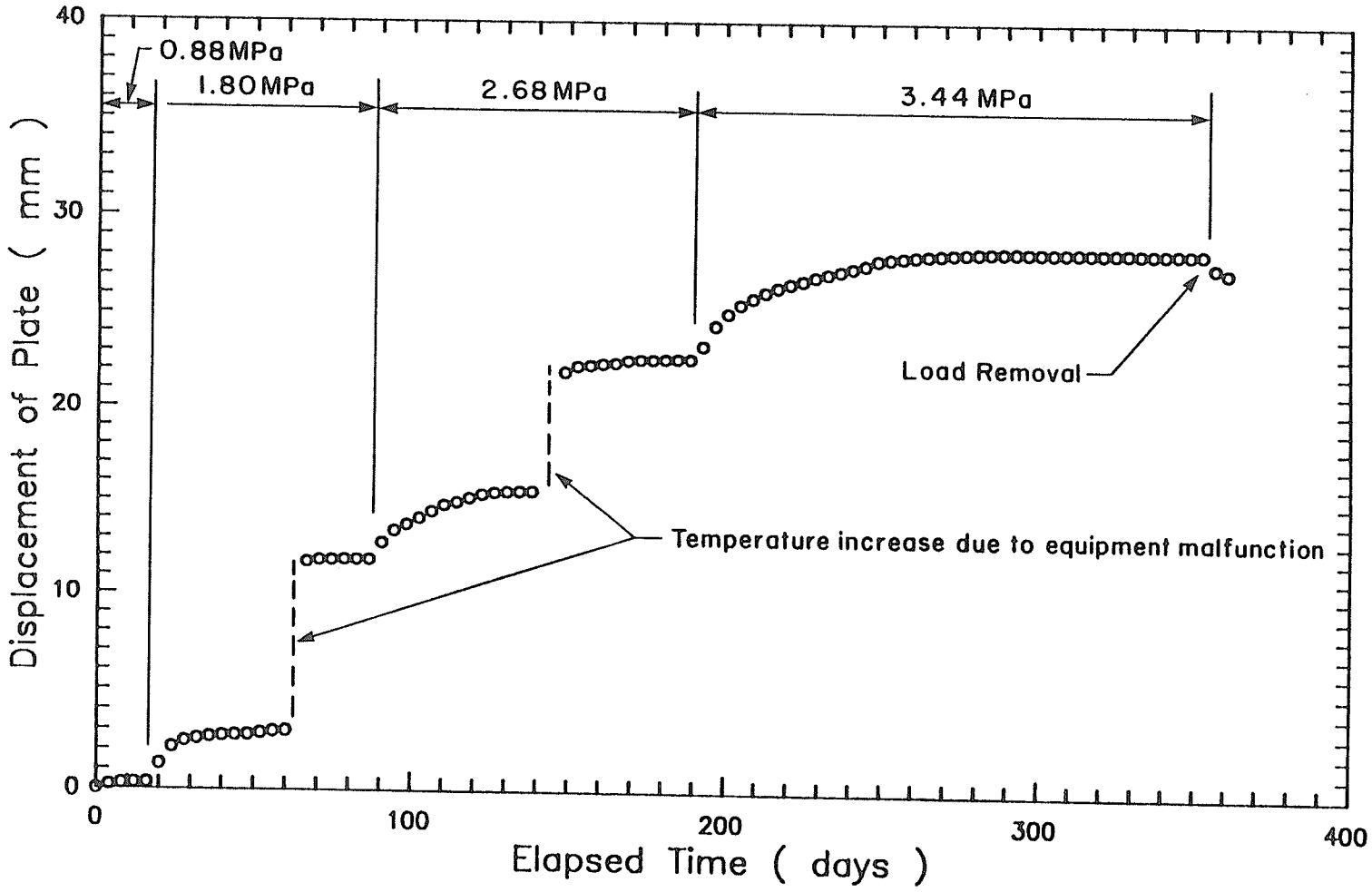

FIGURE 2.9 DISPLACEMENT OF PLATE VERSUS TIME

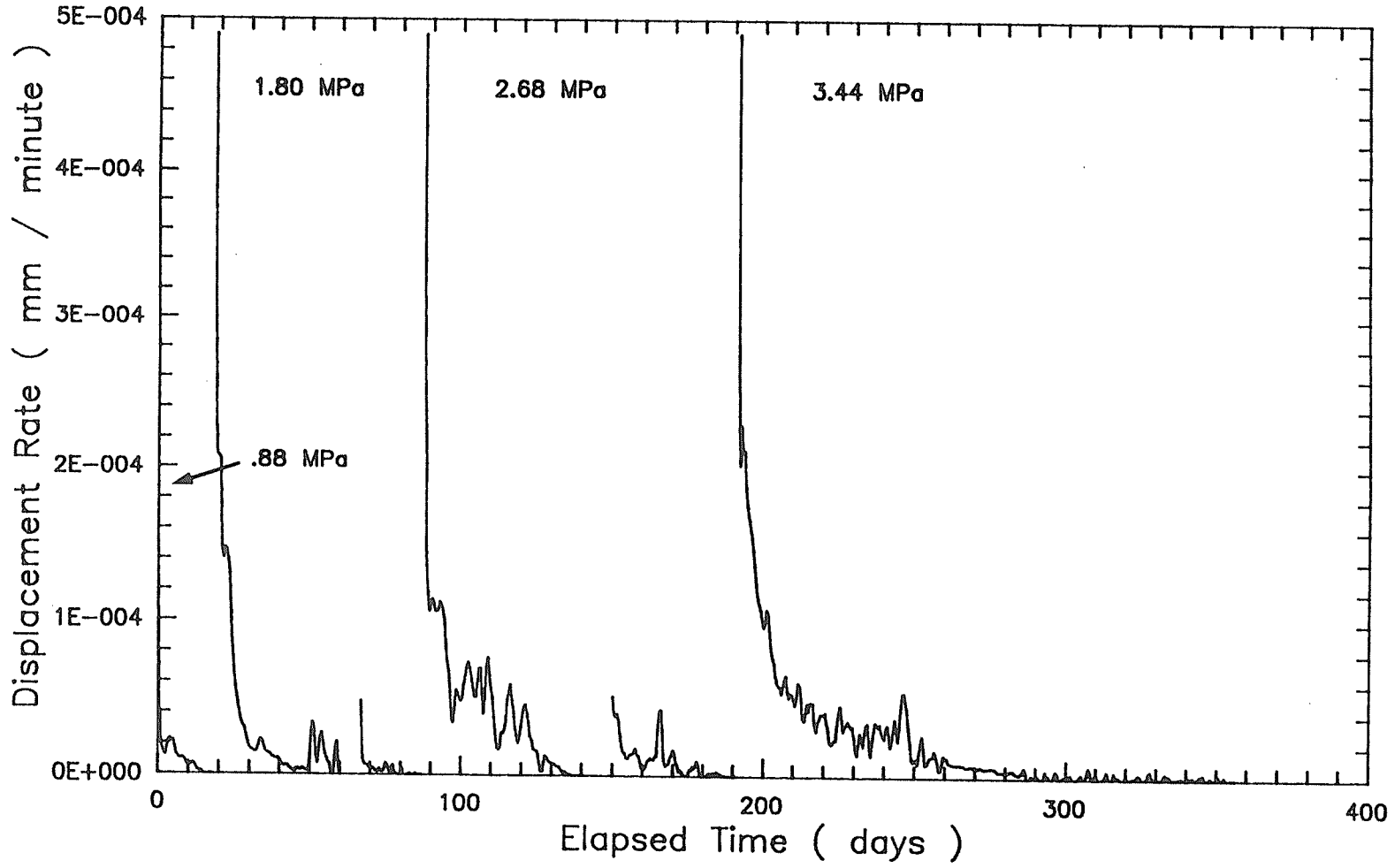

FIGURE 2.10 PLATE DISPLACEMENT RATE VERSUS TIME

in Figure 2.10.

A brief breakdown of the refrigeration system occurred during both the second and third loading stages. In each case, the air temperature in the cold room rose above freezing. There was an accompanying increase in soil temperatures, particularly near the surface. Unfortunately, in the first instance the data acquisition system also failed at the same time so that the temperature changes in the soil were not recorded. In the second instance which was of slightly longer duration, the load was removed and reapplied after the test temperature of the soil was restored. As expected, the increase in soil temperatures resulted in a sharp increase in plate displacement. However, in both instances after temperature test conditions were re-established, the plate continued to deflect at a rate which was essentially the same as the rate which preceded the breakdowns. In the analysis of the results, the displacements that occurred as the result of the breakdowns were omitted.

As previously indicated, the temperature distribution within the test pit was characterized by a slight vertical gradient. Temperatures at depths of 200, 400 and 600 mm below the surface of the frozen soil mass are shown as a function of time in Figure 2.11 for the entire investigation. Average values of the soil temperature measured over the duration of the test at 200, 400 and 600 mm depths were -3.32, -3.15, and -2.99°C, respectively.

The plate displacement attenuated under each load increment. For higher applied loads, longer time intervals were necessary to complete attenuation. The total test duration was approximately one year. The total displacement of the plate, discounting the displacement associated with a breakdown of the refrigeration system, was 12.3 mm. Removal of the load at the conclusion of the test resulted in a total rebound of 0.97 mm, including 0.13 mm of instantaneous rebound and 0.84 mm of time-dependent rebound.

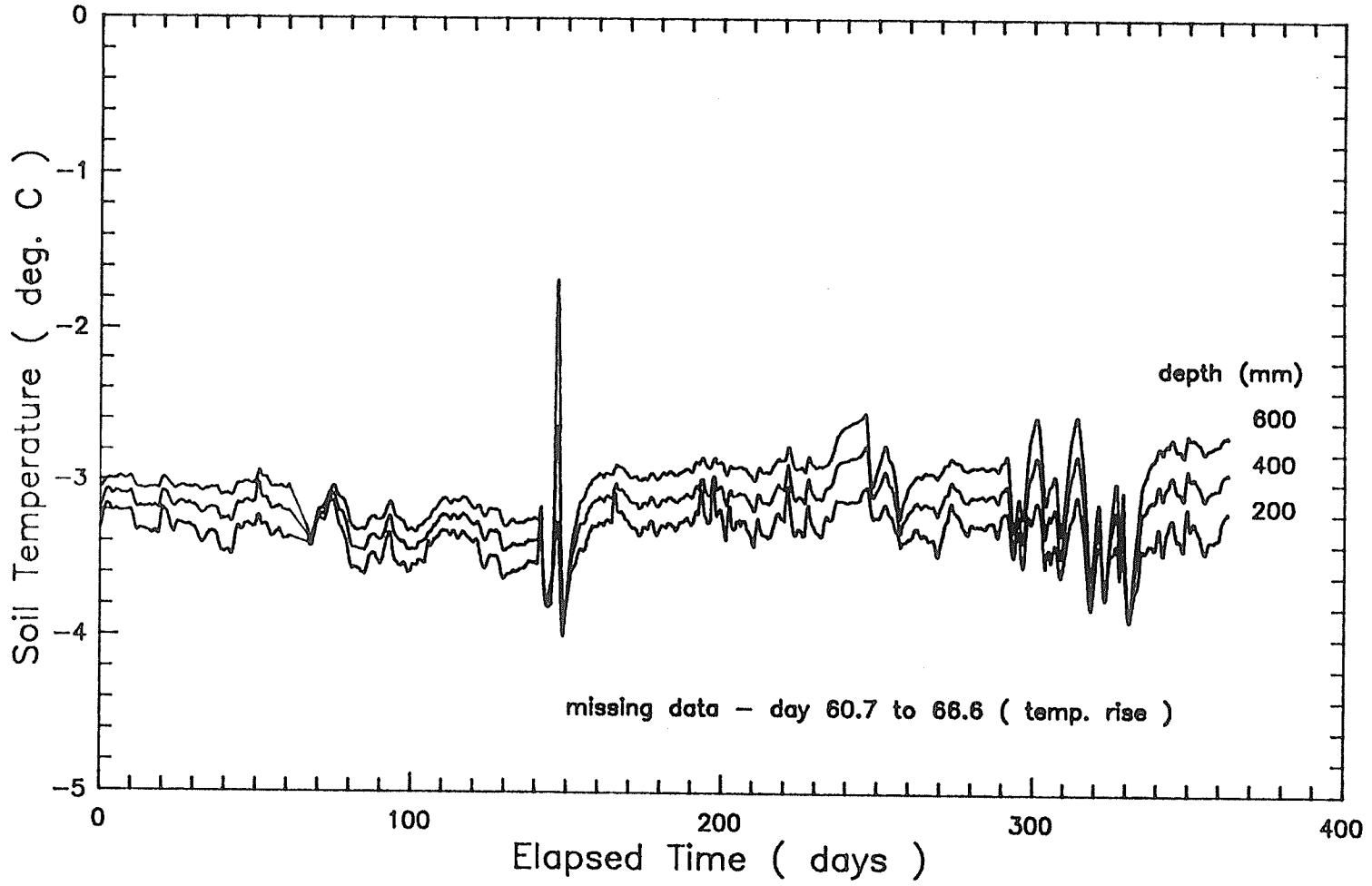

FIGURE 2.11 SOIL TEMPERATURES AT DIFFERENT DEPTHS VERSUS TIME

2.4.2 Test Data - Interpretation

Ideally, to examine both stress level and time effects on the creep behavior of frozen soil, separate plate-load tests should be performed at each stress level. However, this was considered to be impractical because of the high cost and time required to prepare each test. That is to say, the frozen soil in the test pit would have to be thawed, removed, replaced, and refrozen so that the soil conditions at the beginning of each test would be the same. Instead, it was decided to conduct a multi-stage test and to represent the resulting data as a series of equivalent single-stage test results in analyzing the dependence of creep on both stress and time.

A separate plate displacement-time curve was generated for each of the four plate loads by superposition (Figure 2.12). It was assumed that the total displacement under each new total load, at a given elapsed time, was equal to the sum of the displacements that had occurred under all loads, up to and including the load in question, within that same time interval. However, in general, the displacement resulting from an increment in stress in a multi-stage test is less than the displacement set-up by a constant stress of the same magnitude applied over the same period. Studies by Vyalov and Pekarskaya (1968) and Pekarskaya (1973) indicated that this is due to the strain-hardening of soil at a previous loading stage. Therefore, it can be expected that displacement-time relationships developed in the above-stated manner may lack coincidence with single-stage test results. However, performing separate single-stage tests is not always a practical alternative.

The hypothetical instantaneous deformation (measured at t = 1 minute) represented, on average, less than one percent of the total deformation under a given stress increment. Results, as considered subsequently and presented in Figure 2.12, depict only the time-dependent (creep) response.

The creep displacement-time curves are typical of hard-frozen soils

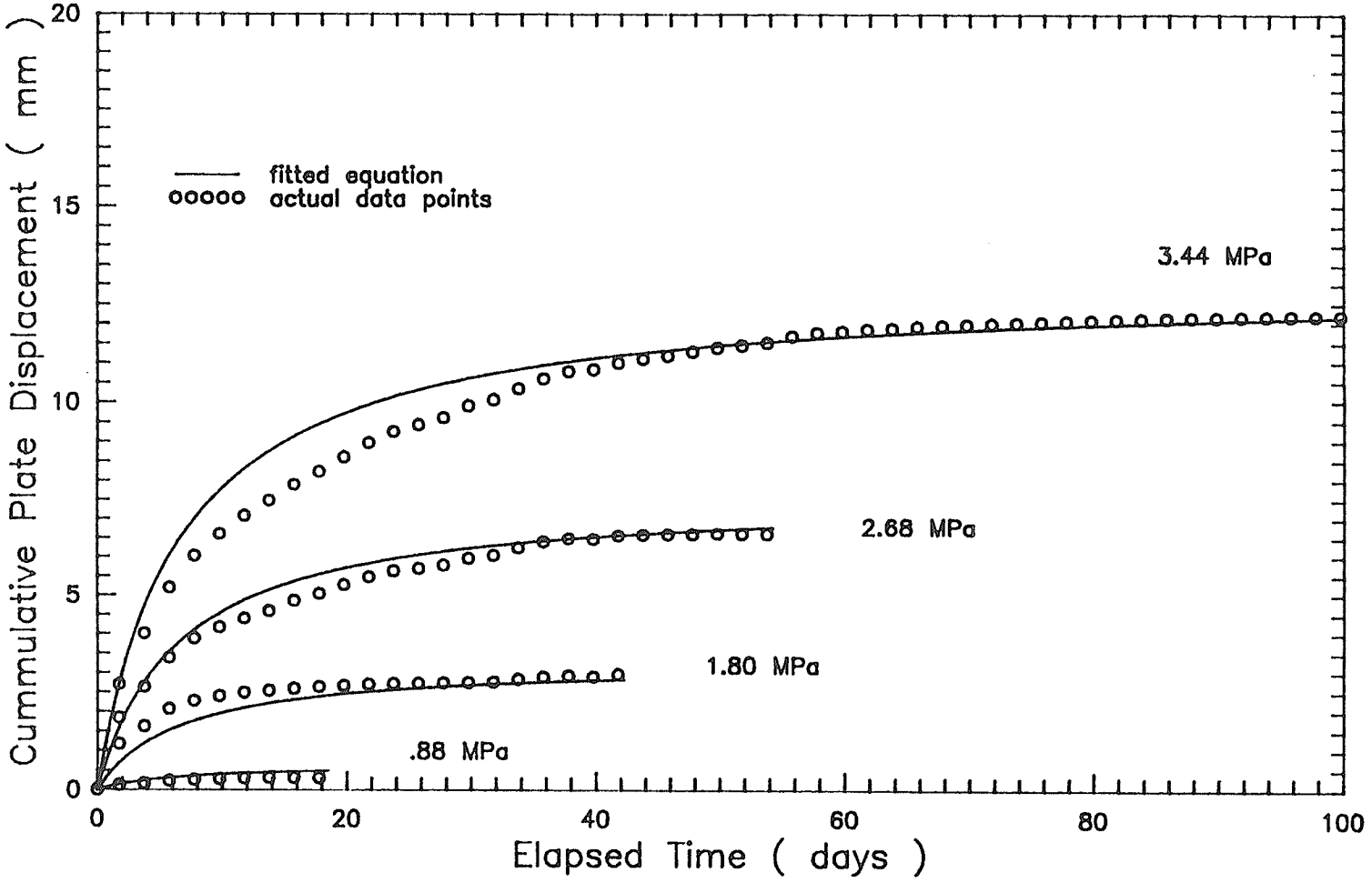

FIGURE 2.12 CUMMULATIVE PLATE DISPLACEMENT VERSUS TIME FOR EACH APPLIED PRESSURE

subjected to stresses below their long-term strength. The displacement attenuated under all of the applied pressures. Plate displacement rates, determined as slopes of the displacement-time curves, are shown plotted against time in Figure 2.13. The rates decreased with time, tending to zero as a limit. A range of time for which rates of deformation were approximately zero was selected for each pressure. These ranges are shown plotted against applied pressure in Figure 2.14. The time to complete attenuation increased approximately linearly with pressure.

The effects of stress and time on the creep deformation (at constant temperature) are commonly expressed by two mutually independent functions. Since the type of function is selected phenomenologically, several expressions have been suggested by different authors to describe the time dependence of the creep response. Some of the more common relations were employed in consideration of their relative effectiveness in representation of the experimental data. Test of fit was assessed by linear regression analysis. A linear-fractional representation (i.e. a hyperbolic type of dependence) of plate displacement on time was found to provide the most satisfactory representation of the experimental data. In addition, the nature of this mathematical form is consistent with the conditions of an attenuating creep (i.e. displacement rates tend to zero with time and the displacement itself tends to a certain finite value with time).

Isochrones representing the non-linear stress-displacement relation were examined in a similar manner. It should be recognized that each curve comprised only four data points, corresponding to respective applied pressure increments. The stress dependence of the creep displacement was best described by a power law. The experimental data was, therefore, most adequately expressed by a relation having the form:

$$y_{cr} = \sigma^{a} \cdot \{ bt / (c + t) \} \quad , \qquad (2.4)$$

in which y_{cr} is the creep displacement, and σ is the stress applied to the frozen

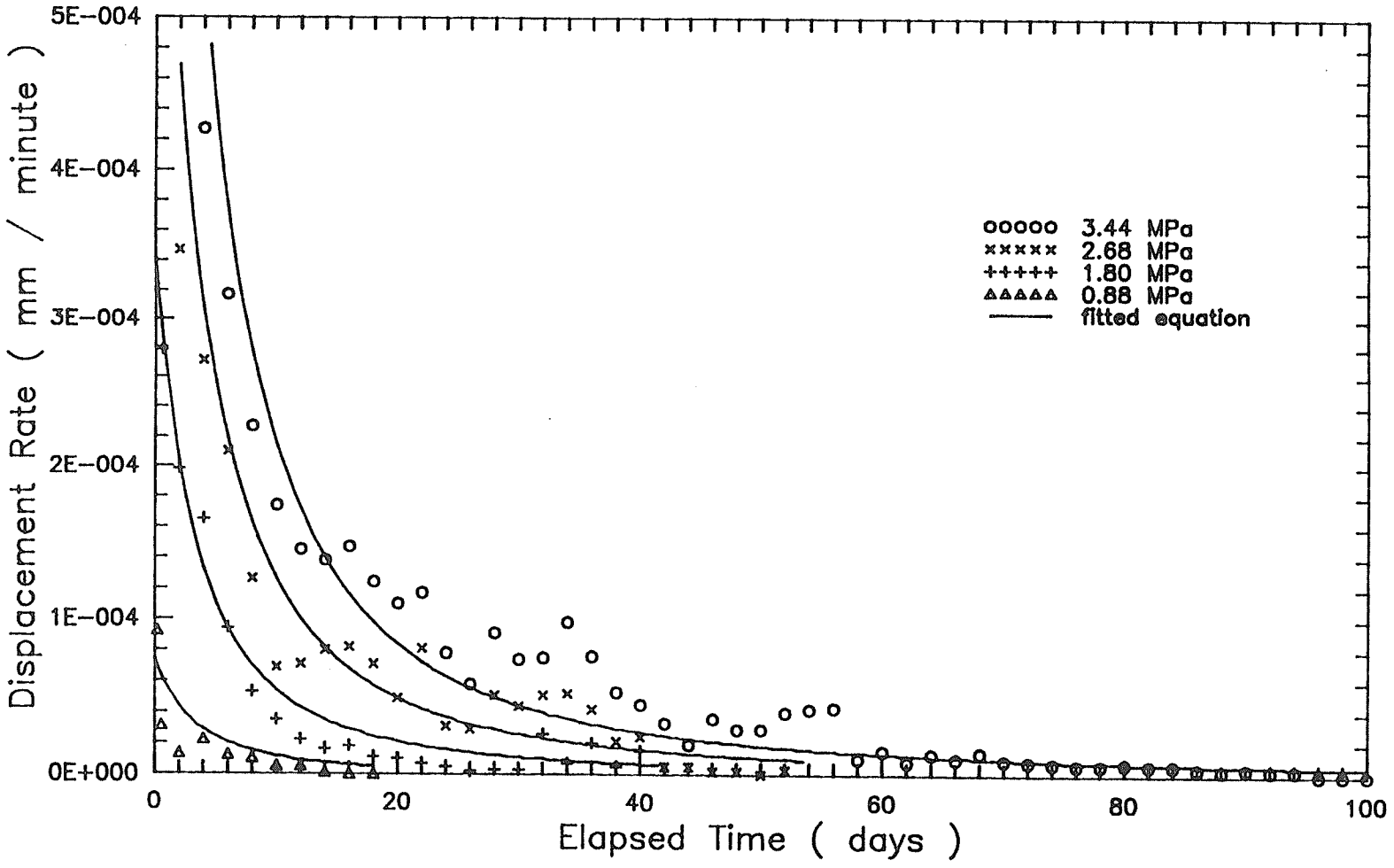

FIGURE 2.13 PLATE DISPLACEMENT RATE VERSUS TIME FOR EACH APPLIED PRESSURE

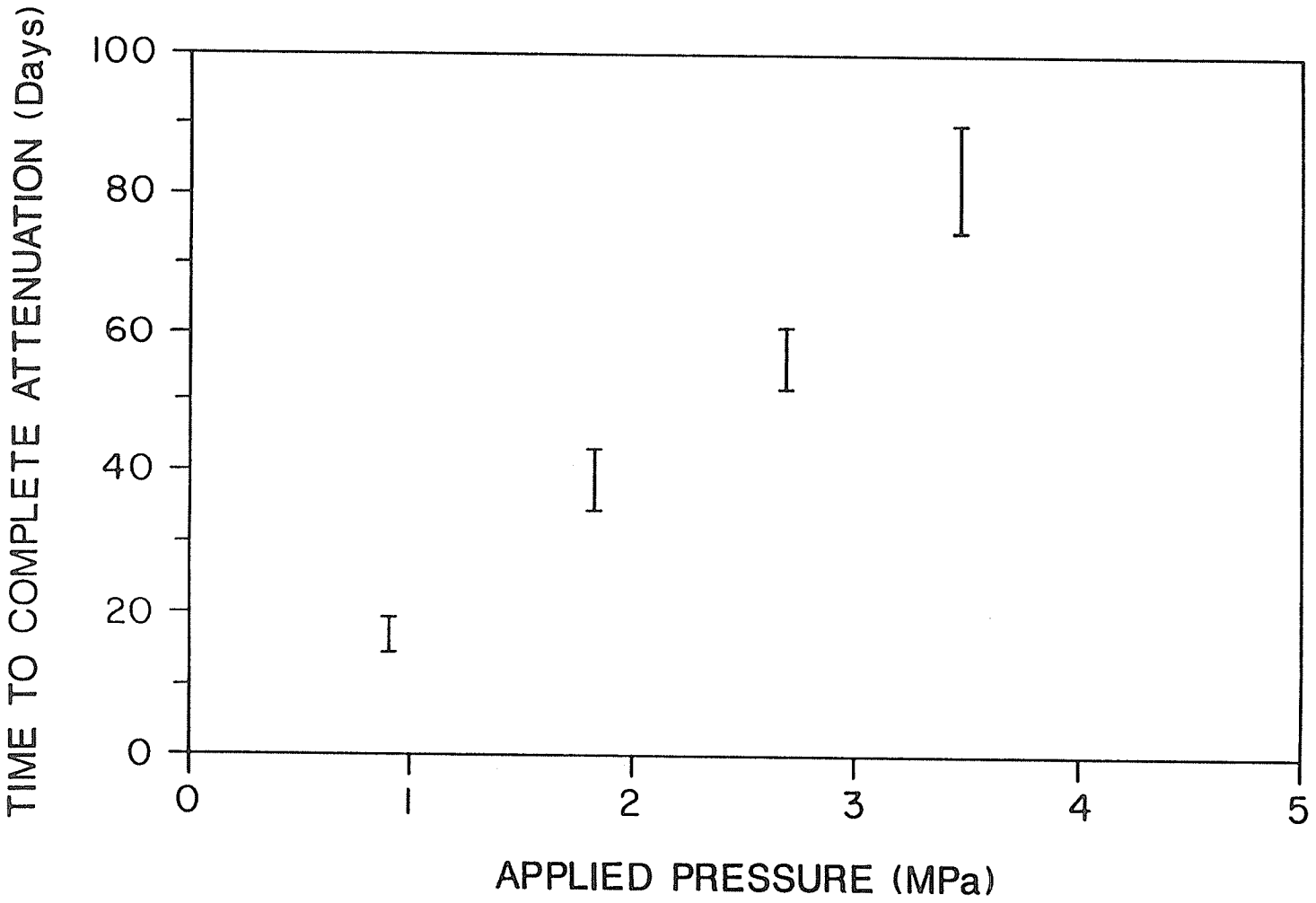

FIGURE 2.14 TIME TO COMPLETE ATTENUATION VERSUS APPLIED PRESSURE

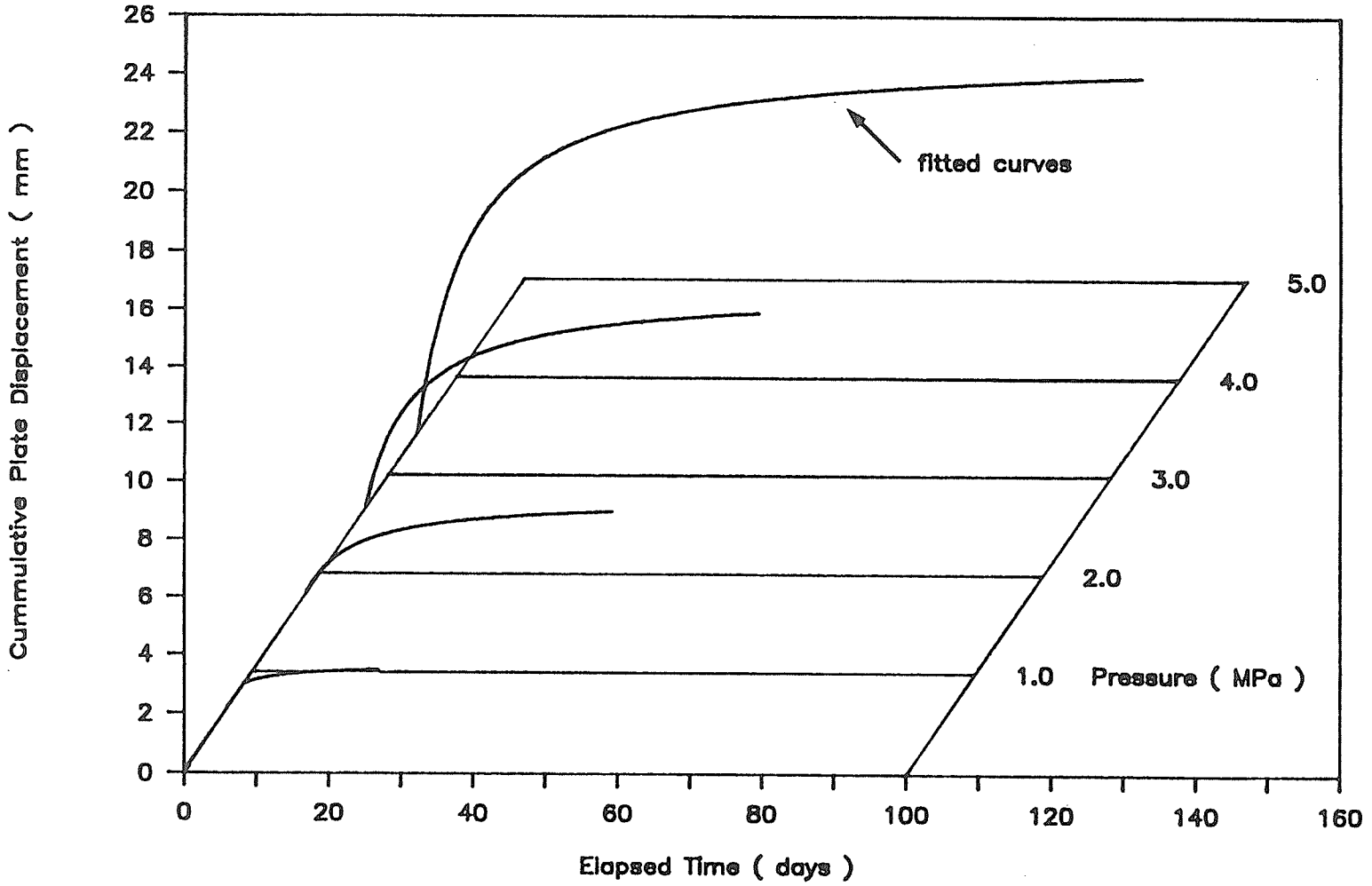

FIGURE 2.15 CUMMULATIVE PLATE DISPLACEMENT VERSUS TIME AND APPLIED PRESSURE

soil by the plate. The three parameters of equation (2.4) as determined for this investigation (for units of displacement in mm, stress in MPa, and time in minutes) are:

$$a = 2.13$$

$$b = 0.935 \text{ MPa}^{-2.13} \cdot \text{mm}$$

and $$c = 9542 \text{ min.}$$

Statistical indices which describe the quality of fit achieved using the above-stated values of the parameters are presented in Table 2.3. Curves described by equation 2.4 are shown in Figure 2.12 along with the actual data points. The development of the creep response in stress-displacement-time space as expressed by equation 2.4 is also shown in Figure 2.15. Equation 2.4 provides good representation of the experimental data for the three highest applied pressures. However, for the lowest applied pressure (0.88 MPa), the equation overestimates the creep displacement. The results should be considered to be applicable only within the range of stresses investigated.

The creep rates, $\dot{y}_{cr}$, shown in Figure 2.13, may be expressed as:

$$\dot{y}_{cr} = \sigma^{a} \cdot \{cb / (c + t)^{2}\} , \qquad (2.5)$$

in accordance with equation 2.4. Curves described by equation 2.5 are also shown in Figure 2.13 along with the actual data points.

The creep data presented in Figure 2.12 was used in the examination of creep effects on the modulus of subgrade reaction of the frozen sand. A plot of the modulus of subgrade reaction versus time is given in Figure 2.16. According to the plot, for a given time, the modulus decreased with an increase in pressure, and for a given pressure, the modulus decreased with time. The modulus decreased very rapidly initially and then tended toward a constant lower-bound value with time. The substantial variation in the modulus with time and pressure is further illustrated in Figure 2.17 where values are shown plotted against pressure for

an elapsed time of one hour and for complete attenuation. The short term (one hour) values decreased from about 24.4 GN/m^3 at a pressure of 0.88 MPa to approximately 6.0 GN/m^3 at a pressure of 3.4 MPa, illustrating the dependence of the modulus on pressure.

The effect of time was also very significant, particularly at low pressures. For example, at a pressure of 0.88 MPa, the modulus corresponding to one hour of elapsed time was 24.4 GN/m^3 and decreased to a lower limiting value of approximately 2.7 GN/m^3 as the result of creep. The difference between short-term and attenuated values of the modulus decreased with an increase in pressure.

TABLE 2.3 PRECISION INDICES (COEFFICIENT OF DETERMINATION, r^2 AND COEFFICIENT OF VARIATION, v) OF THE APPROXIMATION (2.4) (BASED ON DATA POINTS AT SIX HOUR INTERVALS)

Applied Pressure (MPa) (Average)	Indices of Precision	
	v(%)	r^2
0.880	1.10	0.70
1.804	0.25	0.965
2.675	0.08	0.990
3.438	0.05	0.995

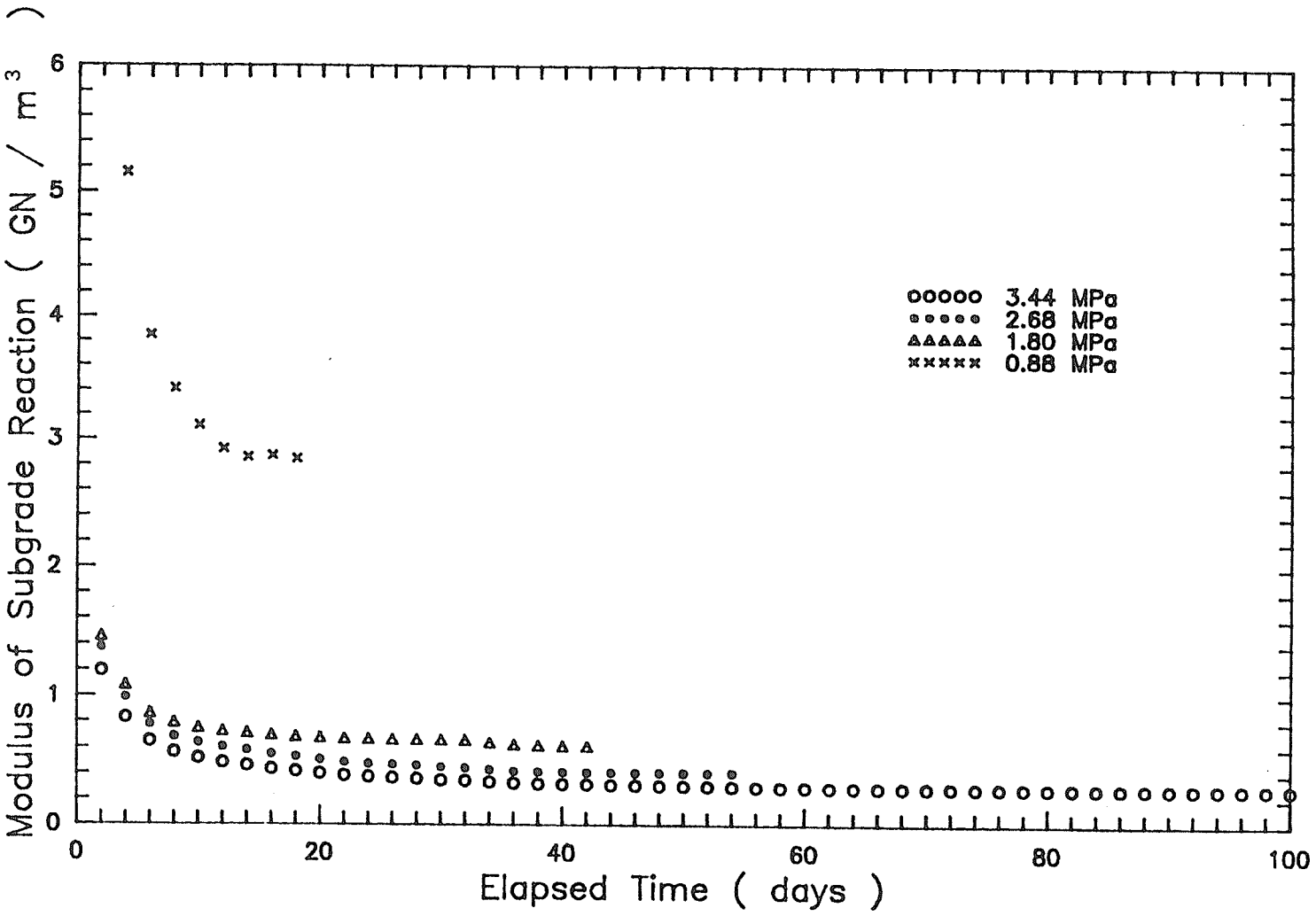

FIGURE 2.16 MODULUS OF SUBGRADE REACTION VERSUS TIME FOR EACH APPLIED PRESSURE

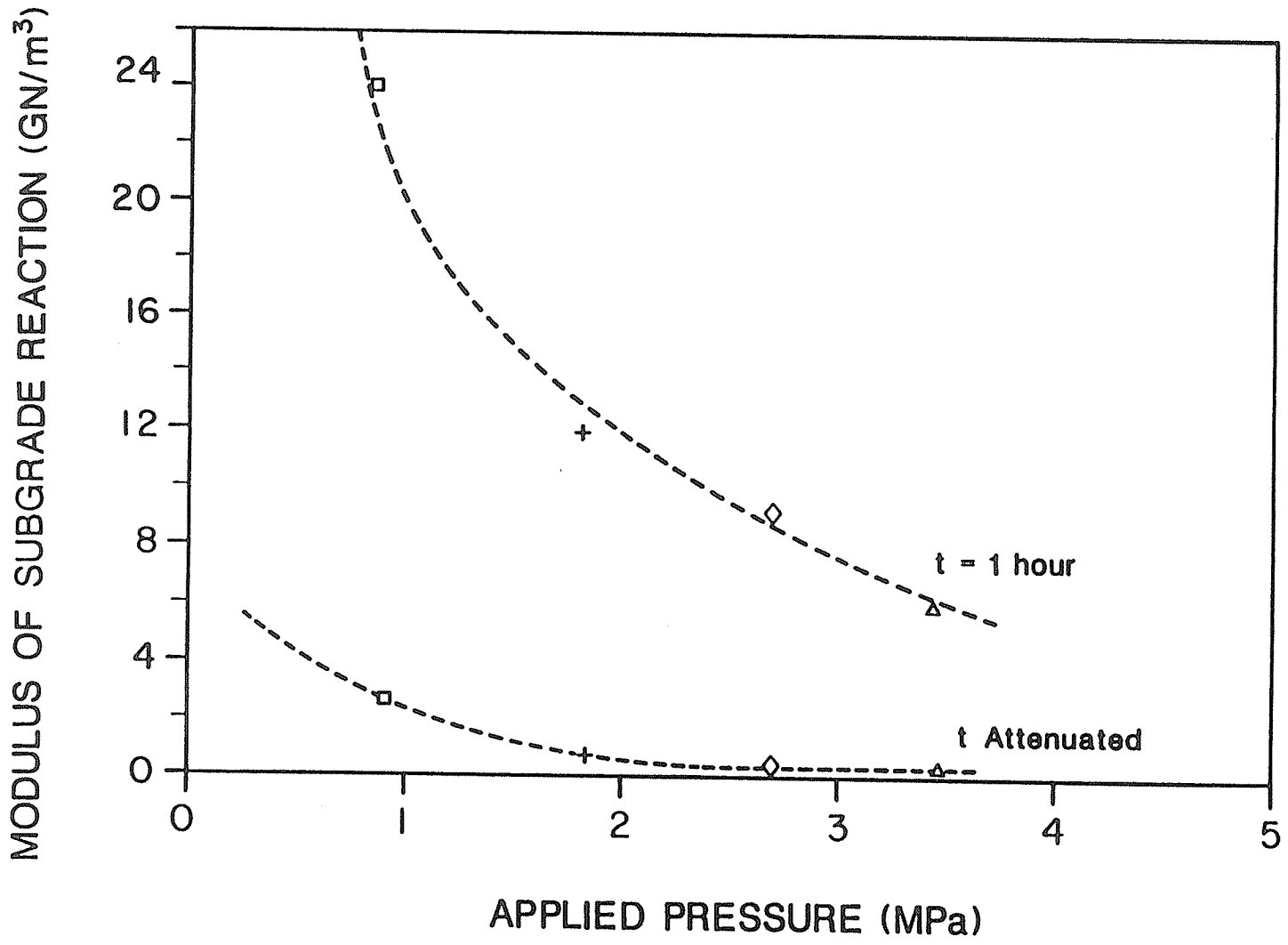

FIGURE 2.17 MODULUS OF SUBGRADE REACTION VERSUS APPLIED PRESSURE FOR ONE HOUR AND ATTENUATED TIMES

CHAPTER 3

PRESSUREMETER CREEP TESTING: EXPERIMENTAL PROGRAM

3.1 INTRODUCTION - REVIEW OF PUBLISHED EXPERIMENTAL DATA

The pressuremeter, introduced initially to the field of frozen soil mechanics in the early 1970's (Ladanyi and Johnston, 1973) (Zaretskiy and Fish, 1973), has since been used with reasonable success in several investigations of both frozen soil and ice. Most of these studies were designed to improve the understanding of the pressuremeter testing method as a tool for the evaluation of rheological properties of frozen materials in-situ. In addition, in recent investigations, pressuremeter tests were carried out in confined thick cylinders of both frozen soil and ice under controlled laboratory conditions. The following is a review of published creep data from pressuremeter testing programs conducted to date.

Ladanyi and Johnston (1973) carried out a field testing program at a permafrost site in Thompson, Manitoba. Tests were conducted using a Ménard pressuremeter (type G) in a warm (-0.1 to -0.3°C), ice-rich, frozen varved clay. Both single and multi-stage (15 minute increment) tests were performed. The primary creep response was described by a power law, having the form:

$$\varepsilon^{(c)} = K \sigma^{a} t^{b} \quad , \quad (b < 1) \quad , \tag{3.1}$$

in which $\varepsilon^{(c)}$ is the creep strain; t is the time; and K, a, and b are temperature-dependent material constants. According to Ladanyi and Johnston, the creep data obtained in a pressuremeter test can be generalized using the solution to the problem of stationary creep of a cylindrical cavity of infinite length, under internal pressure, located in an infinite medium. In order to process the pressuremeter creep data, the only relationship required from the solution relates the creep cavity-expansion rate with the applied internal pressure. The

authors present a procedure, based on this relationship, for the evaluation of the creep modulus σ_c (corresponding to the strain rate $\dot{\varepsilon}_c$) and the two creep exponents b and a. These parameters may then be substituted into an equation of the form:

$$\varepsilon_e^{(c)} = (\dot{\varepsilon}_c / b)^b (\sigma_e / \sigma_c)^a t^b \quad , \tag{3.2}$$

where the subscript e denotes the von Mises equivalent stress and strain. Equation 3.2 then provides a general creep relationship. To apply the procedure, two conditions are necessary: (1) creep curves should linearize in a log-log plot; and (2) creep curves for different pressures should be parallel to each other. Values of the creep parameters b, a and σ_c as deduced from six tests (applied cavity pressures between 0.6 and 1.7 MPa) were given as: 0.4 to 0.67; 0.8 to 2.7; and 0.45 to 2.4 MPa (for $\dot{\varepsilon}_c = 10^{-5}$ min^{-1}), respectively. However, Ladanyi and Johnston indicated that the creep curves presented in a logarithmic plot were distinctly nonlinear. Moreover, such 'creep lines' for different applied pressures were frequently not parallel. Single-stage test results linearized better than multi-stage tests results and in both cases the 'creep lines' for different applied pressures showed a tendency to become parallel after 15 minutes.

Zaretskiy and Fish (1973) conducted creep tests in glacier ice using a D-76 pressuremeter designed by the Scientific Research Institute of Foundations and Underground Structures (NIIOSP) of the Soviet Union. Both single- and multi-stage tests were performed. The former were carried out at pressures of 0.3, 1.2, 1.5, and 1.8 MPa, in separate boreholes. Parameters as evaluated from the single-stage tests were substituted into a generalized relation based on the ageing theory of creep, written as follows:

$$\varepsilon_e^{(c)} = \frac{B \sigma_e^a t^\lambda}{T - (\sigma_e - \sigma_{e(\infty)})^a t^\lambda \eta} \quad , \tag{3.3}$$

in which: a, λ, B and T are parameters; $\sigma_{e(\infty)}$ is the limiting stress (shear

strength); and η is a function, equal to zero when $\sigma_e \leq \sigma_{e(\infty)}$ and to unity otherwise. Creep parameters, derived from the single-stage test data, were reported as: $a = 1.4$; $\lambda = 0.47$; and $B/T = 7.9 \times 10^{-5}$ MPa$^{-1.4}$ min$^{-0.47}$. According to Zaretskiy and Fish, the analysis was also extended to consider multi-stage tests. In addition, the researchers indicated that the creep parameters for ice, determined by pressuremeter tests, agreed closely with values obtained from laboratory uniaxial creep tests.

Rowely et al. (1975) presented the results of pressuremeter creep tests carried out in conjunction with a lateral load pile test program at Inuvik, N.W.T. Pressuremeter creep tests were performed with a Ménard Pressuremeter. The soil was an ice-rich clayey silt permafrost. The average temperature of the soil was -1.6°C. Altogether, four tests were conducted, including three multi-stage tests (15 minutes per stage) and one single-stage test of 10-hour duration. The basic creep parameters b, a, and σ_c of equation 3.2 were determined from the test data, following the procedure suggested by Ladanyi and Johnston (1973). The range of each parameter was as follows: $b = 0.85$ to 0.87; $a = 3.00$ to 3.89; and $\sigma_c = 0.30$ to 0.32 MPa (for $\dot{\varepsilon}_c = 10^{-5}$ min^{-1}).

Ladanyi and Saint-Pierre (1978) carried out a series of pressuremeter creep tests using a Ménard pressuremeter (type G) within a seasonal Arctic sea ice cover at Igloolik, N.W.T. The ice temperature at the level of most of the tests (i.e. at about 50 cm below the ice surface) was about -4°C. Crystallographic analysis of thin sections of ice indicated that the ice was columnar-grained of S2 type. In total, 10 creep tests were performed, of which 6 were multi-stage tests and 4 were relatively long-term single-stage tests. In test No. 13, the length of each stage was 30 minutes, while a 15-minute per stage procedure was used for all other multi-stage tests. Single-stage test durations ranged from 75 minutes up to a maximum of 720 minutes. General test information and creep parameters b, a, and σ_c are shown in Table 3.1. The time exponent b showed an increase

with increasing pressure from about 0.22 to 1.00, the latter value corresponding to steady state creep. There was also a tendency for b to decrease with time. In the evaluation of parameters a and σ_c, an average value of b (valid for 15 minutes and a high stress range) was adopted for each test. These average b values were found to remain approximately within the range of 0.6 to 1.0, with an overall average value of 0.822. There was much less variation in the value of the stress exponent a which remained close to a value of 2.1. However, according to the authors, because of the variation of b with time and stress level, the value of a was also influenced by the two conditions, and may be expected to increase up to 3 or more for longer times and higher stress levels.

TABLE 3.1 LADANYI AND SAINT PIERRE (1978) - RESULTS OF PRESSUREMETER CREEP TEST PROGRAM AT IGLOOLIK, N.W.T. ($\dot{\varepsilon}_c = 10^{-5}$ min^{-1})

Test No.	Applied Pressure (MPa)	Maximum Time per Stage (Min)	b (Average at 15 Min)	a	σ_c (MPa)
3	3.443	15	0.941	-	-
4	0.996-2.989	15	0.933	1.540	0.104
5	3.475	15	1.000	-	-
6	0.995-2.987	15	0.713	4.010	0.494
7	1.494	720	0.620	-	-
8	1.951	75	0.769	-	-
12	1.193-2.388	15	0.745	2.175	0.436
13	0.933-2.188	30	0.706	2.048	0.634
14	0.933-2.388	15	0.805	2.054	0.321
17	0.994-2.189	15	0.882	2.145	0.184
18	1.993	120	0.828	-	-
20	1.595	300	0.740	-	-
22	2.479	20	1.000	-	-

Ladanyi (1982) presented the results of a field study carried out for the National Research Council of Canada at a permafrost site near Inuvik, N.W.T. Tests were conducted with conventional Ménard pressuremeter equipment within ice-saturated clayey silt soils having ice contents of between 50 and 100 percent by weight. The soil temperatures ranged from -1.50 to -2.40°C. A total of four multi-stage tests, three with 15-minute increments and one with 60-minute increments, and seven relatively long-term single-stage pressuremeter creep tests were performed at the site. Test results, given as creep parameters b, a and σ_c of the general expression 3.2, are presented in Table 3.2. According to Ladanyi, two inconsistencies with theory were encountered in processing of the multi-stage test data. Firstly, as was noted by Ladanyi and Johnston (1973), creep curves plotted in logarithmic coordinates did not properly linearize. Rather, in most cases, the slope increased initially, then remained constant over an interval, and finally decreased slightly, especially at low pressures. Secondly, the value of the exponent b showed a definite tendency to increase with pressure. In the evaluation of parameters a and σ_c, an average value of b was adopted. In the solution of practical problems, the use of separate average values for the three creep parameters for low, middle, and high stress ranges, respectively, was suggested. In contrast with multi-stage results, the 'creep lines' developed from single-stage tests had a constant slope after about 15 minutes.

Ladanyi and Eckardt (1983) carried out a series of pressuremeter creep tests under controlled laboratory conditions, at -2.5°C, in confined, large diameter cylinders of frozen sand. The tests were performed with a Ménard pressuremeter (type GC). The cylindrical samples of frozen sand were 500 mm in diameter and 455 mm long. Lateral confinement of a sample was supplied by air-filled rubber cushions placed between the sample and the rigid steel tank wall. Eight multi-stage tests (30 minutes per stage) and seven relatively long-term (maximum 10 days) single-stage tests were conducted. The tests were performed at confining

TABLE 3.2 LADANYI (1982) - RESULTS OF PRESSUREMETER CREEP TEST PROGRAM AT INUVIK, N.W.T. ($\dot{\varepsilon}_c = 10^{-5}$ min^{-1})

Depth (m)	Soil Temp. (°C)	Applied Pressure (MPa)	Max. Time per Stage (Min)	b	b (Average)	a	σ_c (MPa)
2.18	-2.25	0.58	900	0.200	-	-	-
2.26	-2.40	2.48	240	0.549	-	-	-
2.10	-2.20	1.98	150	0.564	-	-	-
1.78	-1.90	1.48	1310	0.434	-	-	-
2.50	-2.50	0.98	1320	0.486	-	-	--
1.98	-2.05	0.75-2.35	15	0.523-1.00	0.746	2.430	0.551
2.02	-2.10	0.95-2.95	15	0.609-0.967	0.786	2.655	0.431
1.78	-1.85	0.95-2.45	60	0.568-0.895	0.688	2.370	0.734
1.90	-2.00	0.95	1590	. 0.377	-	-	-
1.90	-2.00	1.95-2.45	60-75	0.591-0.729	-	-	-
2.10	-2.20	0.95-2.85	15	0.383-0.846	0.780	2.837	0.446

pressures of 0.1, 0.2, and 0.3 MPa. Creep parameter determination from test data followed the procedures of Ladanyi and Johnston (1973), but with modification to account for differences between field and laboratory testing. Parameters b, a, and σ_c were evaluated from multi-stage tests for pressures exceeding 2 MPa. The average values and their ranges were b = 0.80 (0.72 to 0.84), a = 2.40 (1.80 to 3.60), and σ_c = 1.23 MPa (0.82 to 2.00) at $\dot{\varepsilon}_c = 10^{-5}$ min^{-1}. It was suggested that pseudo-instantaneous (1 minute) strains be subtracted from the measured values prior to any interpretation of the test data. According to Ladanyi and Eckardt, two distinct regions of creep behavior were then clearly apparent: one at low stresses, in which b increased noticeably with stress, and another at high stresses, where b remained practically constant. The variation of exponent b with pressure was further evidenced in long-term single-stage test results. The authors indicated that the pressure-dependence of b could be described on average by $b = 0.45\ p^{0.5}$, with an upper bound of $b = 0.52\ p^{0.4}$ and a lower bound of $b = 0.38\ p^{0.6}$, valid for stresses between 0.8 and 5.0 MPa.

Shields et al. (1985) and Fensury (1986) described the results of a laboratory test program designed to assess the reliability of the use of short-term multi-stage

pressuremeter creep tests to predict relatively long-term creep behavior. Tests were performed using an Oyo Elastmeter 100 pressuremeter, in thick cylinders of frozen sand, within a thin-walled steel tank. The temperature of the sand was -3°C. Two multi-stage (45 minutes per stage) pressuremeter creep tests were conducted. Basic creep parameters b, a, and σ_c were evaluated from the test results in accordance with the procedures of Ladanyi and Eckardt (1983). These values (or their ranges) were b = 0.439 to 0.951 , a = 1.70, and σ_c = 1.23 MPa for Test 1 and b = 0.211 to 0.911, a = 1.07 and σ_c = 1.39 MPa for Test 2 ($\dot{\varepsilon}_c = 10^{-5}$ min^{-1} in both cases). Four relatively long-term (maximum 20 days) single-stage pressuremeter creep tests were subsequently conducted. The previously derived parameters were used to predict the long-term creep. Good agreement was obtained only for the test with the highest applied pressure (4 MPa) and the shortest time duration (170 minutes). In all other cases the comparison was very poor, indicating that the method of determining the creep response was not reliable.

Shields et al. (1988a,b) presented the results of a series of single-stage pressuremeter creep tests conducted in large laboratory-prepared samples of polycrystalline freshwater ice, at -2°C. This work represented a portion of a larger program (Kjartanson, 1986) which had two objectives: (1) to investigate the validity of two theories which have been proposed to model the creep deformation of ice: power law theory (Ladanyi and Johnston, 1973) and a modified second-order fluid model (Man et al., 1985); and (2) to examine the influence of loading history through the analysis of both single- and multi-stage test results. Eight single-stage tests were carried out in thick cylinders of ice using an Oyo Elastmeter 100 pressuremeter. The ice was contained in a steel tank, 890 mm in diameter and 800 mm high, which provided semi-rigid bottom and lateral boundaries and no top constraint. In the analysis of primary creep, the authors employed a procedure suggested by Murat et al. (1986) to account for the effect

of stress redistribution on creep parameters. Equation 3.2 was written in the following form:

$$\varepsilon_e^{(c)} = K \sigma_e^a t^b \quad . \tag{3.4}$$

Parameters K, a, and b of equation 3.4 are given in Table 3.3. Reasonably good agreement was found in a comparison of these parameters with those derived in constant stress uniaxial compression tests on polycrystalline ice.

TABLE 3.3 SHIELDS ET AL. (1988a,b) - PRIMARY CREEP PARAMETERS OF POLYCRYSTALLINE ICE ($T = -2°C$)

Pressure (MPa)	b
1.00	0.501
1.25	0.644
1.50	0.601
1.75	0.647
2.00	0.669
2.25	0.642
2.50	0.629

Average b = 0.638 (ignoring b = 0.501 above)

Creep exponent a = 2.47

Creep constant $K = 7.0 \times 10^{-5}$ $MPa^{-2.47}$ $mn^{-0.64}$

The authors also examined the data in the context of secondary creep. Kjartanson et al. (1988a) suggested using Glen's flow law, generalized to multiaxial states of stress by Nye (1957). To simply describe the minimum circumferential strain rates observed in a series of pressuremeter tests at different pressures, Glen's creep equation may be written as:

$$\dot{\varepsilon}_{\theta min} = B p^n \quad , \tag{3.5}$$

in which B and n are material coefficients and the far-field pressure is ignored. Based on the results of the eight pressuremeter tests performed: $B = 2.3 \times 10^{-6}$ $MPa^{-3.76}$ min^{-1} and n = 3.76. Again, relatively good agreement was obtained

in comparing these values with parameters derived from constant stress uniaxial compression tests on polycrystalline ice, following correction to account for differences in stress state between the two types of test.

Shields et al. (1988c) carried out pressuremeter tests of a spray ice island (Mars Island) constructed by AMOCO off the north coast of Alaska. The tests were performed using two Oyo Elastmeter 100 pressuremeters. All tests were run at relatively low pressures and for a relatively short period of time, and as such none attained tertiary creep. The results of sixteen tests are presented in Table 3.4. As can be seen from the table, ice temperatures varied considerably from test to test. The table lists the apparent secondary creep rates, which were measured toward the end of the tests and the equivalent values computed for a reference temperature of -10°C. Primary creep was represented by an equation of the form 3.1 in which, for tests conducted within the range -2 to -3°C: a = 1.83; average b = 0.62; and $K = 2 \times 10^{-8}$ $KPa^{-1.83}$ $mn^{-0.62}$. The authors demonstrated that it was possible to correlate the creep behavior of the spray ice as interpreted from the pressuremeter tests with the creep behavior interpreted from island settlement records.

Table 3.5 provides a summary of the ranges of the creep parameters of equation 3.2 evaluated from pressuremeter creep tests in several of the aforementioned investigations.

TABLE 3.4 SHIELDS ET AL. (1988c) - CREEP DATA FROM PRESSUREMETER TESTS IN SPRAY ICE

Depth (m)	Ice Temperature (°C)	p (kPa)	$\dot{\varepsilon}_s^c$ (10^{-6} mn^{-1})	$\dot{\varepsilon}_s^c(-10°C)$ (10^{-6} mn^{-1})	b	Test Duration (Hrs)
2.58	-10.7	270	4.02	4.42	-	24
2.58	-10.7	470	30.1	33.2	0.60	4
3.25	-11.3	115	2.65	3.20	0.82	23
3.25	-11.3	185	3.88	4.70	-	24
4.60	-9.4	160	2.58	2.40	0.78	23
6.01	-6.1	105	1.66	1.08	-	24
7.89	-2.8	130	8.95	3.10	0.50	12
7.89	-2.8	310	104.5	36.0	0.53	2
7.89	-2.8	485	263	91	0.76	2
7.89	-2.8	650	694	240	-	2
0.44	-22.4	832	62.5	367	0.82	2
0.44	-22.4	1105	115.4	678	0.70	1.5
3.35	-10.4	150	2.00	2.10	0.36	118
4.62	-6.1	105	1.55	1.00	0.38	119
3.39	-8.9	91	0.97	0.87	-	10
4.61	-8.3	195	14.6	12.3	0.34	8

TABLE 3.5 PARAMETERS OF EQUATION 3.2 AS REPORTED FROM VARIOUS PRESSUREMETER CREEP TEST PROGRAMS

Investigator (year)	Material	Temperature (°C)	b	a	σ_c(MPa) (for $\dot{\varepsilon}_c$ = 10^{-5} min^{-1})
Ladanyi and Johnston (1973)	Ice-rich varved clay	-0.1 to -0.3	0.4-0.67	0.8 - 2.7	0.45-2.4
Rowely et al. (1975)	Ice-rich clayey silt	-1.6	0.85-0.87	3.00-3.89	0.30-0.32
Ladanyi and Saint-Pierre (1978)	Sea ice; columnar grained of S2 type	-4.0	0.6-1.0 (Average)	1.54-4.01	0.10-0.63
Ladanyi (1982)	Ice-rich clayey silt	-1.5 to -2.4	0.69-0.78 (Average)	2.37-2.84	0.43-0.73
Ladanyi and Eckardt (1983)	Sand	-2.5	0.72-0.84	1.80-3.60	0.82-2.0
Fensury (1986)	Sand	-3.0	0.21-0.95	1.07-1.70	1.23-1.39
Kjartanson (1986)	Polycrystalline freshwater ice	-2.0	0.50-0.67	2.47	-
Shields et al. (1988c)	Spray ice	-2.0 to -3.0	0.62	1.83	-

3.2 EQUIPMENT AND MATERIALS

The pressuremeter tests were carried out in the same test facility and the same material that was investigated in the plate-load test program. The pressuremeter tests were conducted subsequent to the completion of the plate-load investigation.

3.2.1 Pressuremeter Test Instrumentation

The pressuremeter used in this investigation was the Oyo Elastmeter 100 pressuremeter. This pressuremeter measured changes in the radius of the borehole directly through a caliper arm - LVDT system. The pressure for expanding the probe was supplied by compressed nitrogen gas. The use of pressurized gas removed some of the difficulties associated with low temperature testing. Experience with the Oyo Elastmeter 100 pressuremeter at the University of Manitoba (Fensury, 1985; Kjartanson, 1986; Shields et al., 1988c) demonstrated that the caliper arm measuring system was robust and very accurate at low test temperatures and for long testing periods, under both laboratory and field conditions.

The Oyo Elastmeter 100 pressuremeter equipment used in the present investigation consisted of the probe, a regulated supply of dry nitrogen gas, a caliper arm-LVDT digital indicator, a pressure gauge, a pressure transducer, and a data acquisition system. A schematic of the test pit and pressuremeter testing apparatus is presented in Figure 3.1. The test set-up and instrumentation are also shown in Figure 3.2.

The probe consisted of a steel cylindrical core, over which a 4 mm thick rubber membrane sleeve was fitted. The rubber membrane was rated for applied pressures of up to 3 MPa. The membrane had an outside diameter of 70 mm in its unstressed condition and an effective length of 390 mm, giving a length

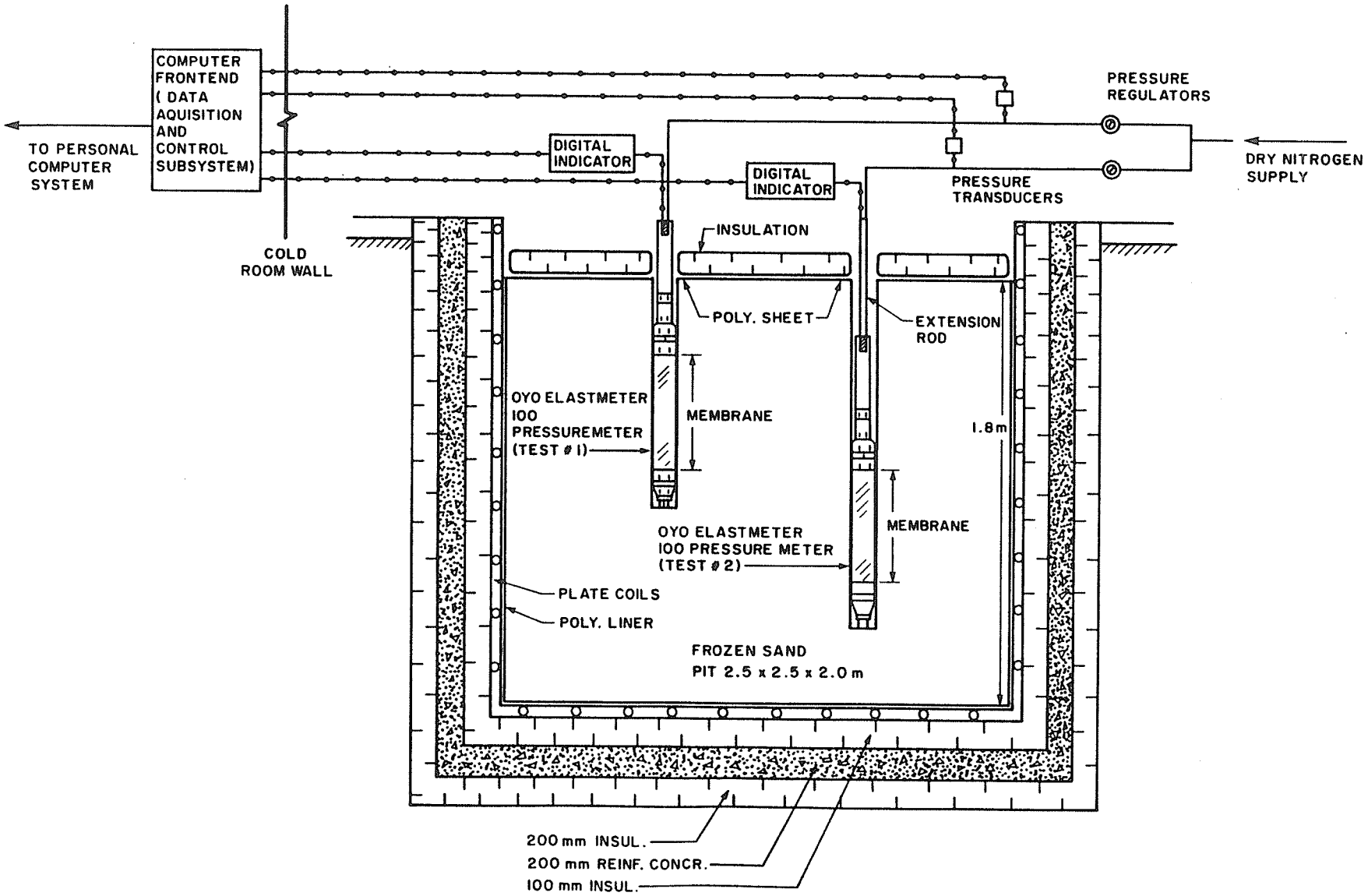

FIGURE 3.1 SECTION THROUGH TEST PIT AND PRESSUREMETER TEST APPARATUS

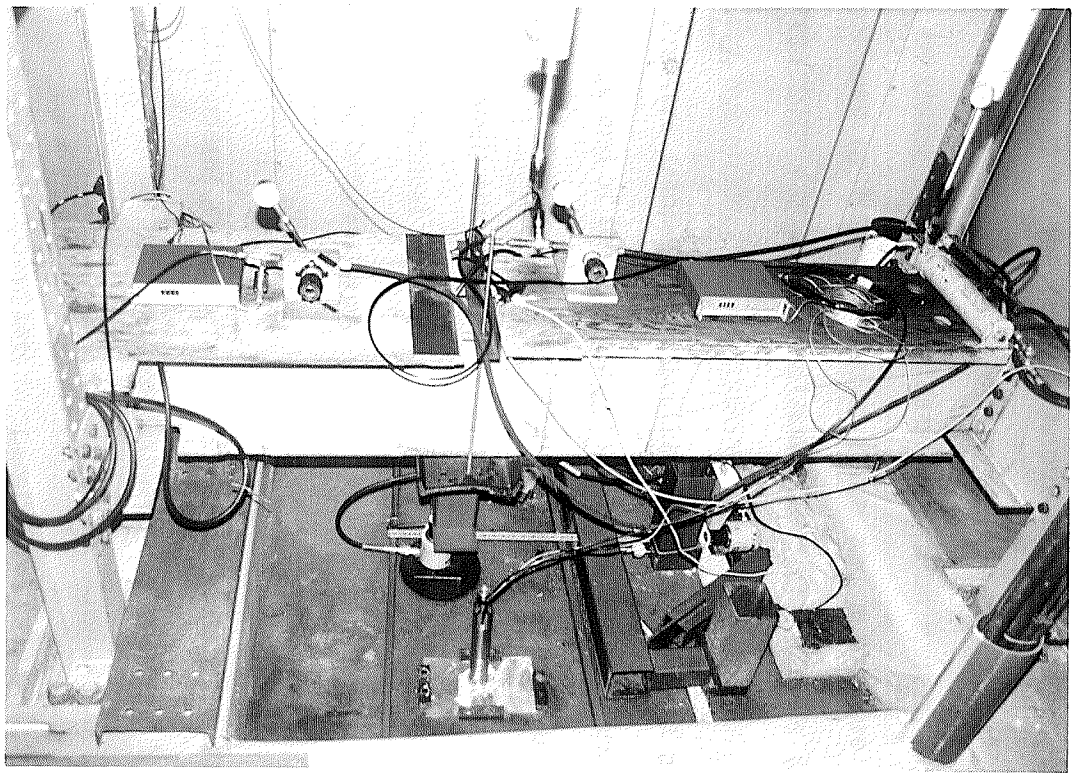

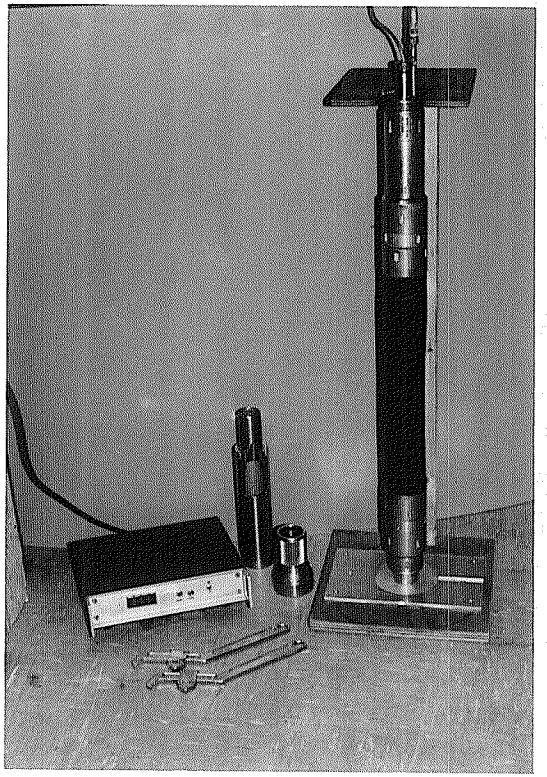

FIGURE 3.2 PRESSUREMETER TEST SET-UP AND OYO ELASTMETER 100 PRESSUREMETER EQUIPMENT

to diameter ratio of 5.6. The caliper arm-LVDT system measured the change in radius of the inside of the rubber membrane, at its center. Calibrations, considered in the following section, were carried out to account for the change in thickness of the membrane with pressure, time, and temperature, to compute its outside diameter, that is, the borehole radius.

The pressure used to inflate the probe was controlled with a Tescom 44 - 1100 series regulator. These regulators provided good setting sensitivity and limited pressure drift to within ±10 KPa over 12 hour time periods (Kjartanson, 1986).

Measured test variables included probe radius, applied pressure, and soil temperatures near to the probe. Output from the pressuremeter displacement transducer was conditioned and displayed in a portable digital indicator which provided an analog output to the data acquisition system. Applied gas pressures were monitored by both a pressure gauge and a pressure transducer (Dynisco Model PT370DHF - 7 MPa). The rated accuracy of this transducer, including nonlinearity, hysteresis, and repeatability, was within ±0.25% of the full scale output. Pressure transducer calibrations were carried out at the beginning and checked at the end of the test program. Frozen soil temperatures were measured with the same thermocouple arrangement as was used in the plate-load test program. As well, the same microcomputer-based data acquisition system was employed for continual monitoring and periodic recording of probe radius, applied pressure, and soil temperatures.

3.2.2 Pressuremeter Calibration

Pressuremeter calibrations were carried out both before and after each test. The procedures followed were those developed by Kjartanson (1986) for relatively long-term creep tests. All of the calibrations were carried out in the cold room at the proposed test temperature.

According to Kjartanson (1986), modifications to the manufacturer's suggested calibration methods were necessary to account for long-term and low temperature tests. The recommended procedures to determine the corrected values of borehole radius and pressure may be grouped into three categories:

1. calibration of the caliper arm-LVDT system,
2. calibration for membrane thickness, and
3. calibration for membrane resistance.

Details of the calibration procedures and results are provided in Appendix A.

3.3 TEST PROCEDURES

As indicated previously, two pressuremeter creep tests were carried out. Test Nos. 1 and 2 were conducted at different locations within the test pit.

Prior to running each test, a borehole was drilled with minimum mechanical and thermal disturbance of frozen soil. A modified CRREL-type core barrel, fabricated at the University of Manitoba, was used for this purpose. The core barrel drilled a 77 mm diameter borehole and produced core samples which were 43 mm in diameter. The core barrel was driven by a variable speed electric drill and was rotated at approximately 60 revolutions per minute. Continuous samples of core were recovered for determining unit weight and ice content, and for visual inspection. As indicated in Section 2.2.2, the range of dry unit weights was 15.2 to 16.2 kN/m^3 and the range of total moisture contents was 20.5 to 23.8%. The specific results are given in Table 3.6. The ratio of the diameter of the borehole to the diameter of the uninflated pressuremeter probe was 1.08 for Test No. 1 and 1.07 for Test No. 2. According to Briaud and Gambin (1983), an acceptable borehole should have a ratio between 1.03 and 1.20.

A polyethelene sheet was placed on the soil surface to minimize sublimation. Fiberglass insulation sheets were placed on the polyethelene, as shown in Figure 3.1.

TABLE 3.6 DRY UNIT WEIGHT AND ICE CONTENT OF FROZEN SAND

Depth Below Sand Surface (mm)	Dry Unit Weight (kN m^{-3})	Moisture Content (%)
TESTHOLE #1 RESULTS		
90	15.4	23.7
240	15.8	21.6
380	15.7	21.1
510	16.1	20.9
650	15.8	21.5
830	15.8	21.6
TESTHOLE #2 RESULTS		
100	15.2	24
290	16.2	20.5
470	16.0	21.5
670	15.7	23.7
890	15.9	22.8
1110	15.9	23.2
1300	15.9	22.8

The boreholes were situated on either side of the plate-test location. The distance from each borehole to the plate-test location was about 0.5 m. Each was drilled to a different depth. For Test No. 1, the probe was seated at the bottom of the shallower borehole. The depth to the center of the probe was approximately 550 mm. For Test No. 2, the probe was seated at the bottom of the deeper borehole. The depth to the center of the probe was approximately 1050 mm.

Multi-stage pressuremeter creep tests were performed. The procedure involved the application of the desired pressure to the probe and the monitoring of changes in borehole radius over time. To start the test, the membrane was first inflated until it came into contact with the cavity wall. This took about 30 seconds and ensured that the probe was properly seated within the hole. The pressure was then rapidly increased to the proposed, first stage, test pressure.

As creep occurred, the probe pressure was adjusted, in accordance with the calibrations, to maintain a constant cavity pressure. After complete attenuation of deformation, the applied pressure was increased to a new level. The pressure increase was usually completed in less than 1 minute.

Pressure increments of similar magnitude to the plate-load test pressures, were applied in both of the pressuremeter tests. In Test No. 1, the mean applied cavity pressures were 0.86, 1.77, 2.83, and 3.47 MPa. In Test No. 2, the mean applied cavity pressures were 0.85, 1.79, and 2.78 MPa.

3.4 TEST RESULTS

3.4.1 Test Data - Summary

The applied cavity pressures, borehole radius, and the temperature of the soil at the depth of the probe are shown as a function of time in Figure 3.3, for Test No. 1. The same information is given for Test No. 2, in Figure 3.4. For clarity, individual plots of applied pressure, soil temperature, and borehole radius are displayed in Figures 3.5, 3.6, and 3.7, respectively, for Test No. 1, and in Figures 3.8, 3.9 and 3.10, respectively, for Test No. 2. The values of pressure shown in the above-mentioned figures were corrected in accordance with the calibration procedures indicated in Section 3.2.2.

A few brief breakdowns of the refrigeration system occurred during the test period. The problems were usually rectified before any soil temperature changes occurred. However, a small rise in soil temperature of brief duration occurred in stage 2 of Test No. 1. This resulted in a small immediate increase in the borehole radius, shown in Figure 3.7. In the analysis of the results, this change in borehole radius was omitted. A small temperature increase also occurred during stage 3 of Test No. 2. It was not possible to determine if this specifically caused any increase in borehole deformation.

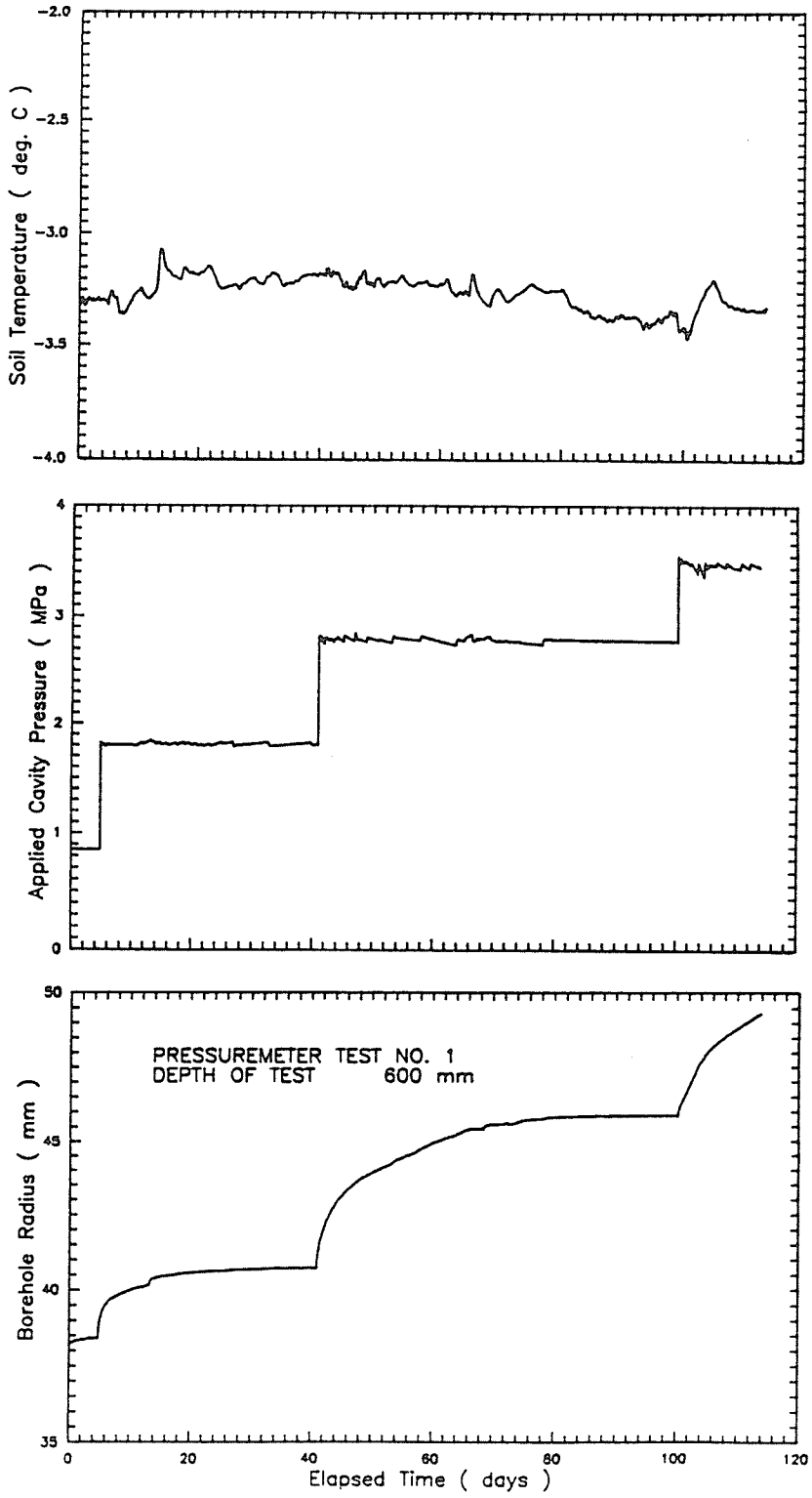

FIGURE 3.3 SOIL TEMPERATURE, APPLIED CAVITY PRESSURE, AND BOREHOLE RADIUS VERSUS TIME (TEST NO. 1)

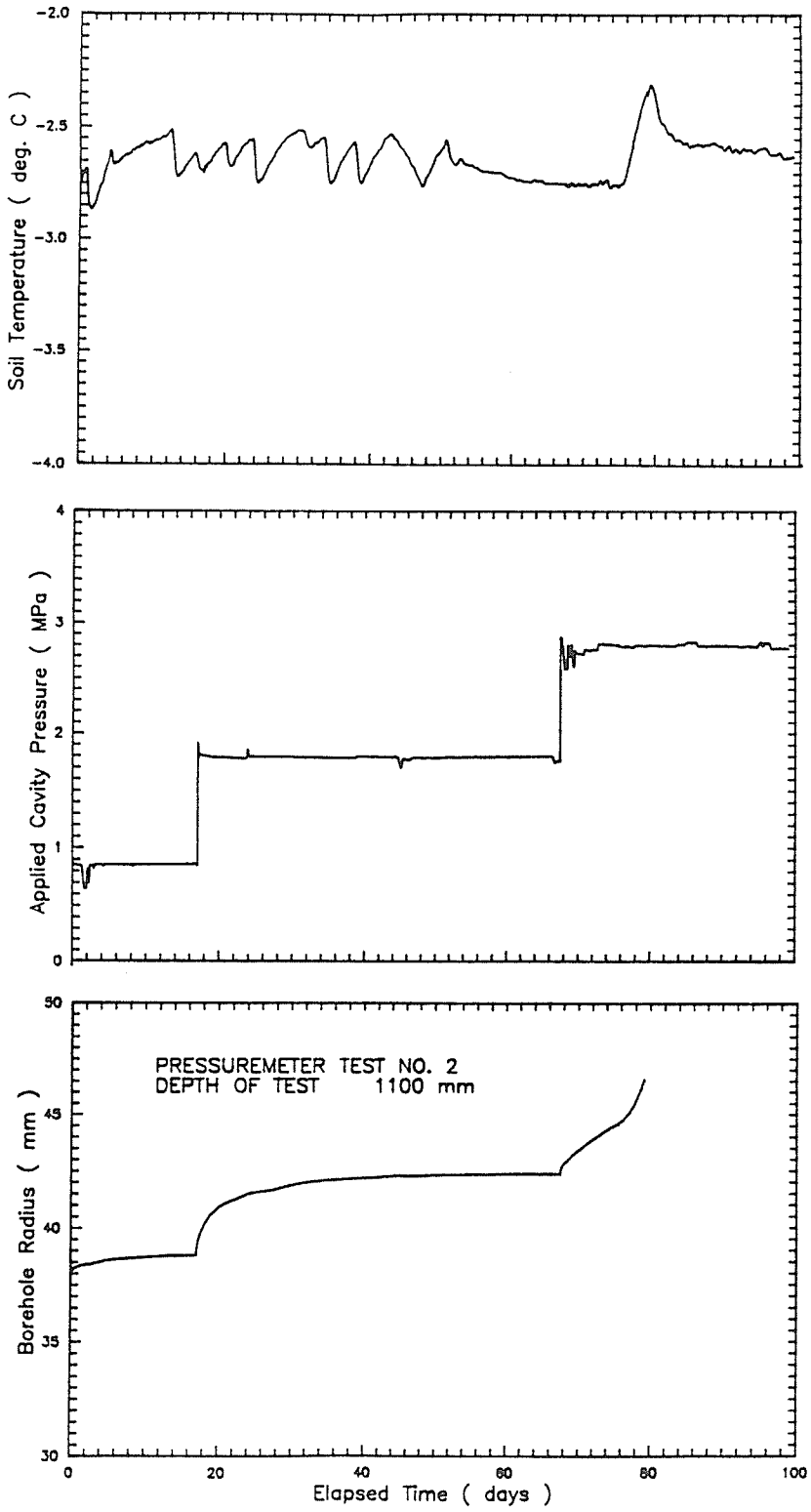

FIGURE 3.4 SOIL TEMPERATURE, APPLIED CAVITY PRESSURE, AND BOREHOLE RADIUS VERSUS TIME (TEST NO. 2)

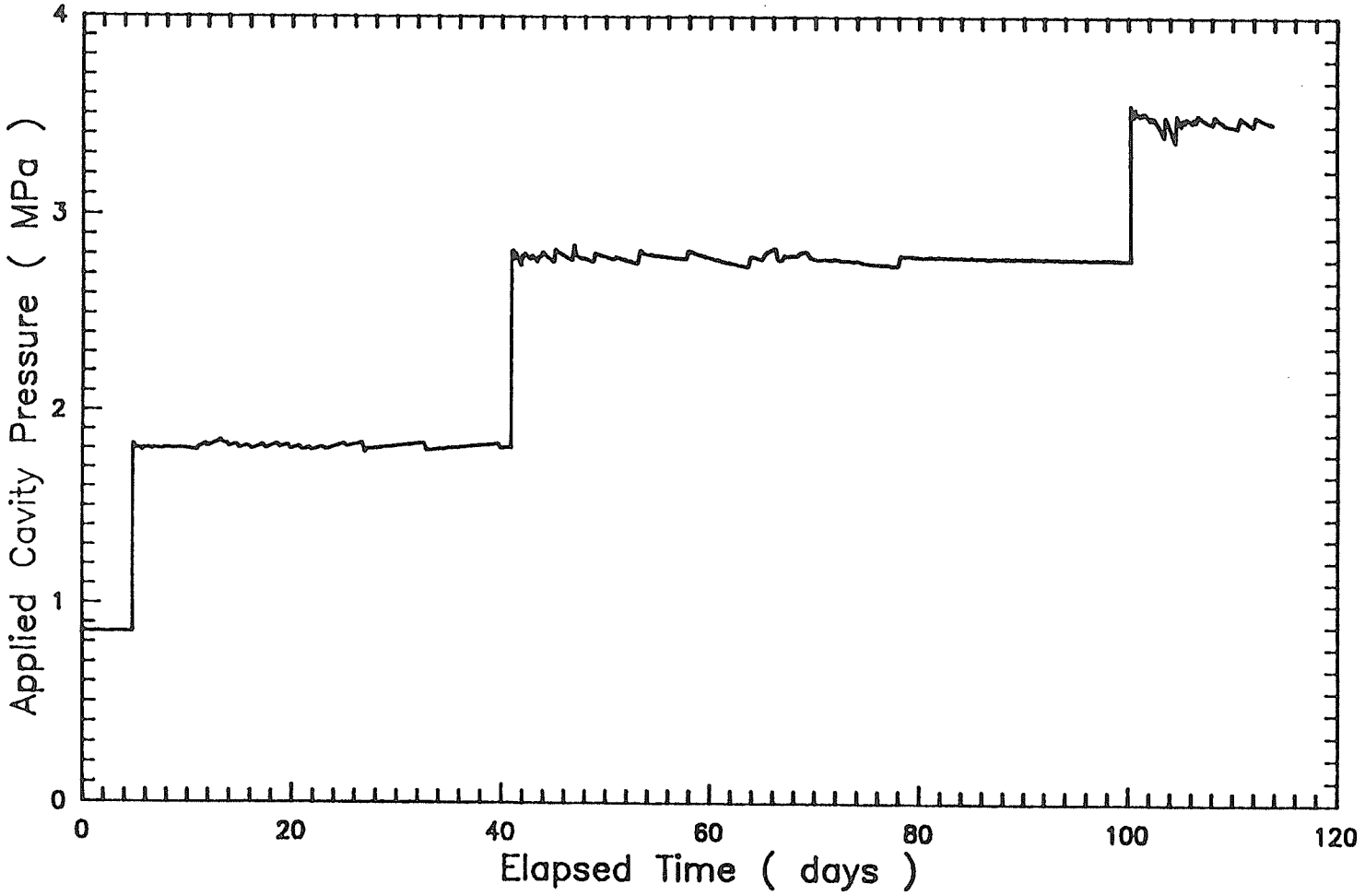

FIGURE 3.5 APPLIED CAVITY PRESSURE VERSUS TIME (TEST NO. 1)

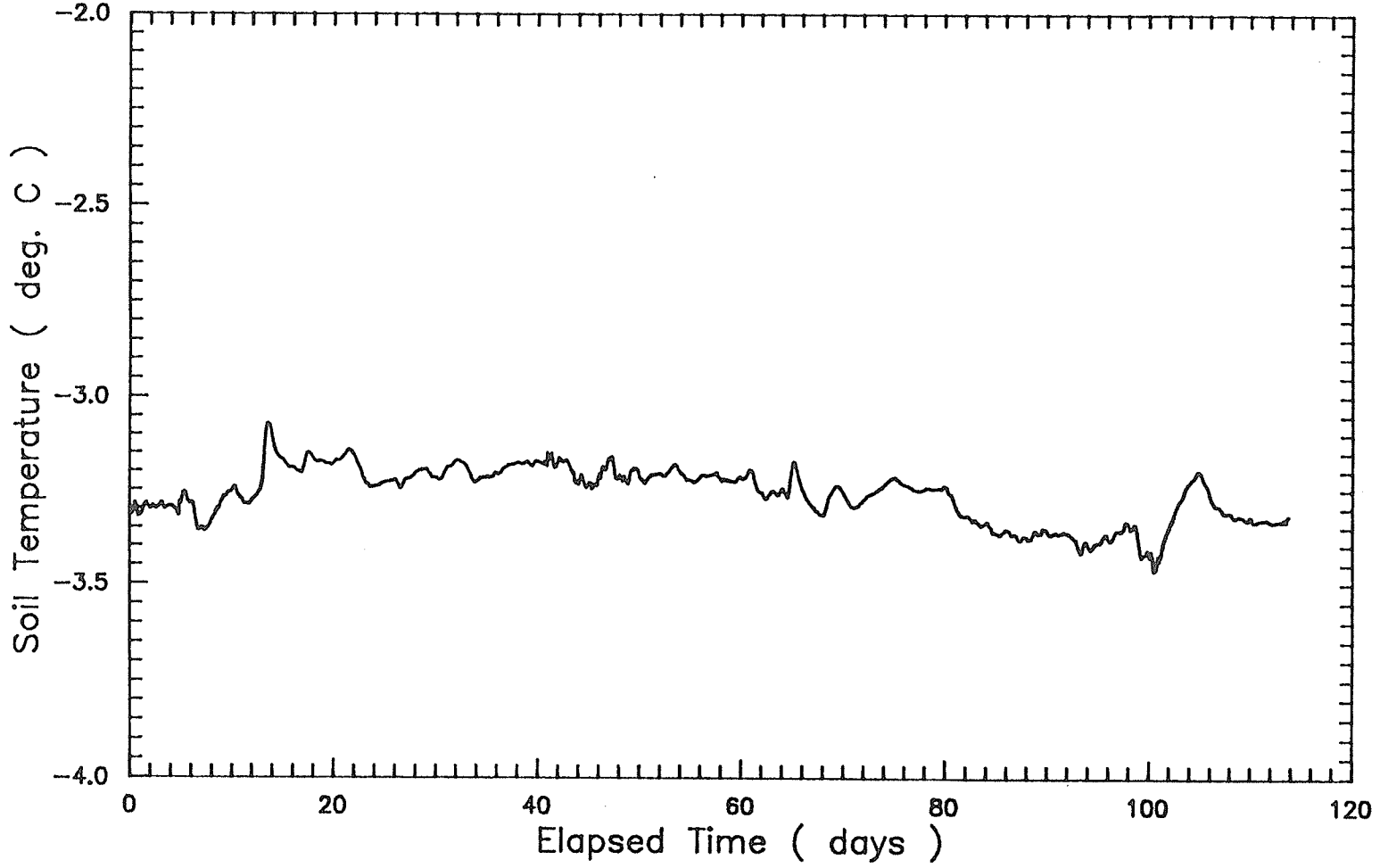

FIGURE 3.6 SOIL TEMPERATURE AT TEST NO. 1 LOCATION VERSUS TIME

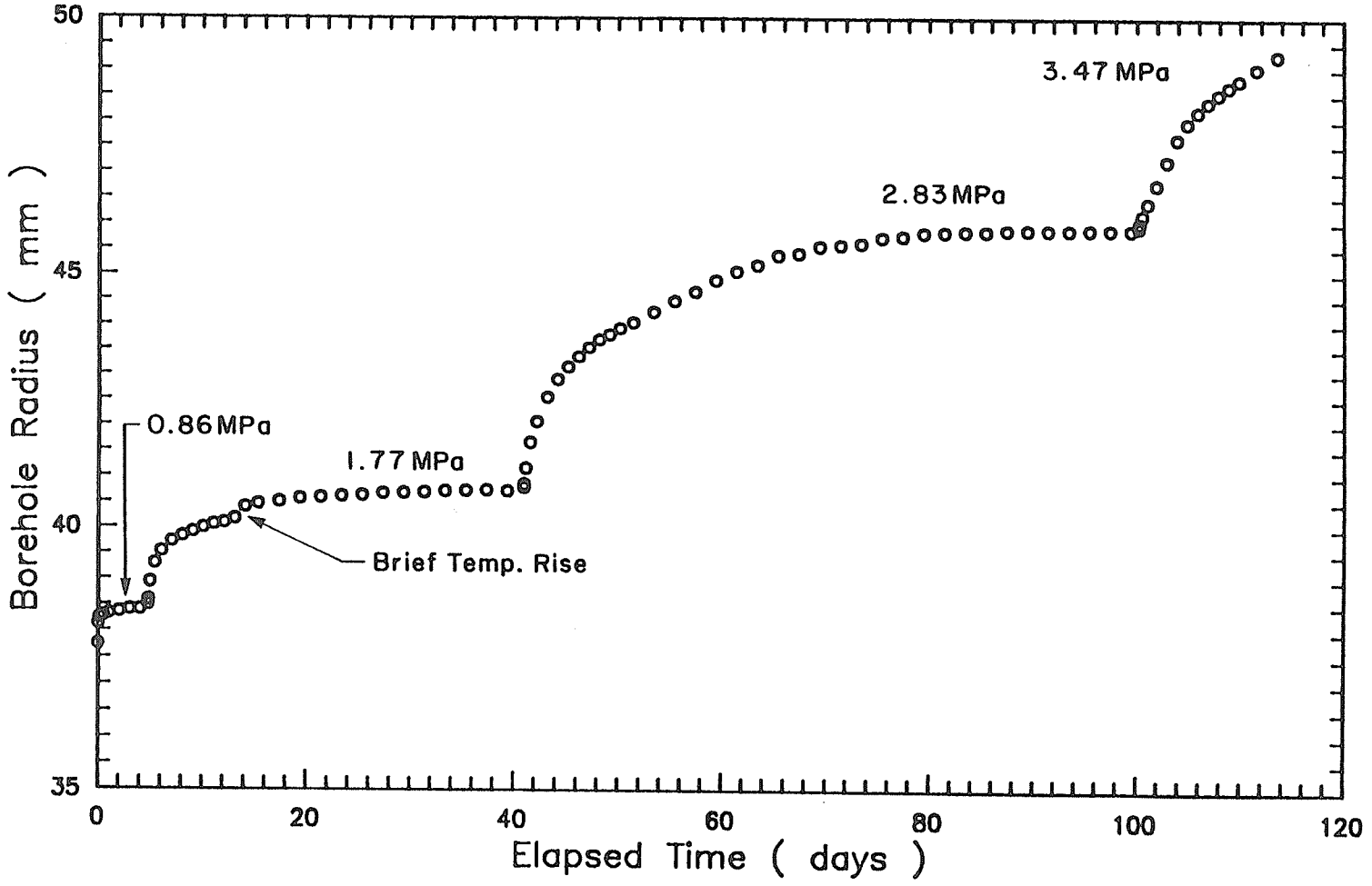

FIGURE 3.7 BOREHOLE RADIUS VERSUS TIME (TEST NO. 1)

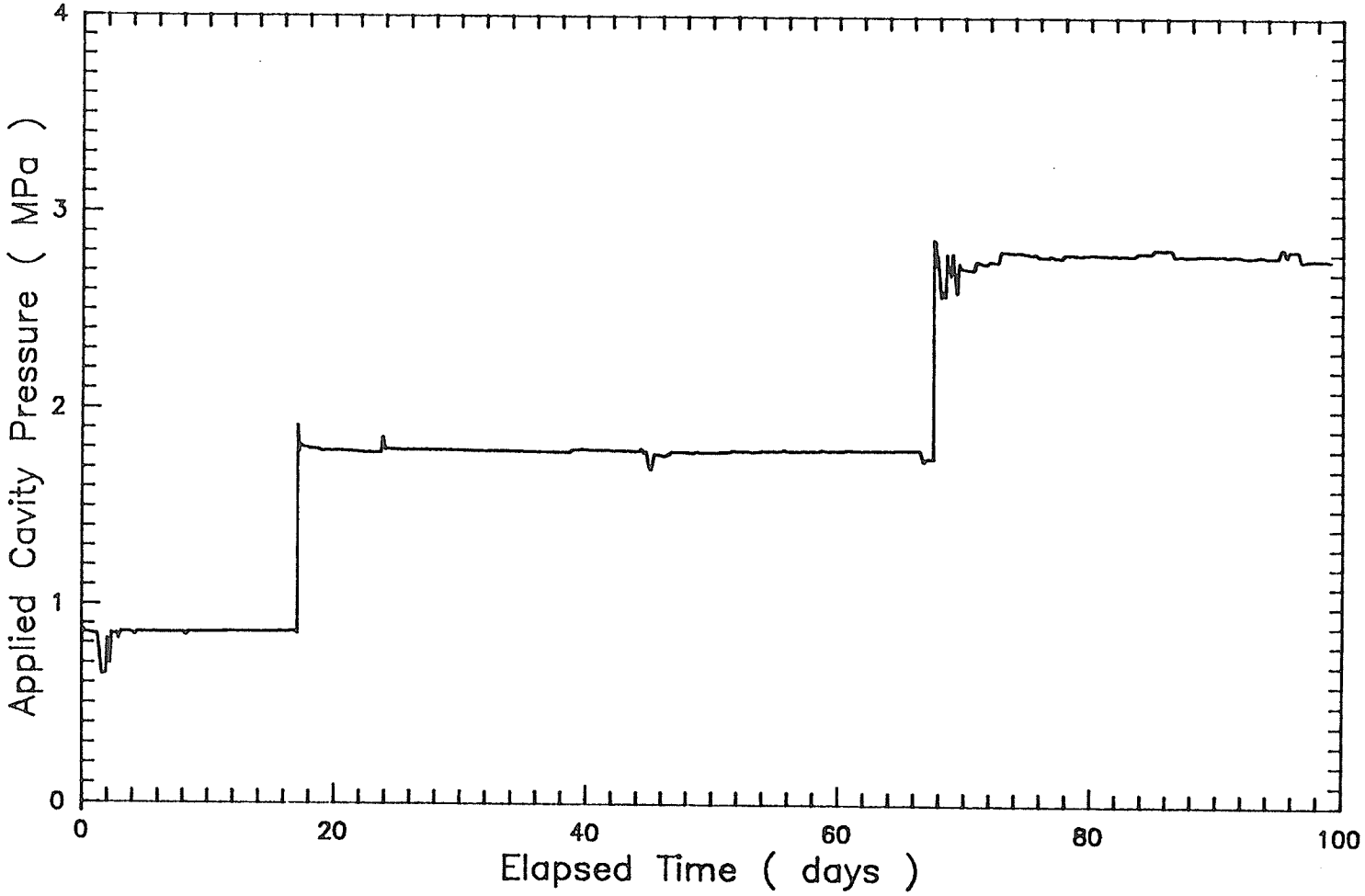

FIGURE 3.8 APPLIED CAVITY PRESSURE VERSUS TIME (TEST NO. 2)

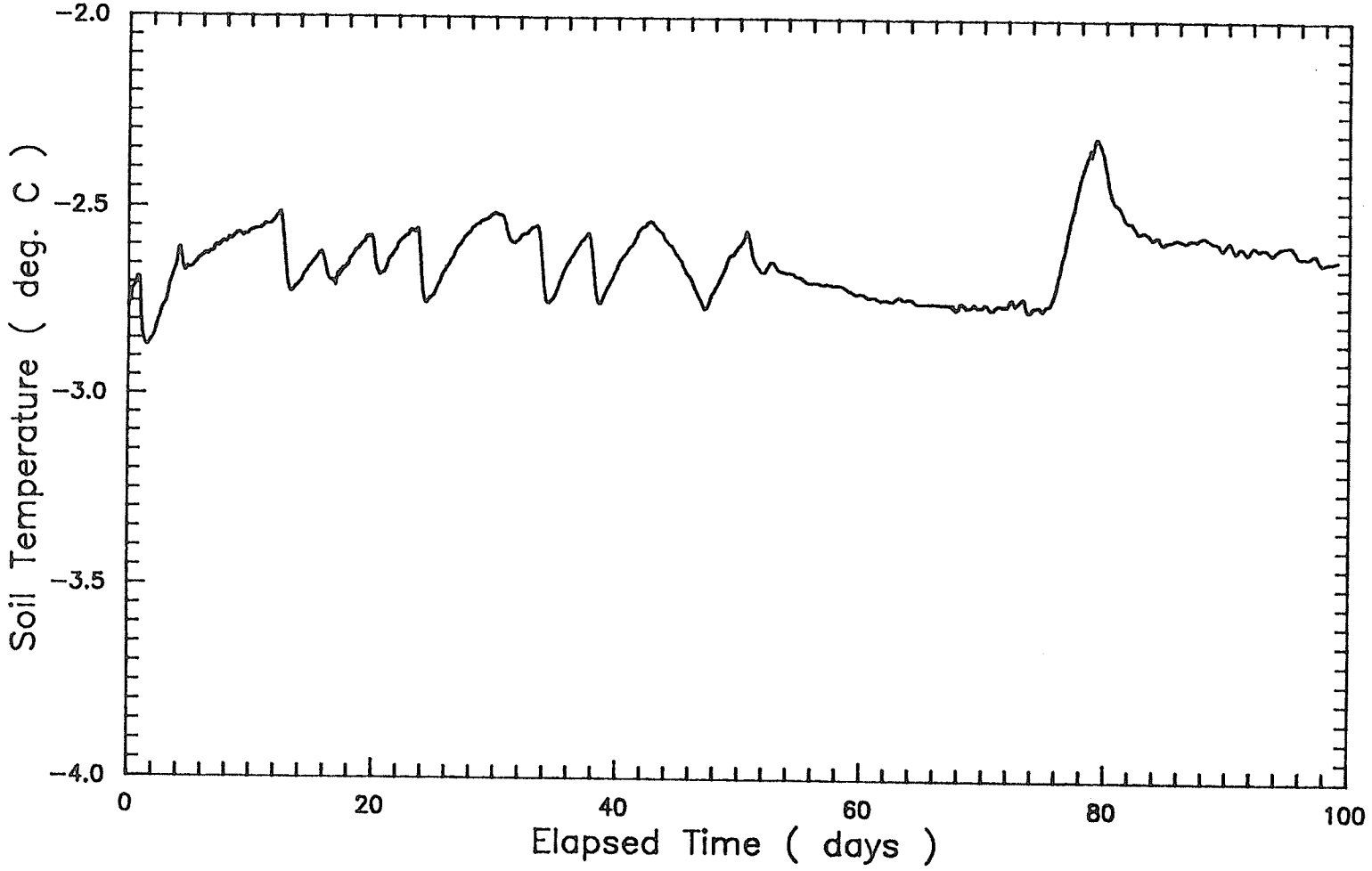

FIGURE 3.9 SOIL TEMPERATURE AT TEST NO. 2 LOCATION VERSUS TIME

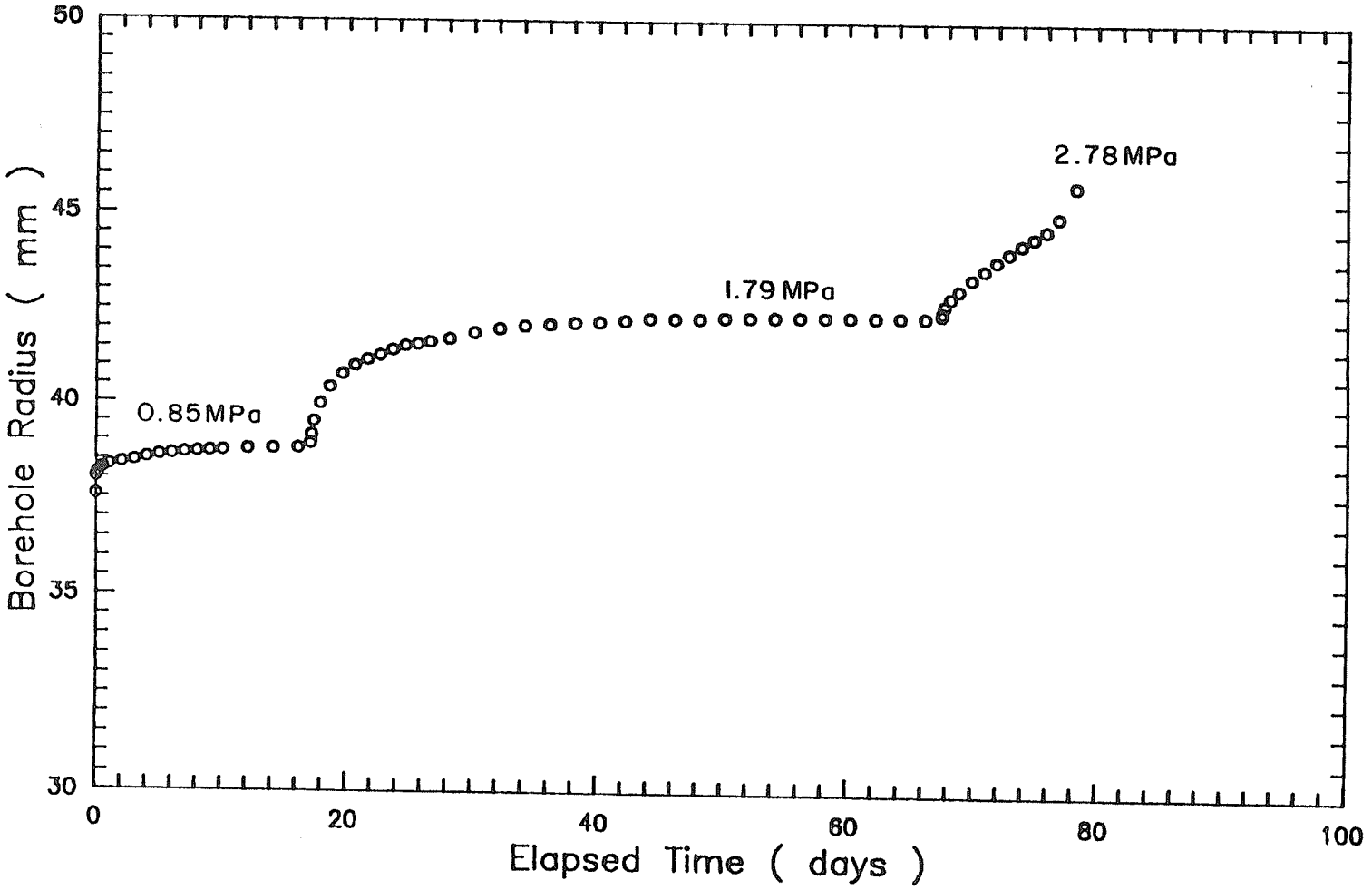

FIGURE 3.10 BOREHOLE RADIUS VERSUS TIME (TEST NO. 2)

As previously mentioned, the temperature distribution in the test pit was characterized by a slight vertical gradient. Soil temperatures at depths of 200, 400, and 600 mm are shown as a function of the elapsed time for Test No. 1, in Figure 3.11. The average value of the soil temperatures measured over the test period, at the approximate depth of Test No. 1, was -3.30.°C. Soil temperatures at depths of 800, 1000, 1200, and 1400 mm are shown as a function of the elapsed time for Test No. 2, in Figure 3.12. The average value of the soil temperatures measured over the test period, at the approximate depth of Test No. 2, was -2.65°C. The temperature data in Figure 3.12 have a cyclic nature. This may be due to periodic circulation of refrigerant through the platecoil panels at the bottom of the test pit.

In stages 1, 2, and 3 of Test No. 1 and stages 1 and 2 of Test No. 2, the borehole deformation attenuated with time. In stage 3 of Test No. 2 the deformation did not attenuate, but instead, continued into tertiary creep. After the limit of the radius measurement system was exceeded, each of the tests was terminated. This limit corresponded to approximately a 25% increase in the borehole radius. Test No. 1 was stopped at stage 4. The total test duration was almost 120 days. Test No. 2 was stopped during stage 3. The total test duration was approximatley 80 days.

3.4.2 Test Data - Interpretation

For small values of strain, the borehole circumferential strain may be defined as:

$$\ln (r/r_i) = \Delta r/r_i = [(r - r_i) / r_i] \quad , \qquad (3.6)$$

in which r denotes the borehole radius and r_i denotes the initial borehole radius. In the present study, only the creep response was considered. In accordance with the approach of Ladanyi and Eckardt (1983), creep strain was assumed to commence at one minute following the application of pressure. All values of

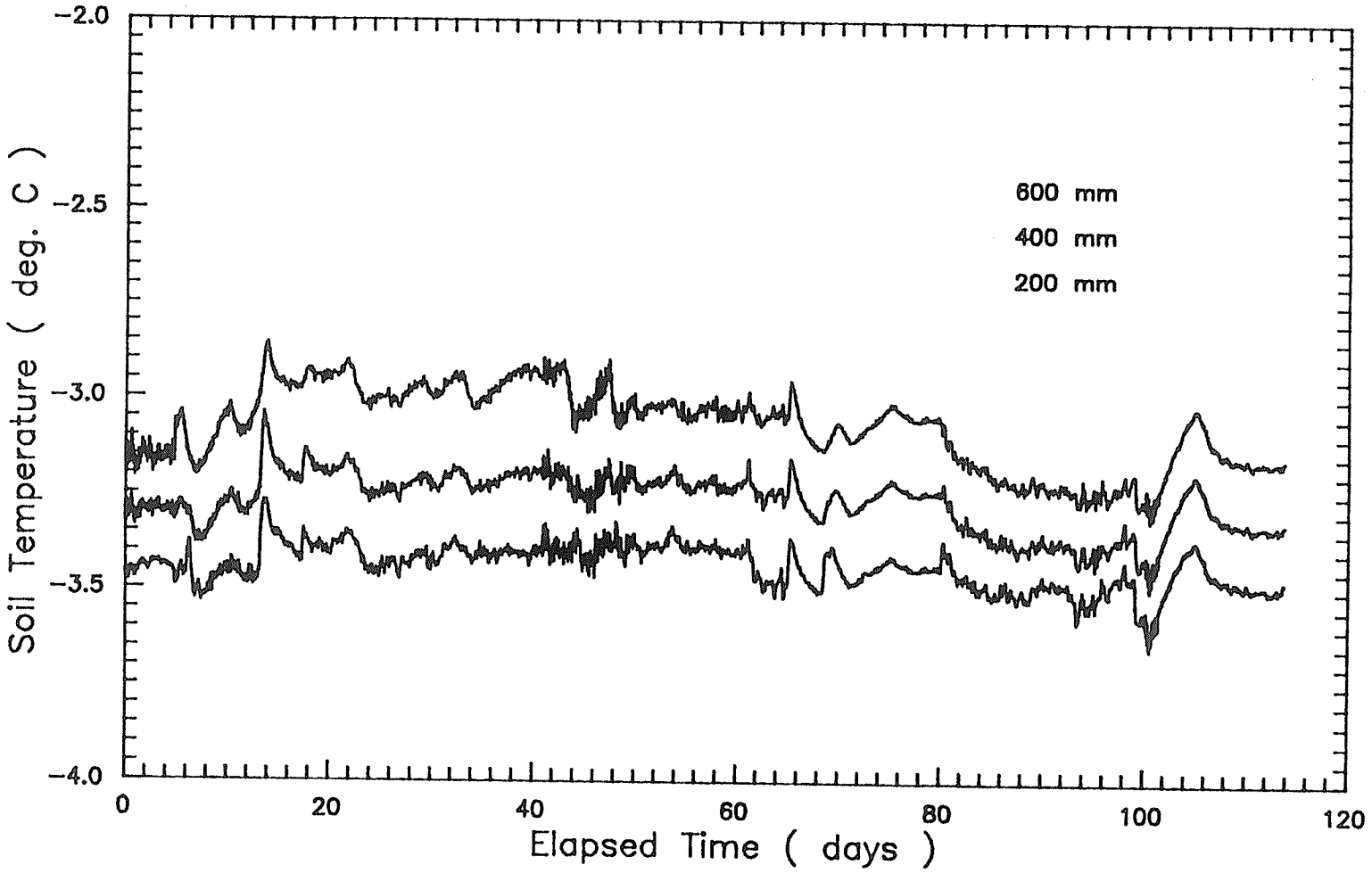

FIGURE 3.11 SOIL TEMPERATURES AT DIFFERENT DEPTHS VERSUS TIME (TEST NO. 1)

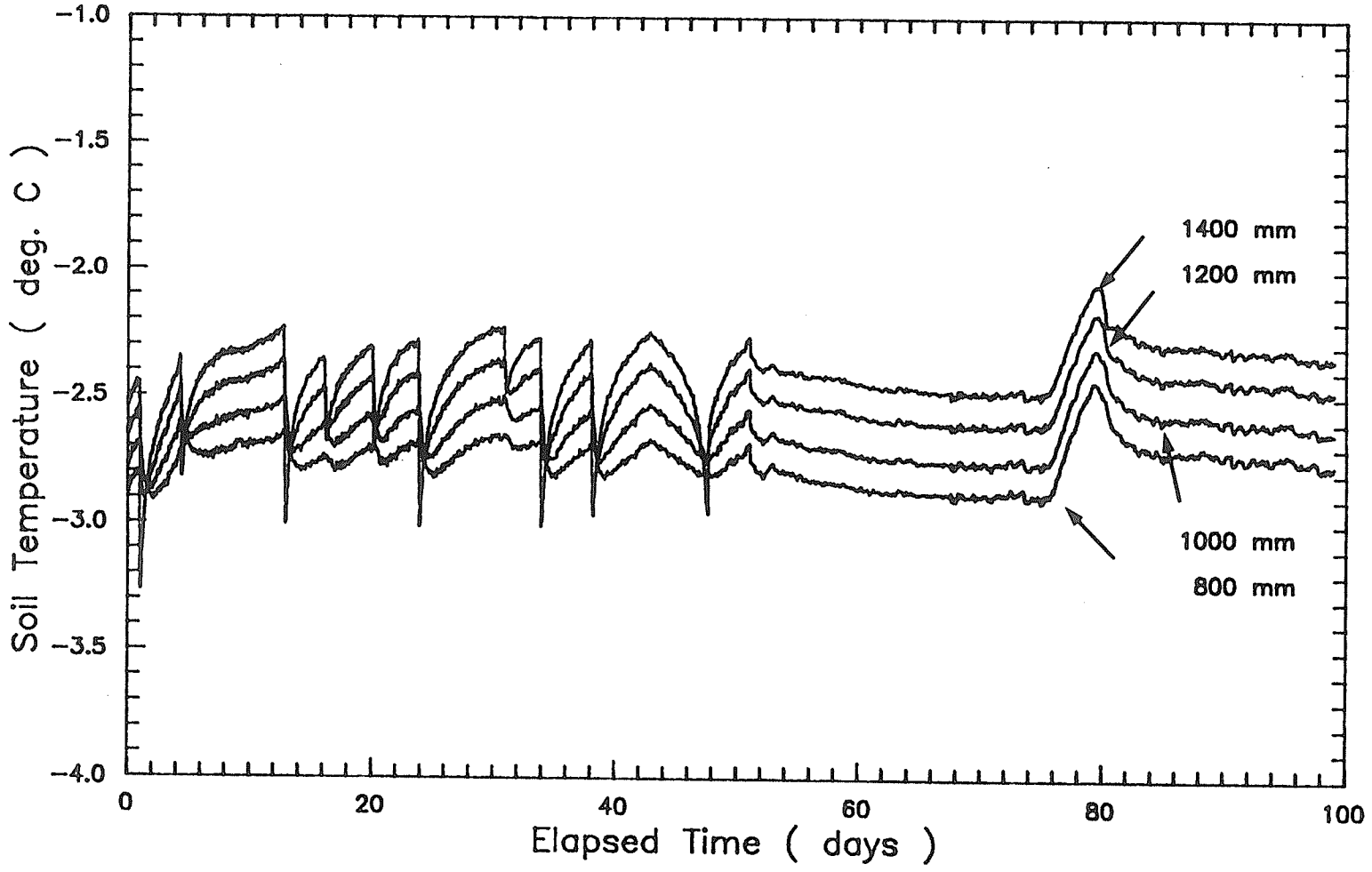

FIGURE 3.12 SOIL TEMPERATURES AT DIFFERENT DEPTHS VERSUS TIME (TEST NO. 2)

creep strain were, therefore, referenced to the borehole radius measured at one minute, that is, r_i in equation 3.6 was defined as the borehole radius at an elapsed time of one minute, for each stage.

To consider the dependence of creep strain on both stress and time, a separate cummulative strain-time curve was generated for each of the applied pressure increments, by superposition. It was assumed that the cummulative strain under each new total pressure, at a given elapsed time, was equal to the sum of the strains that had occurred under all pressures, up to and including the pressure in question, within that same time interval.

Creep circumferential strain-time curves developed from the test data in the above-stated manner are shown in Figure 3.13 for Test No. 1 and in Figure 3.15 for Test No. 2. Curves representing the creep response under pressures imposed in stages 1, 2, and 3 of Test No. 1 and stages 1 and 2 of Test No. 2 show attenuation, which is typical of hard-frozen soils subjected to stresses below their long-term strength. Attenuating creep at relatively large values of strain was a characteristic feature of both the plate-load and pressuremeter creep test results.

Creep circumferential strain rates are shown plotted in Figures 3.17 and 3.18, for Test Nos. 1 and 2, respectively. With the exception of the final stages of each test, creep strain rates decreased, tending to zero as a limit. In the final stage of Test No. 1, the strain rates decreased throughout the period of observation. The test was not continued for a sufficient time period to determine if the strain would attenuate completely. The final stage of Test No. 2 exhibited tertiary creep.

According to the temperature data, there was a small rise in soil temperature near the beginning of stage 3 of Test No. 2 (Figure 3.4). This temperature increase may have contributed to an early development of tertiary creep. Furthermore, it is possible that the development of larger strains, under

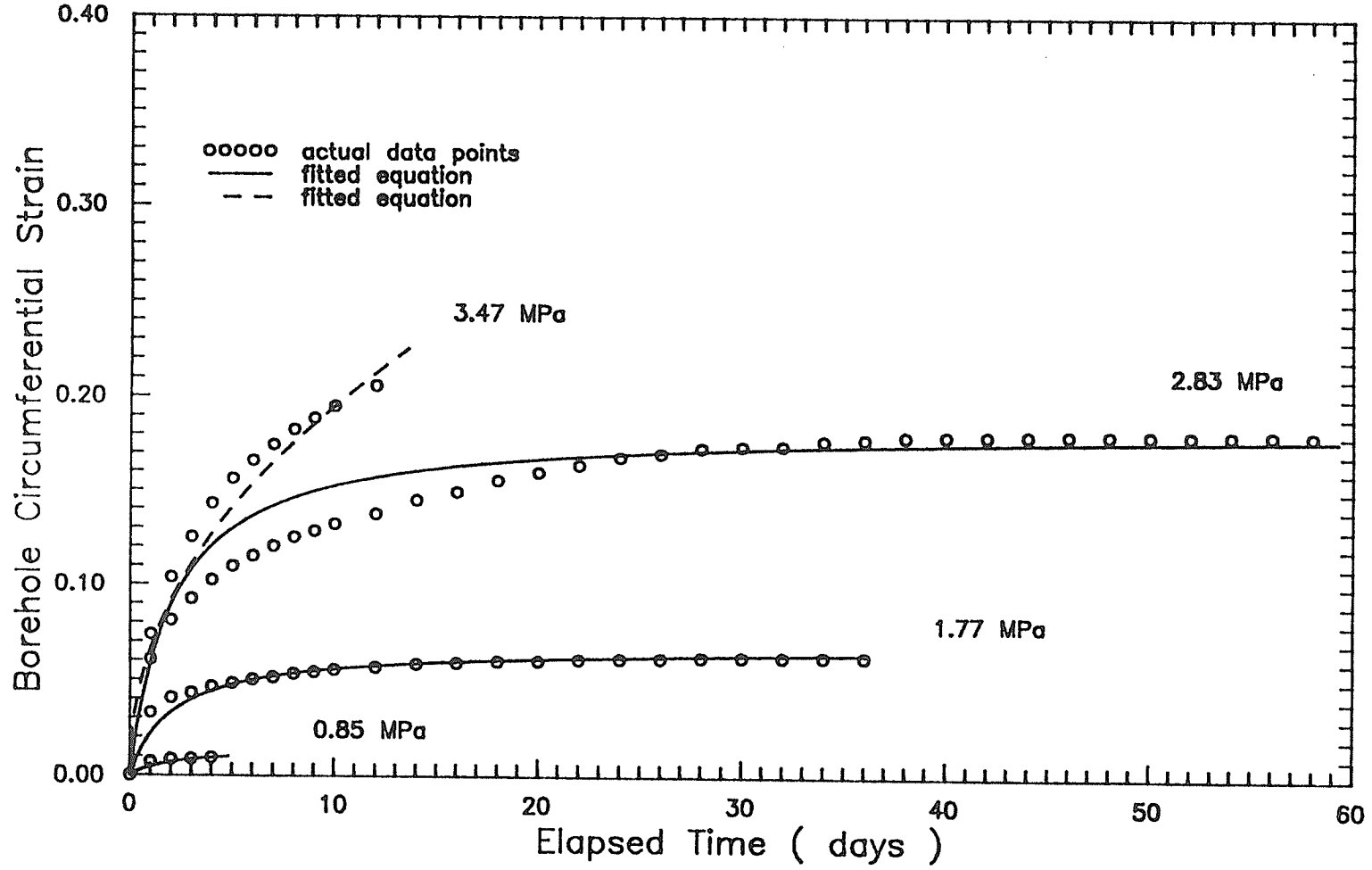

FIGURE 3.13 BOREHOLE CIRCUMFERENTIAL STRAIN VERSUS TIME FOR EACH APPLIED PRESSURE (TEST NO. 1)

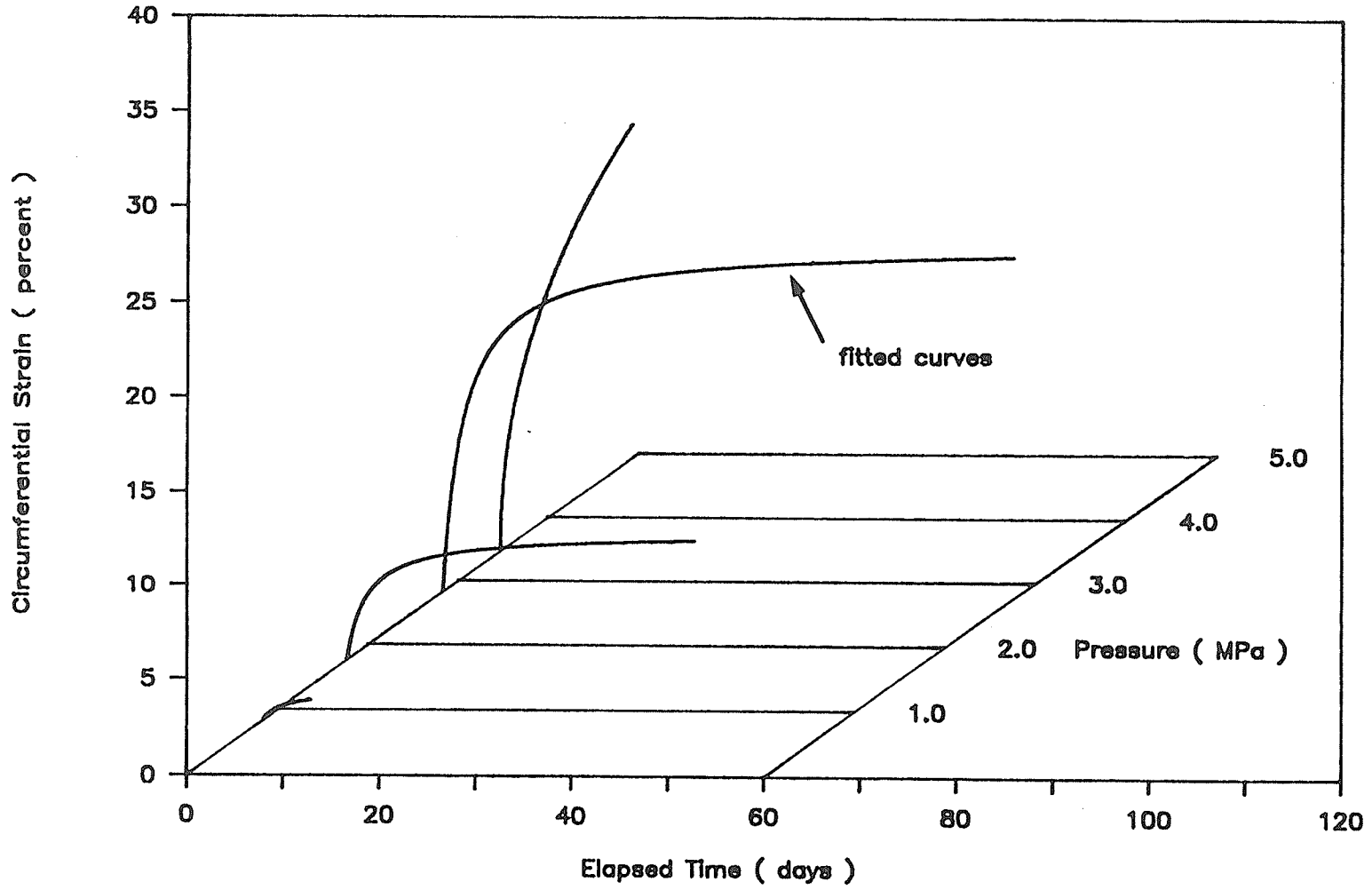

FIGURE 3.14 BOREHOLE CIRCUMFERENTIAL STRAIN VERSUS TIME AND APPLIED PRESSURE (TEST NO. 1)

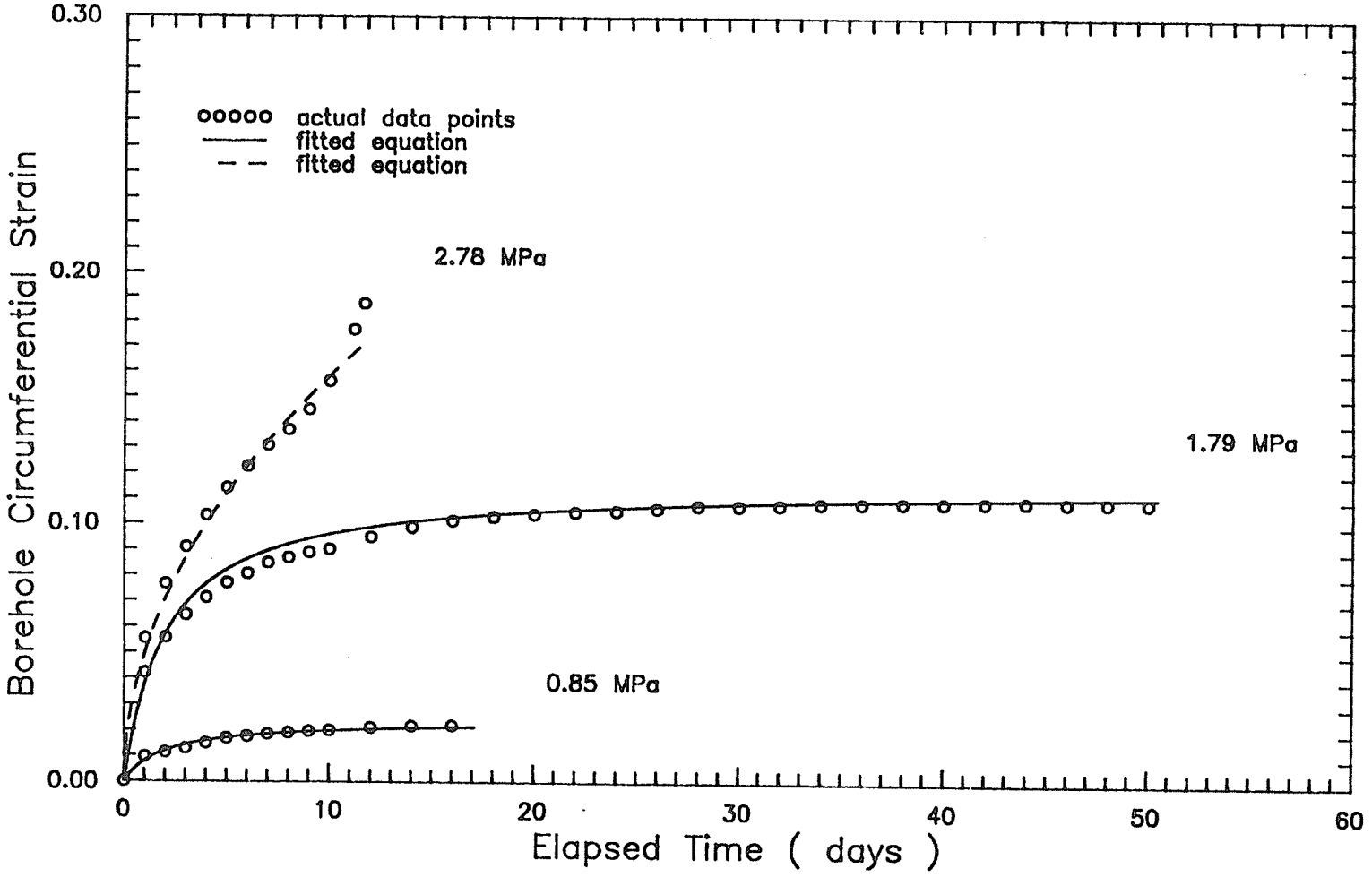

FIGURE 3.15 BOREHOLE CIRCUMFERENTIAL STRAIN VERSUS TIME FOR EACH APPLIED PRESSURE (TEST NO. 2)

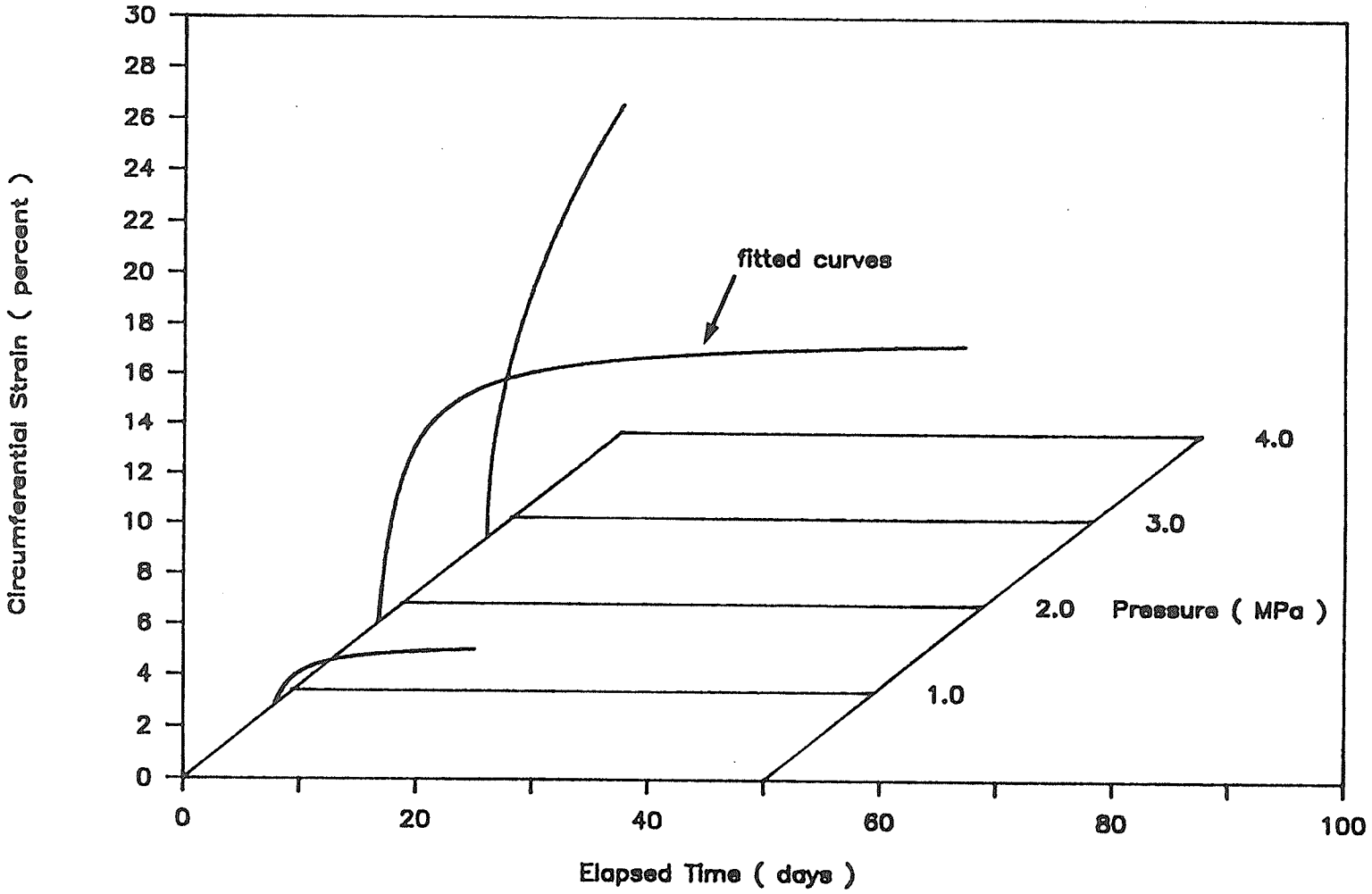

FIGURE 3.16 BOREHOLE CIRCUMFERENTIAL STRAIN VERSUS TIME AND APPLIED PRESSURE (TEST NO. 2)

the same applied pressures, in Test No. 2 as compared with Test No. 1 (Figures 3.13 and 3.15) may be the result of differences in soil temperature at the two test locations. As previously indicated, the average soil temperatures during testing were -3.30 and -2.65°C, at the locations of Test Nos. 1 and 2, respectively. In the present study, no attempt was made to mathematically represent the temperature-dependence of the creep response.

The effects of time and stress on creep strain were expressed by two mutually independent functions. Only primary creep was considered.

Two different types of time function were selected to represent attenuating and non-attenuating creep strain. Ladanyi (1982) made the following statement with regard to the representation of pressuremeter creep test results: "For (the) low stress range, the power law might not be the best solution, and a hyperbolic approximation would probably give a better fit, because, at low stresses, below the long-term strength limit, one can expect to get an attenuating creep and not necessarily continuously increasing creep strains, as implied by the power law". This was observed to be the case for the results of the present study. Stages 1, 2, and 3 of Test No. 1 and stages 1 and 2 of Test No. 2, which displayed attenuating creep, were approximated by a linear-fractional relationship between creep strain and time. The final stages of each test exhibited continuously increasing creep strains. In these cases, a power relation between strain and time was used to represent the test data. In all cases, the nature of the mathematical form selected was compatible with the type of response observed, allowing for consistent extrapolation beyond test results.

The condition of similarity between stress-strain isochrones was approximated by a single function form. Each curve consisted of only four data points in the case of Test No. 1, and three data points in the case of Test No. 2, corresponding to respective applied pressure increments. In each case, the stress-dependence of the creep strain was expressed by a power law.

The following two relationships were, therefore, proposed to represent the experimental data, during primary creep: For attenuating creep,

$$\varepsilon_{cr} = (p - p_o)^a \cdot \{ft / (g + t)\} \quad , \tag{3.7}$$

and, in the case of continuously increasing strains,

$$\varepsilon_{cr} = B(p - p_o)^a t^b \quad , \tag{3.8}$$

in which ε_{cr} is the borehole circumferential creep strain, p is the pressure applied to the walls of the borehole, p_o is the far-field pressure, and a, f, g, B, and b are equation parameters. It was assumed that p_o, the radial pressure in the medium at $r = \infty$, was equal to zero.

For Test No. 1, stages 1, 2, and 3 were represented by equation 3.7, in which:

$a = 2.14$

$f = 0.0199\ \text{MPa}^{-2.14}$

and $g = 3071$ min.

Stage 4 was represented by equation 3.8, in which:

$a = 2.14$

$b = 0.47$

and $B = 1.51 \times 10^{-4}\ \text{MPa}^{-2.14} \cdot \text{min}^{-0.47}$.

Units of stress in MPa and time in minutes were assumed.

For Test No. 2, stages 1 and 2 were represented by equation 3.7, in which:

$a = 2.10$

$f = 0.03040\ \text{MPa}^{-2.10}$

and $g = 2947$ min.

Stage 3 was represented by equation 3.8, in which:

$a = 2.10$

$b = 0.50$

and $B = 1.54 \times 10^{-4}\ \text{MPa}^{-2.10} \cdot \text{min}^{-0.50}$.

Units of stress in MPa and time in minutes were assumed.

Statistical indices which describe the quality of fit achieved using the above-stated values of the parameters are presented in Table 3.7. Curves described by equations 3.7 and 3.8 are shown in Figures 3.13 and 3.15 along with the actual data points. The development of the creep response in stress-strain-time space, as expressed by these equations, is also shown in Figure 3.14, for Test No. 1, and in Figure 3.16, for Test No. 2. The equations provided satisfactory representation of the experimental data, for each of the applied pressures. The results should be considered to be applicable only within the range of stresses investigated.

TABLE 3.7 PRECISION INDICES (COEFFICIENT OF DETERMINATION, r^2, AND COEFFICIENT OF VARIATION, v) OF THE APPROXIMATIONS (3.7) AND (3.8) - (BASED ON DATA POINTS AT ONE HOUR INTERVALS)

Applied Pressure (MPa) (Average)	Equation	Indices of Precision	
		v(%)	r^2
TEST NO. 1:			
0.855	(3.7)	0.89	0.821
1.77	(3.7)	0.08	0.998
2.83	(3.7)	0.04	0.996
3.47	(3.8)	0.01	0.972
TEST NO. 2:			
0.846	(3.7)	0.10	0.998
1.79	(3.7)	0.02	0.999
2.78	(3.8)	0.01	0.984

Cavity circumferential creep strain rates, $\dot{\varepsilon}_{cr}$, may be expressed as:

$$\dot{\varepsilon}_{cr} = (p - p_o)^a \cdot \{fg / (g + t)^2\} \quad , \tag{3.9}$$

in accordance with equation 3.7, or as:

$$\dot{\varepsilon}_{cr} = Bb(p - p_o)^a \, t^{b-1} \quad , \tag{3.10}$$

in accordance with equation 3.8. Curves described by equations 3.9 and 3.10 are shown in Figure 3.17, for Test No. 1, and in Figure 3.18, for Test No. 2, along with the actual data points.

For consistency with the published results presented in Section 3.1, pressuremeter creep test data approximated by equation 3.8 were generalized to the following form:

$$\varepsilon_e^{(c)} = K \, \sigma_e^a \, t^b \quad . \tag{3.11}$$

Equation 3.11 and equation 3.4 are the same. According to Shields et al. (1988b,d), the parameter B of the pressuremeter creep equation 3.8 and the parameter K of the general creep equation 3.11 are related by:

$$B = D \cdot K \quad , \tag{3.12}$$

in which

D = a factor which accounts for the decrease in stress with distance from the borehole wall

$$= (3/4)^{(a+1)/2} \cdot \left\{ \frac{(R_o / R_i)^{2/a}}{(R_o / R_i)^{2/a} - 1} \cdot \frac{2}{a} \right\}^a$$

where

R_o = outside radius of the thick cylinder of soil being tested by the pressuremeter

R_i = internal radius of the thick cylinder of soil, that is, the borehole radius.

In the present study, it was assumed that $R_o \to \infty$, which led to:

$$D = \frac{\sqrt{3}}{2} \left(\frac{\sqrt{3}}{a} \right)^a \quad .$$

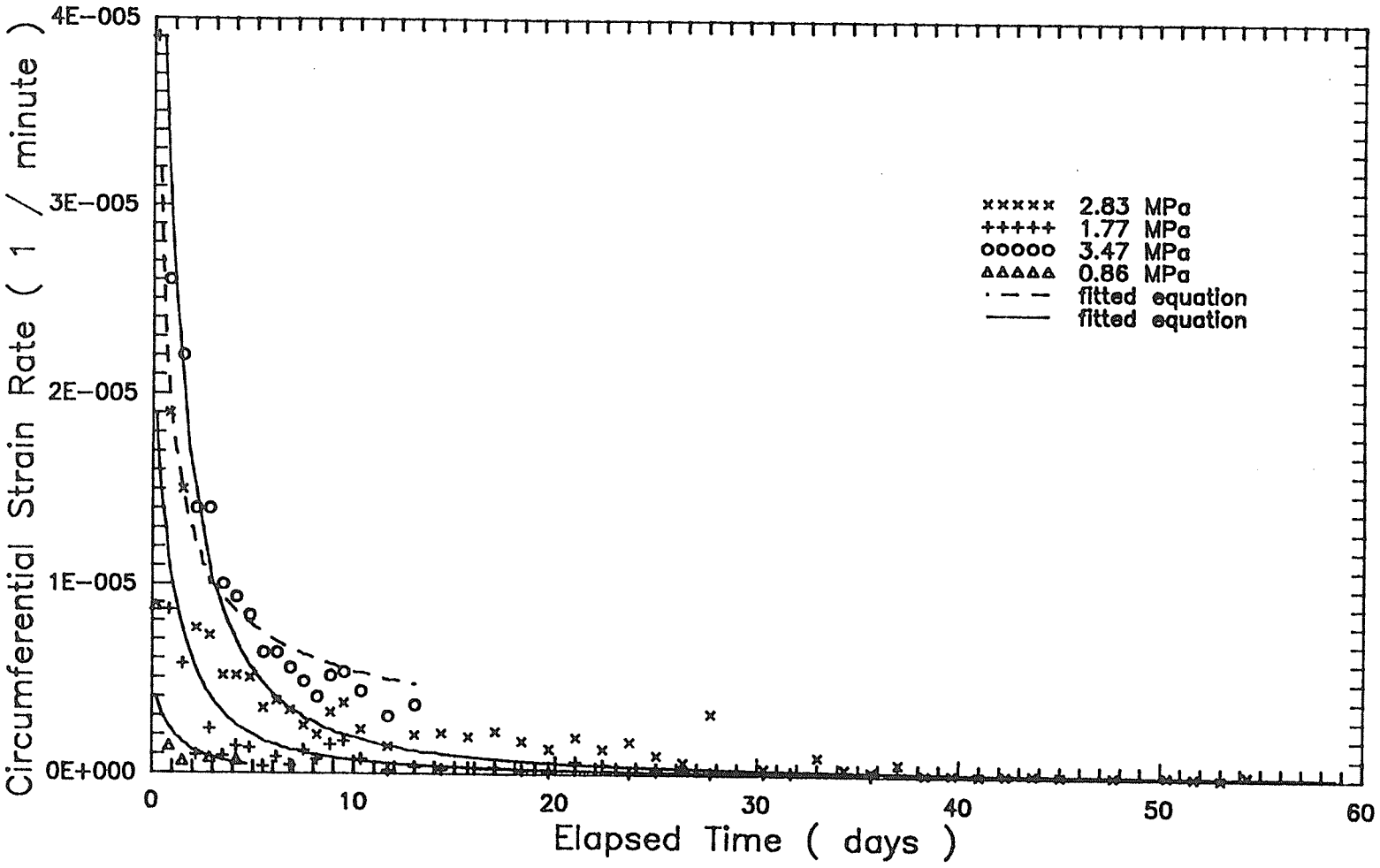

FIGURE 3.17 BOREHOLE CIRCUMFERENTIAL STRAIN RATE VERSUS TIME FOR EACH APPLIED PRESSURE (TEST NO. 1)

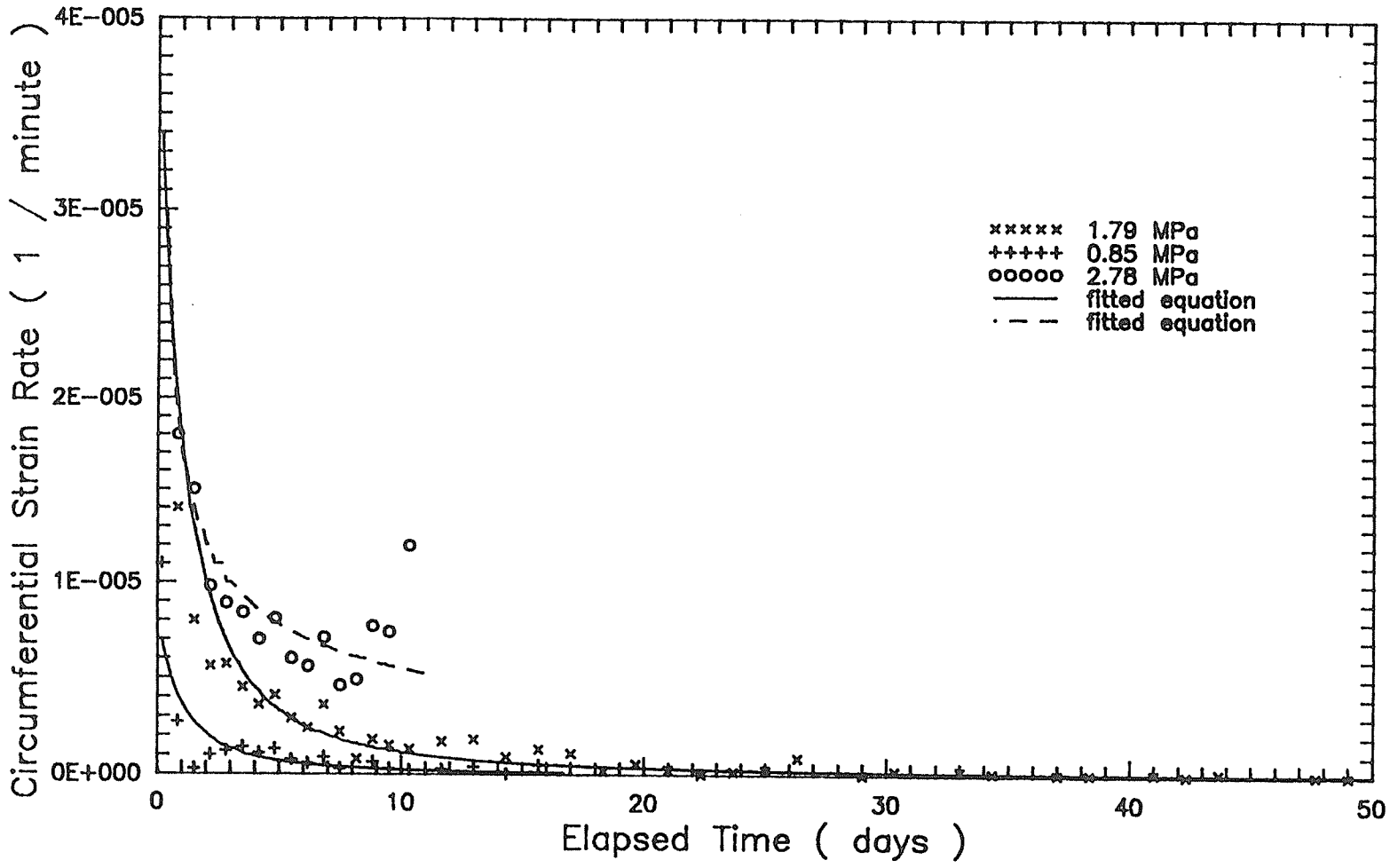

FIGURE 3.18 BOREHOLE CIRCUMFERENTIAL STRAIN RATE VERSUS TIME FOR EACH APPLIED PRESSURE (TEST NO. 2)

The parameters a, b, and B of equation 3.8, determined from Test No. 1 and those determined from Test No. 2 were similar. The average values from the two tests are:

$$a = 2.12$$

$$b = 0.49$$

and $$B = 1.53 \times 10^{-4}\ \text{MPa}^{-2.12} \cdot \text{min}^{-0.49}.$$

Substituting these values of the parameters into equation 3.12 gives:

$$K = 2.70 \times 10^{-4}\ \text{MPa}^{-2.12} \cdot \text{min}^{-0.49}.$$

Therefore, the general creep equation 3.11 is expressed as:

$$\varepsilon_e^{(c)} = 2.70\,(10^{-4}) \cdot \sigma_e^{2.12} \cdot t^{0.49},$$

for units of stress in MPa and time in minutes.

The error rectification algorithm proposed by Murat et al. (1986) to account for the effects of stress redistribution was not employed in the determination of the above-stated parameter values.

Sayles (1968) reported ranges of the creep exponents a and b for various frozen sands: $1.28 < a < 2.63$; and $0.45 < b < 0.63$. The values determined in the present study fall within these ranges.

Secant Creep Shear Modulus

If a cavity of initial radius r_i, located in an infinite medium, is expanded or contracted elastically, due to only a change Δp of the internal stress p, the following relationship is given from the Lamé's theory (Ladanyi, 1982):

$$\Delta r / r_i = \Delta p / 2G, \qquad (3.13)$$

in which Δr is the radial displacement of the cavity wall and G is the shear modulus. From a measured change in the cavity radius Δr, produced by Δp, the value of G is then:

$$G = \Delta p / 2 (\Delta r / r_i). \qquad (3.14)$$

For the pressuremeter creep test data, since the applied pressure - circumferential

creep strain curves are nonlinear, an average (secant) creep shear modulus was determined from the expression:

$$G_{cr} = (p - p_o) / 2\ \varepsilon_{cr} \quad . \tag{3.15}$$

The values of G_{cr} are plotted as a function of time in Figures 3.19 and 3.20 for Test Nos. 1 and 2, respectively. The secant creep shear modulus may be represented by:

$$G_{cr} = \frac{1}{2} (p - p_o)^{1-a} \cdot \{ (g + t) / ft \} \quad , \tag{3.16}$$

in accordance with equation 3.7, or by:

$$G_{cr} = \frac{1}{2} B^{-1} (p - p_o)^{1-a}\ t^{-b} \quad , \tag{3.17}$$

in accordance with equation 3.8. Curves described by equations 3.16 and 3.17 are shown in Figure 3.19, for Test No. 1, and in Figure 3.20, for Test No. 2, along with the actual data points.

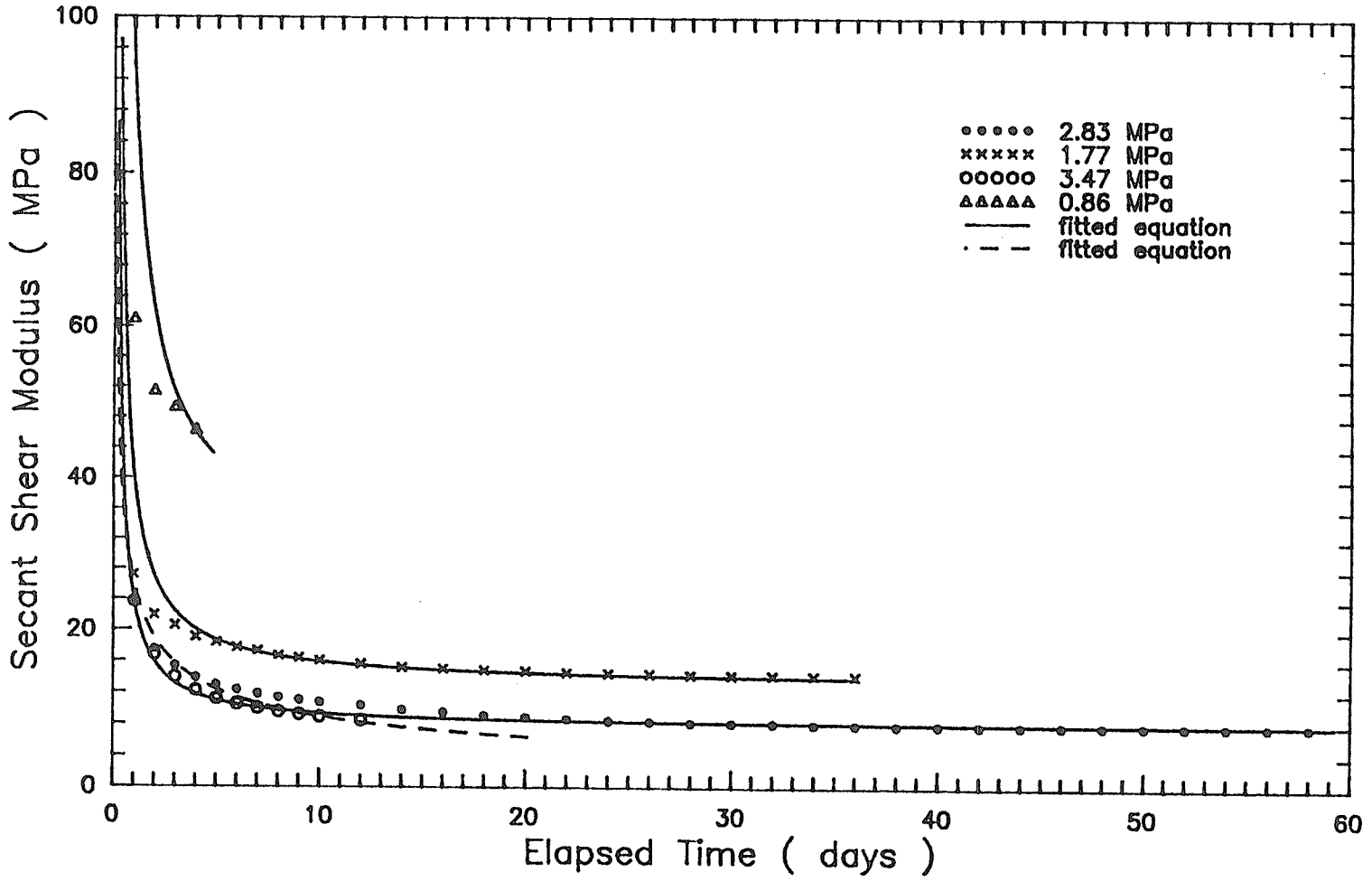

FIGURE 3.19 SECANT CREEP SHEAR MODULUS VERSUS TIME FOR EACH APPLIED PRESSURE (TEST NO. 1)

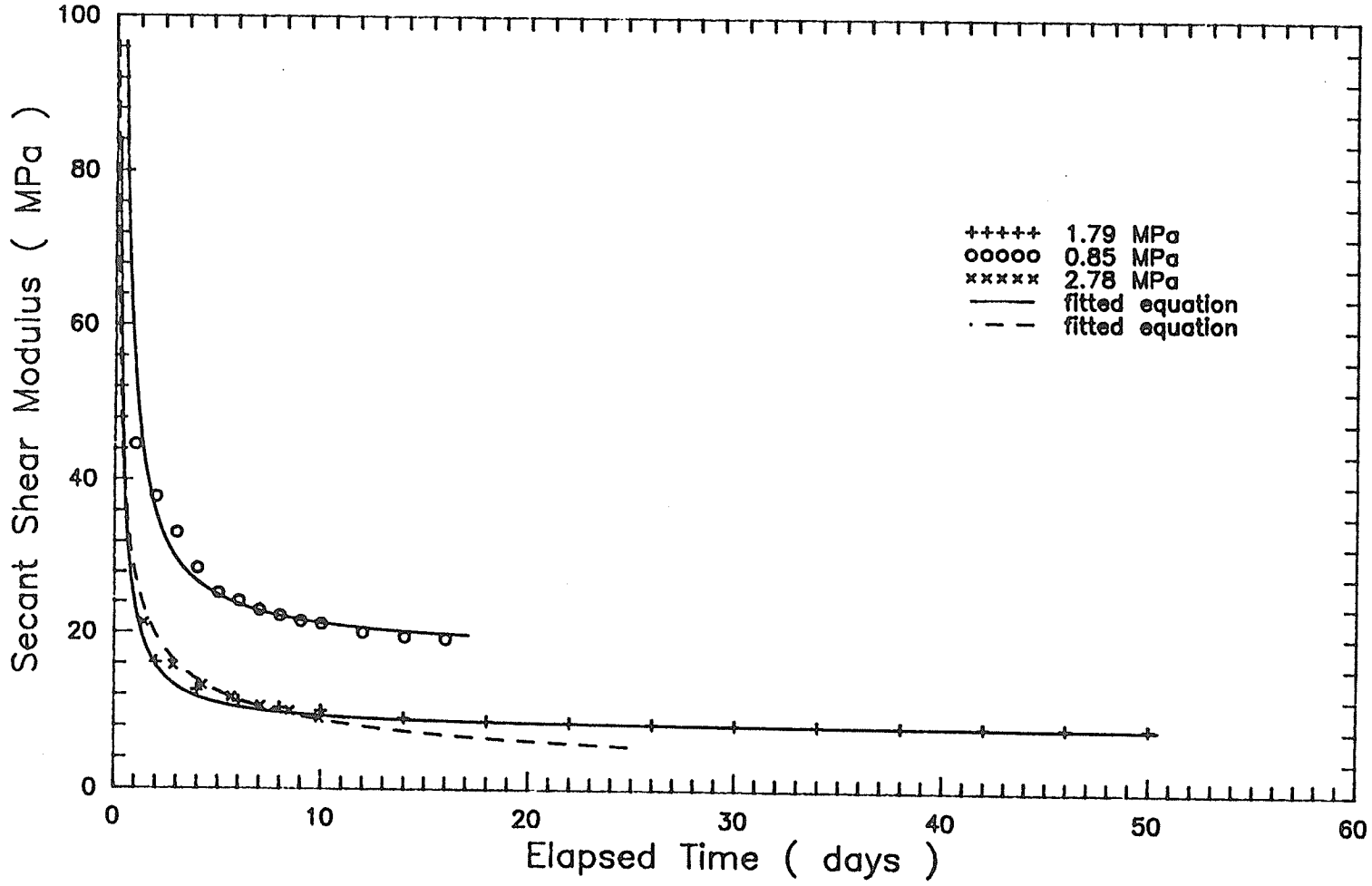

FIGURE 3.20 SECANT CREEP SHEAR MODULUS VERSUS TIME FOR EACH APPLIED PRESSURE (TEST NO. 2)

CHAPTER 4

CREEP ANALYSES AND PREDICTIONS

4.1 INTRODUCTION

Chapters 2 and 3 described two separate experimental investigations of the creep behavior of a frozen sand: (1) a rigid plate-load creep test; and (2) pressuremeter creep tests. The plate-load and pressuremeter creep test problems were subsequently analyzed, based on the constitutive relationships developed by Rahman (1988). In this Chapter, the method of analysis is described and a comparison of the predicted behavior with experimental results is presented.

4.2 REVIEW OF THE CONSTITUTIVE MODEL

The constitutive relationships developed by Rahman (1988) followed an approach suggested by Domaschuk et al. (1983, 1985). This was an extension of an incrementally isotropic stress-strain model proposed by Domaschuk and Wade (1969), for non-frozen soils. Therefore, the model is first described in this context.

The incremental constitutive relations were based on a simple modification of the isotropic linear elastic relations. The constant bulk and shear moduli were replaced with variable, stress-dependent, tangent bulk and shear moduli, K_t and G_t . These are readily related to the two components of material response: K_t is associated with the hydrostatic (volumetric) component and G_t is associated with the deviatoric (shear) component. The incremental stress-strain relations for the two responses were decoupled, for isotropic media, and expressed as:

$$\begin{aligned} \delta\sigma_m &= K_t \ \delta\varepsilon_{kk} \\ \delta s_{ij} &= 2G_t \ \delta e_{ij} \ , \end{aligned} \tag{4.1}$$

in which $\delta\sigma_m$ is the change of the mean normal stress, $\delta\varepsilon_{kk} = \delta\varepsilon_v$ is the volume

change, s_{ij} is the deviatoric stress change, and δe_{ij} is the change of deviatoric strains. The tangent moduli are defined as:

$$K_t = \delta\sigma_m / \delta\varepsilon_v$$
$$G_t = \delta\tau_{oct} / \delta\gamma_{oct} \quad , \tag{4.2}$$

where $\delta\tau_{oct}$ and $\delta\gamma_{oct}$ are the incremental octahedral shear stress and strain, respectively. Expressions were developed for K_t and G_t as functions of the octahedral normal and shear stresses or strains (Domaschuk and Wade, 1969; Domaschuk and Valliappan, 1975). The expressions were substituted into equations 4.1 which, upon addition, provided the following incremental stress-strain relationships:

$$\delta\sigma_{ij} = K_t \ \delta\varepsilon_{kk} \ \delta_{ij} + 2G_t \left(\delta\varepsilon_{ij} - \frac{1}{3} \ \delta\varepsilon_{kk} \ \delta_{ij} \right) \quad , \tag{4.3}$$

in which $\delta\sigma_{ij}$ and $\delta\varepsilon_{ij}$ are the stress and strain increment tensors and δ_{ij} is the Kronecker delta.

For frozen soil, Domaschuk et al. (1983) suggested extension of the constitutive model by the replacement of tangent bulk and shear moduli, K_t and G_t, with tangent bulk and shear creep functions, K_{ct} and G_{ct} . K_{ct} and G_{ct} depend on many factors, including stress level, time, temperature, ice content, unfrozen water content, and mineralogical composition of the soil. The authors used isotropic compression creep tests to determine K_{ct} , for which equation 4.3 was written as:

$$\delta\sigma_m = K_{ct} \ \delta\varepsilon_v \quad , \tag{4.4}$$

and constant mean normal stress triaxial compression creep tests to determine G_{ct}, for which equation 4.3 was written as:

$$\delta S_d = G_{ct} \ \delta\varepsilon_d \quad , \tag{4.5}$$

in which S_d and ε_d are the resultants of the deviatoric components of stress and strain. Hereafter, they are simply referred to as the resultant deviatoric stress

and strain.

Rahman (1988) developed expressions for the tangent bulk and shear creep functions of a frozen sand. The index properties and the temperature (-3°C) of the sand were held constant and K_{ct} and G_{ct} were evaluated as functions of the stress level and time.

Solution for the Bulk Creep Function

A single multi-stage isotropic compression test was performed to evaluate the tangent bulk creep function. Mean normal stress-volumetric strain curves (isochrones) were constructed, for various elapsed times, from the test data.The following linear expression was proposed for the secant bulk creep function, K_{cs} , as a function of the mean normal stress:

$$K_{cs} = \sigma_m / \varepsilon_v = K_o + \beta\sigma_m \quad , \tag{4.6}$$

in which K_o and β are parameters representing the intercept or initial secant bulk creep function and slope, respectively, of the straight line of equation 4.6. The parameter β was observed to be a function of time and the following relationship was suggested:

$$\beta = n\, e^{-mt} \quad , \tag{4.7}$$

where n and m are material constants. The expression for K_{ct} was derived by first rewriting and then differentiating equation 4.6. This expression was given as:

$$K_{ct} = K_o (1 + (\beta / K_o) \sigma_m)^2 \quad , \tag{4.8}$$

which for the particular test data was written as:

$$K_{ct} = 10250 (1 + (\beta / 10250) \sigma_m)^2 \quad ,$$

where $$\beta = 180\, e^{-0.0045\, t}$$

in accordance with equation 4.7. In the above, the time and mean normal stress were expressed in hours and KPa, respectively.

Solution for the Shear Creep Function

A series of constant mean normal stress triaxial compression tests were performed to evaluate the tangent shear creep function. Resultant deviatoric stress-strain curves (isochrones) were constructed, for various elapsed times, from the test data. G_{ct} was determined graphically as the instantaneous slope of the stress-strain curves. The following hyperbolic type of dependence of G_{ct} on the ratio of mean normal stress to the resultant deviatoric stress was proposed:

$$G_{ct} = \frac{\sigma_m / S_d}{a + b\,(\sigma_m / S_d)} \quad , \tag{4.9}$$

in which a and b are equation parameters. The parameter a was observed to be a function of time and the following power relationship was suggested:

$$a = c\,t^{\alpha} \quad , \tag{4.10}$$

where c and α are constants representing the intercept at t = 1 hour and slope, respectively, of the straight line in a logarithmic plot of equation 4.10. In the same manner, the parameter b was observed to be a function of time and the following power relationship was suggested:

$$b = m\,t^{n} \quad . \tag{4.11}$$

where m and n are parameters representing the intercept at t = 1 hour and slope, respectively, of the straight line in a logarithmic plot of equation 4.11. In this equation, the parameter m was observed to be a function of the mean normal stress and the following power relationship was suggested:

$$m = m_1\,\sigma_m^{\beta} \quad . \tag{4.12}$$

where m_1 and β are constants representing the intercept at σ_m = 1 KPa and slope, respectively, of the straight line in a logarithmic plot of equation 4.12. The expression for G_{ct} was, therefore, written as:

$$G_{ct} = \{\, m_1\,\sigma_m^{\beta}\,t^{n} + c\,t^{\alpha}(S_d / \sigma_m)\,\}^{-1} \quad , \tag{4.13}$$

which for the particular test data was given as:

$$G_{ct} = \{3 \times 10^{-5}\, \sigma_m^{-0.205}\, t^{0.147} + 1 \times 10^{-5} t^{0.23} (S_d/\sigma_m)\}^{-1} .$$

In the above, the time is expressed in hours, and the mean normal and resultant deviatoric stresses are expressed in KPa.

Failure Criterion

Rahman (1988) observed that samples underwent volume change during shear deformation in constant mean normal stress triaxial compression tests. The samples initially underwent volume reduction followed by positive dilation. The resultant deviatoric stress at which dilation first occurred coincided with the stress at which accelerating creep (failure) first occurred. The relationship between the resultant deviatoric stress at failure, S_{df} , and the mean normal stress was found to be linear and was expressed as:

$$S_{df} = S_o + m\, \sigma_m \quad , \qquad (4.14)$$

in which S_o and m are parameters representing the intercept and slope, respectively, of the straight line of equation 4.14. For the particular test data, the equation was written as:

$$S_{df} = 100 + 1.3\, \sigma_m \quad ,$$

for stresses expressed in units of KPa. Equation 4.14 was proposed as a failure criterion in which failure is defined as the onset of tertiary creep.

4.3 METHOD OF ANALYSIS

4.3.1 General

In general, to model creep phenomena in practical problems it is necessary to take into account the stress history of the soil. The stresses will be redistributed by the process of creep, even if the applied loads remain constant. To include these effects, creep problems are generally solved using incremental procedures. In most cases, numerical methods are employed. The inclusion of creep behavior

in a finite element approach has been described in several publications. Zienkiewicz (1971) presented an overview of this subject.

There are two approaches to present a constitutive formulation which is valid for variable stress conditions: (1) a memory theory, in which the material remembers its past explicitly and responds to the present in a manner which reflects its past history; and (2) an equation of state theory, in which the response of the material depends on its present state explicitly. An example of the former approach is the theory of non-linear hereditary creep (Rabotnov, 1966). This theory has found some practical application in the field of frozen soil mechanics. In the latter approach, for a constant stress condition, the stress, strain, strain rate, and time are related in their implicit or explicit form. A rule or hypothesis is then proposed to describe the nature of this relation for a variable stress condition. It allows the prediction, from constant stress creep curves, of the effect of varying the stress with time.

These rules are sometimes referred to as engineering theories of creep. The two most widely used are the time-hardening theory and the strain-hardening theory. In the former, it is assumed that the creep strain rate depends on the present values of stress and time. In the latter, it is assumed that the creep strain rate depends on the present values of stress and strain. The simplest formulation is the ageing theory or total strain theory. In this theory, it is assumed that the total strain depends on the present values of stress and time. Many formulations have been proposed for predicting creep strains under a continuously changing stress condition, but none can predict creep behavior in a completely general manner.

In some cases, approximate methods of solution are possible in which incremental procedures are generally not required. These are frequently used to obtain analytical solutions. According to Ladanyi (1972), the following three methods have found increasing application in practice: (1) Hoff's elastic analogue (Hoff, 1954; Finnie and Heller, 1959; Odqvist, 1966); (2) method of time-dependent

strength (Vyalov, 1959; Vyalov et al., 1962) or limiting strain (Turner, 1966); and (3) method of isochronous stress-strain curves (Vyalov, 1959; Vyalov et al., 1962; Smith and Sidebottom, 1965).

The procedure used in the present analysis is directly analogous to the third approximate method stated above. In this method, for a fixed time, the nonlinear creep problem is solved as a nonlinear time-independent problem, using the isochronous stress-strain relationship. The method is based on the ageing theory of creep. The theory states that a strain induced at a specified time is not affected by the stress applied at a preceding time. It is, therefore, strictly applicable only in problems for which the applied load is constant. Moreover, in these cases, it is assumed that the effect of redistribution of stress with time may be neglected.

As previously described, in the development of the constitutive relationships used in the present study, both changes in volume produced by the mean normal stress, and deviatoric strains produced by the resultant deviatoric stress were considered. Expressions were derived for the tangent bulk and shear creep functions. In the analysis, for a fixed time, these creep functions were assumed to represent variable, stress-dependent, tangent bulk and shear moduli, K_t and G_t , and were used in the incremental stress-strain relationships 4.3. Therefore, for a particular problem, a separate solution was obtained, for each specified time, in the same manner as for the corresponding problem in nonlinear elasticity. Specifically, for each fixed value of time, a numerical analysis was carried out using an incremental, time-independent, finite element computer program.

4.3.2 Finite Element Computer Program

The finite element computer program used in the present analysis is a modified version of the program developed by Valliappan (1974). The program was written in FORTRAN IV and was implemented on the AMDAHL 5870 mainframe computer system at the University of Manitoba. A listing of the program and guidelines for data input to the program are given in Appendix B.

The program is limited to linear or physically nonlinear elastic analyses of solids of revolution (axisymmetric solids) subjected to axially symmetric loading. Two types of elements may be used: (1) an axisymmetric ring element of triangular cross-section with a linear displacement model; and (2) an axisymmetric ring element of quadrilateral cross-section (Figure 4.1). In the latter, four triangular elements with linear displacement models are grouped to form a quadrilateral. The stiffness of each triangle adds directly to the quadrilateral element stiffness. The number of unknown displacements is reduced by condensation of the degrees of freedom of the internal node. In addition, the quadrilateral elements ensure that the solution is independent of the skew of a subdivision mesh. As indicated in Figure 4.1, the cylindrical coordinates r, z, and θ are used to denote the radial, vertical, and tangential directions, respectively. For axisymmetric problems, all properties and variables are independent of the θ coordinate.

The solution of problems involving material nonlinearity is accomplished using incremental or stepwise procedures. The program includes two incremental schemes: (1) the basic incremental procedure; and (2) the midpoint Runge-Kutta scheme. In the basic incremental procedure, the load is subdivided into small increments and is applied one increment at a time. During the application of each increment, a linear problem is assumed. For each loading step, the solution is obtained as an increment of the displacements. To compute the increment of the displacements, a fixed value of the stiffness, evaluated at the end of the previous increment, is used. Hence, after the application of the i^{th} increment, the equilibrium equation for a single element is given by:

$$[\, k_{i-1} \,] \{ \Delta q_i \} = \{ \Delta Q_i \}$$

where

$$[\, k_{i-1} \,] = [\, k_{i-1} (\{ q_{i-1} \} , \{ Q_{i-1} \}) \,] \quad , \tag{4.15}$$

in which $[\, k_{i-1} \,]$ is the stiffness evaluated at the end of the previous increment, and $\{ \Delta q_i \}$ and $\{ \Delta Q_i \}$ are the increment in displacements and loads, respectively.

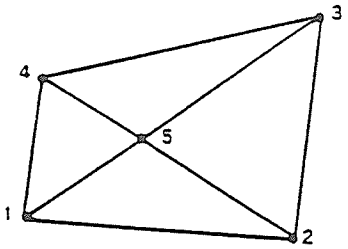

Quadrilateral formed by four triangles

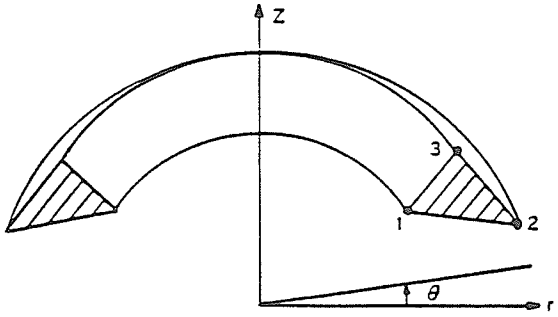

Axisymmetric triangular ring element

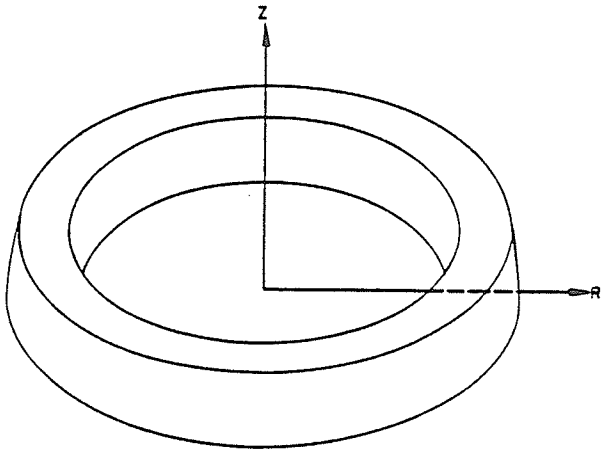

THE FINITE ELEMENT IDEALIZATION

FIGURE 4.1 TRIANGULAR AND QUADRILATERAL AXISYMMETRIC RING ELEMENTS

The **displacement** increments are accumulated to obtain total values at each loading step. The incremental process is repeated until the total load is attained. The basic incremental procedure is shown schematically in Figure 4.2.

The midpoint Runge-Kutta scheme is a modification of the basic incremental procedure. In this scheme, two cycles of analysis are performed for each load increment. In the first cycle, half of the increment of loads is applied and the displacements at the midpoint of the increment $\{q_{i-1/2}\}$ are computed, as follows:

$$\begin{aligned} [\, k_{i-1}\,]\{\Delta q_{i-1/2}\} &= \{\Delta Q_i\}/2 \\ \{q_{i-1/2}\} &= \{q_{i-1}\} + \{\Delta q_{i-1/2}\} \quad . \end{aligned} \tag{4.16}$$

In the second cycle, the stiffness matrix evaluated at the midpoint of the i^{th} increment $[\, k_{i-1/2}\,]$ is used to compute the full displacement increment. Hence, for i^{th} increment, the equilibrium equation for a single element is given by:

$$[\, k_{i-1/2}\,]\ \{\Delta q_i\} = \{\Delta Q_i\} \quad . \tag{4.17}$$

The basic method for a full and halved increment, and the midpoint Runge-Kutta scheme are compared schematically in Figure 4.2. It can be seen that the latter procedure improves the solution. However, it requires additional computational effort.

At every stage of the incremental procedure, new element stiffness matrices are computed. A prerequisite to this computation is the current value of the material parameters. In the case of isotropic elastic behavior, two material parameters, such as the tangent bulk and shear moduli, are required. The moduli are functions of the state of stress within the finite element. In addition, once the increments of displacement are determined, the increments of the strain and stress are evaluated by using the strain-displacement equations and the current stress-strain relationships. The stress increments are accumulated to obtain total values at each loading step. Based on the new state of stress, moduli for the next loading step are calculated for each element.

Valliappan (1974) described the theoretical background of the central features

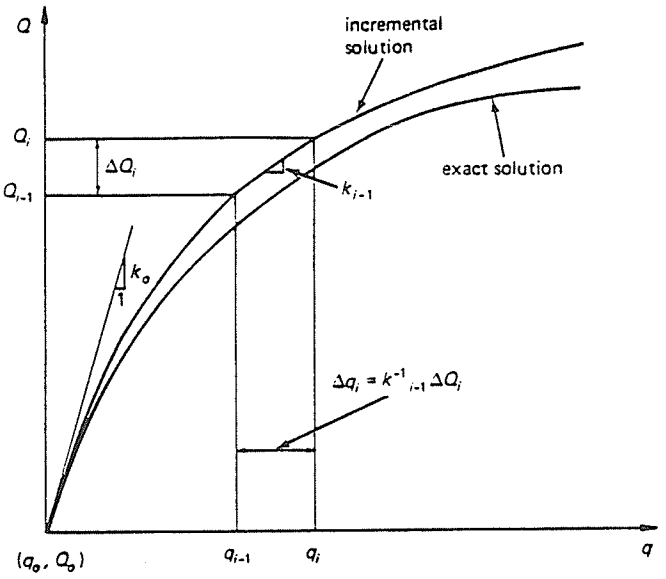

Basic incremental procedure.

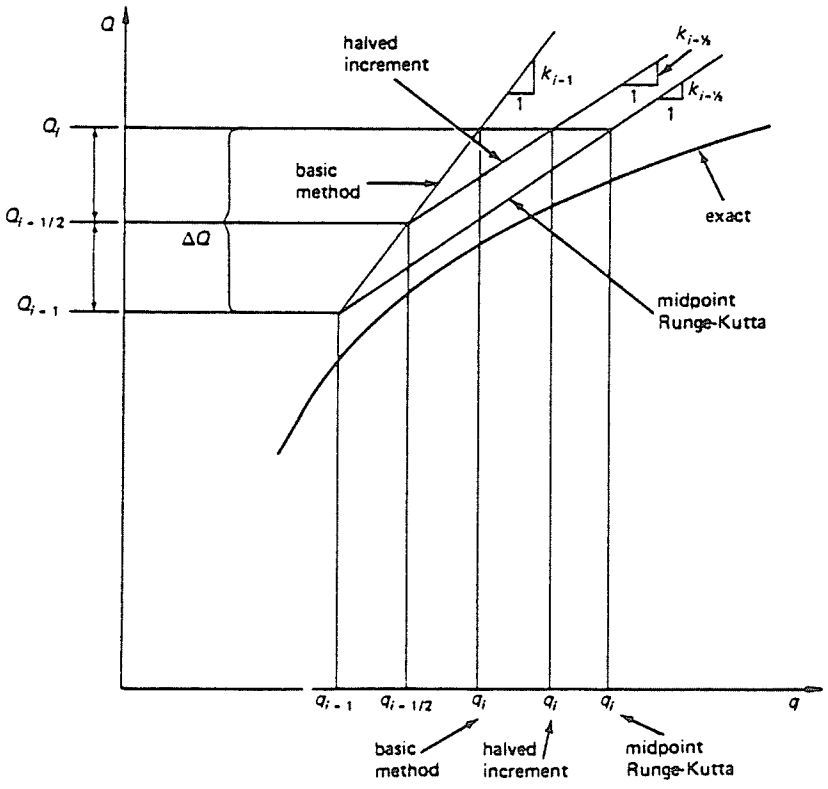

Midpoint Runge-Kutta incremental scheme.

FIGURE 4.2 BASIC INCREMENTAL PROCEDURE AND MIDPOINT RUNGE - KUTTA SCHEME

of the program. In addition, a detailed examination of the finite element method of analysis may be found in several standard textbooks. The principal program modifications required for the present analysis were as follows:

1. The constitutive relationships described in Section 4.2 were incorporated into the program.

   The tangent bulk and shear creep functions were included in separate subroutines. The experimentally determined parameters in each function are specified as input data. The program permits the variation of the parameters from element to element. It also allows selected elements to be treated as linear materials. The proposed failure criterion was also included in the program. The failure condition is checked for individual elements, at each loading step.

2. A procedure to permit the analysis of problems for different values of time was incorporated into the program. The procedure follows the approximate method of solution described in Section 4.3.1.

   The size and number of time steps are specified as input data. At each step, the value of time is held constant in the tangent bulk and shear creep functions. A solution is obtained, using the above-mentioned incremental procedures, in the same manner as for the corresponding problem in nonlinear elasticity. The program writes the solution at the completion of the final loading increment, for the particular time step. Subsequently, the stresses and displacements are initialized at zero and the problem of the succeeding time step is analyzed in the same fashion. The initial moduli values for the new time step are based on the stresses determined following the final load increment of the previous time step.

Solution Algorithm

In accordance with the above-stated program modifications, the procedures

of the analysis may be briefly outlined as follows:

1. The problem specifications were read, including geometry, material properties, boundary load and displacement conditions, and time step information. The program printed this input data. The nodal displacements and element stresses were initialized at zero.

2. The initial or in-situ stresses were computed for each element based on the depth of the element, the average unit weight of the soil, and the coefficient of earth pressure at rest. The mean normal and resultant deviatoric stresses were determined. On the basis of these stresses, the initial tangent bulk and shear moduli were evaluated for each element using equations 4.8 and 4.13, respectively. A value of time of one minute was assumed in these calculations. For elements specified as linear materials, constant tangent bulk and shear moduli values were assigned. The program printed the initial stresses and moduli values for each element. The time was fixed at a constant value for the first time step.

3. The element stiffness matrices were computed based on the current values of the tangent bulk and shear moduli. The element load vectors were determined. Gauss quadrature was used to perform the integrations necessary to obtain the element stiffnesses. The internal degrees of freedom of quadrilateral elements were eliminated by the process of static condensation. The global stiffness matrix and load vector were assembled using the direct stiffness method. If necessary, modifications were made to account for skewed boundary conditions and displacement boundary conditions.

4. The increments of nodal displacement were computed for an applied increment of loading. The system of equilibrium equations was solved by Gaussian elimination. The displacement increments were accumulated to obtain total values at each loading step.

5. The increments of strain were computed for each element from the increments of nodal displacement determined in step 4. The increments of stress were evaluated for each element using the stress-strain equations 4.3. The current values of the tangent bulk and shear moduli were used in the equations. The stress increments were accumulated to obtain total values at each loading step. The mean normal and resultant deviatoric stresses were calculated for each element. In this calculation, both the accumulated values of stress and the in-situ stresses from step 2 were considered. On the basis of these stresses and the current value of the time, new values of tangent bulk and shear moduli were evaluated for each element using equations 4.8 and 4.13, respectively. For elements specified as linear materials, the constant moduli assigned in step 2 were not revised.

6. Steps 3 to 5 were repeated for subsequent loading steps, in accordance with the basic incremental procedure (Figure 4.2). The time was held constant for all load increments during a time step. After the final load increment was applied, the program printed the nodal displacement values as the solution for the particular time step. The program also printed the stresses and current moduli values for each element. In addition, the elements for which the failure condition (equation 4.14) was exceeded were indicated.

7. The time was fixed at a new constant value, for the next time step. The nodal displacements and element stresses were initialized at zero. The initial values of the tangent bulk and shear moduli were computed using equations 4.8 and 4.13, respectively. In this computation, the current value of the time, and the stresses determined following the final load increment of the previous time step, were used. Steps 3 to 6 were repeated beginning with the application of the first load increment.

Any variation of both applied loading increments and time steps could be

considered in a single program run, subject to restrictions on available computer time.

4.4 CREEP DEFORMATION ANALYSES

4.4.1 Plate-Loading Creep Test Problem

Problem Characteristics and Assumptions

Analyses were performed to predict plate displacements for the plate-load creep test described in Chapter 2. A homogeneous soil mass was assumed. The in-situ stresses were computed based on a measured average unit weight of the soil of 15.8 KN/m^3 and an assumed value of 1.0 for the coefficient of earth pressure at rest. For the shallow depths considered, the in-situ stresses did not significantly contribute to the subsequent stresses and therefore did not affect the deformation behavior. As previously mentioned, the tangent bulk and shear creep functions and failure criterion, developed by Rahman (1988) for this soil, were used in the analyses.

Two types of loading conditions were assumed. In the first type, the plate was considered to be completely flexible. In the finite element idealization, a uniform pressure was applied to simulate this condition. Figure 4.3 shows the final mesh layout and the specified boundary conditions used in the analysis. The number of nodal points was 284 and the number of elements was 260. In the second type of loading condition, the plate was considered to be rigid. In the finite element idealization, the plate was represented by elements specified as linear materials. Large values of the bulk and shear moduli were assigned to these elements to simulate the rigid condition. A uniform pressure was applied to the elements representing the plate. This simulation of the problem was considered adequate, since no attempt was made to examine plate-soil interaction or the response of the plate itself. Figure 4.4 shows the final mesh layout and the specified boundary

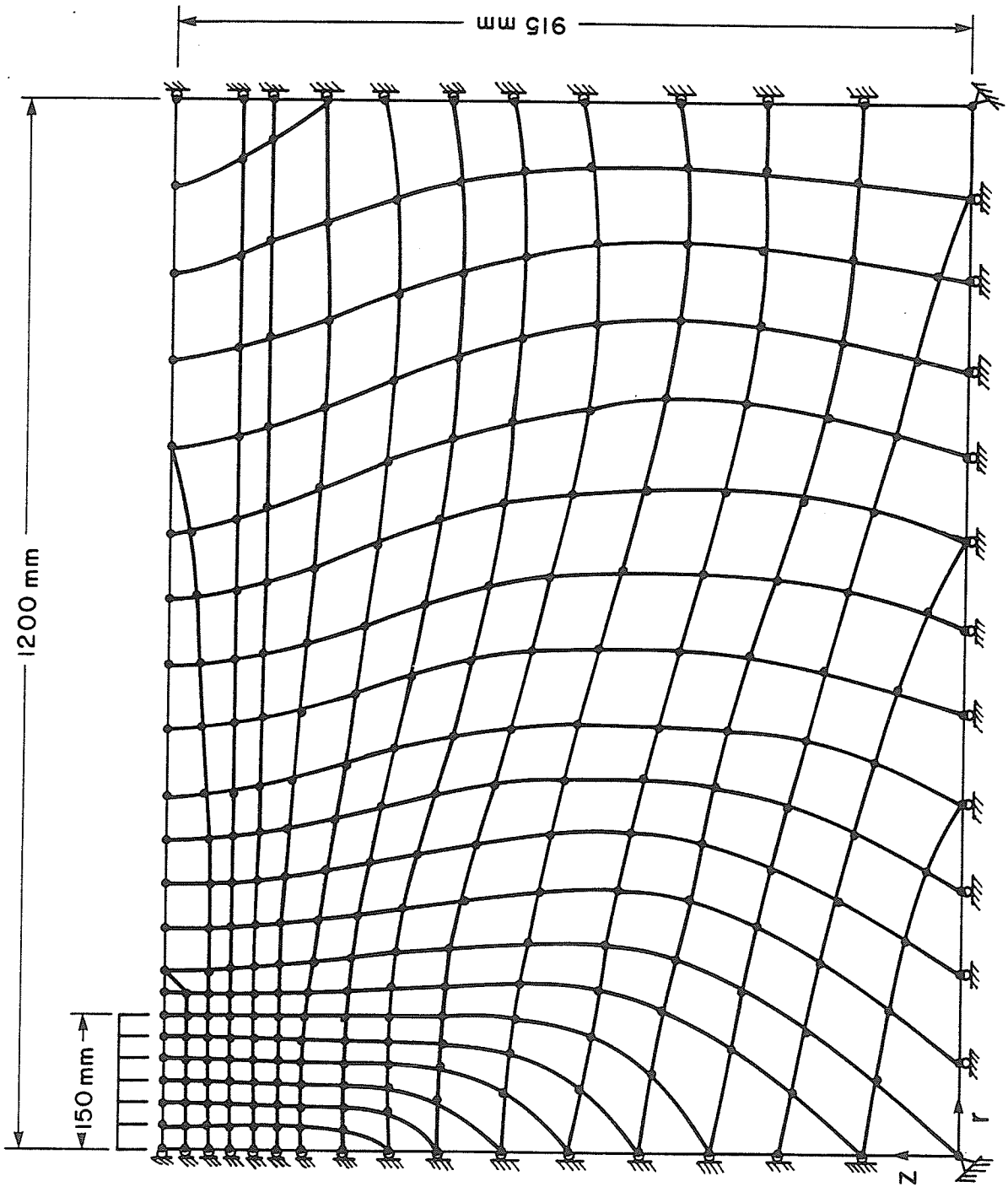

FIGURE 4.3 FINITE ELEMENT IDEALIZATION FOR THE PLATE - LOAD TEST PROBLEM: PERFECTLY FLEXIBLE PLATE CONDITION

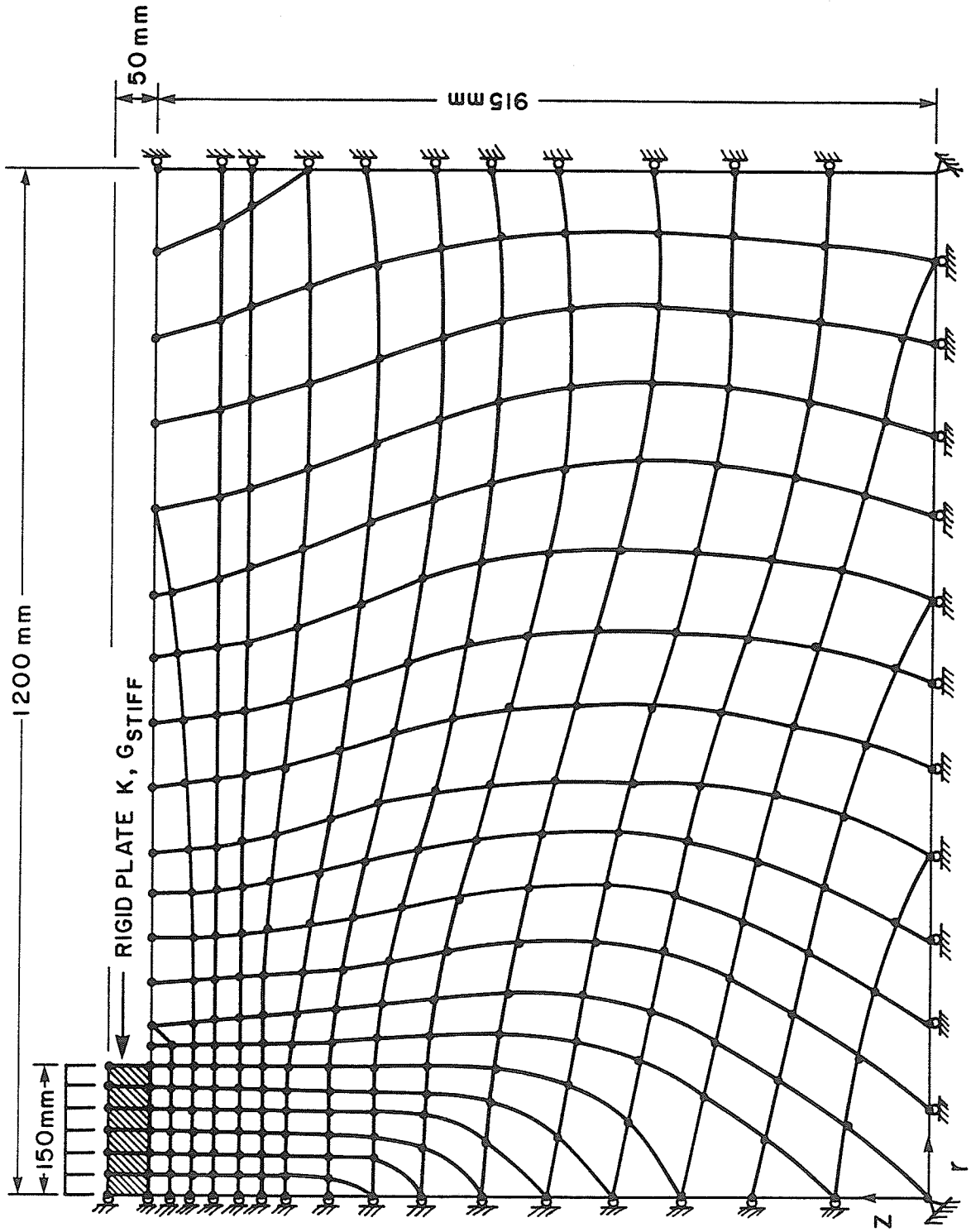

FIGURE 4.4 FINITE ELEMENT IDEALIZATION FOR THE PLATE - LOAD TEST PROBLEM: RIGID PLATE CONDITION

conditions used in the analysis. The number of nodal points was 291 and the number of elements was 266.

The subdivision meshes and boundary conditions used in the flexible and rigid plate analyses were similar. The meshes were made finer near the area of load application. The elements had balanced dimensions and gradually increased in size away from the area of load application. Since the problem was symmetric about the z-axis, it was only necessary to discretize the continuum on one side of this axis. Therefore, the nodal points on the z-axis were restrained against radial displacement. The side and bottom boundaries were placed at a sufficient distance from the area of load application so that, at the boundaries, the radial and vertical displacements, respectively, were negligible. Thus, the nodal points on the side boundary were restrained against radial displacement and the nodal points on the bottom boundary were restrained against vertical displacement.

The basic incremental procedure, described in Section 4.3.2, was used in the analyses. In general, ten load increments were applied at each time step. Improved accuracy could have been obtained by using a greater number of load increments, or by employing the midpoint Runge-Kutta scheme. However, this was not considered to be practical for the present analyses because of the large amount of computational effort required for each time step.

Comparison of Flexible and Rigid Plate Analyses

As indicated above, both a flexible and rigid plate loading condition were considered. The results of analyses based on each of these conditions were compared. Figure 4.5 shows the reactive pressure distributions at a time of one minute for an applied pressure of 0.88 MPa, for both flexible and rigid plate analyses. For the flexible plate, the distribution was approximately uniform, but the pressure decreased near the edge of the plate. For the rigid plate, the pressure increased consistently to a maximum near the edge of the plate. The reactive pressure

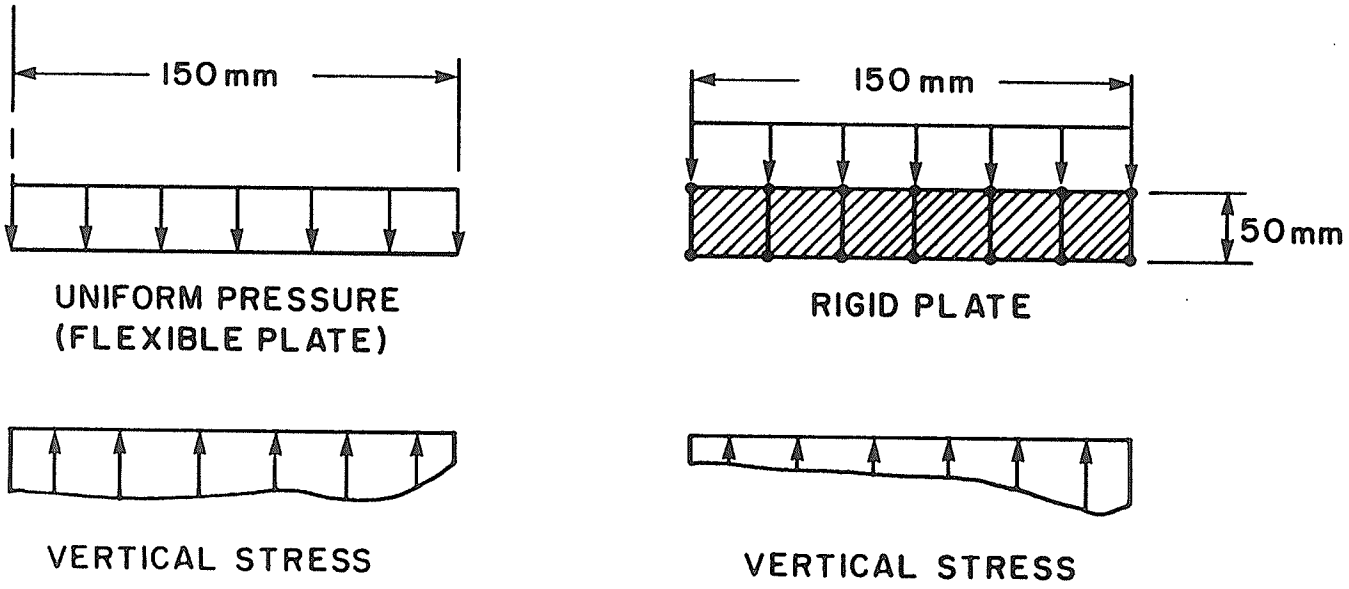

FIGURE 4.5 REACTIVE PRESSURE DISTRIBUTIONS FOR A TIME OF ONE MINUTE: p = 0.88 MPa

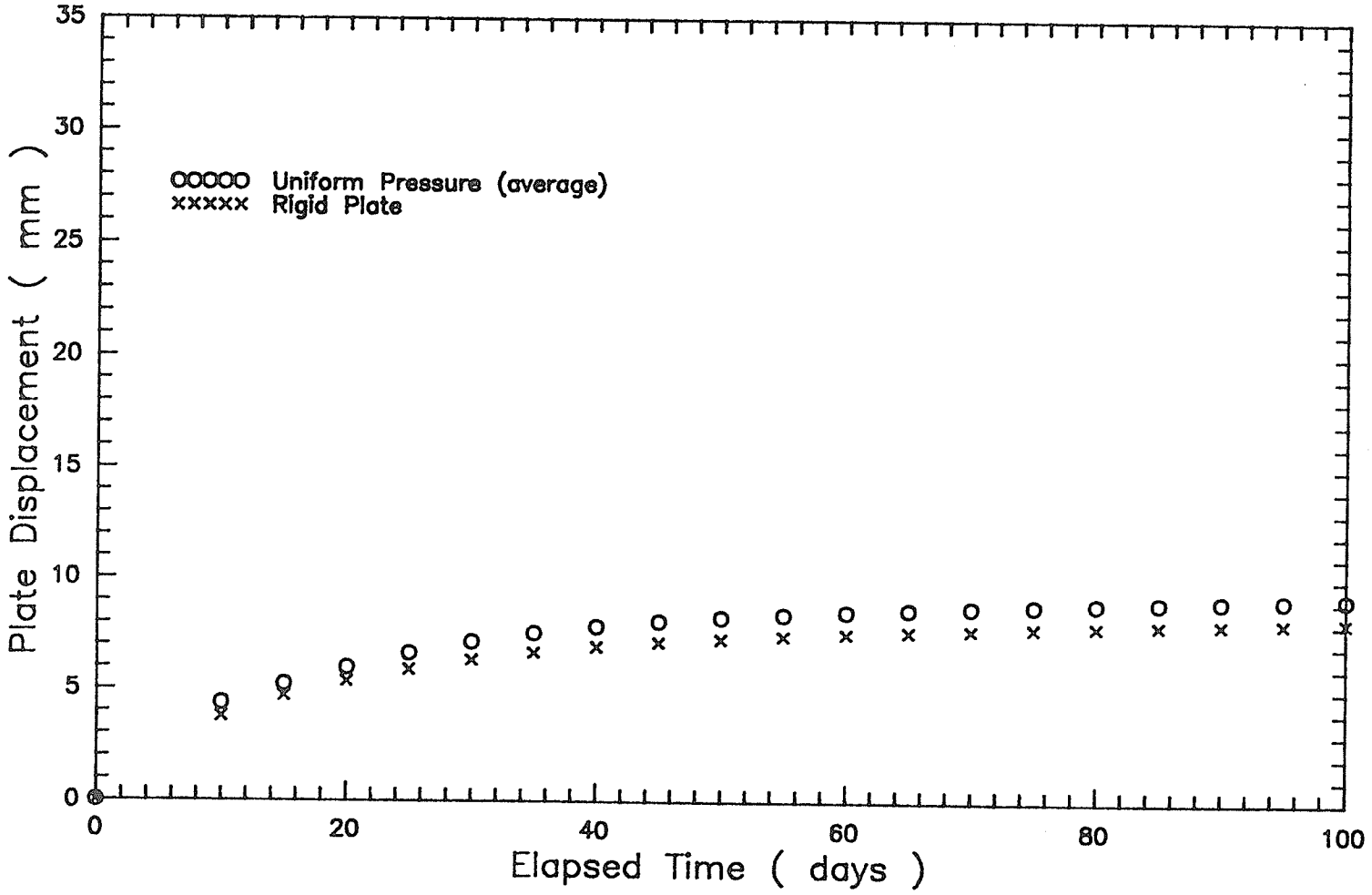

FIGURE 4.6 PLATE DISPLACEMENT VERSUS TIME FOR FLEXIBLE AND RIGID PLATE CONDITIONS: p = 0.88 MPa

distributions changed significantly for different values of the applied pressure.

Figure 4.6 shows the plate displacement as a function of time for an applied pressure of 0.88 MPa, for both flexible and rigid plate analyses. For the flexible plate condition, the displacement was determined as the average displacement of the nodes immediately below the plate. The displacement determined for the rigid plate was slightly smaller than the average displacement determined for the flexible plate. The maximum difference in displacement for the two conditions was about eight percent. The rigid plate condition (Figure 4.4) was used in subsequent analyses, for comparison with the experimental results.

Representation of the Shear Creep Function

As described in Section 4.2, Rahman (1988) developed an expression for the tangent shear creep function. A hyperbolic type of dependence of G_{ct} on the ratio of mean normal stress to the resultant deviatoric stress was proposed (equation 4.9). In order to examine the influence of the form of the function selected to represent G_{ct} , the shear test data obtained by Rahman, were re-fitted using a power relationship, given as:

$$G_{ct} = k (\sigma_m / s_d)^j \quad , \tag{4.18}$$

in which k and j are equation parameters. Expressions were found to relate these parameters with the parameters a and b of equation 4.9, over the range of available data. They were as follows:

$$k = 3369 + 0.464 (1 / a) \tag{4.19}$$

and $$j = 0.226 + 0.164 (a / b) \quad .$$

These expressions permitted incorporating the new representation of G_{ct} (equation 4.18) into the finite element computer program, without making changes to the input data format. A new subroutine was required to evaluate the tangent shear creep function. The subroutine is listed in Appendix B.

The results of analyses, using both function forms for G_{ct} , were compared.

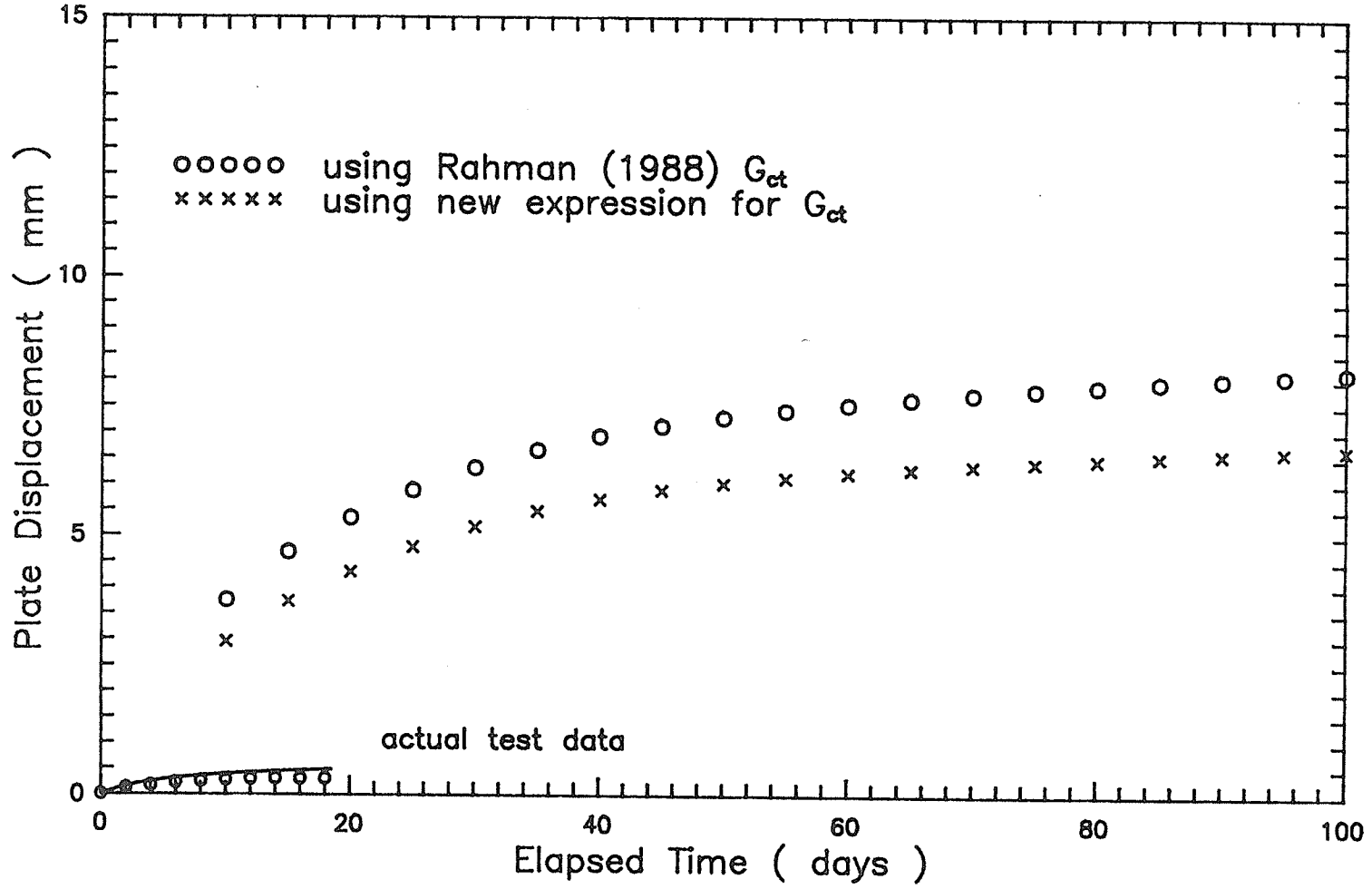

FIGURE 4.7 PLATE DISPLACEMENT VERSUS TIME USING DIFFERENT FUNCTION FORMS FOR G_{ct}: p = 0.88 MPa

Figure 4.7 shows the rigid plate displacement as a function of time for an applied pressure of 0.88 MPa. The displacements determined by analyses using the power function were slightly smaller than the displacements determined by analyses using the hyperbolic function. The maximum difference in displacement for the two cases was about 14 percent. Results based on the power function showed slightly better agreement with actual plate-load creep test data, as shown in Figure 4.7. Therefore, the power function was used in subsequent analyses.

Bulk and Shear Creep Functions

The tangent bulk creep function values, for two elements, are shown as a function of time in Figure 4.8, for an applied pressure of 0.88 MPa. The values shown correspond with the final increment of the applied pressure, at each selected time. Element 4 was situated below the center of the plate and element 59 was near the edge of the plate. The location of each element is indicated in Figure 4.15. Initially, the value of K_{ct} for element 4 was significantly larger than for element 59, at a particular time. However, the values for each element decreased with time to a lower limiting value of K_∞ = 10.25 MPa, which is consistent with equation 4.8.

The tangent shear creep function values, for the same two elements, are shown as a function of time in Figure 4.9, for the same applied pressure. The values shown correspond with the final increment of the applied pressure, at each selected time. The value of G_{ct} for element 4 was always larger than for element 59, at a particular time. The difference between the values for each element decreased slightly with time, but remained approximately constant. For both elements, G_{ct} decreased with time. Over the range of time considered, it appeared to approach a different lower limiting value, for each element.

Comparison of Predicted and Experimental Creep Curves

The plate displacements predicted by analysis are shown as a function of

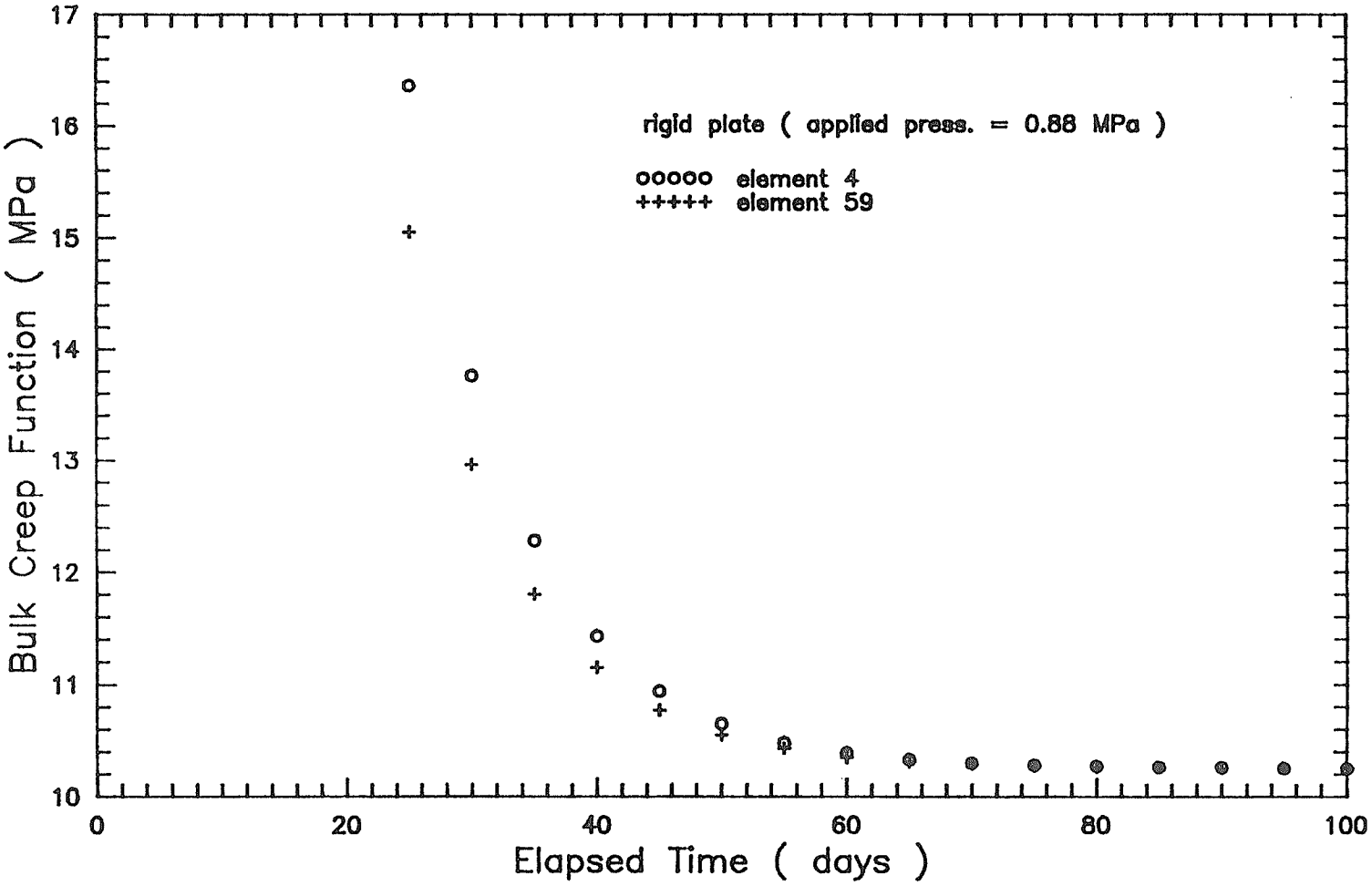

FIGURE 4.8 TANGENT BULK CREEP FUNCTION VERSUS TIME: p = 0.88 MPa

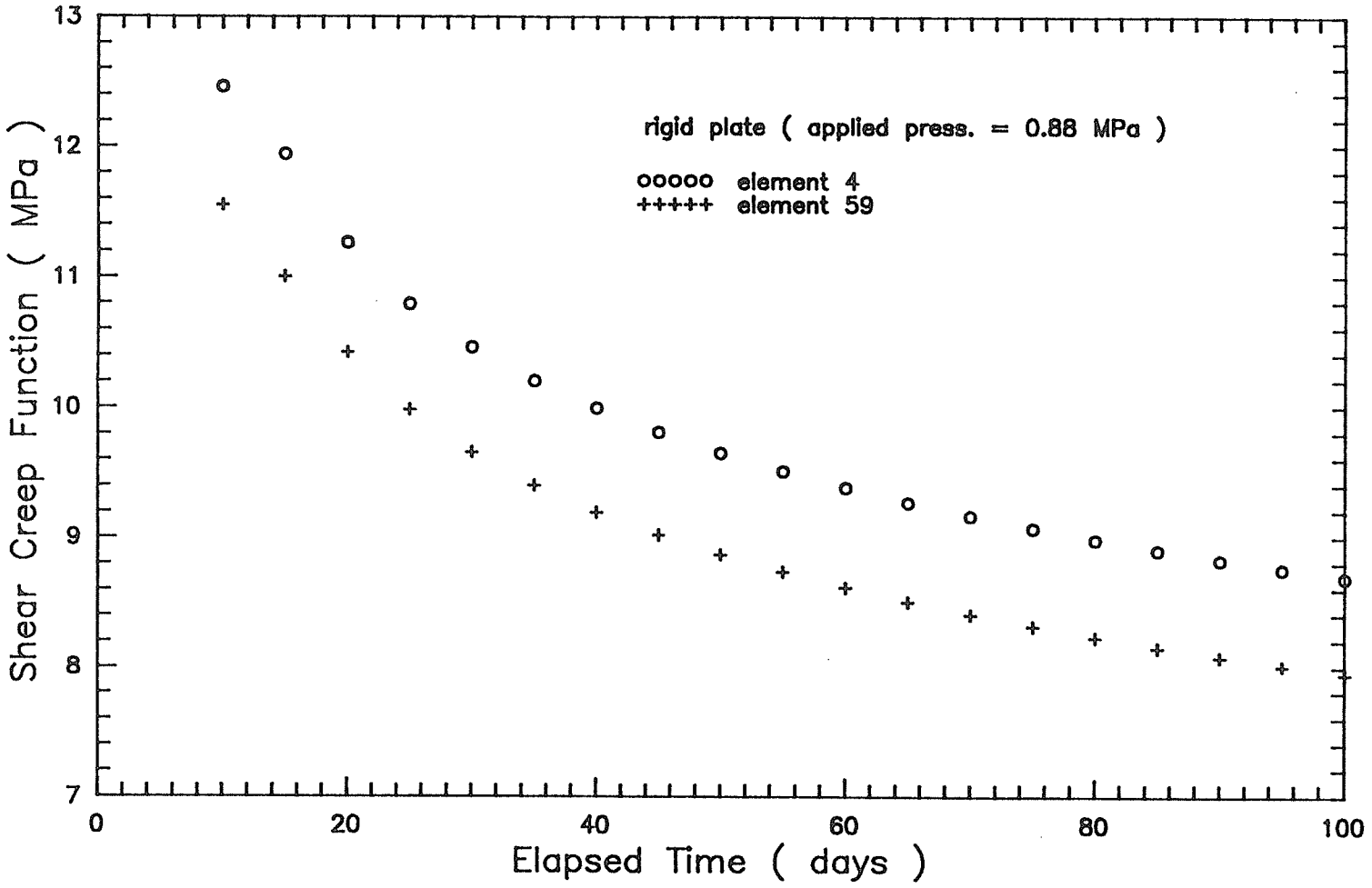

FIGURE 4.9 TANGENT SHEAR CREEP FUNCTION VERSUS TIME: p = 0.88 MPa

time in Figure 4.10, for the same values of pressure as were applied in the plate-load creep test. For comparative purposes, the predicted curves and corresponding experimental results are presented on common plots in Figures 4.11 through 4.14.

Solutions for the plate displacement were obtained for a 100 day time period. The predicted displacements attenuated under each value of the applied pressure. Under applied pressures of 0.88, 1.80, 2.68, and 3.44 MPa, the displacement rates were approximately 0.006, 0.020, 0.032, and 0.042 mm/day, respectively, at the end of the 100 day period. For the same values of the applied pressure, the total displacements were about 6.7, 16.3, 26.0, and 32.2 mm, respectively.

The agreement between the observed plate displacements and the predicted values was very poor. The observed displacement-time curves fell far below the predicted curves, in each case. For applied pressures of 0.88, 1.80, 2.68, and 3.44 MPa, the maximum difference between observed and predicted displacement was roughly 1240, 430, 260, and 160 percent of the observed displacement, respectively. For a particular value of the applied pressure, the difference tended to increase slightly with the elapsed time.

Failure Criterion

The analyses indicated that failure conditions, as defined by equation 4.14, prevailed in several elements below the plate. Figure 4.15 shows the elements which failed, for the lowest applied pressure, 0.88 MPa. The zone of elements which failed extended downward from approximately 50 mm below the plate to about 300 mm below the plate. Most of the elements which failed were directly under the plate.

For elements which failed, the pre-failure shear creep function was assumed to remain valid. To properly account for failure in an element, a shear creep function representative of the failure condition should be assigned to the elment. In general, this would result in larger predicted values of the plate displacement than indicated

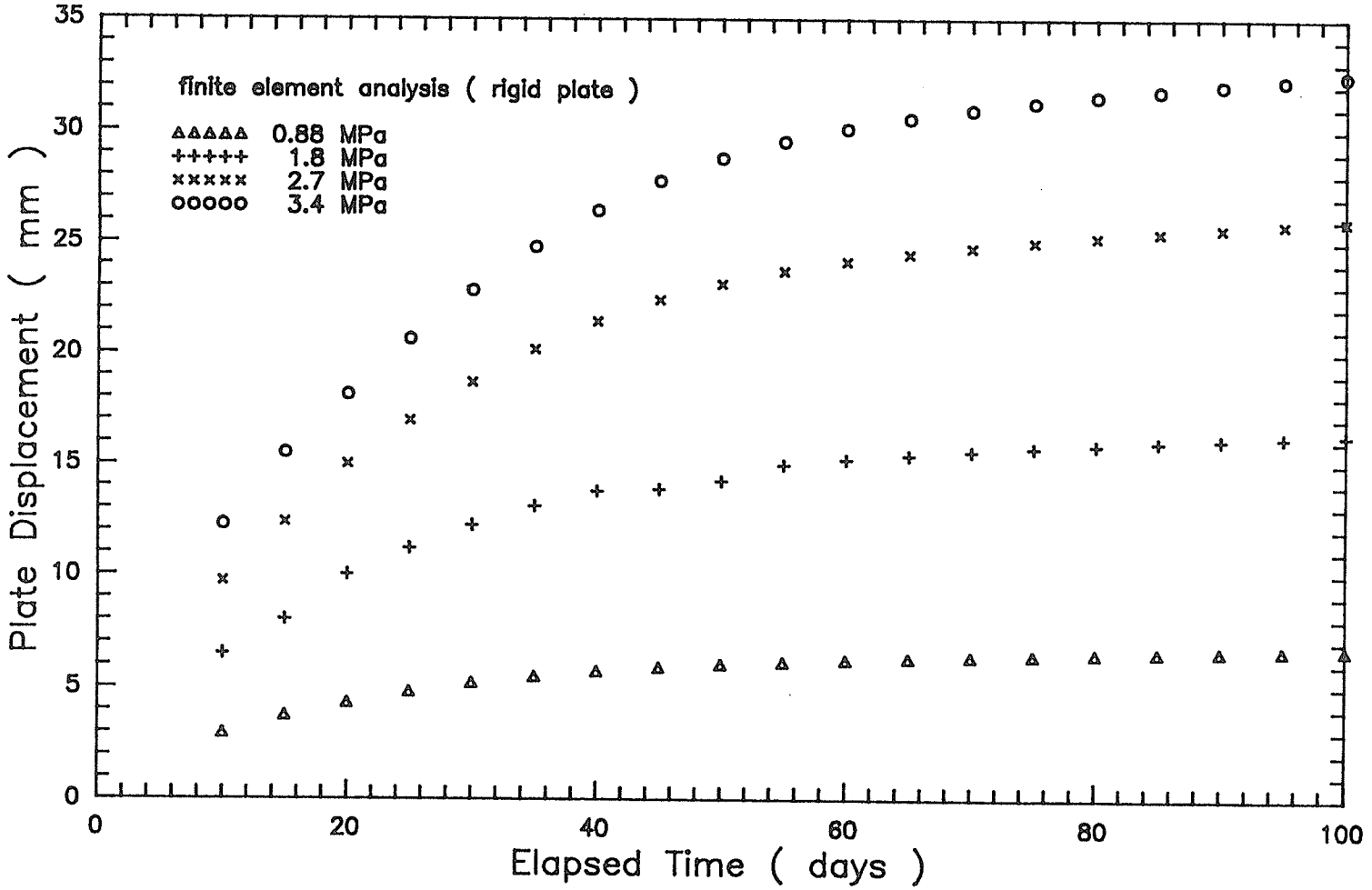

FIGURE 4.10 PREDICTED PLATE DISPLACEMENT VERSUS TIME FOR EACH APPLIED PRESSURE

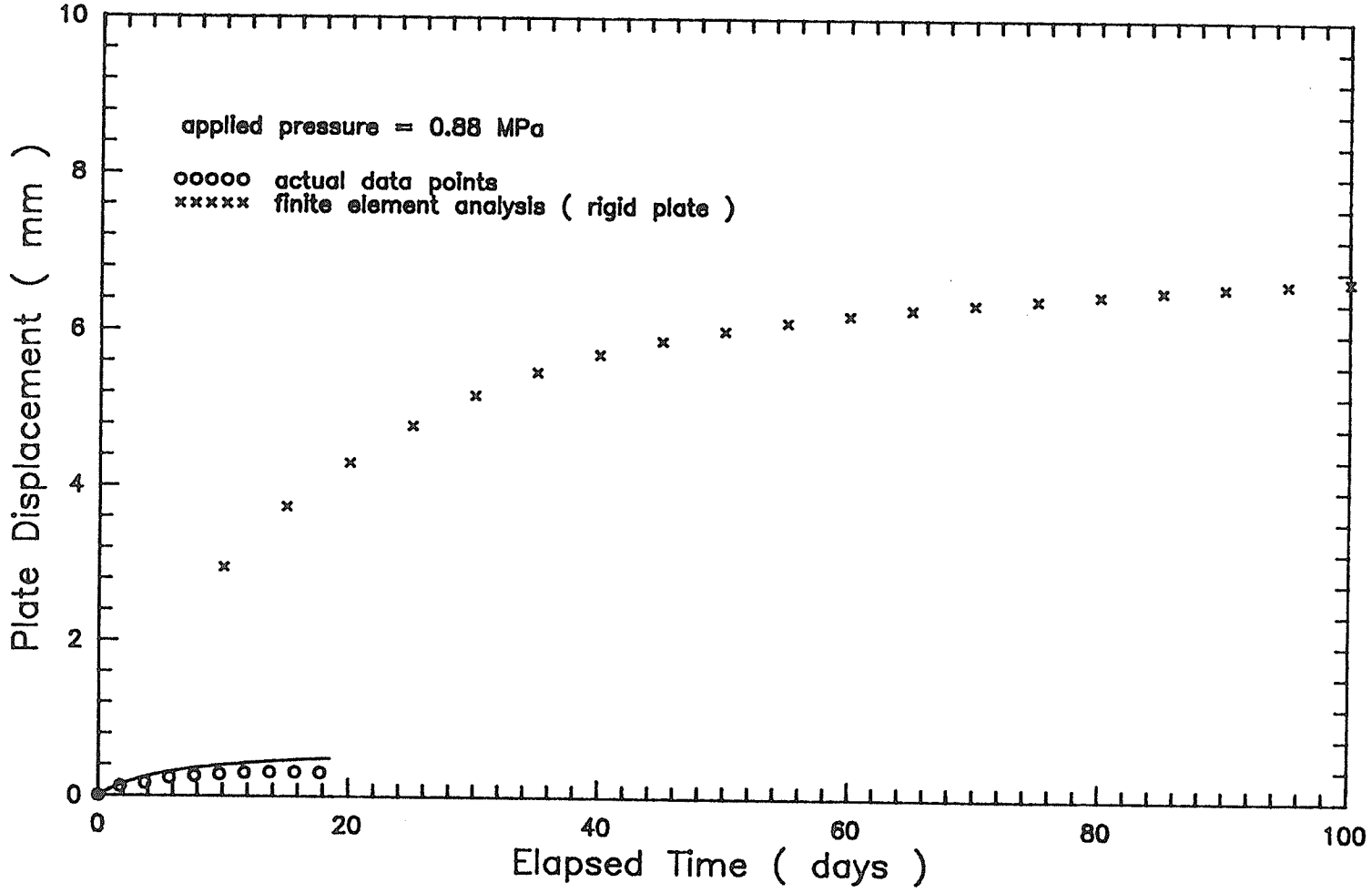

FIGURE 4.11 OBSERVED AND PREDICTED PLATE DISPLACEMENT VERSUS TIME: p = 0.88 MPa

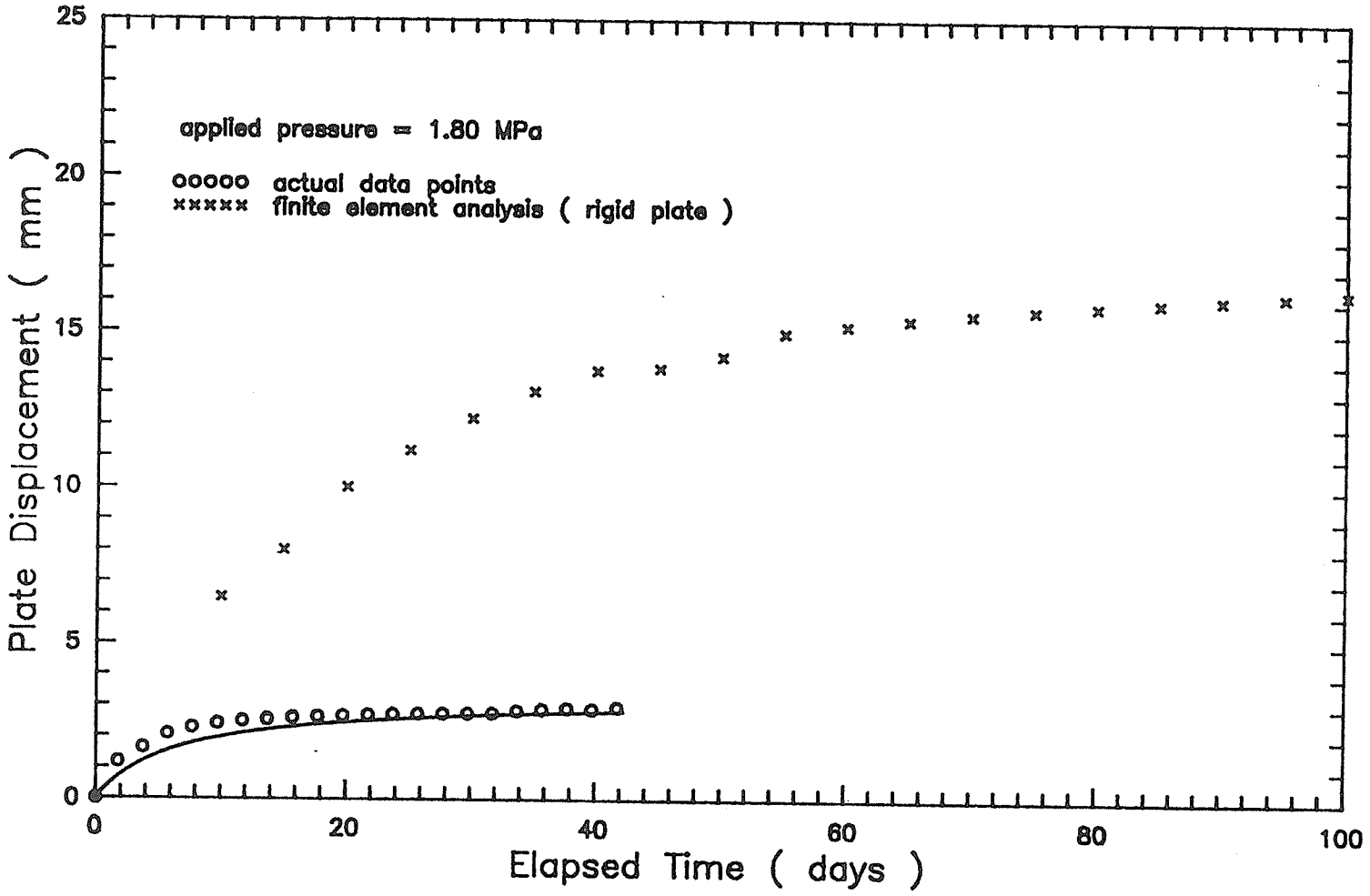

FIGURE 4.12 OBSERVED AND PREDICTED PLATE DISPLACEMENT VERSUS TIME: p = 1.80 MPa

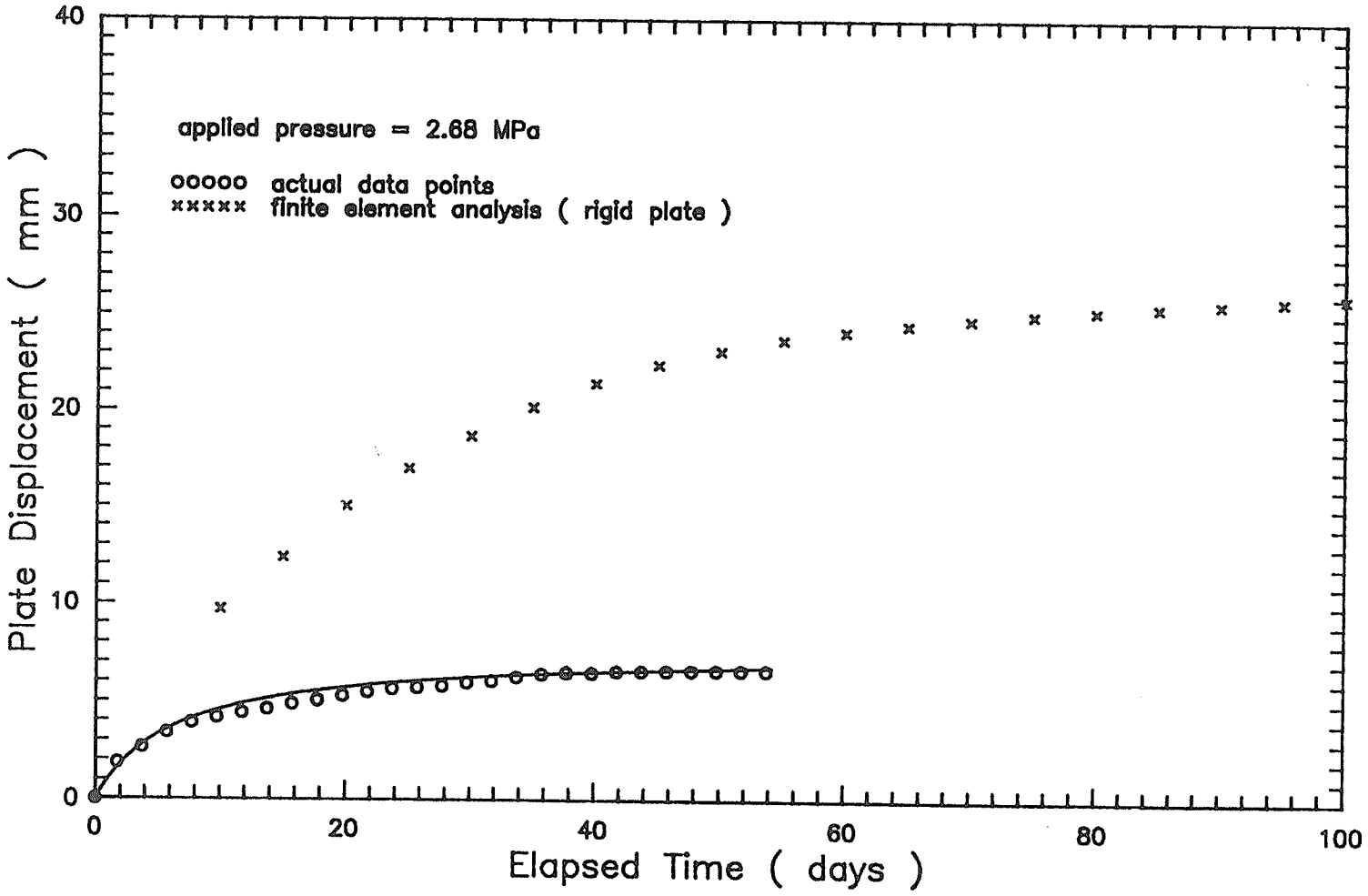

FIGURE 4.13 OBSERVED AND PREDICTED PLATE DISPLACEMENT VERSUS TIME: p = 2.68 MPa

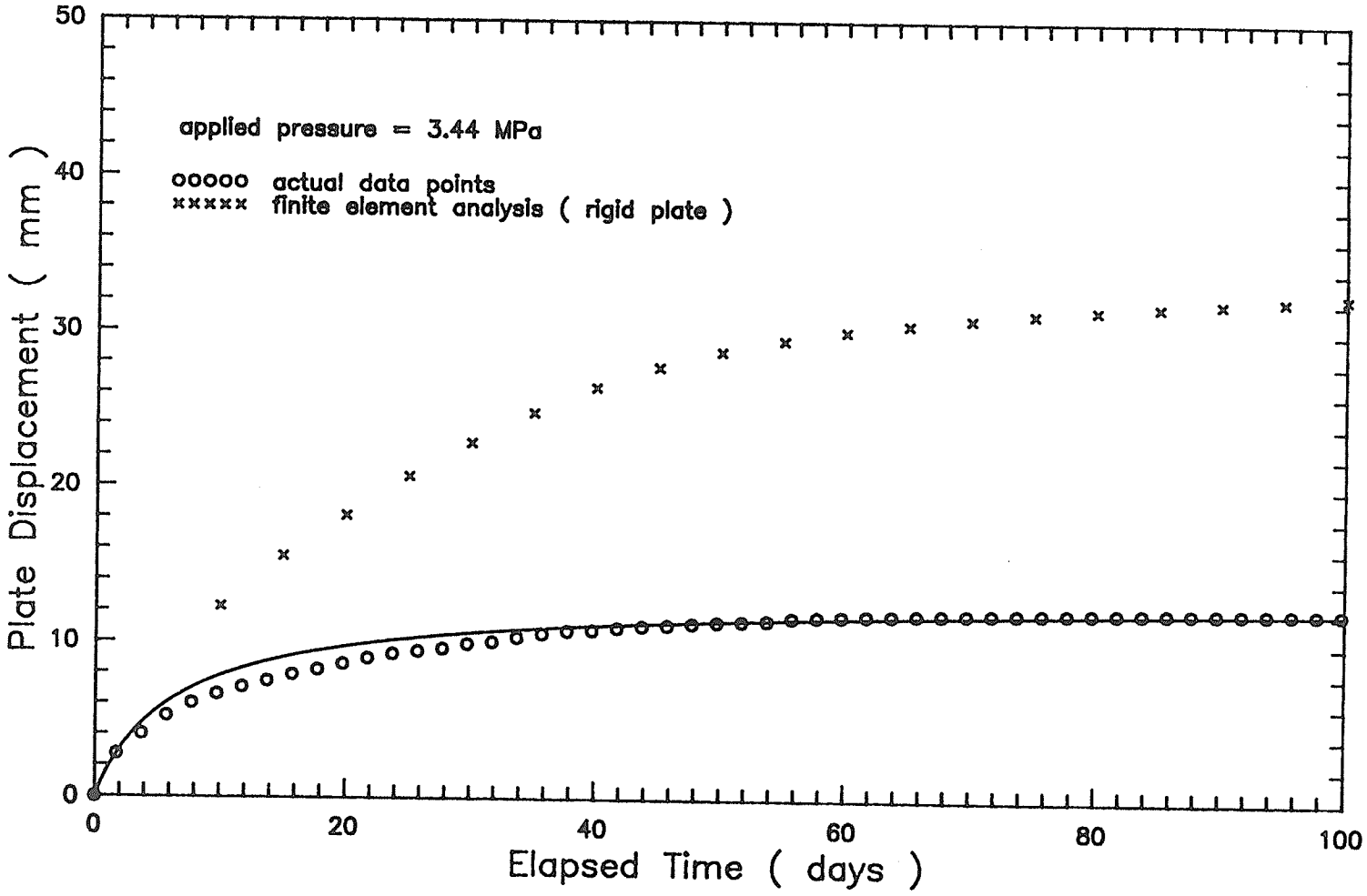

FIGURE 4.14 OBSERVED AND PREDICTED PLATE DISPLACEMENT VERSUS TIME: p = 3.44 MPa

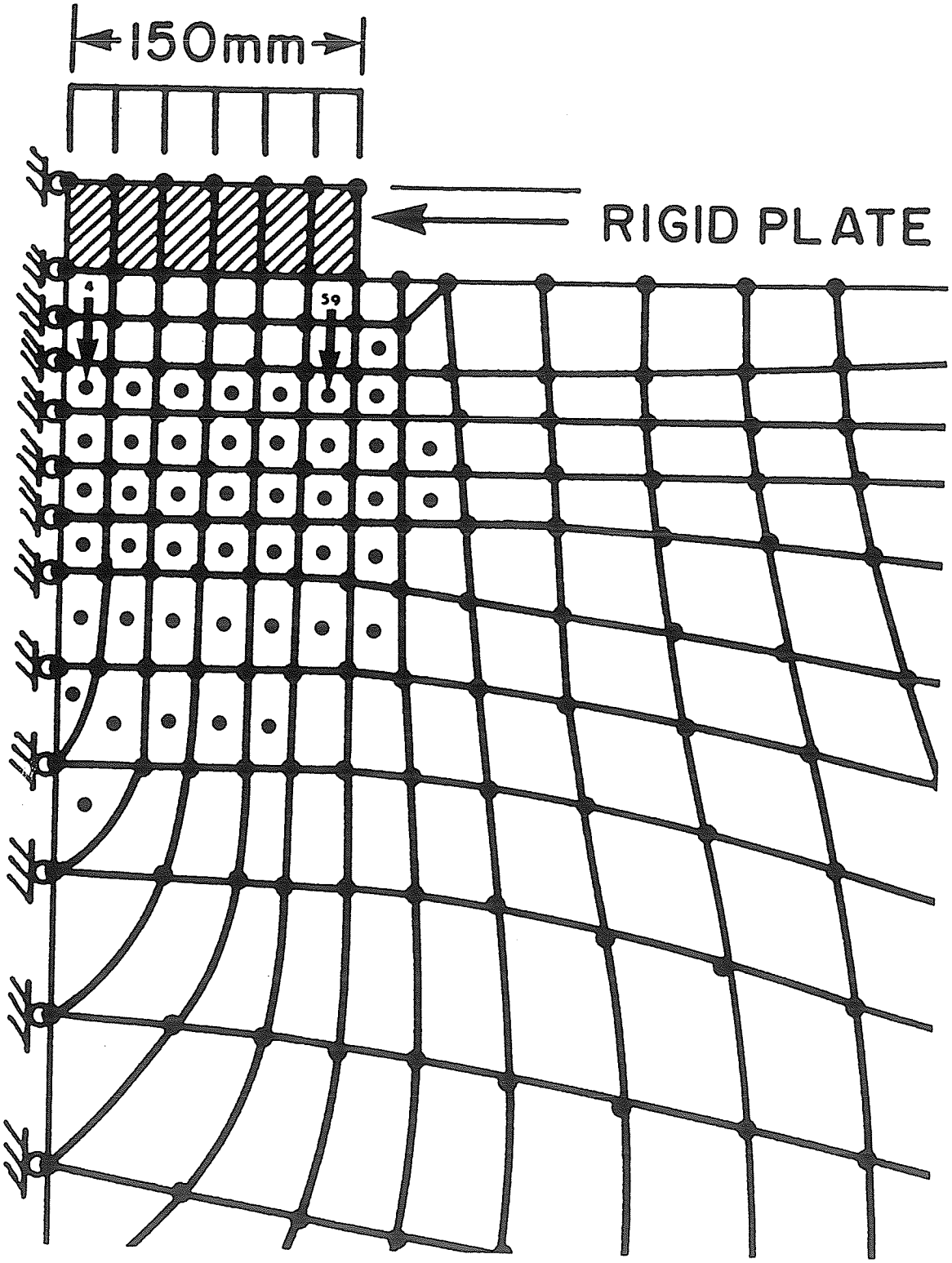

FIGURE 4.15 ELEMENTS WHICH FAILED: p = 0.88 MPa
(DOTS INDICATE FAILED ELEMENTS)

in Figure 4.10, and poorer agreement with observed displacements.

4.4.2 Pressuremeter Creep Test Problem

Problem Characteristics and Assumptions

Analyses were performed to predict the borehole deformations for the pressuremeter creep tests described in Chapter 3. The same assumptions were made regarding soil conditions as those indicated in Section 4.4.1.

As described in Chapter 3, two pressuremeter creep tests were carried out at different depths in the frozen sand. The depth to the center of the probe was approximately 550 mm in Test No. 1 and 1050 mm in Test No. 2. In both cases, the distance from the center of the probe to the bottom of the borehole was about 410 mm. For the shallow depths involved, it can be expected that the depths of the test did not significantly influence the observed creep behavior. Therefore, in the analysis, a single test at an intermediate depth was considered. In the finite element idealization, the depth to the center of the probe was assumed to be 800 mm and the distance from the center of the probe to the base of the borehole was taken to be 410 mm. The initial radius of the borehole was 35 mm. A uniform pressure was applied to the borehole wall, over a vertical distance of 390 mm, the effective length of the pressuremeter membrane.

The final mesh layout and specified boundary conditions used in the analysis are shown in Figure 4.16. The number of nodal points was 302 and the number of elements was 276. The mesh was made finer near the area of pressure application. The stress gradients were comparatively higher in the radial than in the vertical direction, therefore, the dimensions of the elements were generally made larger in the vertical direction. The size of the elements gradually increased away from the area of pressure application. Since the problem was symmetric about the z-axis, the continuum was only discretized on one side of the axis, and the nodal points on the axis were restrained against radial displacement. The nodal points on the

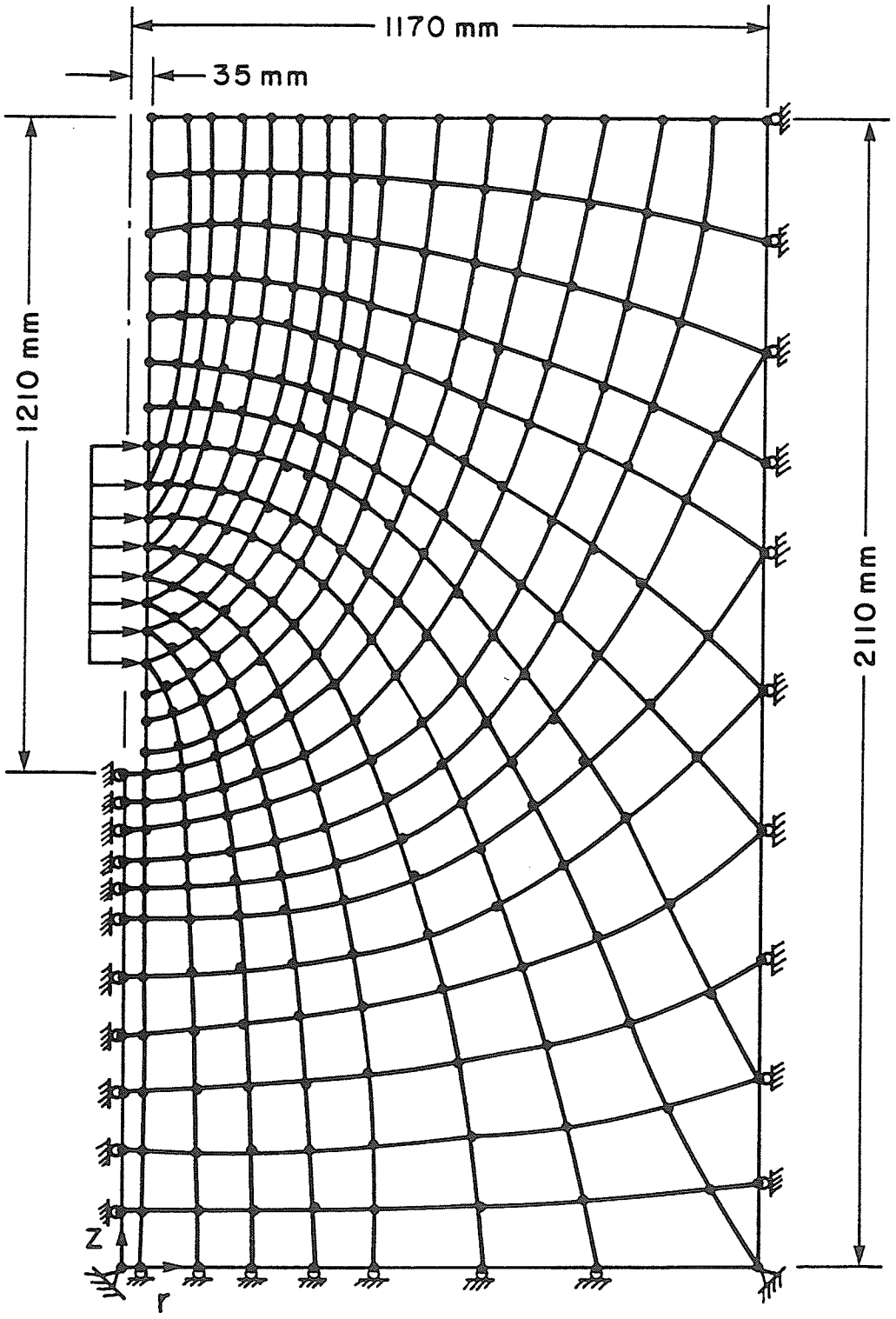

FIGURE 4.16 FINITE ELEMENT IDEALIZATION FOR THE PRESSUREMETER TEST PROBLEM

borehole wall were not restrained. The side and bottom boundaries were placed at sufficient distance from the area of pressure application that the radial and vertical displacements, respectively, were negligible. Thus, the nodal points on the side boundary were restrained against radial displacement, and the nodal points on the bottom boundary were restrained against vertical displacement.

The basic incremental procedure, described in Section 4.3.2, was used in the analysis. In general, ten load increments were applied at each time step.

Bulk and Shear Creep Functions

The tangent bulk creep function values, for two elements, are shown as a function of time in Figure 4.17, for an applied cavity pressure of 0.85 MPa. The values shown correspond with the final increment of the applied pressure, at each selected time. Element 120 was situated near the top and element 220 near the bottom of the region over which the pressure was applied. The elements were at approximately the same radial distance from the borehole wall. The location of each element is indicated in Figure 4.24. For both elements, K_{ct} decreased with time to its lower limiting value of K_{∞} = 10.25 MPa. Initially, the value of K_{ct} for element 120 was slightly larger than for element 220. The difference became insignificant after about 80 days.

The tangent shear creep function values, for the same two elements, are shown as a function of time in Figure 4.18, for the same applied cavity pressure. The values shown correspond with the final increment of the applied pressure, at each selected time. For each element, G_{ct} decreased with time and appeared to approach a different lower limiting value. The value of G_{ct} was larger for element 220 than for element 120 and the difference remained essentially constant with time.

Comparison of Predicted and Experimental Creep Curves

The changes in borehole radius predicted by analysis are shown as a function

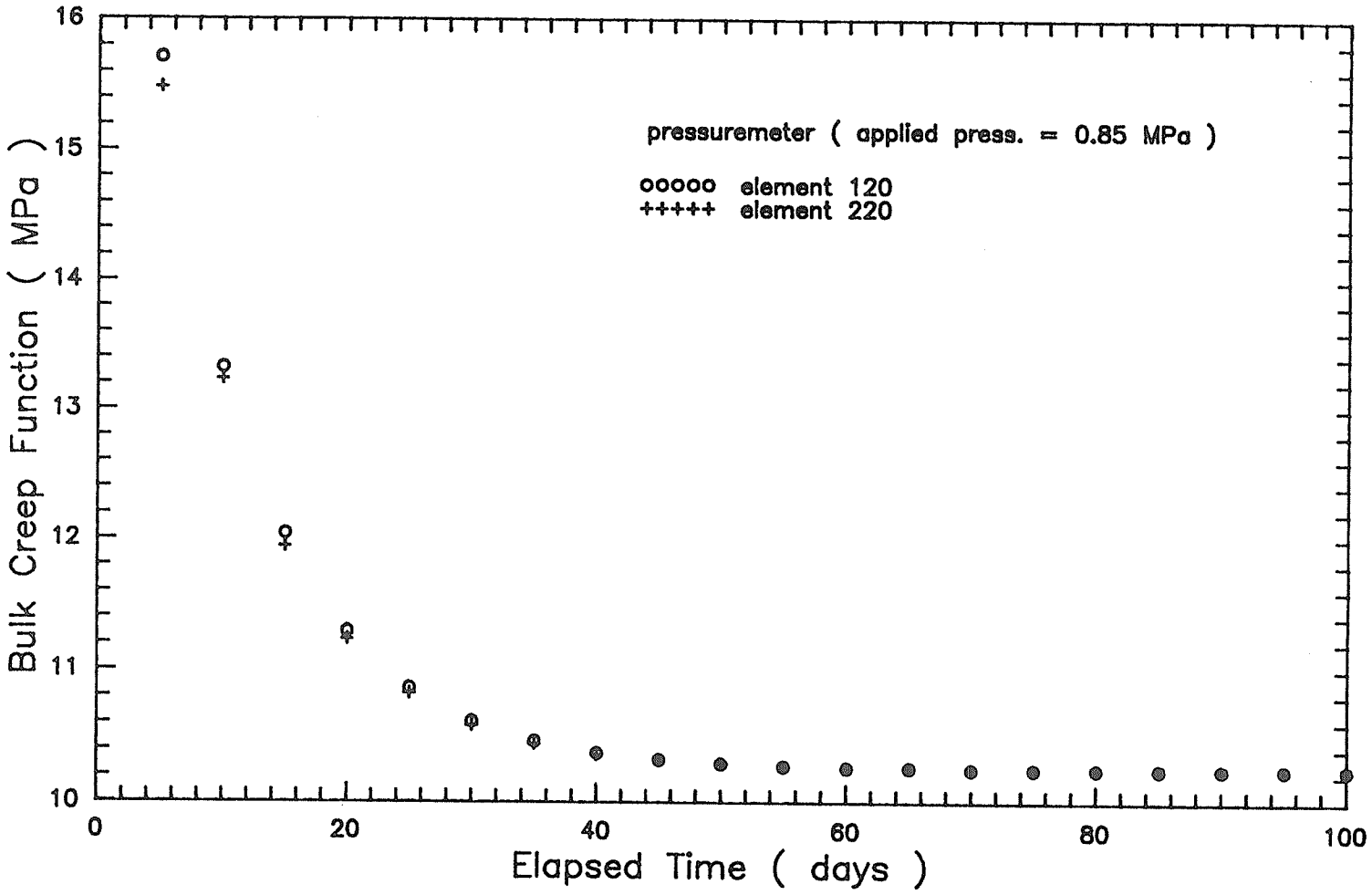

FIGURE 4.17: TANGENT BULK CREEP FUNCTION VERSUS TIME: p = 0.85 MPa

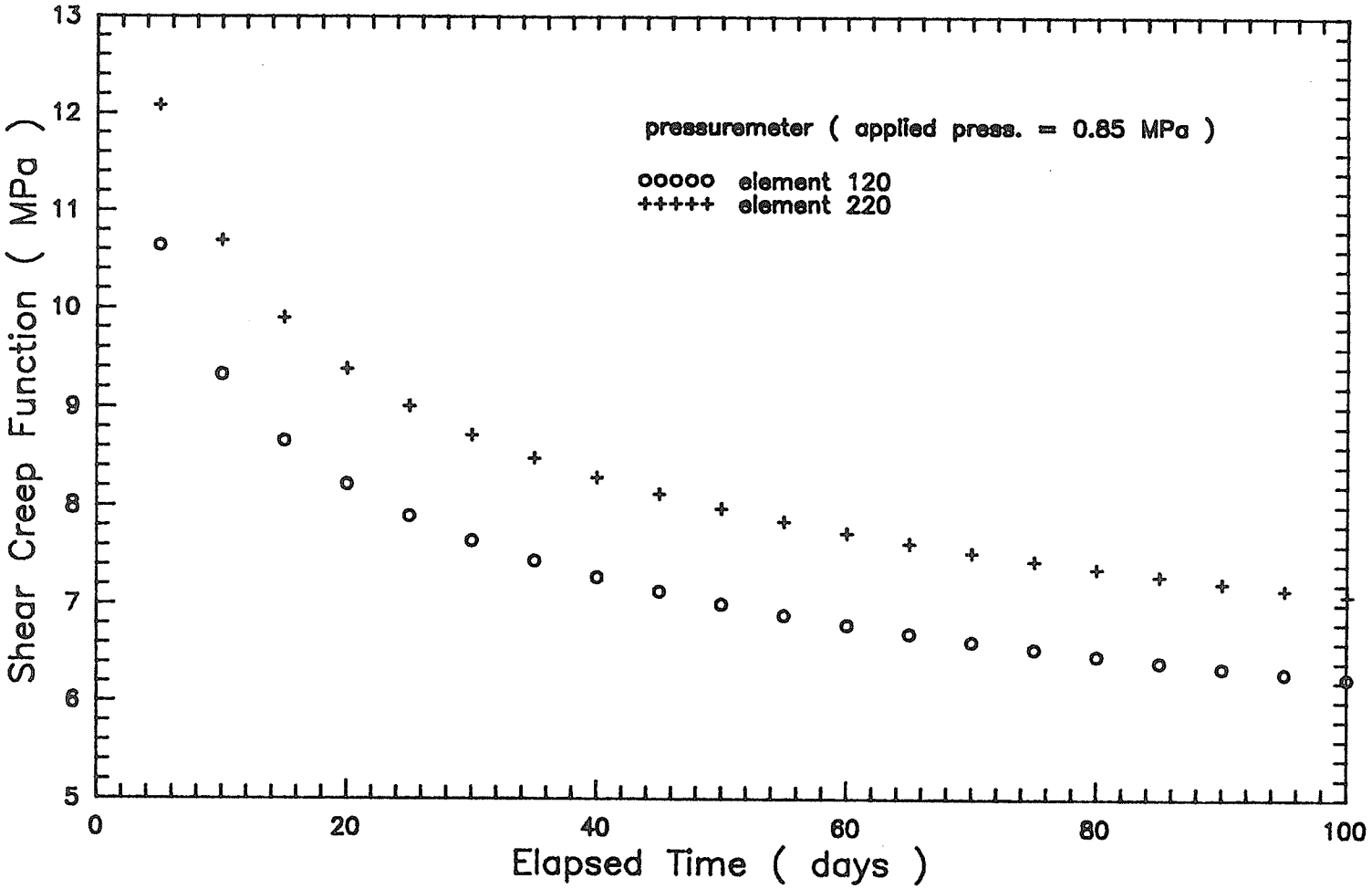

FIGURE 4.18 TANGENT SHEAR CREEP FUNCTION VERSUS TIME: p = 0.85 MPa

of time in Figure 4.19. The values shown were calculated as the average for two nodal points on the borehole wall, which were nearest to the mid-depth of the region over which the pressure was applied. The applied pressures considered in the analyses were 0.85, 1.78, 2.80, and 3.47 MPa. These values were averages of the mean applied cavity pressures for Test Nos. 1 and 2.

Solutions for the change in borehole radius or radial displacement were obtained for a 100 day time period. The predicted radial displacements attenuated under each value of the applied pressure. For applied pressures of 0.85, 1.78, 2.80, and 3.47 MPa, the displacement rates were approximately 0.002, 0.006, 0.008, and 0.016 mm/day, respectively, at the end of the 100 day period. For the same values of the applied pressure, the total displacements were about 2.1, 4.7, 7.4, and 9.2 mm, respectively.

The borehole circumferential strain was computed from the radial displacement in accordance with equation 3.6. For comparative purposes, the predicted borehole circumferential strain-time curves and the corresponding experimental results are presented on common plots in Figures 4.20 through 4.23.

For the applied pressure of 0.85 MPa (Figure 4.20), the observed strain-time curves fell well below the predicted curve. The maximum difference between the observed and predicted strain, over the test duration, was about 220 percent of the observed strain for Test No. 1 and 95 percent for Test No. 2.

For the applied pressure of 1.8 MPa (Figure 4.21), the average of the strains from the two tests was over-predicted. The maximum difference between the observed and predicted strain, over the test duration, was about 74 percent of the observed strain for Test No. 1 and 12 percent for Test No. 2.

For the applied pressure of 2.8 MPa (Figure 4.22), the observed strain-time curve for Test No. 1 fell below the predicted curve initially and above it at greater elapsed times. The maximum difference between the observed and predicted strain,

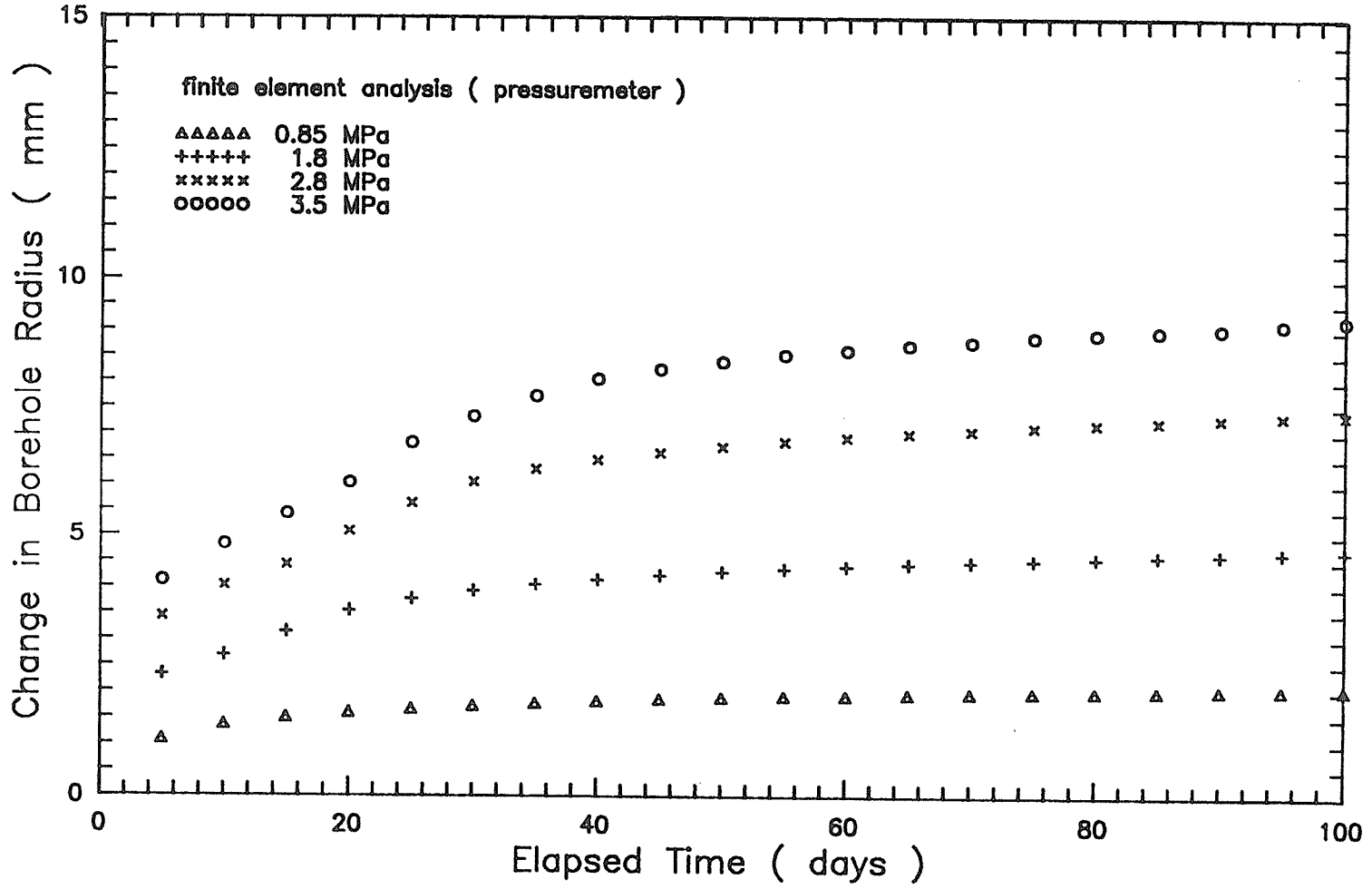

FIGURE 4.19 PREDICTED CHANGE IN BOREHOLE RADIUS VERSUS TIME FOR EACH APPLIED PRESSURE

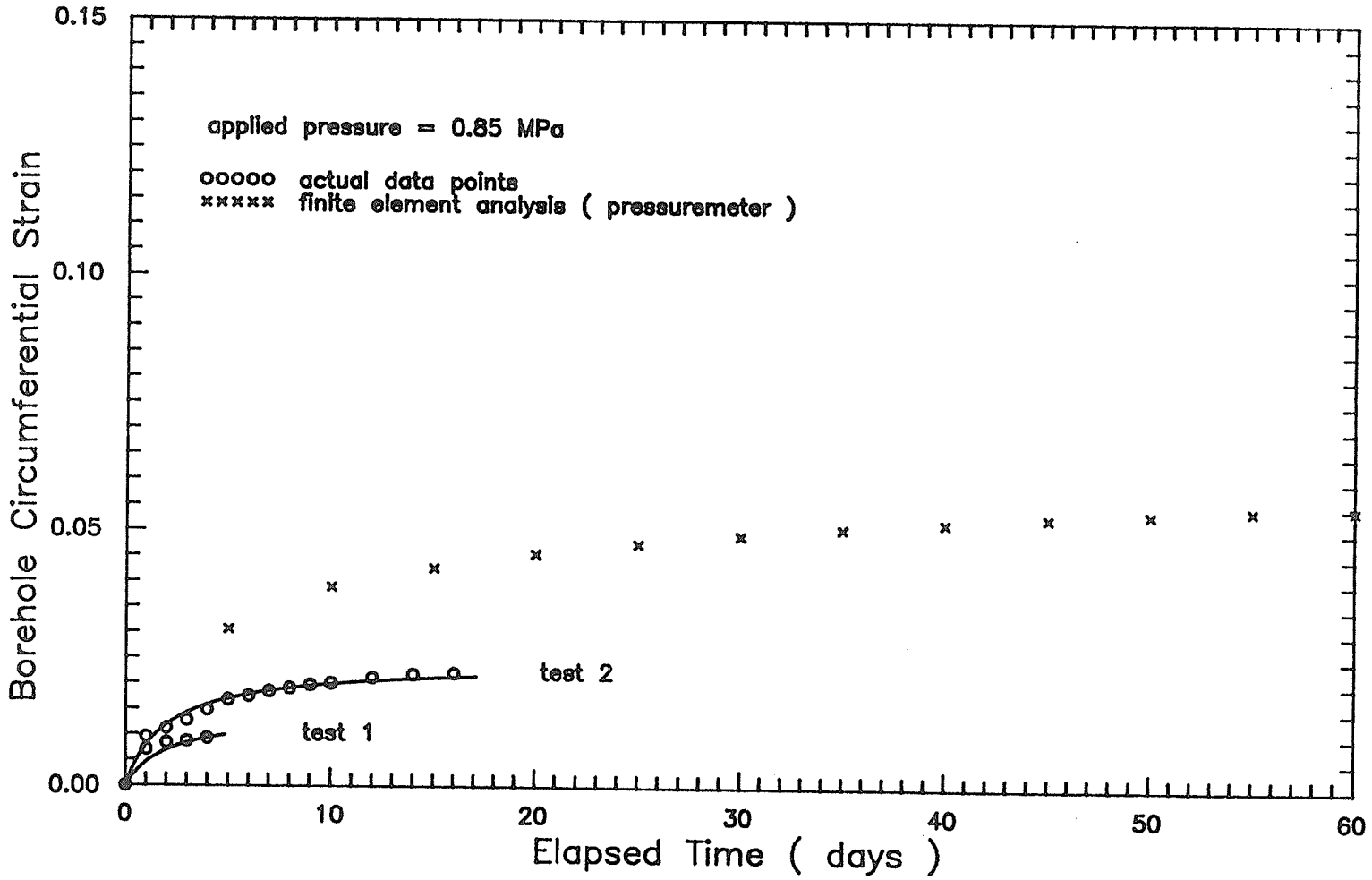

FIGURE 4.20 OBSERVED AND PREDICTED BOREHOLE CIRCUMFERENTIAL STRAIN VERSUS TIME: p = 0.85 MPa

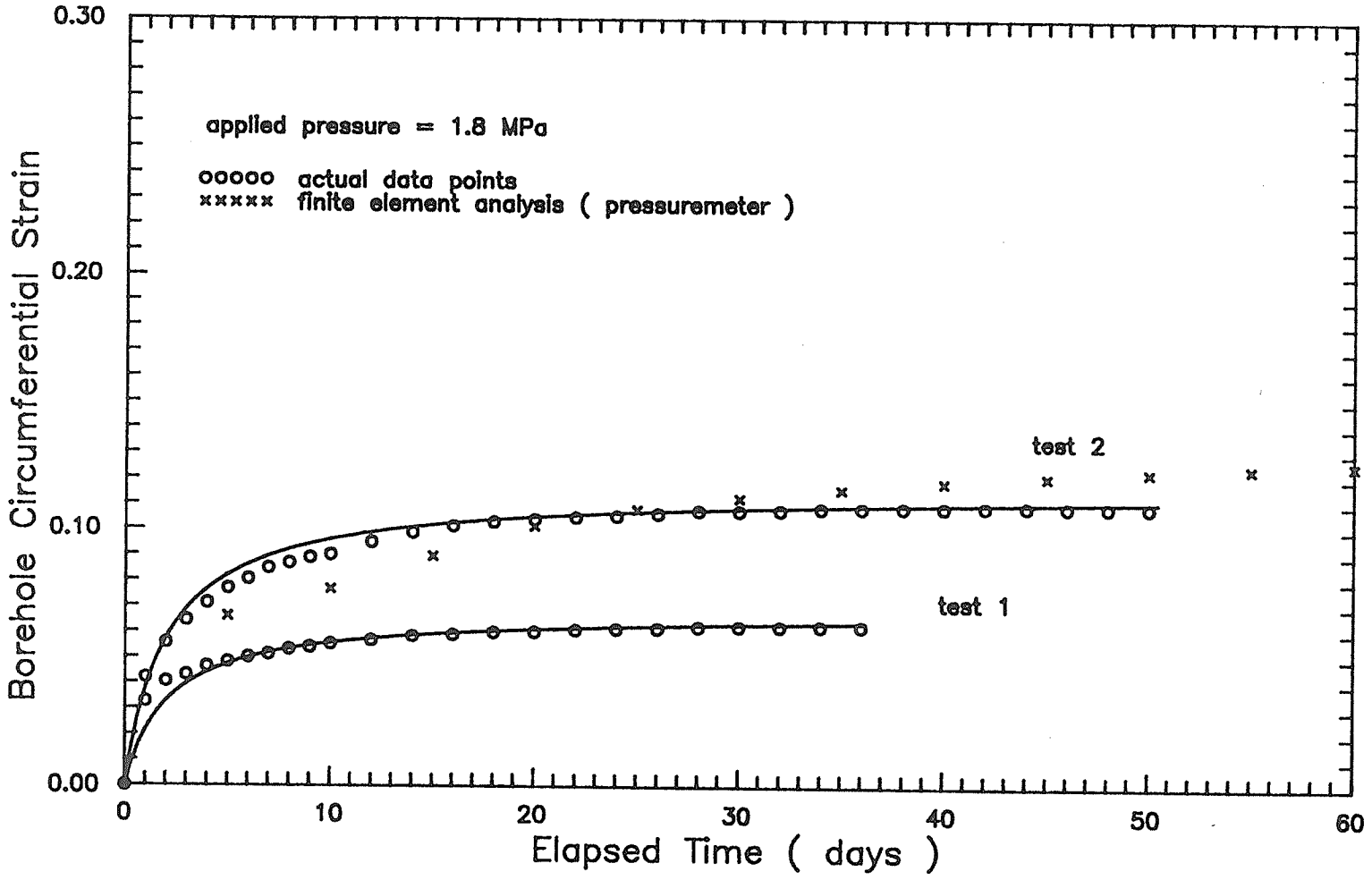

FIGURE 4.21 OBSERVED AND PREDICTED BOREHOLE CIRCUMFERENTIAL STRAIN VERSUS TIME: p = 1.79 MPa

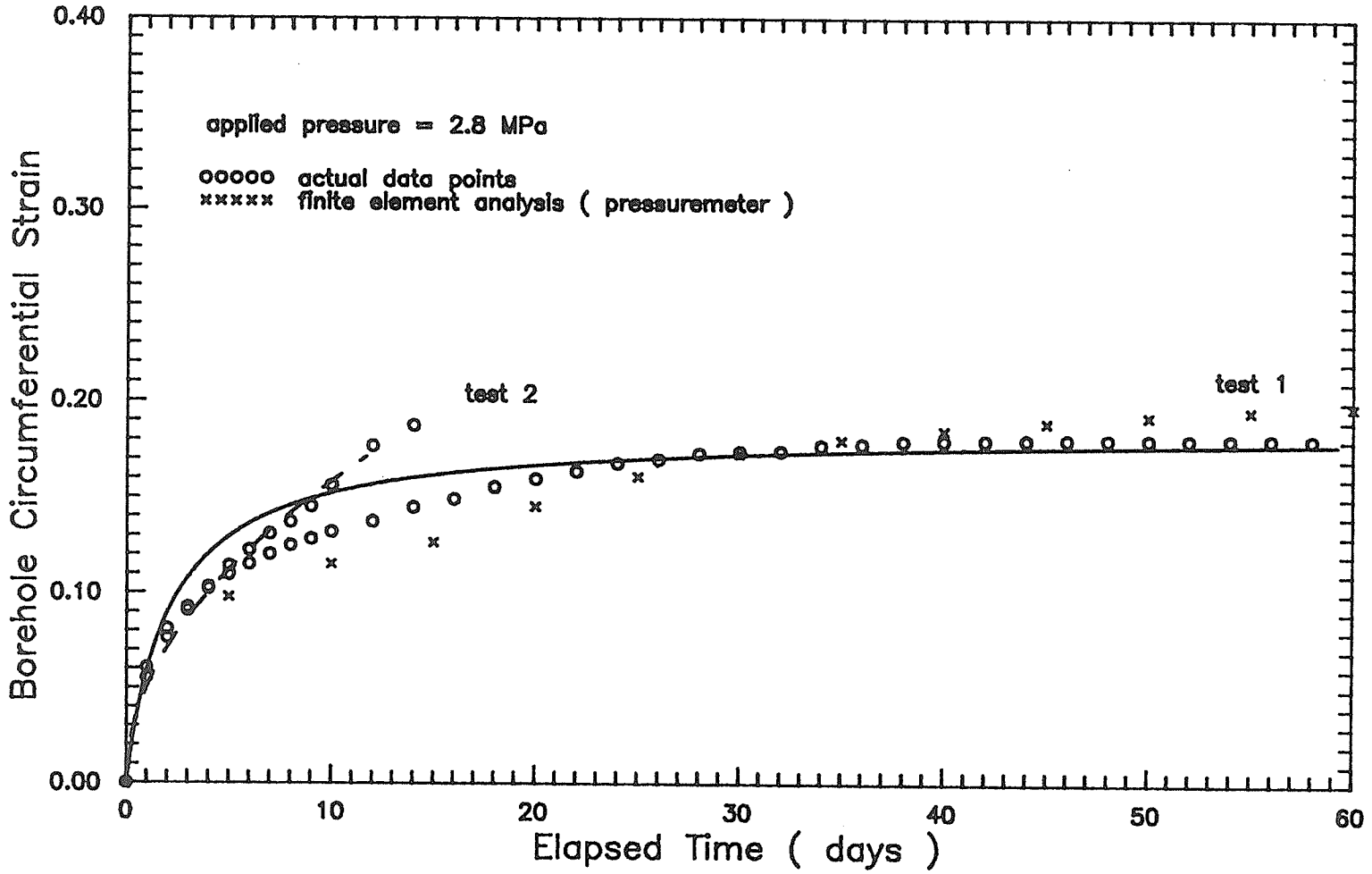

FIGURE 4.22 OBSERVED AND PREDICTED BOREHOLE CIRCUMFERENTIAL STRAIN VERSUS TIME: p = 2.79 MPa

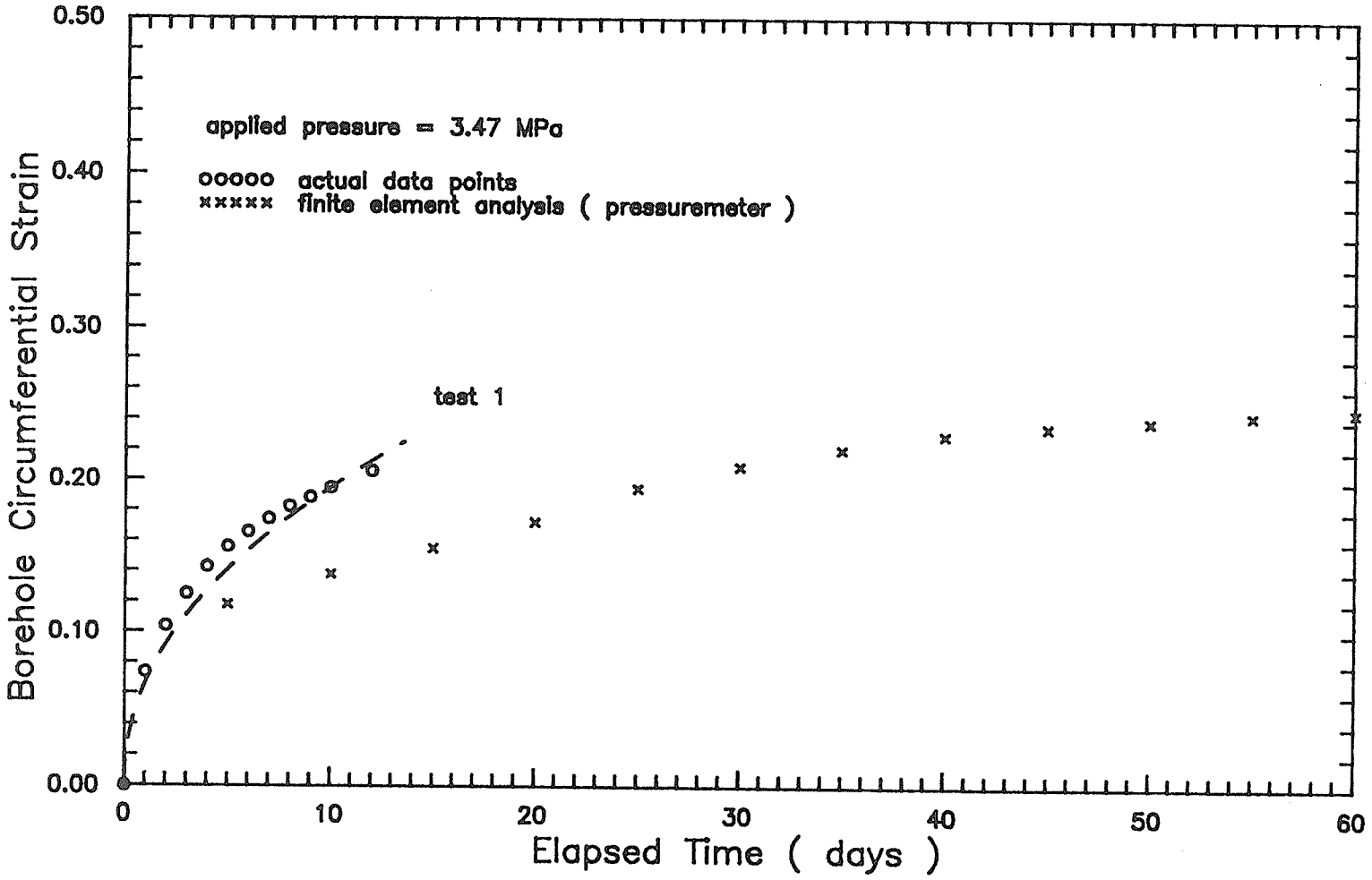

FIGURE 4.23 OBSERVED AND PREDICTED BOREHOLE CIRCUMFERENTIAL STRAIN VERSUS TIME: p = 3.47 MPa

over the test duration, was about 13 percent of the observed strain. In Test No. 2, the strain continued into tertiary creep and, therefore, diverged rapidly from the predicted values.

For the applied pressure of 3.47 MPa (Figure 4.23), the observed strain-time curve for Test No. 1 fell above the predicted curve. The maximum difference between the observed and predicted strain, over the test duration, was about 29 percent of the observed strain.

At the same values of the applied pressure, there was a large difference in the experimental results from Test Nos. 1 and 2. Therefore, a more detailed comparison of the predicted curves with the experimental results was not made. In general, at low applied pressures, the analysis over-predicted the observed strains, whereas, at high applied pressures, the analysis under-predicted the observed strains. For intermediate values of the applied pressure, satisfactory overall agreement between observed and predicted strains was obtained.

Failure Criterion

The analyses indicated that failure conditions, as defined by equation 4.14, prevailed in some elements near to the borehole wall, in the area of the applied pressure. Figure 4.24 shows the elements which failed, for each value of the applied pressure. For the applied pressures of 0.85, 1.79, 2.76, and 3.47 MPa, the zone of elements which failed extended to distances of about 95, 145, 185, and 210 mm, respectively, radially outward from the borehole wall. Most of the elements which failed lied within the vertical extent of the area of the applied pressure.

As indicated in Section 4.4.1, for elements which failed, the pre-failure shear creep function was assumed to remain valid. To properly account for failure in an element, a shear creep function representative of the failure condition should be assigned to the element. In general, this would result in larger predicted values of the borehole circumferential strain and poorer agreement with observed strains.

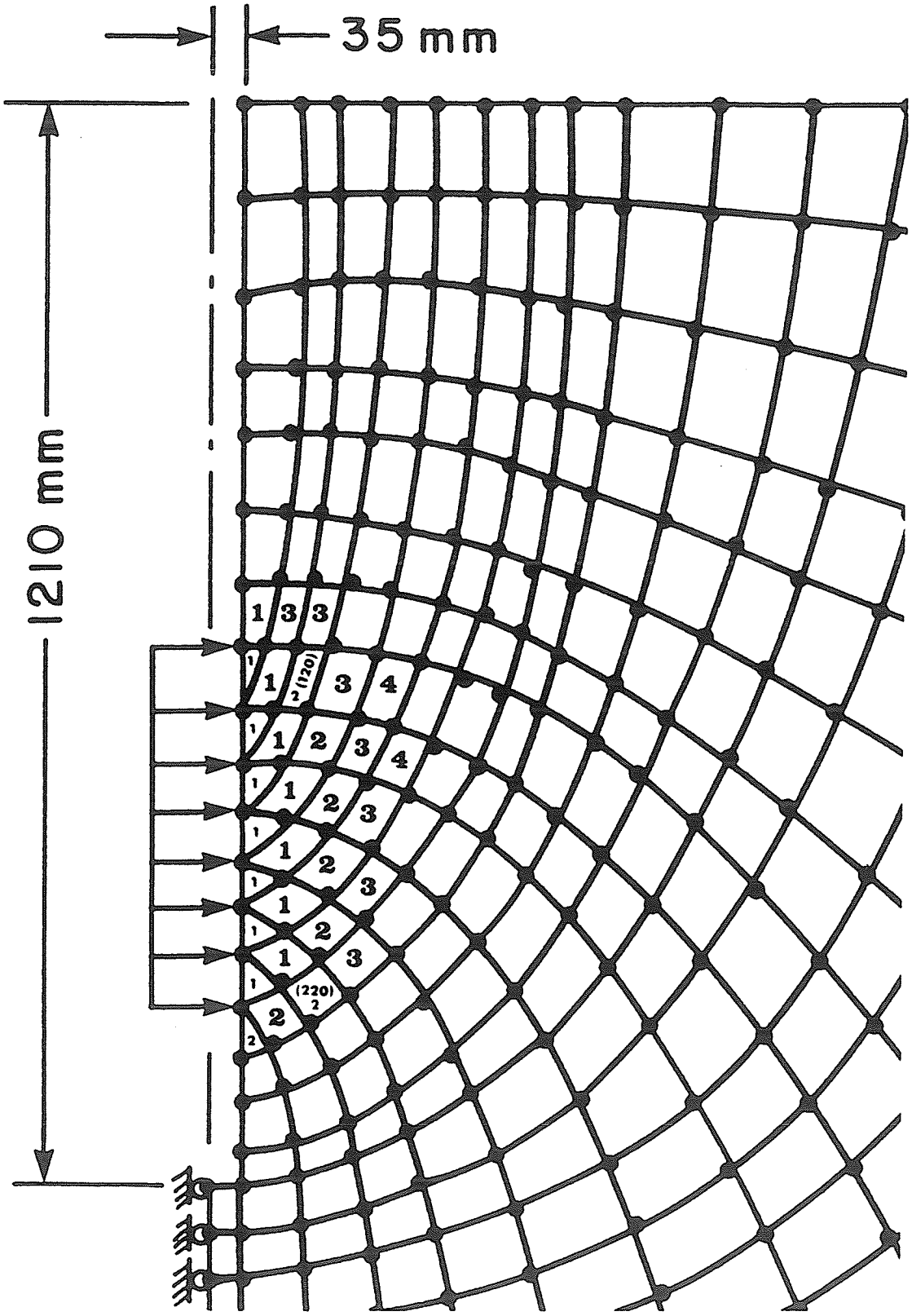

FIGURE 4.24 ELEMENTS WHICH FAILED FOR EACH APPLIED PRESSURE (1, 2, 3, AND 4 FAILED AT 0.85, 1.79, 2.76, AND 3.47 MPa, RESPECTIVELY)

However, it may account for tertiary creep evidenced in the third stage of Test No. 2.

CHAPTER 5

DISCUSSION AND CONCLUSIONS

5.1 INTRODUCTION

Chapter 4 described the creep deformation analyses of the plate-load and pressuremeter test problems. The predicted and experimental creep data were compared. In this Chapter, some of the possible reasons for differences between predicted and observed behavior are discussed. In addition, the observations and conclusions of the study are presented and recommendations for further research are made.

5.2 DISCUSSION

5.2.1 Plate-Loading and Pressuremeter Tests

There is a considerable difference in the way the frozen soil was stressed in the plate-load test, as compared to the pressuremeter tests.

In the plate-load test the soil was subjected to an increase in both vertical and radial stresses, with the former being much larger than the latter. Consequently, there was an increase in both the hydrostatic and deviatoric components of the state of stress. The resulting deformation included both linear strains and distortion.

In the pressuremeter tests, on the other hand, a nearly pure deviatoric state of stress was imposed on the frozen soil. The resulting deformations were primarily distortion.

Since frozen soil behavior is stress-path dependent, it can be expected that the behavior of the frozen sand in the plate-load test would differ from its behavior in the pressuremeter tests.

5.2.2 Limitations of the Study

The limitations of the study may be considered in two general categories:

limitations of the experimental programs; and limitations of the method of analysis.

5.2.2.1 Limitations of the Experimental Programs

Some of the factors which may have influenced experimental results are as follows:

1. **Effect of Variations in Temperature**

In each experimental program, there were deviations from the condition of constant temperature assumed in the analyses. In general, the variation of temperature over the duration of each test was small. There were, however, brief periods of substantial temperature rise associated with breakdowns of the refrigeration system. The immediate displacements which occurred as a result of such temperature increases, were omitted in the analyses. However, the deformations that occurred during these breakdowns may have altered the properties of the soil in the immediate vicinity of the applied pressure. This could not be accounted for in the analyses.

The constitutive relationships used in the analyses were developed for a particular soil at a constant temperature of -3°C. The average soil temperatures measured over the duration of the plate-load test, at 200 mm depth, was -3.32°C. The average soil temperature during pressuremeter testing were -3.30 and -2.65°C, at the locations of Test Nos. 1 and 2, respectively. The development of larger strains, under the same applied pressures, in pressuremeter Test No. 2 as compared with Test No. 1, may have been the result of the higher temperature at the Test No. 2 location. In addition, when comparing the plate-load creep data with predictions, it should be noted that the constitutive model was based on a higher average soil temperature than that in the test pit, near to the plate. This would account for, in part at least, the over-prediction of displacements. The

same is true for pressuremeter Test No. 1.

2. **Effect of Variation in Applied Pressure**

As described in Chapter 2, some difficulty was encountered in maintaining a constant applied pressure in the plate-load test. The variations in applied pressure resulted in some scatter of the test data. In analyzing the problem, a constant pressure was assumed. This could account for some of the difference between the observed and predicted creep.

In both pressuremeter tests, deviations from constant applied pressure conditions were small.

3. **Effect of Variations in Soil Properties**

As indicated above, the constitutive relationships used in the analyses were developed for a particular soil at a constant temperature. Artificially prepared frozen sand samples were used in the associated laboratory testing program. The average dry unit weight of the frozen sand samples was 15.5 KN/m^3 and the maximum difference from the average value was about 2%. The average moisture content of the samples was 25.1% and the maximum difference from the average value was about 5%.

The average dry unit weight of the frozen sand core samples, recovered from the test pit, was 15.9 KN/m^3 and the maximum difference from the average value was about 8%. The average moisture content of the core samples was 21.9% and the maximum difference from the average value was about 3%. Thus, the average value of dry unit weight in the pit was only slightly larger than that of the lab samples, and the average moisture content was significantly smaller. Therefore, from a physical point of view, the frozen sand in the pit would be expected to undergo smaller creep deformations than those predicted by analysis. This may account for some of the over-prediction of observed displacements.

5.2.2.2 Limitations of the Method of Analysis

Some of the factors which may have influenced the results from analysis are as follows:

1. **Constitutive Model - Limitations**

   The time-independent form of the constitutive model used in the present study is a special class of the hypoelastic models in which the behavior is restricted to be incrementally isotropic. In general, cross effects between hydrostatic and deviatoric incremental response components are neglected, since the model is incrementally isotropic. However, for general functions such as K_{ct} and G_{ct} , there is some interaction through the change in magnitude of the moduli with the invariants. The limitations of this class of model were further described by, for example, Chen and Baladi (1985).

2. **Method of Analysis - Limitations**

   The method of analysis used in the study did not account for the stress history. The effect of stress history is significant, even for constant applied loads, since creep results in a redistribution of stress with time. Shanley (1952) indicated that a creep theory, based on the assumption that the effect of stress history can be neglected, will predict deformations that are conservative if the stresses at all points in the body analyzed increase with time, and will predict deformations that are non-conservative if the stresses at all points in the body decrease with time. However, for the problems examined in the present study, different stress histories existed for each element in the body analyzed. Therefore, no general conclusion can be made regarding the error introduced by the assumption that the effect of stress history may be neglected.

The finite element idealization of each problem was described in Chapter 4. The accuracy of the finite element solution may be improved through

further mesh refinement or through the use of higher order displacement models. In addition, other solution techniques for nonlinear problems may be employed, including procedures which account for geometric nonlinearities.

5.3 OBSERVATIONS AND CONCLUSIONS

In the following, observations are presented separately for each different phase of the study.

5.3.1 Plate-Loading Creep Test Program

1. The plate displacement-time curves were typical of hard-frozen soils subjected to stresses below their long-term strength. The hypothetical instantaneous displacement, measured at one minute, represented, on average, less than one percent of the total displacement under a given pressure increment. The displacement attenuated under each of the applied pressures. The time to complete attenuation increased approximately linearly with pressure. The total displacement of the plate, excluding that resulting from equipment failure, was 12.3 mm. Removal of the load at the conclusion of the test resulted in a total rebound of 0.97 mm.

2. Creep displacement-time curves, generated for each of the applied pressures by superposition, were represented by an expression which assumes a hyperbolic type of dependence of displacement on the elapsed time and a power relationship with the applied pressure.

3. The modulus of subgrade reaction of the frozen sand decreased with time under a given applied pressure, and also decreased with pressure for a given time. Modulus values ranged from about 24.4 GN/m^3 at one hour under the smallest applied pressure, to about 0.29 GN/m^3 at complete attenuation under the largest applied pressure.

5.3.2 Pressuremeter Creep Test Program

1. For mean applied cavity pressures of 0.86, 1.77, and 2.83 MPa, in Test

No. 1, and 0.85 and 1.79 MPa, in Test No. 2, the borehole displacements attenuated with time. Test No. 1 was not continued for a sufficient time period, at the applied pressure of 3.47 MPa, to determine if the displacement would attenuate completely. The final stage of Test No. 2, at the applied pressure of 2.78 MPa, exhibited tertiary creep.

2. A larger amount of borehole displacement developed in Test No. 2 than in Test No. 1, under the same applied pressures. This may be partially attributed to the higher soil temperature at the Test No. 2 location.

3. Creep circumferential strain-time curves, generated for each of the applied pressures by superposition, were represented by two equation forms. For attenuating creep, a hyperbolic type of dependence of strain on time was used, whereas, in the case of continuously increasing creep strains, a power relationship between strain and time was used. For both equation forms, a power relationship between the creep strain and the applied pressure provided the best fit. Only primary creep was considered.

4. The pressuremeter test data for which a power relationship between the creep circumferential strain and both time and applied pressure was assumed, was expressed as a general creep power law following Shields et al. (1988b,d). The values determined for the creep exponents were similar to those found in the literature for various frozen sands.

5. The secant creep shear modulus was represented as a function of the elapsed time and the applied pressure, based on the expressions developed for the creep circumferential strain.

5.3.3 Creep Analyses and Predictions

The following observations were made based on the analyses of the plate-load test problem:

1. The agreement between the observed plate displacements and the predicted values was very poor. For each applied pressure, the predicted displacements were much larger than the measured values.
2. The analyses indicated that failure conditions prevailed in very many elements below the plate, even though the observed displacements continued to attenuate. This discrepancy between implied and real behavior could not be accounted for.

The following observations were made based on the analyses of the pressuremeter test problem:

1. In general, at low applied pressures, the analysis over-predicted the observed borehole circumferential strains, whereas, at high applied pressures, the analysis under-predicted observed strains. For intermediate values of the applied pressure, satisfactory agreement between observed and predicted strains was obtained.
2. The analyses indicated that failure conditions prevailed in some elements close to the borehole wall, in the area of the applied pressure.

In summary, it can be stated that there was poor agreement between observed creep displacements of the plate and those predicted by analysis. Although several factors may have contributed to cause the poor agreement, it was not possible to identify them in a quantitative manner. The agreement between observed and predicted creep strains, for the pressuremeter problem, was generally satisfactory. Consequently, no definite conclusion can be drawn regarding the predictive capability of the constitutive model proposed by Rahman (1988).

5.4 RECOMMENDATIONS FOR FURTHER RESEARCH

The following areas of study are suggested for further research:

1. A suitable time-incremental finite element code should be developed which incorporates the constitutive relationships developed by Rahman (1988), to account for the effect of stress history.

2. Additional plate-load and pressuremeter tests should be carried out to verify the experimental results obtained in the present study.

3. For comparative purposes, other constitutive models and available closed-form analytical procedures should be applied in analyses of the problems investigated in the present study.

4. The study should be extended to consider other geotechnical problems having different displacement and stress boundary conditions.

5. The constitutive model should be extended to include different material types and temperature conditions.

REFERENCES

Akagawa, S., 1980. "Poisson's ratio of sandy frozen soil, under long-term stress, by creep tests". Proceedings of the 2nd International Symposium on Ground Freezing, Trondheim, Norway, pp. 235-246.

Alkire, B.D., and Andersland, O.B., 1973. "The effect of confining pressure on the mechanical properties of sand-ice materials". Journal of Glaciology, Vol. 12, No. 66, pp. 469-480.

Andersland, O.B., and Alnouri, I., 1970. "Time-dependent strength behavior of frozen soils". Proceedings ASCE, Journal of the Soil Mechanics and Foundations Division, Vol. 96, No. SM4, pp. 1249-1265.

Andersland, O.B., and Anderson, D.M., eds., 1978. "Geotechnical engineering for cold regions". McGraw-Hill, New York, 566 p.

Anderson, D.M., and Morgenstern, N.R., 1973. "Physics, chemistry, and mechanics of frozen ground: a review". Proceedings of the 2nd International Conference on Permafrost, Yakutsk, North American Contribution, pp. 257-288.

Azizi, F., 1989. "Primary creep of polycrystalline ice under constant stress". Cold Regions Science and Technology, Vol. 16, pp. 159-165.

Baguelin, F., Jezequel, J.F., and Shields, D.H., 1978. "The pressuremeter and foundation engineering". Trans Tech Publications, Clausthal, Germany, 617 p.

Baker, T.H.W., 1979. "Strain rate effect on the compressive strength of frozen sand". Engineering Geology, Vol, 13, pp. 223-231.

Baker, T.H.W., and Kurfurst, P.J., 1985. "Acoustic and mechanical properties of frozen sand". Proceedings of the 4th International Symposium on Ground Freezing, Sapporo, pp. 227-233.

Blatt, J.M., 1969. "Basic Fortran IV programming". Computer Systems (Aust.) Pty. Ltd., Sydney, Australia, 183 p.

Booker, J.R., and Poulos, H.G., 1976. "Finite element analysis of piles in viscoelastic soil". Proceedings of the 2nd International Conference on Numerical Methods in Geomechanics, Blacksburg, New York, pp. 425-437.

Bourbonnais, J., and Ladanyi, B., 1985. "The mechanical behavior of frozen sand down to cryogenic temperatures". Proceedings of the 4th International Symposium on Ground Freezing, Sapporo, pp. 235-243.

Bragg, R.A., and Andersland, O.B., 1980. "Strain rate, temperature, and sample size effects on compression and tensile properties of frozen sand". Proceedings of the 2nd International Symposium on Ground Freezing, Trondheim, Norway, pp. 34-47.

Briaud, J.-L., and Shields, D.H., 1981. "Pressuremeter tests at very shallow depth". ASCE Journal of the Geotechnical Division, Vol. 107, No. GT8, pp. 1023-1040.

Briaud, J.-L., and Gambin, M., 1983. "Suggested practice for drilling boreholes for pressuremeter testing", to appear.

Briaud, J.-L., 1986. "Pressuremeter and foundation design". Use of In-situ Tests in Geotechnical Engineering, Proceedings of a Specialty Conference sponsored by the Geotechnical Engineering Division of the ASCE, Blackburg, Virginia, pp. 74-115.

Carter, J.P., Booker, J.R., and Poulos, H.G., 1982. "Finite element analysis of the creep behavior of laterally loaded piles". Proceedings of the 4th International Conference in Australia on Finite Element Methods, Melbourne, pp. 99-103.

Chamberlain, E., Groves, C., and Perham, R., 1972. "The mechanical behavior of frozen earth materials under high pressure triaxial test conditions". Geotechnique, Vol. 22, No. 3, pp. 469-483.

Chen, W.F., and Saleeb, A.F., 1982. "Constitutive equations for engineering materials, volume I: elasticity and modeling". John Wiley and Sons, Inc., 580 p.

Chen, W.F., and Baladi, G.Y., 1985. "Elastic-plastic constitutive modelling of soils". Soil Plasticity Theory and Implementation, Elsevier, New York, Chapter 2.

Clough, R.W., and Rashid, Y., 1965. "Finite element analysis of axi-symmetric solids". Proceedings ASCE, Journal of the Engineering Mechanics Division, Vol. 91, No. EM1, pp. 71-85.

Desai, C.S., "Solution of stress-deformation problems in soil and rock mechanics using finite element methods". Ph.D. Thesis, The University of Texas at Austin, 247 p.

Desai, C.S., and Reese, L.C., 1970. "Analysis of circular footings on layered soils". Proceedings ASCE, Journal of the Soil Mechanics and Foundations Division, Vol. 96, No. SM4, pp. 1289-1311.

Desai, C.S., and Abel, J.F., 1972. "Introduction to the finite element method, a numerical method for engineering analysis". Van Nostrand Reinhold Company Inc., New York, 477 p.

Domaschuk, L., and Wade, N.H., 1969. "A study of the bulk and shear moduli of a sand". Proceedings ASCE, Journal of the Soil Mechanics and Foundations Division, Vol. 95, No. SM2, pp. 561-581.

Domaschuk, L., and Valliappan, P., 1975. "Nonlinear settlement analysis by finite element". Proceedings ASCE, Journal of the Geotechnical Engineering Division, Vol. 101, No. GT7, pp. 601-614.

Domaschuk, L., Man, C.S., Shields, D.H., and Yong, E., 1983. "Creep behavior of frozen saline silt under isotropic compression". Proceedings of the 4th International Conference on Permafrost, National Academy Press, Washington, D.C., pp. 238-242.

Domaschuk, L., Knuttson, S., Shields, D.H., and Rahman, M.G., 1985. "Creep of frozen sand under isotropic and deviatoric components of stress". Proceedings ASME, Journal of Energy Resources Technology, Vol. 107, pp. 199-203.

Domaschuk, L., Shields, D.H., and Rahman, M.G., 1987. "Effect of hydrostatic stress on creep of a frozen sand". Proceedings of the 6th International Offshore Mechanics and Arctic Engineering Symposium, pp. 119-124.

Domaschuk, L., Fransson, L., and Shields, D.H., 1988. "Interaction between a laterally loaded pile and frozen soil". 5th International Conference on Permafrost, Trondheim, Norway.

Eckardt, H., 1981. "Creep behavior of frozen soils in uniaxial compression tests". Proceedings of the 4th Canadian Permafrost Conference, Calgary, pp. 394-405.

Emery, J.J., 1971. "Finite element analysis of creep problems in soil mechanics". Ph.D. Thesis, The University of British Columbia, Vancouver, B.C., 154 p.

Fensury,H., 1985. "Determination of creep parameters of frozen soil using the pressuremeter test". M.Sc. Thesis, University of Manitoba, Winnipeg, Manitoba, 209 p.

Finnie, I., and Heller, W.R., 1959. "Creep of engineering materials". McGraw-Hill Book Company, Inc., New York.

Fish, A.M., 1982. "Comparative analysis of the U.S.S.R. Construction Codes and the U.S. Army Technical Manual for design of foundations on permafrost". Report 82-14, U.S. Army CRREL, Hanover, N.H., 28 p.

Fish, A.M., 1983. "Thermodynamic model of creep at constant stresses and constant strain rates". Report 83-33, U.S. Army CRREL, Hanover, N.H., 25 p.

Fish, A.M., 1987. "Shape of creep curves in frozen soils and polycrystalline ice". Canadian Geotechnical Journal, Vol. 24, pp. 623-629.

Gioda, G., 1981. "A finite element solution of non-linear creep problems in rocks". Int. J. Rock Mech. Min. Sci. and Geomech. Abstr., Vol. 18, pp. 35-46.

Girijavallabhan, C.V., and Reese, L.C., 1968. "Finite element method for problems in soil mechanics". Proceedings ASCE, Journal of the Soil Mechanics and Foundations Division, Vol. 94, No. SM2, pp. 473-496.

Gonze, P., Lejeune, M.I., Thimus, J.F., and Monjoie, A., 1985. "Sand ground freezing for the construction of a subway station in Brussels". Proceedings of the 4th International Symposium on Ground Freezing, Sapporo, pp. 277-283.

Gorodetsky, S.E., 1975. "Creep and strength of frozen soils under combined stress". Soil Mechanics and Foundation Engineering, Vol. 12, No. 3, pp. 205-209.

Goughnour, R.R., and Andersland, O.B., 1968. "Mechanical properties of a sand-ice system". Proceedings ASCE, Journal of the Soil Mechanics and Foundations Division, Vol. 94, No. SM4, pp. 923-950.

Greenbaum, G.A., 1966. "Creep analysis of axisymmetric bodies". Ph.D. Thesis, University of California, Los Angeles, California, 99 p.

Greenbaum, G.A., and Rubinstein, M.F., 1968. "Creep analysis of axisymmetric bodies using finite elements". Nuclear Engineering and Design, Vol. 7, pp. 379-397.

Hoff, N.J., 1954. "Approximate analysis of structures in the presence of moderately large creep deformations". Quart. Appl. Math., Vol. 12, pp. 49-55.

Hooke, R.L., Dahlin, B.B., and Kauper, M.T., 1972. "Creep of ice containing dispersed fine sand". Journal of Glaciology, Vol. 11, No. 63, pp. 327-336.

Huang, Y.H., 1966. "Stresses and displacements in viscoelastic layered systems under circular loaded areas". Doctor of Science Dissertation, University of Virginia.

Hult, J.A.H., 1966. "Creep in engineering structures". Blaisdell Publishing Company, Waltham, Mass., 115 p.

Johansen, N.I., Chalich, P.C., Wellen, E.W., 1980. "Sublimation and sublimation control in the CRREL tunnel". Proceedings of the 2nd International Symposium on Ground Freezing, Trondheim, Norway, pp. 952-968.

Jones, S.J., and Parameswaran, V.R., 1983. "Deformation behavior of frozen sand-ice materials under triaxial compression". Proceedings of the 4th International Conference on Permafrost, Fairbanks, Vol. 4, pp. 560-565.

Kjartanson, B.H., 1986. "Pressuremeter creep testing in laboratory ice". Ph.D. Thesis, University of Manitoba, Winnipeg, Manitoba, 400 p.

Kjartanson, B.H., Shields, D.H., Domaschuk, L., and Man, C.-S., 1988a. "The creep of ice measured with the pressuremeter". Canadian Geotechnical Journal, Vol. 25, pp. 250-261.

Kjartanson, B.H., Shields, D.H., and Domaschuk, L., 1988b. "Pressuremeter creep testing in ice: calibration and test procedures", accepted for publication in ASTM Geotechnical Testing Journal.

Klein, J., 1981. "Finite element method for time-dependent problems of frozen soils". International Journal for Numerical and Analytical Methods in Geomechanics, Vol. 5, pp. 263-283.

Ladanyi, B., 1972. "An engineering theory of creep of frozen soils". Canadian Geotechnical Journal, Vol. 9, No. 1, pp. 63-80.

Ladanyi, B., 1974. "Bearing capacity of frozen soils". Proceedings of the 27th Canadian Geotechnical Conference, Edmonton, Alberta, pp. 97-107.

Ladanyi, B., 1975. "Bearing capacity of strip footings in frozen soils". Canadian Geotechnical Journal, Vol. 12, pp. 393-407.

Ladanyi, B., 1979. "Borehole relaxation test as a means of determining the creep properties of ice covers". Proceedings of the 5th POAC Conference, Trondheim, Norway, Vol. 1, pp. 757-770.

Ladanyi, B., 1982. "Borehole creep and relaxation tests in ice-rich permafrost". Proceedings of the 4th Canadian Permafrost Conference, R.J.E. Brown Memorial Volume, National Research Council of Canada, Ottawa, pp. 406-415.

Ladanyi, B., 1983. "Shallow foundations on frozen soil: creep settlement". Proceedings ASCE, Journal of the Geotechnical Engineering Division, Vol. 109, No. 11, pp. 1434-1448.

Ladanyi, B., 1985. "Stress transfer mechanism in frozen soils". Proceedings of the 10th Canadian Congress of Applied Mechanics, The University of Western Ontario, London, pp. 11-23.

Ladanyi, B., and Johnston, G.H., 1972. "In-situ testing of frozen soils". Northern Engineer, Vol. 4, No. 1, pp. 6-8.

Ladanyi, B., and Johnston, G.H., 1973. "Evaluation of the in-situ creep properties of frozen soils with the pressuremeter". Proceedings of the 2nd International Conference on Permafrost, Yakutsk, North American Contribution, National Acdemy of Sciences, Washington, pp. 310-318.

Ladanyi, B., and Johnston, G.H., 1974a. "Field tests of deep power-installed screw anchors in permfrost". Canadian Geotechnical Journal, Vol. 11, No. 3, pp. 348-358.

Ladanyi, B., and Johnston, G.H., 1974b. "Behavior of circular footings and plate anchors embedded in permafrost". Canadian Geotechnical Journal, Vol. 11, pp. 531-553.

Ladanyi, B., and Paquin, J., 1978. "Creep behavior of frozen sand under a deep circular load". Proceedings of the 3rd International Conference on Permafrost, Edmonton, Canada, Vol. 1, pp. 679-686.

Ladanyi, B., and Saint-Pierre, R., 1978. "Evaluation of creep properties of sea ice by means of a borehole dilatometer". Proceedings of the IAHR Symposium on Ice Problems, Lulea, Sweden, Vol. 1, pp. 97-115.

Ladanyi, B., Barthelemy, E., and Saint-Pierre, R., 1979. "In-situ determination of creep properties of ice covers by means of borehole creep and relaxation tests". Proceedings of a Workship on the Bearing Capacity of Ice Covers, Winnipeg, Canada, NRCC-ACGR Technical Memo., No. 123, pp. 44-64.

Ladanyi, B., and Sayles, F.H., 1979. "General report II: mechanical properties". Engineering Geology, Vol. 13, pp. 7-18.

Ladanyi, B., and Eckardt, H., 1983. "Dilatometer testing in thick cylinders of frozen sand". Proceedings of the 4th International Conference on Permafrost, Fairbanks, Alaska, Nat. Acad. Press, Washington, D.C., pp. 677-682.

Ladanyi, B., Murat, J.R. and Huneault, P., 1984. "A parametric study of long-term borehole dilatometer tests in ice". Proceedings of the 7th IAHR Symposium on Ice, Hamburg, Vol. 2, pp. 393-404.

Lade, P.V., Jessberger, H.L., and Dickmann, N., 1980. "Stress-strain and volumetric behavior of frozen soil". Proceedings of the 2nd International Symposium on Ground Freezing, Trondheim, Norway, pp. 48-64.

Lade, P.V., 1988. "Effects of voids and volume changes on the behavior of frictional materials". Interntional Journal for Numerical and Analytical Methods in Geomechanics, Vol. 12, pp. 351-370.

Linell, K.A., and Lobacz, E.F., 1980. "Design and construction of foundations in areas of deep seasonal frost and permafrost". Special Report 80-34, U.S. Army CRREL, Hanover, N.H., 320 p.

Liu, Y.J., and Hsu, T.R., 1982. "On the multidimensional creep deformation of ice by finite element analysis". Transactions ASME, Journal of Energy Resources Technology, Vol. 104, kpp. 193-198.

Lunne, T., and Eidsmoen, T., 1988. "Long-term plate load tests on marine clay in Svea, Svalbard". Proceedings of the 5th International Conference on Permafrost, Trondheim, Norway, pp. 1282-1287.

McRoberts, E.C., 1982. "Shallow foundations in cold regions: design". Proceedings ASCE, Journal of the Geotechnical Engineering Division, Vol. 108, No. GT10, pp. 1338-1349.

Murat, J.R., 1976. "Axi-symmetric finite element formulation of non-homogeneous floating ice sheets - Part II: Creep analysis". Ecole Polytechnique de Montreal, Report EP-76-R.37, 83 p.

Murat, J.R., Huneault, P., and Ladanyi, B., 1986. "Effects of stress redistribution on creep parameters determined by a borehole dilatometer test". 5th Intl. Symposium on Offshore Mechanics and Arctic Engineering, Tokyo, Vol. 4, pp. 58-64.

Murat, J.R., and Lemoigne, Y., 1988. "Improved calibration and correction techniques for pressuremeters", accepted for publication in ASTM Geotechnical Testing Journal.

Nixon, J.F., 1978. "First Canadian geotechnical colloquim: foundation design approaches in permafrost areas". Canadian Geotechnical Journal, Vol. 15, pp. 96-112.

Nye, J.F., 1957. "The distribution of stress and velocity in glaciers and ice-sheets". Proceedings of the Royal Society of London, Vol. A239, pp. 113-133.

Odqvist, F.K.G., 1966. "Mathematical theory of creep and creep rupture". Clarendon Press, London, England, 168 p.

Ohya, S., 1982. "Modification of the Elastmeter - 100 to apply in more soft or loose soil ground". Report prepared for the OYO Corporation, Japan, 20 p.

Orth, W., 1985. "Deformation of frozen sand and its physical interpretation". Proceedings of the 4th International Symposium on Ground Freezing, Sapporo, pp. 245-253.

Parameswaran, V.R., 1980. "Deformation behavior and strength of frozen sand". Canadian Geotechnical Journal, Vol. 17, pp. 74-88.

Parameswaran, V.R., 1985. "Attenuating creep of piles in frozen soils". Foundations in Permafrost and Seasonal Frost, Proceedings of a session sponsored by the ASCE Technical Council on Cold Regions Engineering, Denver, Colorado, pp. 16-28.

Parameswaran, V.R., and Jones, S.J., 1981. "Triaxial testing of frozen sand". Journal of Glaciology, Vol. 27, No. 95, pp. 147-155.

Parameswaran, V.R., and Roy, M., 1982. "Strength and deformation of frozen saturated sand at -30°C". Canadian Geotechnical Journal, Vol. 19, pp. 104-107.

Pekarskaya, N.K., 1973. "The strain-hardening of frozen ground during the creep process". Proceedings of the 2nd International Conference on Permafrost, Yakutsk, U.S.S.R. Contribution, pp. 841-842.

Penny, R.K., and Marriott, D.L., 1971. "Design for creep". McGraw-Hill Book Company (UK) Ltd., 291 p.

Pusch, R., 1980. "Creep of frozen soil: a preliminary physical interpretation". Proceedings of the 2nd International Symposium on Ground Freezing, Trondheim, Norway, pp. 190-201.

Puswewala, U.G.A., 1988. "Constitutive relations for frozen soils". Internal Report, University of Manitoba, Winnipeg, Manitoba. 121 p.

Rabotnov, Y.N., 1966. "Creep problems in structural members". Transl. from Russian. North Holland Publishing Company, 1969.

Rahman, M.G., 1988. "The creep of frozen sands". Ph.D. Thesis, University of Manitoba, Winnipeg, Manitoba, 268 p.

Rein, R.G., Vidyutkumar, V.H., and Sliepcevich, C.M., 1975. "Creep of sand-ice system". Proceedings ASCE, Journal of the Geotechnical Engineering Division, Vol. 101, No. GT2, pp. 115-128.

Rowley, R.K., Watson, G.H., and Ladanyi, B., 1973. "Vertical and lateral pile load tests in permafrost". Proceedings of the 2nd International Conference on Permafrost, Yakutsk, USSR, North American Contribution, pp. 712-721.

Rowley, R.K., Watson, G.H., and Ladanyi, B., 1975. "Prediction of pile performance in permafrost under lateral load". Canadian Geotechnical Journal, Vol. 12, pp. 510-523.

Sanger, F.J., 1969. "Foundations of structures in cold regions". Monograph 111-C4, U.S. Army CRREL, Hanover, N.H., 93 p.

Sayles, F.H., 1968. "Creep of frozen sands". Technical Report 190, U.S. Army CRREL, Hanover, N.H., 60 p.

Sayles, F.H., 1973. "Triaxial and creep tests on frozen Ottawa sands". Proceedings of the 2nd International Conference on Permafrost, Yakutsk, North American Contribution, pp. 384-392.

Sayles, F.H., 1974. "The use of frozen soil mechanics in the design of structures in permafrost". Acres Geotechnical Seminar, 37 p.

Sayles, F.H., 1985. "Creep of a strip footing on ice-rich permafrost". Foundations in Permafrost and Seasonal Frost, Proceedings of a session sponsored by the ASCE Technical Council on Cold Regions Engineering, Denver, Colorado, pp. 29-51.

Scott, R.F., 1969. "The freezing process and mechanics of frozen ground". Monograph II-DI, U.S. Army CRREL, Hanover, N.H., 65 p.

Sego, C., and Morgenstern, N.R., 1985. "Punch indentation of polycrystalline ice". Canadian Geotechnical Journal, Vol. 22, pp. 226-233.

Shanley, F.R., 1952. "Weight-strength analysis of aircraft structures". McGraw-Hill Book Company, Inc., 394 p.

Shibata, T. et al., 1985. "Time-dependence and volumetric change characteristics of frozen sand under triaxial stress condition". Proceedings of the 4th International Symposium on Ground Freezing, Sapporo, pp. 173-179.

Shields, D.H., Domaschuk, L., Azizi, F., and Kjartanson, B.H., 1988a. "Primary creep parameters for ice measured in-situ", submitted to Cold Regions Science and Technology.

Shields, D.H., Domaschuk, L., Kjartanson, B.H., and Azizi, F., 1988b. "Measuring the creep properties of ice in-situ". Proceedings of the 24th Annual Conference of the Engineering Group of the Geological Society, Field Testing in Engineering Geology, Newcastle-on-Tyne, England.

Shields, D.H., Domaschuk, L., Funegard, E., and Azizi, F., 1988c. "Creep rates of spray ice". Proceedings of the 41st Canadian Geotechnical Conference, Waterloo, Ontario.

Shields, D.H., Domaschuk, L., Kjartanson, B.H., and Azizi, F., 1988d. "Measuring the creep of ice in place". Proceedings of the International Conference on Technology for Polar Areas: Polartech 88, Trondheim, Norway.

Singh, A., and Mitchell, J.K., 1968. "General stress-strain-time function for soils". Proceedings ASCE, Journal of the Soil Mechanics and Foundations Division, Vol. 94, No. SM1, pp. 21-46.

Smith, J.O., and Sidebottom, O.M., 1965. "Inelastic behavior of load-carrying members". John Wiley and Sons, New York, 447 p.

Sun, Q., Domaschuk, L., and Rahman, M.G., 1989. "A viscoelastic constitutive model for creep of frozen soil". Proceedings of the 3rd International Symposium on Numerical Models in Geomechanics, Niagara Falls, Canada.

Sweanum, S., Wen, R.K., and Andersland, O.B., 1987. "Finite element method for analysis of frozen earth structures". Cold Regions Science and Technology, Vol. 13, pp. 121-129.

Terzaghi, K., 1955. "Evaluation of coefficients of subgrade reaction". Geotechnique, Vol. 5, pp. 297-326.

Thompson, E.G., and Sayles, F.H., 1972. "In-situ creep analysis of room in frozen soil". Proceedings ASCE, Journal of the Soil Mechanics and Foundations Division, Vol. 98, No. SM9, pp. 899-915.

Ting, J.M., 1981. "The creep of frozen sands: qualitative and quantitative models". Research Report No. R81-5, U.S. Army CRREL, Hanover, N.H., 432 p.

Ting, J.M., 1983. "Tertiary creep model for frozen sands". Proceedings ASCE, Journal of Geotechnical Engineering, Vol. 109, No. 7, pp. 932-945.

Ting, J.M., Martin, R.T., and Ladd, C.C., 1983. "Mechanisms of strength for frozen sand". Proceedings ASCE, Journal of Geotechnical Engineering, Vol. 109, No. 10, pp. 1286-1302.

Tsytovich, N.A., 1957. "The fundamentals of frozen ground mechanics". Proceedings of the 4th International Conference on Soil Mechanics and Foundation Engineering, London, Vol. 1, pp. 116-119.

Tsytovich, N.A., 1960. "Bases and foundations on frozen soil". Highway Research Board, Special Report 58, 93 p.

Tsytovich, N.A., 1975. "The mechanics of frozen ground". McGraw-Hill, New York, 426 p.

Tsytovich, N.A., and Cherkasov, I.I., 1970. "Determining the compressibility factor of soils from the impression of test plates". Soil Mechanics and Foundation Engineering, No. 6, pp. 379-381.

Turner, S., 1966. "The foundations of possible engineering design methods for plastics". Trans. J. Plastics Inst., Vol. 34, pp. 127-135.

Valliappan, P., 1974. "Nonlinear stress-deformation analysis of Lake Agassiz clays using the finite element method". Ph.D. Thesis, University of Manitoba, Winnipeg, Manitoba.

Voytkovskiy, K.F., 1960. "The mechanical properties of ice". Izrestia Adademia Nauk, Moscow, USSR. English translation AMS-T-R-391. United States Department of Commerce, Washington, D.C.

Vyalov, S.S., 1957. "Creep and long-term strength of frozen soils". Tran. Dok. Akad. Nauk. Vol. 104, No. 6, pp. 5-9.

Vyalov, S.S., 1959. "Rheological properties and bearing capacity of frozen soils". Transl. 74, U.S. Army CRREL, Hanover, N.H., 1965, 219 p.

Vyalov, S.S., 1963. "Rheology of frozen soils". Proceedings of the 1st International Conference on Permafrost, Lafayette, Indiana, pp. 332-338.

Vyalov, S.S., 1973. "Long-term failure of frozen soil as a thermally activated process". Proceedings of the 2nd International Conference on Permafrost, Yakutsk, U.S.S.R. Contribution, pp. 222-228.

Vyalov, S.S., 1978. "Long-term settlement of foundations on permafrost". Proceedings of the 3rd International Conference on Permafrost, Edmonton, Canada, pp. 899-903.

Vyalov, S.S., 1979. "Settlements of experimental plates on plastic-frozen soils". Soil Mechanics and Foundation Engineering, Vol. 15, No. 5, pp. 328-334.

Vyalov, S.S., 1986. "Rheological fundamentals of soil mechanics". Elsevier Science Publishing Company Inc., New York, 564 p.

Vyalov, S.S. et al., 1962. "The strength and creep of frozen soils and calculations for ice-soil retaining structures". Transl. 76, U.S. Army CRREL, Hanover, N.H., 300 p.

Vyalov, S.S., and Pekarskaya, N.K., 1968. "Long-term strength of soils". Pro. Coordinating Conf. Hydraul. Eng., Issue 38, Study of Rheological Properties of Soils.

Vyalov, S.S., Dokuchayev, V.V., and Sheyukman, D.R., 1973. "Ground ice as a bearing stratum for construction". Proceedings of the 2nd International Conference on Permafrost, Yakutsk, U.S.S.R. Contribution, pp. 537-545.

Vyalov, S.S., Manimyak, R.V., Razbegin, V.N., Slepak, M.E., and Chapayev, A.A., 1988. "Stress-strain behavior of frozen soils". Proceedings of the 5th International Conference on Permafrost, Trondheim, Norway, pp. 1186-1191.

Wilson, E.L., 1965. "Structural analysis of axisymmetric solids". AIAA Journal, Vol. 3, pp. 2269-2274.

Zaretskii, Y.K., 1972. "Rheological properties of plastic frozen soils and determination of settlement of a test plate with time". Soil Mechanics and Foundation Engineering, Vol. 9, No. 2, pp. 81-85.

Zaretskii, Y.K., and Fish, A.M., 1973. "A study of the rheological properties of ice using a pressuremeter". Proceedings of the 2nd International Conference on Permafrost, Yakutsk, USSR Contribution, National Academy of Sciences, pp. 846-847.

Zaretskii, Y.K., and Gorodetskii, S.E., 1975. "Dilatancy of frozen soil and development of a strain theory of creep". Hydrotechnical Construction, No. 2, pp. 127-132.

Zaretskii, Y.K., and Schebolev, A.G., 1983. "A mathematical model for the viscoplastic deformation of frozen soils". Proceedings of the 4th International Conference on Permafrost, Fairbanks, Alaska, Vol. 1, pp. 1457-1462.

Zaretskii, Y.K., Ter-Martirosyan, Z.G., and Shchobolev, A.G., 1988. "Stress-strain prediction of frozen retaining structures regarding the frozen soil creep". Proceedings of the 5th International Conference on Permafrost, Trondheim, Norway, pp. 533-536.

Zatsarnaya, A.G., 1973. "Calculating the settlement of foundations on plastically frozen ground". Proceedings of the 2nd International Conference on Permafrost, Yakutsk, U.S.S.R. Contribution, pp. 647-650.

Zienkiewicz, O.C., 1971. "The finite element method in engineering science". McGraw-Hill Publishing Company Ltd.

APPENDIX A

PRESSUREMETER CREEP TEST CALIBRATIONS

PRESSUREMETER CALIBRATION

According to Kjartanson (1986) and Kjartanson et al. (1988b), modifications to the manufacturer's suggested calibration methods are necessary to account for long-term and low temperature tests. The recommended procedures to determine corrected values of the borehole radius and pressure may be grouped into three categories:

1. calibration of the caliper arm - LVDT system
2. calibration for membrane thickness, and
3. calibration for membrane resistance.

In the following, these calibrations are described with regard to the present study.

1. Caliper Arm - LVDT System

The following relationships were required in order to calculate the internal radius of the rubber membrane. Based on the geometry of the caliper arm - LVDT system, the internal radius, r_i , is related to the travel, x , of the LVDT core by:

$$r_i = 2x + 6[1 - (x/25)^2]^{\frac{1}{2}} + 16 \text{ mm} . \quad (1)$$

The digital indicator reading, r_n , is related to x by:

$$x = c_1 + c_2 r_n , \quad (2)$$

in which c_1 and c_2 are calibration constants. To determine r_i , the value of x was first calculated from equation 2 and then substituted into equation 1.

For calibration of the caliper arm - LVDT system, a calibration ring was slid along the pressuremeter core. In setting the zero and gain potentiometers, the manufacturer's calibration ring, with two radius settings, 1 and 2, was used. For radius setting 1, the internal radius, r_i , is 23.500 mm, and the digital indicator reading, r_n , was set to -2.00. For radius setting 2, the internal radius, r_i , is 33.500 mm, and the digital indicator reading, r_n , was set to -12.00. To establish the relationship between the digital indicator reading, r_n , and the travel, x ,

of the LVDT core, the x values corresponding to these radius settings were back-calculated from equation 1. The values of the calibration constants, c_1 and c_2, in equation 2, were determined to be 6.8493 and 0.5082, respectively. To verify these values, a calibration ring with three additional radius settings, 3, 4, and 5, was used. Digital indicator readings, r_n, were obtained for these radius settings and the corresponding values of the internal radius, r_i, were calculated from equations 1 and 2. The calculated radii and the actual radii are given in Table 1. The maximum error in nonlinearity, based on radius settings 3, 4, and 5, was in the order of 0.03 and 0.02 mm, for pressuremeter Test Nos. 1 and 2, respectively.

TABLE 1 CALIPER ARM - LVDT SYSTEM CALIBRATION RESULTS

Radius Setting No.	Actual r_i (mm)	r_n	x(mm)	Computed r_i (mm)
TEST NO. 1:				
1	23.500	-12.00	0.7514	23.500
2	33.500	-2.00	5.833	33.500
3	38.485	3.09	8.420	38.489
4	41.980	6.73	10.269	42.008
5	45.995	10.93	12.403	46.016
TEST NO. 2:				
1	23.500	-12.00	0.7514	23.500
2	33.500	-2.00	5.833	33.500
3	38.485	3.10	8.425	38.498
4	41.980	6.72	10.264	41.999
5	45.995	10.92	12.398	46.007

Drift of the caliper arm radius measuring system was small. Table 2 gives the results of calibrations performed before and immediately after pressuremeter testing. For Test Nos. 1 and 2, the test duration was about 120 and 80 days, respectively. Based on an average of the before and after test readings, the maximum error in the system was determined to be in the order of 0.06 mm for Test No. 1 and 0.03 mm for Test No. 2.

TABLE 2 DRIFT OF THE RADIUS MEASURING SYSTEM

Radius Setting No.	r_n (before test)	r_n (after test)
TEST NO. 1:		
1	-12.00	-11.89
2	-2.00	-2.00
TEST NO. 2:		
1	-12.00	-11.94
2	-2.00	-2.00

2. Membrane Thickness

Two types of calibrations were necessary to relate the caliper arm inside radius reading to the outside radius of the rubber membrane, that is, the borehole radius:

(a) calibration to account for change in membrane thickness with expansion of the probe, and

(b) calibration to account for compression of the membrane due to applied pressures.

(a) Membrane Thickness Change Due to Probe Expansion

To calibrate for change in membrane thickness, the probe was placed in each of five thick-walled steel tubes having inside radii ranging from 37.84 to 47.58 ± 0.01 mm, which represented the common range of probe expansion during a test. The probe was inflated until it just came into contact with each tube, by increasing the probe pressure in 13.79 KPa increments. Each increment was maintained for one minute. The digital indicator reading, r_n , corresponding to the initial contact of the probe with the steel tube wall, was then converted to an inside radius value, r_i , using equations 1 and 2. Therefore, both the inside radius of the membrane, r_i , and the outside radius of the membrane, r_o , were known. The cross-sectional area of the membrane, s , was then calculated, as

follows:

$$s = \pi[(r_o / 10.0)^2 + (r_i / 10.0)^2] \, cm^2 \quad . \qquad (3)$$

In this manner, an s/π value was determined for each steel tube, both before and after each pressuremeter test. The s/π versus r_n relationship was expressed as:

$$s/\pi = (c_3 + c_4 \, r_n) \, cm^2 \quad , \qquad (4)$$

in which c_3 and c_4 are calibration constants. The relationship is shown plotted in Figures 1 and 2. The values of the calibration constants c_3 and c_4, in equation 4, were determined to be 2.3137 and 0.09476, respectively, for Test No. 1, and 2.2394 and 0.09719, respectively, for Test No. 2.

(b) Membrane Compression Due to Pressure

The change in membrane thickness with pressure calibration was performed in the thick-walled steel tube closest in radius to the initial test cavity radius. To determine the zero reading for the calibration test, the probe was first inflated sufficiently to provide contact with the tube. The pressure was then rapidly increased to the proposed test pressure and held constant. The changes in the digital indicator reading, r_n, with time, were then recorded. The relationsip between the observed change in membrane thickness, P_g, and the time, t, in minutes was expressed as:

$$P_g = (c_5 + c_6 \ln (t)) \, mm \quad , \qquad (5)$$

in which c_5 and c_6 are calibration constants. Since the pressuremeter tests were multi-stage tests, staged calibrations were performed. The constants, c_5 and c_6, in equation 5, were determined for each pressure increment. The calibrations were carried out both before and after the pressuremeter tests. The results of the calibrations are given in Tables 3 through 6.

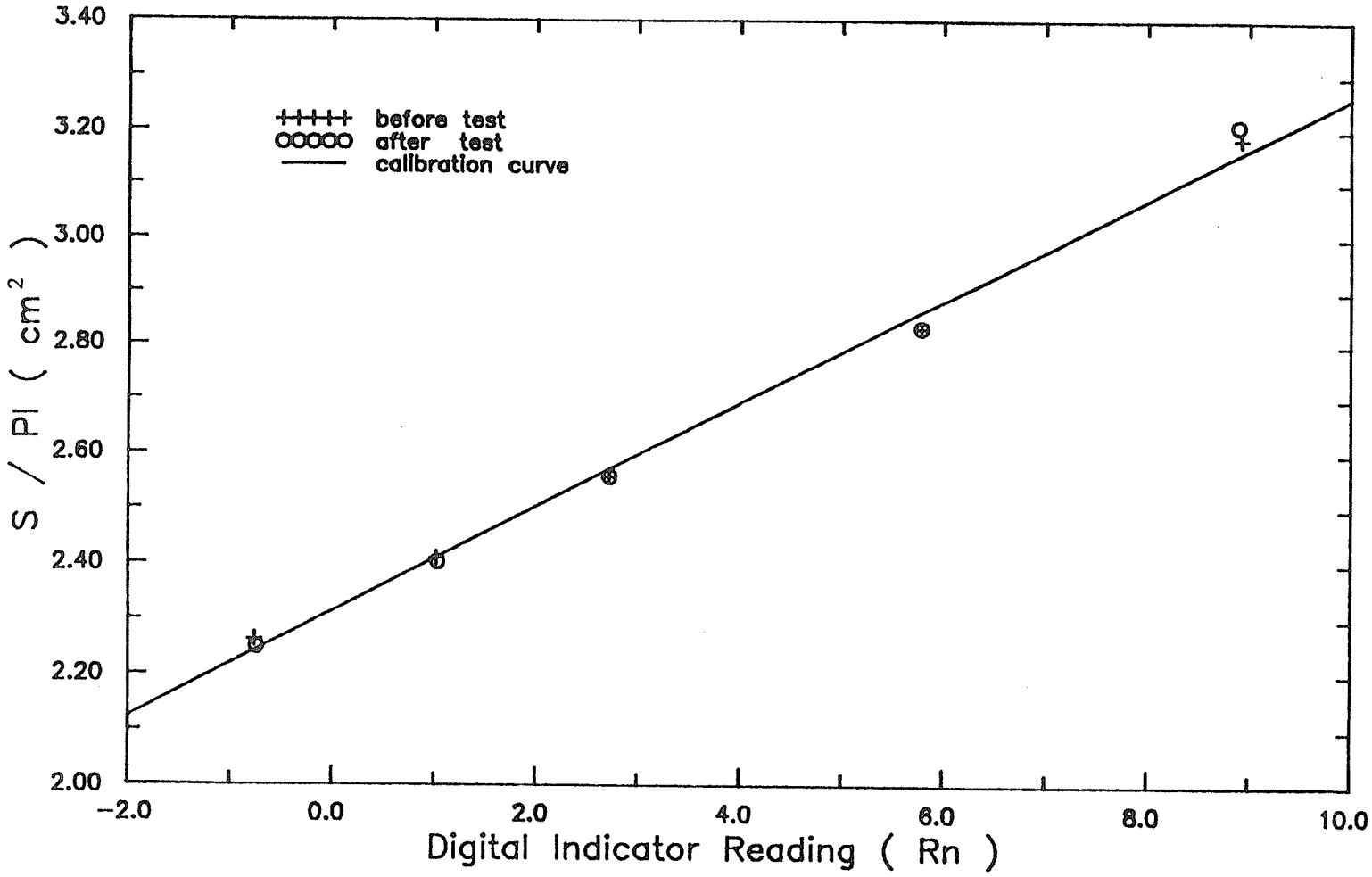

FIGURE 1 CROSS-SECTIONAL AREA OF MEMBRANE - DIGITAL INDICATOR READING RELATIONSHIP (TEST NO. 1)

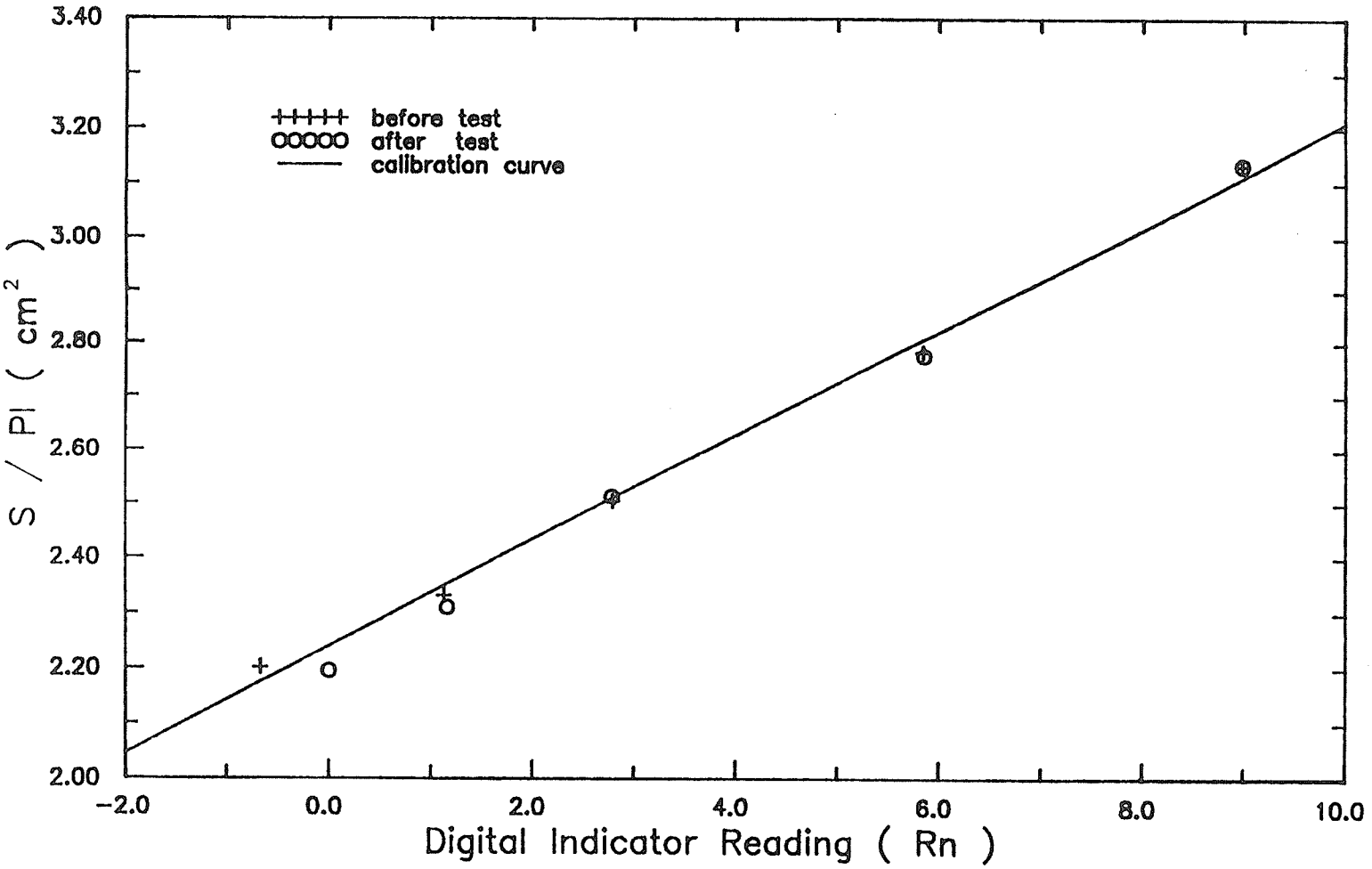

FIGURE 2 CROSS-SECTIONAL AREA OF MEMBRANE - DIGITAL INDICATOR READING RELATIONSHIP (TEST NO. 2)

TABLE 3 CHANGE IN MEMBRANE THICKNESS WITH TIME
CALIBRATION: BEFORE TEST RESULTS
TEST #1

Elapsed Time (min)	Pressure (MPa)	r_n	Change in r_i (mm)
STAGE 1:			
0	(membrane in contact)	1.06	--
1	0.8543	1.14	0.078
2	0.8571	1.15	0.088
3	0.859	1.15	0.088
5	0.8585	1.15	0.088
10	0.8507	1.15	0.088
20	0.8502	1.15	0.088
30	0.8525	1.15	0.088
60	0.8516	1.15	0.088
120	0.8497	1.16	0.098
240	0.8516	1.16	0.098
$c_5(1) = 0.0822$	$c_6(1) = 0.0026$		
STAGE 2:			
1	1.797	1.16	0.098
5	1.799	1.17	0.108
15	1.798	1.17	0.108
$c_5(2) = 0.108$	$c_6(2) = 0.0$		
STAGE 3:			
1	2.805	1.18	0.117
5	2.811	1.18	0.117
15	2.811	1.18	0.117
$c_5(3) = 0.117$	$c_6(3) = 0.0$		
STAGE 4:			
1	3.509	1.19	0.127
5	3.499	1.19	0.127
15	3.498	1.19	0.127
$c_5(4) = 0.127$	$c_6(4) = 0.0$		

TABLE 4 CHANGE IN MEMBRANE THICKNESS WITH TIME
CALIBRATION: AFTER TEST RESULTS
TEST #1

Elapsed Time (min)	Pressure (MPa)	r_n	Change in r_i (mm)
STAGE 1:			
0	(membrane in contact)	1.05	----
1	0.8521	1.10	0.049
2	0.8535	1.10	0.049
5	0.8542	1.10	0.049
10	0.8499	1.11	0.059
20	0.8462	1.11	0.059
30	0.8461	1.11	0.059
60	0.8512	1.14	0.088
120	0.8526	1.16	0.108
240	0.8525	1.16	0.108
$c_5(1) = 0.03596$	$c_6(1) = 0.01199$		
STAGE 2:			
1	1.821	1.17	0.118
5	1.820	1.18	0.127
15	1.821	1.18	0.127
$c_5(2) = 0.127$	$c_6(2) = 0.0$		
STAGE 3:			
1	2.836	1.19	0.137
5	2.839	1.19	0.137
15	2.841	1.19	0.137
$c_5(3) = 0.137$	$c_6(3) = 0.0$		
STAGE 4:			
1	3.531	1.20	0.147
5	3.509	1.20	0.147
15	3.524	1.20	0.147
$c_5(4) = 0.147$	$c_6(4) = 0.0$		

TABLE 5 CHANGE IN MEMBRANE THICKNESS WITH TIME
CALIBRATION: BEFORE TEST RESULTS
TEST #2

Elapsed Time (min)	Pressure (MPa)	r_n	Change in r_i (mm)
STAGE 1:			
0	(membrane in contact)	1.23	----
1	0.8583	1.26	0.030
2	0.8499	1.26	0.030
3	0.8495	1.26	0.030
5	0.8718	1.26	0.030
10	0.8541	1.26	0.030
20	0.8439	1.26	0.030
30	0.8578	1.26	0.030
60	0.8639	1.27	0.039
120	0.8500	1.27	0.039
240	0.8499	1.27	0.039
$c_5(1) = 0.0276$	$c_6(1) = 0.0019$		
STAGE 2:			
1	1.812	1.28	0.049
5	1.803	1.28	0.049
15	1.806	1.28	0.049
$c_5(2) = 0.049$	$c_6(2) = 0.0$		
STAGE 3:			
1	2.858	1.29	0.059
5	2.820	1.29	0.059
15	2.781	1.29	0.059
$c_5(3) = 0.059$	$c_6(3) = 0.0$		
STAGE 4:			
1	3.489	1.30	0.069
5	3.484	1.31	0.079
15	3.544	1.31	0.079
$c_5(4) = 0.079$	$c_6(4) = 0.0$		

TABLE 6 CHANGE IN MEMBRANE THICKNESS WITH TIME
CALIBRATION: AFTER TEST RESULTS
TEST #2

Elapsed Time (min)	Pressure (MPa)	r_n	Change in r_i (mm)
STAGE 1:			
0	(membrane in contact)	1.19	--
1	0.8552	1.22	0.029
2	0.8517	1.22	0.029
3	0.8520	1.22	0.029
5	0.8630	1.22	0.029
10	0.8520	1.22	0.029
20	0.8451	1.22	0.029
30	0.8519	1.22	0.029
60	0.8575	1.24	0.049
120	0.8513	1.24	0.049
240	0.8513	1.24	0.049
$c_5(1) = 0.02360$	$c_6(1) = 0.00431$		
STAGE 2:			
1	1.817	1.26	0.069
5	1.812	1.26	0.069
15	1.814	1.26	0.069
$c_5(2) = 0.069$	$c_6(2) = 0.0$		
STAGE 3:			
1	2.847	1.27	0.078
5	2.830	1.27	0.078
15	2.811	1.27	0.078
$c_5(3) = 0.078$	$c_6 = 0.0$		
STAGE 4:			
1	3.510	1.27	36.713
5	3.497	1.27	36.713
15	3.534	1.28	36.723
$c_5(4) = 0.088$	$c_6(4) = 0.0$		

In order to determine the outside radius, r_o , of the membrane, the results of the two membrane thickness calibrations, (a) and (b), were applied independently. First, a corrected inside radius, r_s , was calculated by subtracting the change in membrane thickness, P_g, from the inside radius, r_i :

$$r_s = [(r_i - P_g) / 10.0] \text{ cm} \quad . \tag{6}$$

Next, the value of s/π , in which s is the cross-sectional area of the membrane, was calculated from equation 4. Finally, the outside radius, r_o , was determined using the following expression:

$$r_o = [(s/\pi + r_s^2)^{1/2} 10.0] \text{ mm} \quad . \tag{7}$$

3. Membrane Resistance Correction

On expansion of the rubber membrane during testing, a difference existed between the recorded internal pressure and the pressure actually applied by the probe to the borehole wall. This difference was due to the resistance of the rubber membrane. Therefore, it was necessary to obtain the resistance to inflation of the membrane by calibration, and to subtract it from the measured probe pressure, in order to determine the true pressure applied to the soil. The calibration involved unrestrained inflation of the probe in air in increments of 20 kPa, to the capacity of the radius measurement system. Each increment was maintained for a period of 60 minutes. The 60-minute digital indicator readings, r_n , are shown as a function of applied pressure, for Test Nos. 1 and 2, in Figures 3 and 4, respectively.

In a similar manner, Kjartanson (1986) studied the change of membrane resistance during pressuremeter creep tests at -2°C. In order to compensate for the loss of membrane stiffness during a test, Kjartanson used a composite curve (also shown in Figures 3 and 4) to reflect the membrane resistance of the 'before test' curves early in the test and the less stiff 'after test' curves near the end of the test. The composite curve was developed from the calibration

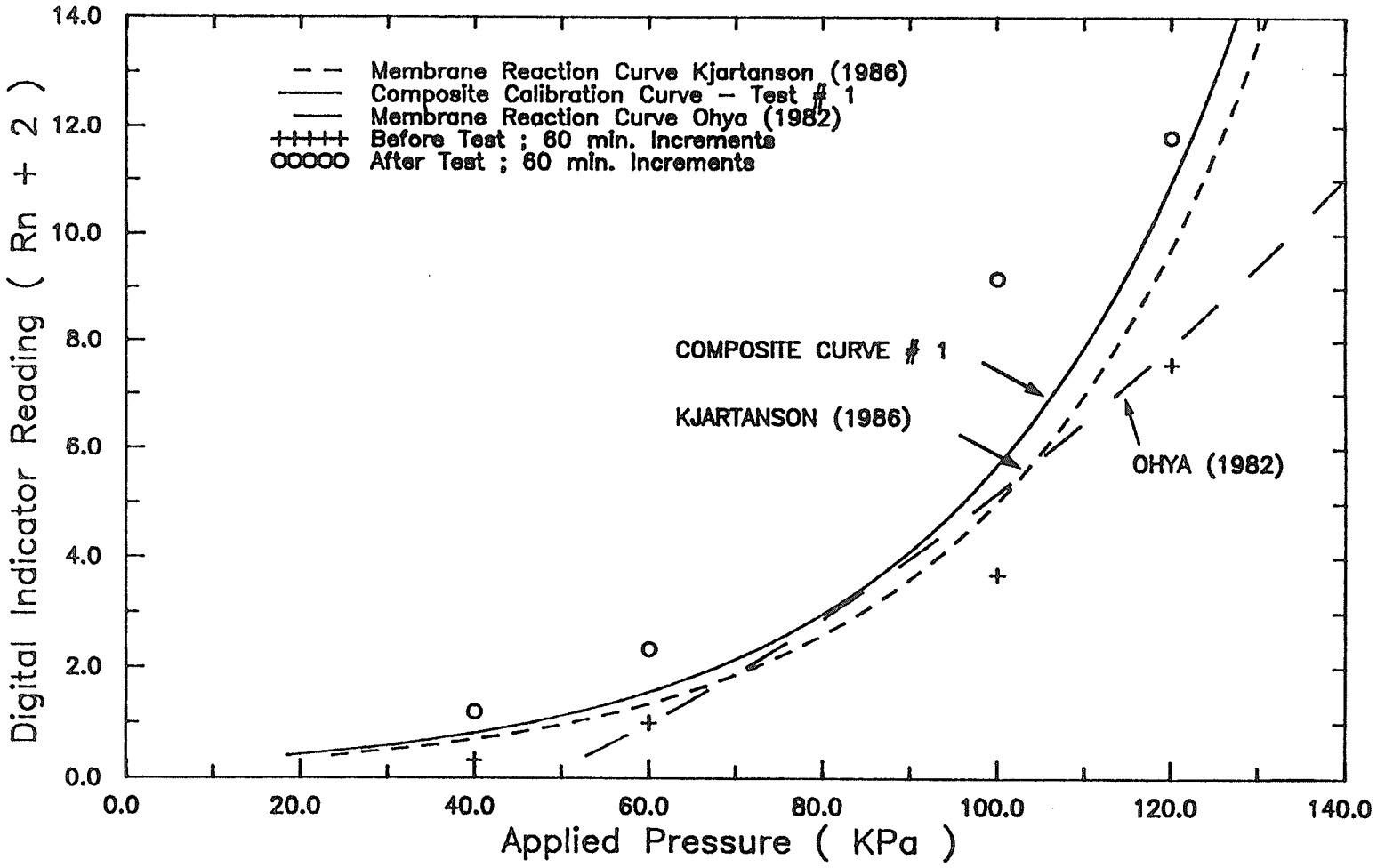

FIGURE 3 MEMBRANE REACTION CURVES INCLUDING COMPOSITE CALIBRATION CURVE FOR TEST NO. 1

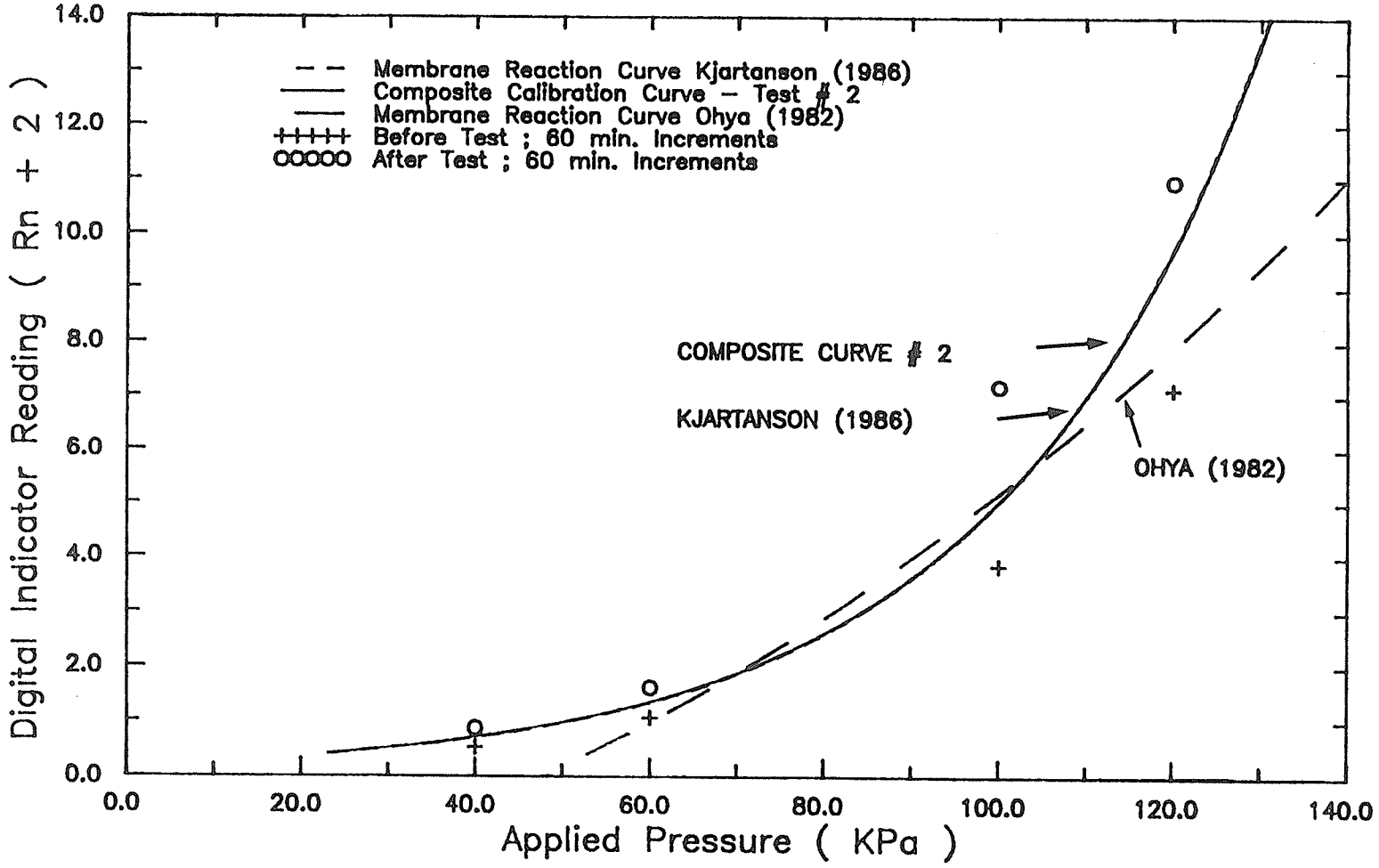

FIGURE 4 MEMBRANE REACTION CURVES INCLUDING COMPOSITE CALIBRATION CURVE FOR TEST NO. 2

results of two pressuremeter tests of durations 52 and 26 days. There was no apparent change in resistance for different membranes. The membrane reaction curve suggested by Ohya (1982), based on tests conducted in steel tubes at room temperature, is also presented in Figures 3 and 4.

In the present study, composite calibration curves were developed for pressuremeter Test Nos. 1 and 2. These are shown in Figures 3 and 4. The membrane resistance correction, R_g , or composite calibration curve, was given by:

$$R_g = 46.57 + 30.695 \ln (r_n + 2) \text{ KPa}$$

for Test No. 1, and by:

$$R_g = 50.94 + 30.37 \ln (r_n + 2) \text{ KPa}$$

for Test No. 2. These curves were used to calculate the true pressure applied to the cavity wall, P_{cav} , from the applied internal pressure, Pa, according to:

$$P_{cav} = Pa - (R_g / 1000.0) \text{ MPa} \quad . \qquad (8)$$

It was also necessary to adjust the internal pressure in the probe throughout the duration of each test. This was required to account for the current membrane resistance, in order to apply the proposed constant test pressure to the cavity wall. Since it was not possible to develop a composite calibration curve until 'after test' calibrations had been performed, the curve suggested by Kjartanson (1986) given by:

$$R_g = 51.28 + 30.18 \ln (r_n + 2) \text{ KPa}$$

was used for this purpose. It was observed that the 'before test' calibration results of Kjartanson were similar to those of the present study.

In summary, the results from all of the above-described calibrations allowed for: the calculation of the cavity radius based on the digital indicator reading; the calculation of the true pressure applied to the cavity based on the measured

internal pressure; and conversely, the calculation of the internal pressure required to apply a desired constant cavity pressure. Simple computer programs were written to perform these calculations as required, during testing.

APPENDIX B

COMPUTER PROGRAM FOR FINITE ELEMENT ANALYSIS

GUIDELINES FOR DATA INPUT

A. Problem Heading (20A4)

Columns 1 - 80 contain alphanumeric data to be printed as titles on the output.

B. Problem Details (15, 5X, 17A4)

Columns 1 - 5 Problem number

11 - 80 Problem details

C. Logical Keys: Options to Keep Prior Information (715)

One for retaining or using the information previously read, zero otherwise.

Column 5 Control information (KCINF)

10 Linear material type (KLMTYP)

15 Nodal point data (KNPDT)

20 Element data (KELDT)

25 Non linear data (KNLIN)

30 Soil conditions (KSCON)

35 Constant moduli information (KPLE)

D. Time Increment Specification (15, E10.3)

Column 1 - 5 Number of time increments (NTINCR)

6 - 15 Size of time increments (STINCR)

E. General Information and Options (11I5)

Columns 1 - 5 Number of nodal points (NNP); 400 maximum

6 - 10 Number of elements (NEL); 300 maximum

11 - 15 Number of linear or nonlinear materials (NMAT); 10 maximum

16 - 20 Number of boundary pressure cards (NBPC); 30 maximum

21 - 25 Number of increments (NINCR)

26 - 30 Number of concentrated load or deformation points (NUMLPC)

35 Option for full or half step method of analysis (NRNGKT). Set the value = 0 for half step and to one for full step.

40 Option for linear or nonlinear analysis (LIN). Set the value = 0 for linear analysis and to one for nonlinear analysis.

45 Option for analysis of materials with constant K and G (MPILE). Set the value = 1 for such analysis; zero otherwise.

50 Option for different increment of loading (KINEXC) set the value = 1 for different increment of loading; zero otherwise.

55 Number of elements to be modified in a stage (NELEX).

F. Linear Material Properties (3E 10.3)

Required if the option for linear material type (KLMTYP) is specified as zero in Section C. As many number of cards as the number of linear materials (NMAT) specified in Section E.

Columns 1 - 10 Elastic modulus (E)

11 - 20 Poisson's ratio (NU)

21 - 30 Density (RO)

G. Soil Conditions (3F10.0)

Required if the option for soil conditions (KSCON) is specified as zero in Section C.

Columns 1 - 10 Coefficient of earth pressure at rest (CEPAR)

11 - 20 Depth of bottom boundary (DEPB)

21 - 30 Average unit weight of soil (UWT)

H. Nodal Point Cards (15, 5X, 5F10.3)

Required if the option for nodal point data (KNPDT) is specified as zero in Section C. One card for each nodal point with the following information.

Columns 1 - 5 Nodal point number (N)

11 - 20 Code number which indicates if displacements or forces to be specified.

21 - 30 R - ordinate (R)

31 - 40 Z - ordinate (Z)

41 - 50 Specified load or displacement in R-direction (UR)

51 - 60 Specified load or displacement in Z-direction (UZ)

If the nodal points are on a straight line and equidistant then the first and last nodal points need to be input and intermediate nodal points are generated by the program. The code number for the generated nodal point is assigned as 0.0.

If the number in columns 11 - 20 is:

0.0 UR is the specified load in R-direction

UZ is the specified load in Z-direction

1.0 UR is the specified displacement in R-direction

UZ is the specified load in Z-direction

2.0 UR is the specified load in R-direction

UZ is the specified displacement in Z-direction

3.0 UR is the specified displacement in R-direction

UZ is the specified displacement in Z-direction

All loads are considered to be total forces acting in one radial segment,

Skew Boundaries

If the number in columns 11 - 20 is other than 0.0, 1.0, 2.0 or 3.0, it is interpreted as the magnitude of an angle in degrees. The terms in columns 41 - 60 of the nodal point card are then interpreted as follows:

UR is the specified load in 1-direction and

UZ is the specified displacement in 2-direction.

The directions 1 and 2 are indicated with reference to coordinate system in Figure 1. The angle must always be input as a negative angle and can range from -.001 to -180.0 degrees. Hence, +1.0 degree is the same as - 179.0 degrees. The displacements of these nodal points which are printed by the program are:

UR = the displacement in 1-direction and

US = the displacement in 2-direction.

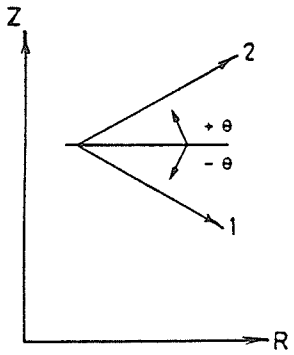

Figure 1 Skew Boundary

I. Load or Deformation Addition at Certain Nodal Points (15, 5X, 5F10.3).

Required if the option for element data (KELDT) is specified as zero in Section C and if the option for linear or nonlinear analysis (LIN) is specified as zero in Section E. One card for each element. Order nodal points counter-clockwise around element. Identification of nodal points according to Figure 2.

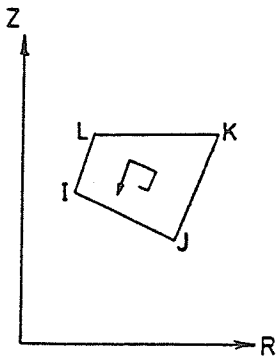

Figure 2 Quadrilateral Element

Columns 1 - 5 Element number (M)

6 - 10 Nodal point I (IX (M,1))

11 - 15 Nodal point J (IX (M,2))

16 - 20 Nodal point K (IX (M,3))

21 - 25 Nodal point L (IX (M,4))

26 - 30 Material identification (IX (M,5))

For triangular elements repeat the last nodal point, i.e. (I,J,K,K). If the elements are in the same row and of same size and material then the first and last elements need be input and the omitted elements between two input elements will be generated automatically by the program.

J. Element Cards for Linear Materials (not applicable in this study).

K. Element Cards for Nonlinear Materials (615)

Required if the option for element data (KELDT) is specified as zero in Section C and if the option for linear or nonlinear analysis is specified as one in Section E. Identification of nodal points according to Figure 2. One card for each element. No provision for automatic generation of left out elements.

Columns 1 - 5 Element number (M)

6 - 10	Nodal point I (I X (M,1))
11 - 15	Nodal point J (I X (M,2))
16 - 20	Nodal point K (I X (M,3))
21 - 25	Nodal point L (IX (M,4))
26 - 30	Material identification (IX (M,5))
	For constant K, G materials this should be specified as 200.

L. Elements to be Modified (615, 3F10.0)

Required if the number of elements under excavation (NELEX) is specified in Section E. One card for each element to be modified. Arrangement of data as outlined in Section K.

M Distributed Boundary Loads (215,E10.3)

Required if the number of boundary pressure cards (NBPC) is specified in Section E. One card for each boundary pressure according to Figure 3.

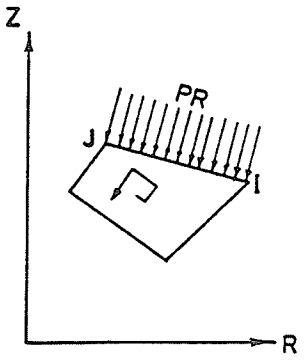

Figure 3 Boundary Pressure on an Element

N. Moduli for the Analysis of Constant, K, G Materials (2F10.0)

Required if the option for analysis of constant moduli materials (MPILE) is specified as one in Section E and the option (KPLE) in Section C is specified as zero.

Columns 1 - 20 Shear Modulus (SMPL)

21 - 40 Bulk Modulus (BMPL)

O. Nonlinear Material Property Cards (8F8.0)

Required if the option for linear or nonlinear analysis (LIN) is specified as one in Section E and the option for nonlinear data is specified as each nonlinear material.

Columns 1 - 8 Parameter K_o in equation 4.8 (AAA)

9 - 16 Parameter n in equation 4.8 (BBB)

17 - 24 Parameter m in equation 4.8 (CCC)

25 - 32 Parameter m_1 in equation 4.13 (DDD)

33 - 40 Parameter β in equation 4.13 (EEE)

41 - 48 Parameter n in equation 4.13 (FFF)

49 - 56 Parameter c in equation 4.13 (GGG)

57 - 64 Parameter α in equation 4.13 (HHH)

P. Stop Card (Blank)

For normal termination of execution the complete deck finishes with a blank card. A non zero value encountered in columns 1 - 5 is considered a subsequent problem number and the program continues with new specification of input parameters as desired. As such, there are no restrictions on the variations in the number and size of time increments which may be considered.

PROGRAM LISTING

```
//LACH    JOB ',,,L=15,T=42M,I=20','FORTX'
// EXEC FORTXCLG,REGION=2048K,MAP=NOMAP
//FORT.SYSIN DD *
      IMPLICIT REAL * 8(A-H,O-Z)
      DIMENSION AN1(20), AN2(17)
      COMMON / TIME / DT
      COMMON / GENCON / DEPB, UWT, CEPAR, NNP, NEL, NMAT, NBPC,
     &LIN, NRNGKT, NINCR, NCOUNT, IHALF, MTYP, IMOD, NTINCR, STINCR
      COMMON / MATYP / ES(300), E(10), RO(10), NU(10)
      COMMON / NPDATA / R(400), Z(400), UR(400), UZ(400), CODE(400)
      COMMON / ELDATA / BD(800), SIG1(300), SIG2(300), SIG3(300), SIG4(
     &300), SIG5(300), SIG6(300), S1BY(300), S2BY(300), PR(30),
     &SIG(10), ANGLE(4), IBC(30), JBC(30)
      COMMON / MODLS / BMOD(300), SMOD(300), AAA(15), BBB(15), CCC(15),
     &DDD(15), EEE(15), FFF(15), GGG(15), HHH(15), SMPL, BMPL
      COMMON / ARG / RRR(5), ZZZ(5), S(10, 10), P(10), LM(4), DD(3, 3),
     &HH(6, 10), RR(4), ZZ(4), C(4, 4), H(6, 10), D(6, 6), F(6, 10), TP(
     &6), XI(10), IX(400, 5)
      COMMON / SOLVR / MBAND, NUMBLK, B(108), A(108, 54)
      REAL NU
      REAL*8 IHC208
      REAL*8 IHC265
      CALL ERRSAV(208, IHC208)
      CALL ERRSAV(265, IHC265)
      CALL ERRSET(208, 999, - 1, 1)
      CALL ERRSET(265, 999, - 1, 1)
      IMOD = 0
C     PROBLEM IDENTIFICATION  &  DESCRIPTION
      READ (5,385) (AN1(N), N = 1, 20)
5     WRITE (6,390)
      READ (5,395) NPROB, (AN2(N), N = 1, 17)
      IF (NPROB) 10,380,10
10    WRITE (6,400) (AN1(N), N = 1, 20)
      WRITE (6,405) NPROB, (AN2(N), N = 1, 17)
C     READ & PRINT CONTROL INFORMATION & MATERIAL PROPERTIES
      READ (5,410) KCINF, KLMTYP, KNPDT, KELDT, KNLIN, KSCON, KPLE
      WRITE (6,415) KCINF, KLMTYP, KNPDT, KELDT, KNLIN, KSCON, KPLE
      WRITE (6,416)
C     NELEX: NUMBER OF ELEMENTS TO BE ALTERED AT EACH STAGE
C     NRNGKT: SET THE VALUE =0 FOR HALF STEP, & TO 1 FOR FULL STEP
C     NINCR: NUMBER OF INCREMENTS OF LOAD
C     LIN: SET THE VALUE =0 FOR LINEAR ANALYSIS
C     MPILE: SET THE VALUE =1 FOR ANALYSIS OF CONST. MODULUS MATERIALS
C     SET THE MATERIAL #=200 FOR CONSTANT K G MATERIAL (eg pile)
C     KINEXC:SET THE VALUE=1 IF DIFF.INCR. OF LOADING IS DESIRED & ALSO
C     FOR EXCN. PROBLEMS FROM 2ND STAGE. FOR EXCN.PROBLEMS ELEMENTS TO
C     BE EXCAVATED ARE TO BE INDICATED AT EACH STAGE. EVERY STAGE OF
C     EXCN. & EVERY DIFF. INCREMENT ARE TO BE ANALYSED AS A SEPERATE
C     PROBLEM.
C     READ & PRINT NUMBER AND SIZE OF TIME INCREMENTS
C     TINCR: NUMBER OF TIME INCREMENTS
C     STINCR: SIZE OF TIME INCREMENT
      READ (5,417) TINCR, STINCR
      WRITE (6,418) TINCR, STINCR
      IF (IMOD) 14,14,12
12    TT = DT + TINCR * STINCR
      DT = DT + STINCR
14    IF (KCINF) 20,15,20
15    READ (5,420) NNP, NEL, NMAT, NBPC, NINCR, NUMLPC, NRNGKT, LIN,
     &MPILE, KINEXC, NELEX
20    WRITE (6,425)
      WRITE (6,430) NNP, NEL, NMAT, NBPC, NINCR, NUMLPC, NRNGKT, LIN,
     &MPILE, KINEXC, NELEX
30    CONTINUE
```

```
      IF (LIN) 35,35,50
35    WRITE (6,445)
      IF (KLMTYP) 45,40,45
40    READ (5,450) (E(M), NU(M), RO(M), M=1, NMAT)
      WRITE (6,455)
      WRITE (6,460) (M, E(M), NU(M), RO(M), M=1,NMAT)
      GO TO 65
45    WRITE (6,465)
      GO TO 65
50    IF (KSCON) 60,55,60
55    READ (5,470) CEPAR, DEPB, UWT
      WRITE (6,475) CEPAR, DEPB, UWT
      GO TO 65
60    WRITE (6,480)
C     READ AND PRINT NODAL POINT DATA
65    WRITE (6,485)
      WRITE (6,490)
      IF (KNPDT) 105,70,105
70    L = 0
75    READ (5,495) N, CODE(N), R(N), Z(N), UR(N), UZ(N)
      NL = L + 1
      IF (L .EQ. 0) GO TO 80
      ZX = N - L
      DR = (R(N) - R(L)) / ZX
      DZ = (Z(N) - Z(L)) / ZX
80    L = L + 1
      IF (N-L) 95,90,85
85    CODE(L) = 0.0
      R(L) = R(L - 1) + DR
      Z(L) = Z(L - 1) + DZ
      UR(L) = 0.0
      UZ(L) = 0.0
      GO TO 80
90    WRITE (6,500) (K, CODE(K), R(K), Z(K), UR(K), UZ(K), K = NL, N)
      IF (NNP - N) 95,100,75
95    WRITE (6,505) N
      GO TO 380
100   CONTINUE
      GO TO 110
C     LOAD OR DEFORMATION ADDITION AT CERTAIN NODAL POINTS
105   WRITE (6,510)
110   IF (NUMLPC) 115,125,115
115   WRITE(6,515)
      DO 120 I = 1, NUMLPC
      READ (5,495) N,CODE(N), R(N), Z(N), UR(N), UZ(N)
      WRITE (6,500) N, CODE(N), R(N), Z(N), UR(N), UZ(N)
120   CONTINUE
C     READ AND PRINT ELEMENT PROPERTIES
125   WRITE (6,520)
      WRITE (6,525)
      IF (KELDT) 190,130,190
130   N = 0
135   IF (LIN) 140,140,145
140   READ (5,530) M, (IX(M, I), I = 1, 5)
      GO TO 150
145   READ (5,535) M, (IX(M, I), I = 1, 5)
150   N = N + 1
      IF (M - N) 160,160,155
155   IX(N, 1) = IX(N - 1, 1) + 1
      IX(N, 2) = IX(N - 1, 2) + 1
      IX(N, 3) = IX(N - 1, 3) + 1
      IX(N, 4) = IX(N - 1, 4) + 1
      IX(N, 5) = IX(N - 1, 5) + 1
160   IF (LIN) 165,165,170
```

```
165   WRITE (6,540) N, (IX(N, I), I = 1, 5)
      GO TO 175
170   WRITE (6,545) N, (IX(N, I), I = 1, 5)
175   IF (M - N) 180,180,150
180   IF (NEL - N) 185,185,135
185   CONTINUE
      GO TO 195
190   WRITE(6,550)
195   IF (NELEX) 200,210,200
200   WRITE (6,555)
      DO 205 J = 1, NELEX
      READ (5,535) M, (IX(M, I), I = 1, 5)
      WRITE (6,545) M, (IX(M, I), I = 1, 5)
205   CONTINUE
C     READ AND PRINT PRESSURE BOUNDARY CONDITIONS
210   IF (NBPC) 215,225,215
215   WRITE (6,560)
      WRITE (6,565)
      DO 220 L = 1, NBPC
      READ (5,570) IBC(L), JBC(L), PR(L)
220   WRITE (6,575) IBC(L), JBC(L), PR(L)
225   CONTINUE
C     INPUT OF BACKFILL & PILE MATERIAL PARAMETERS
      IF (MPILE) 265,265,230
230   IF (KPLE) 240,235,240
235   READ (5,580) SMPL, BMPL
      WRITE (6,585) SMPL,BMPL
      GO TO 265
240   WRITE (6,590)
265   CONTINUE
C     INPUT OF NON LINEAR STRESS STRAIN RELATIONSHIP;OPTION LIN IS FOR
C     LINEAR OR NON LINEAR ANALYSIS. IF LIN=0 LINEAR ANALYSIS IS DONE.
      IF (LIN) 270,285,270
270   WRITE (6,610)
      IF (KNLIN) 280,275,280
275   READ(5,615) (AAA(N), BBB(N), CCC(N), DDD(N), EEE(N), FFF(N), GGG(N
     &), HHH(N), N = 1, NMAT)
      WRITE (6,620)
      WRITE (6,625) (N, AAA(N), BBB(N), CCC(N), DDD(N), EEE(N), FFF(N),
     &GGG(N), HHH(N), N = 1, NMAT)
      GO TO 285
280   WRITE (6,630)
C     COMPUTATION OF BAND WIDTH
285   J = 0
      DO 297 N = 1, NEL
      DO 297 I = 1, 4
      DO 295 L = 1, 4
      KK = IABS(IX(N, I) - IX(N, L))
      IF (KK - J) 295,295,290
290   J = KK
295   CONTINUE
297   CONTINUE
      MBAND = 2 * J + 2
      NNC = 2 * NNP
      WRITE (6,635) MBAND
      IF (IMOD) 298,298,300
298   DT = STINCR
      TT = TINCR * STINCR
300   IF (IMOD) 304,304,301
301   WRITE (6,636)
      WRITE (6,637) DT
C     WRITE (6,642)
      DO 303 N = 1, NEL
      IF (MTYP - 200) 302,303,303
```

```
302   SM = (SIG5(N) + SIG6(N) + (SIG3(N) - S2BY(N))) / 3.0
      S1 = SIG5(N) - SM
      S2 = SIG6(N) - SM
      S3 = SIG3(N) - SM - S2BY(N)
      SDSQ = DABS(S1 ** 2 + S2 ** 2 + S3 ** 2)
      SD = DSQRT(SDSQ)
      X = NINCR
      NINCR = -1
      CALL PARAM(N, SM, SD)
      NINCR = X
C     WRITE (6,643) N, SIG5(N), SIG6(N), SM, SD, SMOD(N), BMOD(N)
303   CONTINUE
      GO TO 325
304   IF (LIN) 315,315,305
305   IF (KINEXC) 310,310,315
310   WRITE (6,637) DT
312   WRITE (6,640)
315   CONTINUE
      IF (KINEXC) 325,325,320
320   IMOD = 1
      GO TO 340
325   DO 330 I = 1, NNC
330   BD(I) = 0.0
      DO 335 N = 1, NEL
      SIG1(N) = 0.0
      SIG2(N) = 0.0
      SIG3(N) = 0.0
      SIG4(N) = 0.0
      SIG5(N) = 0.0
335   SIG6(N) = 0.0
      NCOUNT = 0
340   IF (NRNGKT) 345,355,345
345   IHALF = 1
C     FORMATION OF STIFFNESS MATRIX
      CALL STIFF
C     SOLVE FOR DISPLACEMENTS
      CALL EQSOLV
      DO 350 I = 1,NNC
350   BD(I) = BD(I) + B(I)
      KCOUNT = NCOUNT + 1
      IF (NINCR - KCOUNT) 351,351,352
351   WRITE (6,390)
      WRITE (6,645)
      WRITE (6,650) (N, BD(2 * N - 1), BD(2 * N), N = 1, NNP)
352   IMOD = 1
C     COMPUTATION OF STRESSES
      CALL STRESS
      NCOUNT = NCOUNT + 1
      IF (NINCR - NCOUNT) 353,353,354
353   WRITE (6,655) NCOUNT
354   IF (NINCR - NCOUNT) 375,375,345
355   DO 360 I = 1, NNP
360   UZ(I) = UZ(I) / 2.0
      IHALF = 0
      CALL STIFF
      CALL EQSOLV
      IMOD = 1
      CALL STRESS
      IHALF = 1
      DO 365 I = 1, NNP
365   UZ(I) = UZ(I) + UZ(I)
      CALL STIFF
      CALL EQSOLV
      DO 370 I = 1, NNC
```

```
370   BD(I) = BD(I) + B(I)
      KCOUNT = NCOUNT + 1
      IF (NINCR - KCOUNT) 371,371,372
371   WRITE (6,650) (N, BD(2 * N - 1), BD(2 * N), N = 1, NNP)
372   CALL STRESS
      NCOUNT = NCOUNT + 1
      IF (NINCR - NCOUNT) 373,373,374
373   WRITE (6,655) NCOUNT
374   IF (NINCR - NCOUNT) 375,375,355
375   IF (TT - DT) 5,5,376
376   DT = DT + STINCR
      GO TO 301
380   CONTINUE
      CALL ERRSTR(208, IHC208)
      CALL ERRSTR(265, IHC265)
385   FORMAT (20A4)
390   FORMAT (1H1)
395   FORMAT (I5, 5X, 17A4)
400   FORMAT (5X, 20A4)
405   FORMAT ( /, 8H    PROB, /, 5X, I5, 5X, 17A4)
410   FORMAT (7I5)
415   FORMAT (5X, /, 29H OPTIONS TO RETAIN PRIOR DATA, /, 39H     SET TH
     &E VALUE=1 FOR RETAINING      , /, 39H     CONTROL INFORMATION
     &         , I3, /, 39H     MATERIAL PROPERTIES (LINEAR CASE) , I3,
     & /, 39H     NODAL POINT DATA                    , I3, /, 39H     ELE
     &MENT DATA                    , I3, /, 39H     NON LINEAR INFORMA
     &TION             , I3, /, 39H     SOIL CONDITIONS
     & , I3, /, 39H     CONSTANT DEFORMATION MODULI DATA  , I3, / )
416   FORMAT (//, 5X, 'TIME - RELATED CONTROL INFORMATION', / )
417   FORMAT (E10.3, E10.3)
418   FORMAT ( / , 5X, 'NUMBER OF TIME INCREMENTS = ',F10.3, /, 5X, 'SIZ
     &E OF TIME INCREMENT = ',F10.3, /)
420   FORMAT (11I5)
425   FORMAT (5X, 9H TABLE  1, 5X, 'CONTROL INFORMATION', / )
430   FORMAT ( /, 39H     NUMBER OF NODAL POINTS             , I5, /, 39H
     &     NUMBER OF ELEMENTS                , I5, /, 39H     NUMBER OF
     &DIFFERENT MATERIALS      , I5, /, 39H     NUMBER OF PRESSURE CARDS
     &         , I5, /, 39H     NUMBER OF LOAD INCREMENTS          , I5,
     & /, 39H     NUMBER OF LOAD POINTS              , I5, /, 39H     OPT
     &ION FOR HALF OR FULL STEP       , I5, /, 39H     OPTION FOR LINEAR
     &ANALYSIS         , I5, /, 39H     OPTION FOR CONST. K G ELEMENTS
     & ,I5, /, 39H     SPECIAL OPTION FOR DIFF. INCREMENT , I5, /, 39H
     &   NUMBER OF ALTERED ELEMENTS         , I5, / )
445   FORMAT (5X, 9H TABLE 1A, 5X, 'LINEAR ANALYSIS', 5X, 'MATERIAL PROP
     &ERTIES', / )
450   FORMAT (3E10.3)
455   FORMAT (10H MATERIAL , 5X, 10HMODULUS OF, 5X, 9HPOISSON-S, 5X, 9HM
     &ATERIAL, /, 9H   NUMBER, 6X, 10HELASTICITY, 7X, 7H  RATIO, 7X, 8HD
     &ENSITY, / )
460   FORMAT (I6, 7X, E12.4, 3X, E12.4, 5X, E12.4)
465   FORMAT (5X, 42H ELASTIC AND MATERIAL PROPERTIES AS BEFORE, / )
470   FORMAT (3F10.0)
475   FORMAT ( /, 39H     COEFFT.OF EARTH PRESSURE AT REST= , F6.2, /,
     &39H     DEPTH OF BOTTOM BOUNDARY         = , F6.2, /, 39H     AVERA
     &GE UNIT WT. OF SOIL         = , F6.2, / )
480   FORMAT (5X, 26H SOIL CONDITIONS AS BEFORE, / )
485   FORMAT (5X, 9H TABLE 2, / )
490   FORMAT (5X, 83H  NODAL POINT     TYPE     R-ORDINATE     Z-ORDINATE
     & R-LOAD OR DISP   Z-LOAD OR DISP, / )
495   FORMAT (I5, 5X, 5F10.3)
500   FORMAT (10X, I5, 5X, F10.3, 2X, E10.3, 1X, E10.3, 3X, F10.3, 7X,
     &F10.3)
505   FORMAT (1X, 28H NODAL POINT CARD ERROR N=   , I5, / )
510   FORMAT (5X, 27H NODAL POINT DATA AS BEFORE, / )
```

```
515   FORMAT (5X, 10H TABLE 2A, /, 47H MODIFIED LOADS OR DISPS=PREVIOUS
     &   +INCREMENT, / )
520   FORMAT (5X, 9H TABLE  3, / )
525   FORMAT (5X, 49H ELEMENT NO.       I     J     K     L   MATERIAL,
     & / )
530   FORMAT (6I5)
535   FORMAT (6I5)
540   FORMAT (7X, I5, 8X, I5, 1X, I5, 1X, I5, 1X, I5, 4X, I5)
545   FORMAT (7X, I5, 8X, I5, 1X, I5, 1X, I5, 1X, I5, 4X, I5)
550   FORMAT (5X, 30H ELEMENT PROPERTIES AS BEFORE , / )
555   FORMAT (5X, 10H TABLE 3A, /, 5X, 55HMODIFIED ELEMENTS = PREVIOUS +
     & ELEMENTS TO BE EXCAVATED, / )
560   FORMAT (5X, 9H TABLE  4, / )
565   FORMAT (5X, 30H  PRESSURE BOUNDARY CONDITIONS, /, 25H       I
     &J   PRESSURE, / )
570   FORMAT (2I5,E10.3)
575   FORMAT (3X, I5, 1X, I5, 3X, F10.3)
580   FORMAT (2F20.0)
585   FORMAT (5X, 'FOR PLATE ; CONSTANT G VALUE = ', E10.3, 'KPa', /,
     &24X, ' K VALUE   = ', E10.3, 'KPa', / )
590   FORMAT (5X, 'PARAMETERS FOR CONSTANT K ; G MATERIAL AS BEFORE', /
     &)
610   FORMAT (5X, 33H TABLE 5 NON LINEAR ANALYSIS DATA, / )
615   FORMAT (8F8.0)
620   FORMAT (T5, 'MATERIAL #', T20, 'AAA', T30, 'BBB', T40, 'CCC', T50,
     & 'DDD', T60, 'EEE', T70, 'FFF', T80, 'GGG', T90, 'HHH', / )
625   FORMAT (I10, 5X, 8E10.3)
630   FORMAT (5X, 26H NON LINEAR DATA AS BEFORE, / )
635   FORMAT (20X, 'BAND WIDTH=', I7, / )
636   FORMAT ( /, 10X, 90H**********************************************
     &*****************************************)
637   FORMAT ( ///, 5X, 'TIME = ', F10.3)
640   FORMAT ( / /, 25X, 'OUTPUT; INSITU STRESSES AND ASSOCIATED MODULI'
     &, / /, 7X, 8HELEMENT#, 2X, 10HMAX-STRESS, 2X, 10HMIN-STRESS, 2X,
     &11HMEAN-STRESS, 2X, 10HDEV-STRESS, 9X, 9HSHEAR MOD, 2X, 8HBULK MOD
     &, / )
C 642 FORMAT ( / /, 25X, 'OUTPUT; CURRRENT STRESSES AND ASSOC. MODULI  '
C     &, / /, 7X, 8HELEMENT#, 2X, 10HMAX-STRESS, 2X, 10HMIN-STRESS, 2X,
C     &11HMEAN-STRESS, 2X, 10HDEV-STRESS, 9X, 9HSHEAR MOD, 2X, 8HBULK MOD
C     &, / )
C 643 FORMAT (7X, I7, F10.2, 2X, F10.2, 2X, F10.2, 3X, F10.2, 9X, 2E10.3
C     &)
645   FORMAT (5X, 49HRESULTS,NODAL DISPLACEMENTS AND ELEMENT STRESSES, /
     &)
650   FORMAT (12H N.P. NUMBER, 18X, 2HUR, 18X, 2HUZ, /, (1I12, 2F20.7))
655   FORMAT (5X, 32H NUMBER OF FULL LOAD INCREMENT =, I5)
      STOP
      END
      SUBROUTINE STIFF
      IMPLICIT REAL * 8(A - H, O - Z)
      COMMON / TIME / DT
      COMMON / GENCON / DEPB, UWT, CEPAR, NNP, NEL, NMAT, NBPC,
     &LIN, NRNGKT, NINCR, NCOUNT, IHALF, MTYP, IMOD, NTINCR, STINCR
      COMMON / MATYP / ES(300), E(10), RO(10), NU(10)
      COMMON / NPDATA / R(400), Z(400), UR(400), UZ(400), CODE(400)
      COMMON / ELDATA / BD(800), SIG1(300), SIG2(300), SIG3(300), SIG4(
     &300), SIG5(300), SIG6(300), S1BY(300), S2BY(300), PR(30),
     &SIG(10), ANGLE(4), IBC(30), JBC(30)
      COMMON / MODLS / BMOD(300), SMOD(300), AAA(15), BBB(15), CCC(15),
     &DDD(15), EEE(15), FFF(15), GGG(15), HHH(15), SMPL, BMPL
      COMMON / ARG / RRR(5), ZZZ(5), S(10, 10), P(10), LM(4), DD(3, 3),
     &HH(6, 10), RR(4), ZZ(4), C(4, 4), H(6, 10), D(6, 6), F(6, 10), TP(
     &6), XI(10), IX(400, 5)
      COMMON / SOLVR / MBAND, NUMBLK, B(108), A(108,54)
```

```
      REAL NU
C     INITIALISE
      REWIND 9
C     NB;PARAMETER RELATED TO THE SIZE OF A BLOCK. ITS VALUE CAN BE
C     SPECIFIED DEPENDING ON THE CORE STORAGE AVAILABLE IN THE COMPUTER
      NB = 27
      ND = 2 * NB
      ND2 = 2 * ND
      STOPP = 0.0
      NUMBLK = 0
      DO 10 N = 1, ND2
      B(N) = 0.0
      DO 10 M = 1, ND
10    A(N, M) = 0.0
C     FORM THE STIFFNESS MATRIX IN BLOCKS
20    NUMBLK = NUMBLK + 1
      NH = NB * (NUMBLK + 1)
      NM = NH - NB
      NL = NM - NB + 1
      KSHIFT = 2 * NL - 2
      DO 180 N = 1, NEL
      IF (IX(N, 5)) 180,180,30
30    DO 50 I = 1, 4
      IF (IX(N, I) - NL) 50,40,40
40    IF (IX(N, I) - NM) 60,60,50
50    CONTINUE
      GO TO 180
60    CALL QUDSTF(N, VOL)
      IF (VOL) 70,70,80
70    WRITE (6,470) N
      STOPP = 1.0
80    IF (IX(N, 3) - IX(N, 4)) 90,120,90
C     ELIMINATE THE FIFTH NODAL POINT
90    DO 100 II = 1, 9
      CC = S(II, 10) / S(10 , 10)
      P(II) = P(II) - CC * P(10)
      DO 100 JJ = 1, 9
100   S(II, JJ) = S(II, JJ) - CC * S(10, JJ)
      DO 110 II = 1, 8
      CC = S(II, 9) / S(9, 9)
      P(II) = P(II) - CC * P(9)
      DO 110 JJ = 1, 8
110   S(II, JJ) = S(II, JJ) - CC * S(9, JJ)
C     ADD ELEMENT STIFFNESS TO TOTAL STIFFNESS. DIRECT STIFFNESS METHOD
120   DO 130 I = 1, 4
130   LM(I) = 2 * IX(N, I) - 2
      DO 170 I = 1, 4
      DO 170 K = 1, 2
      II = LM(I) + K - KSHIFT
      KK = 2 * I - 2 + K
      B(II) = B(II) + P(KK)
      DO 170 J = 1, 4
      DO 170 L = 1, 2
      JJ = LM(J) + L - II + 1 - KSHIFT
      LL = 2 * J - 2 + L
      IF (JJ) 170,170,140
140   IF (ND - JJ) 150,160,160
150   WRITE (6,480) N
      STOPP = 1.0
      GO TO 180
160   A(II, JJ) = A(II, JJ) + S(KK, LL)
170   CONTINUE
180   CONTINUE
C     ADD CONCENTRATED FORCES WITHIN BLOCKS
```

```
      DO 190 N = NL, NM
      K = 2 * N - KSHIFT
      B(K) = B(K) + UZ(N)
190   B(K - 1) = B(K - 1) + UR(N)
C     BOUNDARY CONDITIONS
C     1. PRESSURE BOUNDARY CONDITIONS
      IF (NBPC) 200,340,200
200   DO 330 L = 1, NBPC
      I = IBC(L)
      J = JBC(L)
      IF (IHALF) 220,210,220
210   PP = PR(L) / 12.0
      GO TO 230
220   PP = PR(L) / 6.0
230   DZ = (Z(I) - Z(J)) * PP
      DR = (R(J) - R(I)) * PP
      RX = 2.0 * R(I) + R(J)
      ZX = R(I) + 2.0 * R(J)
      II = 2 * I - KSHIFT
      JJ = 2 * J - KSHIFT
      IF (II) 280,280,240
240   IF (II - ND) 250,250,280
C     MODIFY FOR SKEW BOUNDARIES
250   SINA = 0.0
      COSA = 1.0
      IF (CODE(I)) 260,270,270
260   SINA = DSIN(CODE(I) / 57.29577)
      COSA = DCOS(CODE(I) / 57.29577)
270   B(II - 1) = B(II - 1) + RX * (COSA * DZ + SINA * DR)
      B(II) = B(II) - RX * (SINA * DZ - COSA * DR)
280   IF (JJ) 330,330,290
290   IF (JJ - ND) 300,300,330
300   SINA = 0.0
      COSA = 1.0
      IF (CODE(J)) 310,320,320
310   SINA = DSIN(CODE(J) / 57.29577)
      COSA = DCOS(CODE(J) / 57.29577)
320   B(JJ - 1) = B(JJ - 1) + ZX * (COSA * DZ + SINA * DR)
      B(JJ) = B(JJ) - ZX * (SINA * DZ - COSA * DR)
330   CONTINUE
C     2. DISPLACEMENT BOUNDARY CONDITIONS
340   DO 420 M = NL, NH
      IF (M - NNP) 350,350,420
350   U = UR(M)
      N = 2 * M - 1 - KSHIFT
      IF (CODE(M)) 410,420,360
360   IF (CODE(M) - 1.0) 370,390,370
370   IF (CODE(M) - 2.0) 380,410,380
380   IF (CODE(M) - 3.0) 410,400,410
390   CALL MODIFY(A, B, ND2, MBAND, N, U)
      GO TO 420
400   CALL MODIFY(A, B, ND2, MBAND, N, U)
410   U = UZ(M)
      N = N + 1
      CALL MODIFY(A, B, ND2, MBAND, N, U)
420   CONTINUE
C     WRITE BLOCK OF EQUATIONS ON TAPE AND SHIFT UP LOWER BLOCK
      WRITE (9) (B(N), (A(N, M), M = 1, MBAND), N = 1, ND)
      DO 430 N = 1, ND
      K = N + ND
      B(N) = B(K)
      B(K) = 0.0
      DO 430 M = 1, ND
      A(N, M) = A(K, M)
```

```
430   A(K, M) = 0.0
C     CHECK FOR THE LAST BLOCK
      IF (NM - NNP) 20,440,440
440   CONTINUE
      IF (STOPP) 450,460,450
450   CALL EXIT
460   RETURN
470   FORMAT (5X, 25HNEGATIVE AREA ELEMENT NO., I5, / )
480   FORMAT (5X, 30HBAND WIDTH EXCEEDS ALLOWABLE  , I5, / )
      END
      SUBROUTINE QUDSTF(N, VOL)
      IMPLICIT REAL * 8(A - H, O - Z)
      COMMON / TIME / DT
      COMMON / GENCON / DEPB, UWT, CEPAR, NNP, NEL, NMAT, NBPC,
     &LIN, NRNGKT, NINCR, NCOUNT, IHALF, MTYP, IMOD, NTINCR, STINCR
      COMMON / MATYP / ES(300), E(10), RD(10), NU(10)
      COMMON / NPDATA / R(400), Z(400), UR(400), UZ(400), CODE(400)
      COMMON / ELDATA / BD(800), SIG1(300), SIG2(300), SIG3(300), SIG4(
     &300), SIG5(300), SIG6(300), S1BY(300), S2BY(300), PR(30),
     &SIG(10), ANGLE(4), IBC(30), JBC(30)
      COMMON / MODLS / BMOD(300), SMOD(300), AAA(15), BBB(15), CCC(15),
     &DDD(15), EEE(15), FFF(15), GGG(15), HHH(15), SMPL, BMPL
      COMMON / ARG / RRR(5), ZZZ(5), S(10, 10), P(10), LM(4), DD(3, 3),
     &HH(6, 10), RR(4), ZZ(4), C(4, 4), H(6, 10), D(6, 6), F(6, 10), TP(
     &6), XI(10), IX(400, 5)
      COMMON / SOLVR / MBAND, NUMBLK, B(108), A(108, 54)
      REAL NU
10    I = IX(N, 1)
      J = IX(N, 2)
      K = IX(N, 3)
      L = IX(N, 4)
      MTYP = IX(N, 5)
      IX(N, 5) = - IX(N, 5)
C     DEVELOPEMENT OF STRESS STRAIN RELATIONSHIPS
C     FOR PLANE STRAIN OR STRESS INSERT CORRESPONDING C MATRIX
      IF (LIN) 20,20,50
20    IF (NCOUNT) 30,30,40
C     COMPUTE C MATRIX FOR LINEAR CASE INVOLVING E & NU
30    ES(N) = E(MTYP)
40    XNUM = ES(N) * (1.0 - NU(MTYP))
      XDEN = (1.0 + NU(MTYP)) * (1.0 - 2.0 * NU(MTYP))
      COMMR = XNUM / XDEN
      COMMR1 = NU(MTYP) / (1.0 - NU(MTYP))
      C(1, 1) = COMMR
      C(1, 2) = COMMR * COMMR1
      C(1, 3) = C(1, 2)
      C(1, 4) = 0.0
      C(2, 1) = C(1, 2)
      C(2, 2) = C(1, 1)
      C(2, 3) = C(1, 2)
      C(2, 4) = 0.0
      C(3, 1) = C(1, 2)
      C(3, 2) = C(1, 2)
      C(3, 3) = C(1, 1)
      C(3, 4) = 0.0
      C(4, 1) = 0.0
      C(4, 2) = 0.0
      C(4, 3) = 0.0
      XN = (1.0 - 2.0 * NU(MTYP)) * COMMR
      XD = 2.0 * (1.0 - NU(MTYP))
      C(4, 4) = XN / XD
      GO TO 130
C     C MATRIX FOR NON LINEAR ANALYSIS
50    IF (NRNGKT) 60,100,60
```

```
60    IF (NCOUNT) 90,70,90
70    IF (IMOD) 80,80,90
80    CALL BFORCE(N, I, J, K, L)
90    ESH = SMOD(N)
      EBK = (SMOD(N) / 3.0) + BMOD(N)
      GO TO 120
100   IF (NCOUNT) 110,110,90
110   IF (IHALF) 70,70,90
120   C(1, 1) = EBK + ESH
      C(1, 2) = EBK - ESH
      C(1, 3) = C(1, 2)
      C(1, 4) = 0.0
      C(2, 1) = C(1, 2)
      C(2, 2) = C(1, 1)
      C(2, 3) = C(1, 2)
      C(2, 4) = 0.0
      C(3, 1) = C(1, 3)
      C(3, 2) = C(2, 3)
      C(3, 3) = C(1, 1)
      C(3, 4) = 0.0
      C(4, 1) = 0.0
      C(4, 2) = 0.0
      C(4, 3) = 0.0
      C(4, 4) = ESH
C     DEVELOPEMENT OF QUADRILATERAL STIFFNESS MATRIX
130   RRR(5) = (R(I) + R(J) + R(K) + R(L)) / 4.0
      ZZZ(5) = (Z(I) + Z(J) + Z(K) + Z(L)) / 4.0
      DO 170 M = 1, 4
      MM = IX(N, M)
      IF (R(MM)) 160,140,160
140   R(MM) = 0.01 * RRR(5)
      IF (CODE(MM)) 160,150,160
150   CODE(MM) = 1.0
160   RRR(M) = R(MM)
170   ZZZ(M) = Z(MM)
      DO 190 II = 1, 10
      P(II) = 0.0
      DO 180 JJ = 1, 6
180   HH(JJ, II) = 0.0
      DO 190 JJ = 1, 10
190   S(II, JJ) = 0.0
      DO 200 II = 1, 4
      JJ = IX(N, II)
200   ANGLE(II) = CODE(JJ) / 57.3
      IF (K - L) 220,210,220
210   CALL TRISTF(1, 2, 3)
      RRR(5) = (RRR(1) + RRR(2) + RRR(3)) / 3.0
      ZZZ(5) = (ZZZ(1) + ZZZ(2) + ZZZ(3)) / 3.0
      VOL = XI(1)
      GO TO 240
220   VOL = 0.0
      CALL TRISTF(4, 1, 5)
      VOL = VOL + XI(1)
      CALL TRISTF(1, 2, 5)
      VOL = VOL + XI(1)
      CALL TRISTF(2, 3, 5)
      VOL = VOL + XI(1)
      CALL TRISTF(3, 4, 5)
      VOL = VOL + XI(1)
      DO 230 II = 1, 6
      DO 230 JJ = 1, 10
230   HH(II, JJ) = HH(II, JJ) / 4.0
240   RETURN
      END
```

```
      SUBROUTINE TRISTF(II, JJ, KK)
      IMPLICIT REAL * 8(A - H, O - Z)
      COMMON / TIME / DT
      COMMON / GENCON / DEPB, UWT, CEPAR, NNP, NEL, NMAT, NBPC,
     &LIN, NRNGKT, NINCR, NCOUNT, IHALF, MTYP, IMOD, NTINCR, STINCR
      COMMON / MATYP / ES(300), E(10), RO(10), NU(10)
      COMMON / NPDATA / R(400), Z(400), UR(400), UZ(400), CODE(400)
      COMMON / ELDATA / BD(800), SIG1(300), SIG2(300), SIG3(300), SIG4(
     &300), SIG5(300), SIG6(300), S1BY(300), S2BY(300), PR(30),
     &SIG(10), ANGLE(4), IBC(30), JBC(30)
      COMMON / MODLS / BMOD(300), SMOD(300), AAA(15), BBB(15), CCC(15),
     &DDD(15), EEE(15), FFF(15), GGG(15), HHH(15), SMPL, BMPL
      COMMON / ARG / RRR(5), ZZZ(5), S(10, 10), P(10), LM(4), DD(3, 3),
     &HH(6, 10), RR(4), ZZ(4), C(4, 4), H(6, 10), D(6, 6), F(6, 10), TP(
     &6), XI(10), IX(400, 5)
      REAL NU
C     INITIALIZATION
      LM(1) = II
      LM(2) = JJ
      LM(3) = KK
      RR(1) = RRR(II)
      RR(2) = RRR(JJ)
      RR(3) = RRR(KK)
      RR(4) = RRR(II)
      ZZ(1) = ZZZ(II)
      ZZ(2) = ZZZ(JJ)
      ZZ(3) = ZZZ(KK)
      ZZ(4) = ZZZ(II)
10    DO 30 I = 1, 6
      DO 20 J = 1, 10
      F(I, J) = 0.0
20    H(I, J) = 0.0
      DO 30 J = 1, 6
30    D(I, J) = 0.0
C     COMPUTE INTEGRAL (G)T * (C) * (G)
C     FOR PLANE STRAIN AND STRESS CASES ,THE ELEMENT PER UNIT LENGTH IS
C     COMPUTED BY MULTIPLYING WIDTH BY DEPTH . SUBROUTINE NUMINT IS
C     NEEDED FOR AXI-SYMMETRICAL CASE .
      CALL NUMINT(XI, RR, ZZ)
      D(2, 6) = XI(1) * (C(1, 2) + C(2, 3))
      D(3, 5) = XI(1) * C(4, 4)
      D(5, 5) = XI(1) * C(4, 4)
      D(6, 6) = XI(1) * C(2, 2)
      D(1, 1) = XI(3) * C(3, 3)
      D(1, 2) = XI(2) * (C(1, 3) + C(3, 3))
      D(1, 3) = XI(5) * C(3, 3)
      D(1, 6) = XI(2) * C(2, 3)
      D(2, 2) = XI(1) * (C(1, 1) + 2.0 * C(1, 3) + C(3, 3))
      D(2, 3) = XI(4) * (C(1, 3) + C(3, 3))
      D(3, 3) = XI(6) * C(3, 3) + XI(1) * C(4, 4)
      D(3, 6) = XI(4) * C(2, 3)
      DO 40 I = 1, 6
      DO 40 J = 1, 6
40    D(J, I) = D(I, J)
C     DEVELOPEMENT OF COEFFICIENT DISPLACEMENT TRANSFORMATION MATRIX
      COMM = RR(2) * (ZZ(3) - ZZ(1)) + RR(1) * (ZZ(2) - ZZ(3)) + RR(3) *
     &(ZZ(1) - ZZ(2))
      DD(1, 1) = (RR(2) * ZZ(3) - RR(3) * ZZ(2)) / COMM
      DD(1, 2) = (RR(3) * ZZ(1) - RR(1) * ZZ(3)) / COMM
      DD(1, 3) = (RR(1) * ZZ(2) - RR(2) * ZZ(1)) / COMM
      DD(2, 1) = (ZZ(2) - ZZ(3)) / COMM
      DD(2, 2) = (ZZ(3) - ZZ(1)) / COMM
      DD(2, 3) = (ZZ(1) - ZZ(2)) / COMM
      DD(3, 1) = (RR(3) - RR(2)) / COMM
```

```
      DD(3, 2) = (RR(1) - RR(3)) / COMM
      DD(3, 3) = (RR(2) - RR(1)) / COMM
      DO 50 I = 1, 3
      J = 2 * LM(I) - 1
      H(1, J) = DD(1, I)
      H(2, J) = DD(2, I)
      H(3, J) = DD(3, I)
      H(4, J + 1) = DD(1, I)
      H(5, J + 1) = DD(2, I)
50    H(6, J + 1) = DD(3, I)
C     ROTATE UNKNOWNS IF NECESSARY
      DO 80 J = 1, 2
      I = LM(J)
      IF (ANGLE(I)) 60,80,80
60    SINA = DSIN(ANGLE(I))
      COSA = DCOS(ANGLE(I))
      IJ = 2 * I
      DO 70 K = 1, 6
      TEM = H(K, IJ - 1)
      H(K, IJ - 1) = TEM * COSA + H(K, IJ) * SINA
70    H(K, IJ) = - TEM * SINA + H(K, IJ) * COSA
80    CONTINUE
C     DEVELOP ELEMENT STIFFNESS MATRIX (H)T * (D) * NH
      DO 110 J = 1, 10
      DO 110 K = 1, 6
      IF (H(K, J)) 90,110,90
90    DO 100 I = 1, 6
100   F(I, J) = F(I, J) + D(I, K) * H(K, J)
110   CONTINUE
      DO 140 I = 1, 10
      DO 140 K = 1, 6
      IF (H(K, I)) 120,140,120
120   DO 130 J = 1, 10
130   S(I, J) = S(I, J) + H(K, I) * F(K, J)
140   CONTINUE
      IF (LIN) 150,150,170
C     DEVELOPMENT OF BODY FORCE MATRIX
150   TBODYF = XI(1) * RO(MTYP)
      BODYF = - TBODYF / 3.0
      DO 160 I = 1, 3
      J = 2 * LM(I)
160   P(J) = P(J) + BODYF
C     DEVELOPMENT OF STRAIN TRANSFORMATION MATRIX
170   DO 180 I = 1, 6
      DO 180 J = 1, 10
180   HH(I, J) = HH(I, J) + H(I, J)
      RETURN
      END
      SUBROUTINE BFORCE(N, I, J, K, L)
      IMPLICIT REAL * 8(A - H, O - Z)
      COMMON / TIME / DT
      COMMON / GENCON / DEPB, UWT, CEPAR, NNP, NEL, NMAT, NBPC,
     &LIN, NRNGKT, NINCR, NCOUNT, IHALF, MTYP, IMOD, NTINCR, STINCR
      COMMON / NPDATA / R(400), Z(400), UR(400), UZ(400), CODE(400)
      COMMON / ELDATA / BD(800), SIG1(300), SIG2(300), SIG3(300), SIG4(
     &300), SIG5(300), SIG6(300), S1BY(300), S2BY(300), PR(30),
     &SIG(10), ANGLE(4), IBC(30), JBC(30)
      COMMON / MODLS / BMOD(300), SMOD(300), AAA(15), BBB(15), CCC(15),
     &DDD(15), EEE(15), FFF(15), GGG(15), HHH(15), SMPL, BMPL
      IF (K - L) 20,10,20
10    RCENT = (R(I) + R(J) + R(K)) / 3.0
      ZCENT = (Z(I) + Z(J) + Z(K)) / 3.0
      GO TO 30
20    RCENT = (R(I) + R(J) + R(K) + R(L)) / 4.0
```

```
      ZCENT = (Z(I) + Z(J) + Z(K) + Z(L)) / 4.0
30    DEL = DEPB - ZCENT
C     TOTAL STRESS ANALYSIS
      S1BY(N) = DEL * UWT
      S2BY(N) = S1BY(N) * CEPAR
      IF (MTYP - 200) 80,70,70
70    SMOD(N) = SMPL
      BMOD(N) = BMPL
      GO TO 90
80    SM = (S1BY(N) + 2.0 * S2BY(N)) / 3.0
      S1B = S1BY(N) - SM
      S2B = S2BY(N) - SM
      SDSQB = DABS(S1B ** 2 + 2.0 * (S2B ** 2))
      SD = DSQRT(SDSQB)
      CALL PARAM(N, SM, SD)
      WRITE (6,100) N, S1BY(N), S2BY(N), SM, SD, SMOD(N), BMOD(N)
90    CONTINUE
      RETURN
100   FORMAT (7X, I7, F10.2, 2X, F10.2, 2X, F10.2, 3X, F10.2, 9X,
     &2F10.1)
      END
      SUBROUTINE PARAM(N, SM, SD)
      IMPLICIT REAL * 8(A - H, O - Z)
      COMMON / TIME / DT
      COMMON / GENCON / DEPB, UWT, CEPAR, NNP, NEL, NMAT, NBPC,
     &LIN, NRNGKT, NINCR, NCOUNT, IHALF, MTYP, IMOD, NTINCR, STINCR
      COMMON / NPDATA / R(400), Z(400), UR(400), UZ(400), CODE(400)
      COMMON / ELDATA / BD(800), SIG1(300), SIG2(300), SIG3(300), SIG4(
     &300), SIG5(300), SIG6(300), S1BY(300), S2BY(300), PR(30),
     &SIG(10), ANGLE(4), IBC(30), JBC(30)
      COMMON / MODLS / BMOD(300), SMOD(300), AAA(15), BBB(15), CCC(15),
     &DDD(15), EEE(15), FFF(15), GGG(15), HHH(15), SMPL, BMPL
      CALL BULKM(N, SM)
C     CHECK FAILURE CRITERION
      SDF = 100.0 + (1.3 * DABS(SM))
      IF (SD - SDF) 6,6,4
4     KCOUNT = NCOUNT + 1
      IF (NINCR - KCOUNT) 6,5,6
5     WRITE (6,110) N
6     IF (DT) 10,10,20
10    WRITE(6, 100)
      CALL EXIT
20    IF (IMOD) 25,25,30
25    X = DT
      DT = 0.016667
30    W0=DABS(SM)
      W1=W0**EEE(MTYP)
      W2=DT**FFF(MTYP)
      W3=DT**HHH(MTYP)
      W4=SD/W0
      W5=(DDD(MTYP)*W1*W2)+(GGG(MTYP)*W3*W4)
      SMOD(N)=1.0/W5
      IF (IMOD) 35,35,40
35    DT = X
40    EMOD = (9.0 * BMOD(N) * SMOD(N)) / (SMOD(N) + (3.0 * BMOD(N)))
      POIR = (3.0 * BMOD(N) - 2.0 * SMOD(N)) / (6.0 * BMOD(N) + 2.0 *
     &SMOD(N))
100   FORMAT (5X, 'INVALID (NEGATIVE OR ZERO) TIME STEP SPECIFIED IN PRO
     &GRAM' )
110   FORMAT (5X, 'FAILURE CRITERION EXCEEDED IN ELEMENT NO.', I5 )
      RETURN
      END
      SUBROUTINE BULKM(N, SM)
      IMPLICIT REAL * 8(A - H, O - Z)
```

```
      COMMON / TIME / DT
      COMMON / GENCON / DEPB, UWT, CEPAR, NNP, NEL, NMAT, NBPC,
     &LIN, NRNGKT, NINCR, NCOUNT, IHALF, MTYP, IMOD, NTINCR, STINCR
      COMMON / NPDATA / R(400), Z(400), UR(400), UZ(400), CODE(400)
      COMMON / ELDATA / BD(800), SIG1(300), SIG2(300), SIG3(300), SIG4(
     &300), SIG5(300), SIG6(300), S1BY(300), S2BY(300), PR(30),
     &SIG(10), ANGLE(4), IBC(30), JBC(30)
      COMMON / MODLS / BMOD(300), SMOD(300), AAA(15), BBB(15), CCC(15),
     &DDD(15), EEE(15), FFF(15), GGG(15), HHH(15), SMPL, BMPL
      IF (IMOD) 10,10,20
10    X = DT
      DT = 0.016667
20    W0=DABS(SM)
      W1=1.0/AAA(MTYP)
      W2=-CCC(MTYP)*DT
      W3=DEXP(W2)
      W4=1.0+(W1*BBB(MTYP)*W3*W0)
      W5=W4**2
      BMOD(N)=AAA(MTYP)*W5
      IF (IMOD) 30,30,40
30    DT = X
40    RETURN
      END
      SUBROUTINE MODIFY(A, B, NEQ, MBAND, N, U)
      IMPLICIT REAL * 8(A - H, O - Z)
      DIMENSION A(108, 54), B(108)
      DO 40 M = 2, MBAND
      K = N - M + 1
      IF (K) 20,20,10
10    B(K) = B(K) - A(K, M) * U
      A(K, M) = 0.0
20    K = N + M - 1
      IF (NEQ - K) 40,30,30
30    B(K) = B(K) - A(N, M) * U
      A(N, M) = 0.0
40    CONTINUE
      A(N, 1) = 1.0
      B(N) = U
      RETURN
      END
      SUBROUTINE NUMINT(XI, RR, ZZ)
      IMPLICIT REAL * 8(A - H, O - Z)
      DIMENSION RR(4), ZZ(4), XI(10), XM(6), RN(6), ZN(6), XX(6)
      DO 10 I = 1, 3
      XX(I) = 1.0
10    XX(I + 3) = 3.0
      COMM = RR(2) * (ZZ(3) - ZZ(1)) + RR(1) * (ZZ(2) - ZZ(3)) + RR(3) *
     &(ZZ(1) - ZZ(2))
      COMM = COMM / 24.0
      RN(1) = RR(1)
      RN(2) = RR(2)
      RN(3) = RR(3)
      RN(4) = (RN(1) + RN(2)) / 2.0
      RN(5) = (RN(2) + RN(3)) / 2.0
      RN(6) = (RN(3) + RN(1)) / 2.0
      ZN(1) = ZZ(1)
      ZN(2) = ZZ(2)
      ZN(3) = ZZ(3)
      ZN(4) = (ZN(1) + ZN(2)) / 2.0
      ZN(5) = (ZN(2) + ZN(3)) / 2.0
      ZN(6) = (ZN(3) + ZN(1)) / 2.0
      DO 20 I = 1, 6
20    XM(I) = XX(I) * RN(I)
      DO 30 I = 1, 10
```

```
30    XI(I) = 0.0
      DO 40 I = 1, 6
      XI(1) = XI(1) + XM(I)
      XI(2) = XI(2) + XM(I) / RN(I)
      XI(3) = XI(3) + XM(I) / (RN(I) ** 2)
      XI(4) = XI(4) + XM(I) * ZN(I) / RN(I)
      XI(5) = XI(5) + XM(I) * ZN(I) / (RN(I) ** 2)
      XI(6) = XI(6) + XM(I) * ZN(I) ** 2 / (RN(I) ** 2)
      XI(7) = XI(7) + XM(I) * RN(I)
      XI(8) = XI(8) + XM(I) * ZN(I)
      XI(9) = XI(9) + XM(I) * (RN(I) ** 2)
      XI(10) = XI(10) + XM(I) * RN(I) * ZN(I)
40    CONTINUE
      DO 50 I = 1, 10
50    XI(I) = XI(I) * COMM
      RETURN
      END
      SUBROUTINE STRESS
      IMPLICIT REAL * 8(A - H, O - Z)
      COMMON / TIME / DT
      COMMON / GENCON / DEPB, UWT, CEPAR, NNP, NEL, NMAT, NBPC,
     &LIN, NRNGKT, NINCR, NCOUNT, IHALF, MTYP, IMOD, NTINCR, STINCR
      COMMON / MATYP / ES(300), E(10), RO(10), NU(10)
      COMMON / NPDATA / R(400), Z(400), UR(400), UZ(400), CODE(400)
      COMMON / ELDATA / BD(800), SIG1(300), SIG2(300), SIG3(300), SIG4(
     &300), SIG5(300), SIG6(300), S1BY(300), S2BY(300), PR(30),
     &SIG(10), ANGLE(4), IBC(30), JBC(30)
      COMMON / MODLS / BMOD(300), SMOD(300), AAA(15), BBB(15), CCC(15),
     &DDD(15), EEE(15), FFF(15), GGG(15), HHH(15), SMPL, BMPL
      COMMON / ARG / RRR(5), ZZZ(5), S(10, 10), P(10), LM(4), DD(3, 3),
     &HH(6, 10), RR(4), ZZ(4), C(4, 4), H(6, 10), D(6, 6), F(6, 10), TP(
     &6), XI(10), IX(400, 5)
      COMMON / SOLVR / MBAND, NUMBLK, B(108), A(108,54)
      REAL NU
C     COMPUTATION OF ELEMENT STRESSES
      MPRINT = 0
      DO 360 M = 1, NEL
      N = M
      IX(N, 5) = IABS(IX(N, 5))
      MTYP = IX(N, 5)
      CALL QUDSTF(N, VOL)
      IX(N, 5) = MTYP
C     PLACE NODAL DISPLACEMENT IN ARRAY P FROM ARRAY B
      DO 10 I = 1, 4
      II = 2 * I
      JJ = 2 * IX(N, I)
      P(II - 1) = B(JJ - 1)
10    P(II) = B(JJ)
C     MODIFY TO ACCOUNT FOR THE FIFTH NODAL POINT
      DO 20 I = 1, 2
      RR(I) = P(I + 8)
      DO 20 K = 1, 8
20    RR(I) = RR(I) - S(I + 8, K) * P(K)
      COMM = S(9, 9) * S(10, 10) - S(9, 10) * S(10, 9)
      IF (COMM) 30,40,30
30    P(9) = (S(10, 10) * RR(1) - S(9, 10) * RR(2)) / COMM
      P(10) = ( - S(10, 9) * RR(1) + S(9, 9) * RR(2)) / COMM
C     COMPUTATION OF THE STRAINS
40    DO 50 I = 1, 6
      TP(I) = 0.0
      DO 50 K = 1, 10
50    TP(I) = TP(I) + HH(I, K) * P(K)
      RR(1) = TP(2)
      RR(2) = TP(6)
```

```
      RR(3) = (TP(1) + TP(2) * RRR(5) + TP(3) * ZZZ(5)) / RRR(5)
      RR(4) = TP(3) + TP(5)
C     COMPUTATION OF THE RADIAL,VERTICAL,TANGENTIAL AND SHEAR STRESSES
60    DO 70 I = 1, 3
      SIG(I) = 0.0
      DO 70 K = 1, 3
70    SIG(I) = SIG(I) + C(I, K) * RR(K)
      SIG(4) = (C(4, 4)) * RR(4)
C     COMPUTATION OF THE PRINCIPAL STRAINS ; STORE IN RR
      CC = (RR(1) + RR(2)) / 2.0
      CR1 = DABS(((RR(2) - RR(1)) / 2.0) ** 2 + (RR(4) / 2.0) ** 2)
      CR = DSQRT(CR1)
      RR(1) = CC + CR
      RR(2) = CC - CR
C     COMPUTE PRINCIPAL STRESSES AND ANGLE BETWEEN STRESS DIRECTIONS
      CC = (SIG(1) + SIG(2)) / 2.0
      BB = DABS(SIG(1) - SIG(2)) / 2.0
      CR = DSQRT(BB ** 2 + SIG(4) ** 2)
      TOT1 = CC + CR
      SIG(5) = TOT1
      TOT2 = CC - CR
      SIG(6) = TOT2
      SIG(7) = 28.648 * (DATAN2(SIG(4), BB))
C     MODIFY FOR SKEW BOUNDARIES
C     STRESSES PARALLEL TO THE LINE I-J
      I = IX(N, 1)
      J = IX(N, 2)
      XXN = Z(J) - Z(I)
      XXD = R(J) - R(I)
      ANG = 2.0 * DATAN2(XXN, XXD)
      COS2A = DCOS(ANG)
      SIN2A = DSIN(ANG)
      CX = 0.5 * (SIG(1) - SIG(2))
      SIG(8) = CX * (COS2A) + SIG(4) * (SIN2A) + CC
      SIG(9) = 2.0 * CC - SIG(8)
      SIG(10) = - CX * (SIN2A) + SIG(4) * (COS2A)
      IF (NRNGKT) 80,120,80
C     FULL INCREMENTAL METHOD
80    SIG1(N) = SIG1(N) + SIG(1)
      SIG2(N) = SIG2(N) + SIG(2)
      SIG3(N) = SIG3(N) + SIG(3)
      SIG4(N) = SIG4(N) + SIG(4)
      IF (LIN) 90,90,100
90    CCI = (SIG1(N) + SIG2(N)) / 2.0
      BBI = DABS(SIG1(N) - SIG2(N)) / 2.0
      GO TO 110
100   CCI = ((SIG1(N) - S2BY(N)) + (SIG2(N) - S1BY(N))) / 2.0
      BBI = DABS((SIG1(N) - S2BY(N)) - (SIG2(N) - S1BY(N))) / 2.0
110   CRI = DSQRT(BBI ** 2 + SIG4(N) ** 2)
      SIG5(N) = CCI + CRI
      SIG6(N) = CCI - CRI
      GO TO 170
120   IF (IHALF) 80,130,80
C     HALF INCREMENT METHOD
130   SIG11 = SIG1(N) + SIG(1)
      SIG22 = SIG2(N) + SIG(2)
      SIG33 = SIG3(N) + SIG(3)
      SIG44 = SIG4(N) + SIG(4)
      IF (LIN) 140,140,150
140   CCIH = (SIG11 + SIG22) / 2.0
      BBIH = DABS(SIG11 - SIG22) / 2.0
      GO TO 160
150   CCIH = ((SIG11 - S2BY(N)) + (SIG22 - S1BY(N))) / 2.0
      BBIH = DABS((SIG11 - S2BY(N)) - (SIG22 - S1BY(N))) / 2.0
```

```
160   CRIH = DSQRT(BBIH ** 2 + SIG44 ** 2)
      SIG55 = CCIH + CRIH
      SIG66 = CCIH - CRIH
      GO TO 205
170   IF (LIN) 175,175,205
175   KCOUNT = NCOUNT + 1
      IF (NINCR - KCOUNT) 180,180,205
180   IF (MPRINT) 200,190,200
190   WRITE (6, 380)
      MPRINT = 50
200   MPRINT = MPRINT - 1
      WRITE (6,390) N, RRR(5), ZZZ(5), SIG1(N), SIG2(N), SIG3(N), SIG4(N
     &), SIG5(N), SIG6(N)
      GO TO 205
205   IF (LIN) 360,360,210
210   IF (MTYP .EQ. 200) GO TO 360
      IF (IHALF) 220,220,230
220   SM = (SIG55 + SIG66 + (SIG33 - S2BY(N))) / 3.0
      S1 = SIG55 - SM
      S2 = SIG66 - SM
      S3 = SIG33 - SM - S2BY(N)
      GO TO 240
230   SM = (SIG5(N) + SIG6(N) + (SIG3(N) - S2BY(N))) / 3.0
      S1 = SIG5(N) - SM
      S2 = SIG6(N) - SM
      S3 = SIG3(N) - SM - S2BY(N)
240   SDSQ = DABS(S1 ** 2 + S2 ** 2 + S3 ** 2)
      SD = DSQRT(SDSQ)
250   KCOUNT = NCOUNT + 1
      IF (NINCR - KCOUNT) 260,260,350
260   IF (MPRINT) 280,270,280
270   WRITE (6,400)
      MPRINT = 300
280   MPRINT = MPRINT - 1
      WRITE (6,410) N, RRR(5), ZZZ(5), SIG1(N), SIG2(N), SIG3(N), SIG4(N
     &), SM, SD, SMOD(N), BMOD(N)
350   CALL PARAM(N, SM, SD)
360   CONTINUE
370   RETURN
380   FORMAT (1H1, 7HEL.NO. , 4X, 1HR, 7X, 1HZ, 8X, 8HR-STRESS, 5X, 8HZ-
     &STRESS, 6X, 8HT-STRESS, 6X, 9HRZ-STRESS, 4X, 10HMAX-STRESS, 4X, 10
     &HMIN-STRESS)
390   FORMAT (I7, 2F8.2, 2X, 1PE12.4, 2X, 1PE12.4, 2X, 1PE12.4, 2X,
     &1PE12.4, 2X, 1PE12.4, 2X, 1PE12.4)
400   FORMAT (1H1, 85X, 18HCOMBINED  STRESSES, /, 1X, 7HEL.NO. , 4X, 1HR
     &, 7X, 1HZ, 8X, 8HR-STRESS, 5X, 8HZ-STRESS, 6X, 8HT-STRESS, 6X, 9HR
     &Z-STRESS, 4X,11HMEAN-STRESS, 4X, 10HDEV-STRESS, 2X, 9HSHEAR MOD,
     &2X, 8HBULK MOD)
410   FORMAT (I7, 2F8.2, 2X, 1PE12.4, 2X, 1PE12.4, 2X, 1PE12.4, 2X,
     &1PE12.4, 2X, 1PE12.4, 2X, 1PE12.4, 2X, 1PE9.3, 2X, 1PE9.3)
420   FORMAT (I4, 2F8.2, 4F15.5)
      END
      SUBROUTINE EQSOLV
      IMPLICIT REAL * 8(A - H, O - Z)
      COMMON / SOLVR / MM, NUMBLK, B(108), A(108, 54)
      NN = 54
      NL = NN + 1
      NH = NN + NN
      REWIND 8
      REWIND 9
      NB = 0
      GO TO 30
C     REDUCE EQUATIONS BY BLOCKS
C     1. SHIFT BLOCK OF EQUATIONS
```

```
10    NB = NB + 1
      DO 20 N = 1, NN
      NM = NN + N
      B(N) = B(NM)
      B(NM) = 0.0
      DO 20 M = 1, MM
      A(N, M) = A(NM, M)
20    A(NM, M) = 0.0
C     2. READ NEXT BLOCK OF EQUATIONS INTO THE CORE
      IF (NUMBLK - NB) 30,40,30
30    READ (9) (B(N), (A(N, M), M = 1, MM), N = NL, NH)
      IF (NB) 40,10,40
C     3. REDUCE BLOCK OF EQUATIONS
40    DO 90 N = 1, NN
      IF (A(N, 1)) 50,90,50
50    B(N) = B(N) / A(N, 1)
      DO 80 L = 2, MM
      IF (A(N, L)) 60,80,60
60    C = A(N, L) / A(N, 1)
      I = N + L - 1
      J = 0
      DO 70 K = L, MM
      J = J + 1
70    A(I, J) = A(I, J) - C * A(N, K)
      B(I) = B(I) - A(N, L) * B(N)
      A(N, L) = C
80    CONTINUE
90    CONTINUE
C     WRITE BLOCK OF REDUCED EQUATIONS OF TAPE 9
      IF (NUMBLK - NB) 100,110,100
100   WRITE(8) (B(N), (A(N, M), M = 2, MM), N = 1, NN)
      GO TO 10
C     BACK SUBSTITUTION
110   DO 130 M = 1, NN
      N = NN + 1 - M
      DO 120 K = 2, MM
      L = N + K - 1
120   B(N) = B(N) - A(N, K) * B(L)
      NM = N + NN
      B(NM) = B(N)
130   A(NM, NB) = B(N)
      NB = NB - 1
      IF (NB) 140,150,140
140   BACKSPACE 8
      READ (8) (B(N), (A(N, M), M = 2, MM), N = 1, NN)
      BACKSPACE 8
      GO TO 110
C     ORDER UNKNOWNS IN B ARRAY
150   K = 0
      DO 160 NB = 1, NUMBLK
      DO 160 N = 1, NN
      NM = N + NN
      K = K + 1
160   B(K) = A(NM, NB)
      RETURN
      END
```

REVISED SUBROUTINE TO EVALUATE THE SHEAR CREEP FUNCTION

```
      SUBROUTINE PARAM(N, SM, SD)
      IMPLICIT REAL * 8(A - H, O - Z)
      COMMON / TIME / DT
      COMMON / GENCON / DEPB, UWT, CEPAR, NNP, NEL, NMAT, NBPC,
     &LIN, NRNGKT, NINCR, NCOUNT, IHALF, MTYP, IMOD, NTINCR, STINCR
      COMMON / NPDATA / R(400), Z(400), UR(400), UZ(400), CODE(400)
      COMMON / ELDATA / BD(800), SIG1(300), SIG2(300), SIG3(300), SIG4(
     &300), SIG5(300), SIG6(300), S1BY(300), S2BY(300), PR(30),
     &SIG(10), ANGLE(4), IBC(30), JBC(30)
      COMMON / MODLS / BMOD(300), SMOD(300), AAA(15), BBB(15), CCC(15),
     &DDD(15), EEE(15), FFF(15), GGG(15), HHH(15), SMPL, BMPL
      CALL BULKM(N, SM)
C     CHECK FAILURE CRITERION
      SDF = 100.0 + (1.3 * DABS(SM))
      IF (SD - SDF) 6,6,4
4     KCOUNT = NCOUNT + 1
      IF (NINCR - KCOUNT) 6,5,6
5     WRITE (6,110) N
6     IF (DT) 10,10,20
10    WRITE(6, 100)
      CALL EXIT
20    IF (IMOD) 25,25,30
25    X = DT
      DT = 0.016667
30    W0=DABS(SM)
      IF (SD) 31,31,32
31    SD=1.0E-12
32    W1=W0**EEE(MTYP)
      W2=DT**FFF(MTYP)
      W3=DT**HHH(MTYP)
      W4=SD/W0
      W5=DDD(MTYP)*W1*W2
      W6=GGG(MTYP)*W3
      W7=3369.31+.46355*(1.0/W6)
      W8=0.22563+0.16386*(W6/W5)
      W9=1.0/W4
      SMOD(N)=W7*(W9**W8)
      IF (IMOD) 35,35,40
35    DT = X
40    EMOD = (9.0 * BMOD(N) * SMOD(N)) / (SMOD(N) + (3.0 * BMOD(N)))
      POIR = (3.0 * BMOD(N) - 2.0 * SMOD(N)) / (6.0 * BMOD(N) + 2.0 *
     &SMOD(N))
100   FORMAT (5X, 'INVALID (NEGATIVE OR ZERO) TIME STEP SPECIFIED IN PRO


     &GRAM' )
110   FORMAT (5X, 'FAILURE CRITERION EXCEEDED IN ELEMENT NO.', I5 )
      RETURN
      END
```